Dipl.-Ing. Thomas Eixelsberger, BSc

Mechanistic analysis and synthetic application of nucleotide sugar oxidoreductases

DOCTORAL THESIS

to achieve the university degree of

Doktor der technischen Wissenschaften

submitted to

Graz University of Technology

Supervisor

Univ.-Prof. Dipl.-Ing. Dr. techn. Bernd Nidetzky

Institute of Biotechnology and Biochemical Engineering

Faculty of Technical Chemistry, Chemical and Process Engineering and Biotechnology

Graz, June 2015

AFFIDAVIT

I declare that I have authored this thesis independently, that I have not used other than the declared sources/resources, and that I have explicitly indicated all material which has been quoted either literally or by content from the sources used. The text document uploaded to TUGRAZonline is identical to the present doctoral thesis.

Date	Signature

Danksagung

Auf diesem lehrreichen Abschnitt meines Lebensweges haben mich viele Menschen begleitet. Rückblickend wird mir immer mehr bewusst, wie wichtig es ist, Menschen zu haben, die einen fördern, in schwierigen Zeiten Rat geben und mit denen man Erfolge teilen kann.

Ich danke meinem Betreuer Univ.-Prof. Dr. Bernd Nidetzky dafür, die Möglichkeit bekommen zu haben, meine Dissertation im Rahmen eines spannenden und fordernden Projekts zu verfassen und an vielfältigen Themen zu forschen. Die Diskussion mit ihm stellte für mich immer wieder eine Förderung meiner fachlichen und persönlichen Entwicklung dar. Für die Finanzierung des Projekts bedanke ich mich beim DK Molekulare Enzymologie.

Ebenso möchte ich meinen Projektpartnern Doroteja Horvat, Silvia Maitz, Claudia Puchner, Ao.Univ.-Prof. Dr. Hansjörg Weber und Assoc.-Prof. Dr. Lothar Brecker meinen Dank aussprechen. Die Zusammenarbeit mit ihnen ermöglichte erst das Entstehen dieser Arbeit. Einen wichtigen Beitrag stellte auch die Unterstützung meiner Kollegen am Institut für Biotechnologie und Bioprozesstechnik sowie von außerhalb dar. Für das angenehme Arbeitsklima im Büro danke ich Manuel Eibinger und Dr. Alexander Gutmann.

Große Unterstützung während der vergangenen Jahre fand ich nicht nur an meinem Arbeitsplatz, sondern auch in meinem Freundeskreis, durch den ich den manchmal stressigen Arbeitsalltag hinter mir lassen konnte. Ein ganz besonderer Dank gebührt meiner Familie und meiner Freundin. Meine Eltern standen das gesamte Studium hindurch hinter mir und bestärkten mich in schwierigen Momenten und wenn es darum ging, Entscheidungen zu treffen. Sie waren ebenso wie meine Schwester Christina und Josef ein großer Rückhalt für mich. Meiner Liebe Sarah danke ich für ihren Beistand in allen Lebenslagen, der einen wesentlichen Anteil am Gelingen dieser Arbeit hatte. Sie war, ist und wird immer für mich da sein.

Abstract

Nucleotide sugars act as donor substrates in enzymatic glycosylation reactions and thus play central roles in cellular metabolism. Their lack can lead to defective macromolecular structures, resulting in interference with growth and cell signaling. In humans, uridine 5'-diphosphate (UDP)-glucose (UDP-Glc) is utilized by UDP-Glc dehydrogenase (hUGDH) to produce UDP-glucuronic acid (UDP-GlcUA), which in turn acts as substrate in synthesis of UDP-xylose (UDP-Xyl) by UDP-Xyl synthase (hUXS). The products of these complex nicotinamide adenine dinucleotide (NAD^+)-dependent multi-step transformations are vital in build-up of extracellular matrix proteoglycans.

In situ ^{1}H NMR studies were used to investigate interaction between hUGDH and a thio-hemiacetal intermediate. In the case of hUXS, a combination of structural studies, reaction course analysis and molecular dynamics simulations served to elucidate the three distinct steps in the enzyme-catalyzed oxidative decarboxylation. The results revealed that distortion of the pyranoside ring through a group of highly conserved residues in the active site of hUXS is strongly conducive to catalysis by optimally aligning reactive side groups of the ligand with the enzyme and led to a detailed mechanistic proposal for the reaction catalyzed by hUXS. The significance of residue conservation in hUXS was further explored by mutational studies that gave insights into structure-function relationships in the enzyme.

Notwithstanding their high biological importance, synthetic ways towards both UDP-GlcUA and UDP-Xyl are not well established. Therefore, an enzymatic redox cascade employing hUGDH and hUXS for production of these compounds from UDP-Glc was developed. Coupling of the biosynthetic reaction to three-step chemo-enzymatic co-enzyme regeneration by *Candida tenuis* xylose reductase and bovine liver catalase was crucial to overcome inhibitory effects of reduced NAD^+ and to achieve high product yields.

Production of ^{2}*H*- and ^{13}*C*-labeled as well as deoxygenated UDP-GlcUA was a prerequisite for subsequent investigation of UDP-apiose (UDP-Api)/UDP-Xyl synthase (UAXS). D-apiose (Api), a branched carbohydrate unique to plants, serves to crosslink different polysaccharide chains in glycoconjugates in the cell wall. UAXS catalyzes the chemically intriguing decarboxylation/pyranoside ring contraction reaction from UDP-GlcUA to the Api precursor UDP-Api. Comprehensive probing of the enzymatic reaction using the synthesized compounds allowed to decipher the elusive mechanism of UAXS and delineated how the enzyme chemically achieves a reorganization of the carbon skeleton from pyranoside to furanoside.

Zusammenfassung

Nukleotidzucker sind Donorsubstrate in enzymatischen Glykosylierungsreaktionen und haben daher wichtige metabolische Funktionen. Ihr Fehlen kann zu defekten makromolekularen Strukturen führen, was Wachstum und zelluläre Kommunikation beeinträchtigt. Im Menschen verwendet Uridin-5'-Diphosphat (UDP)-Glucose (UDP-Glc)-Dehydrogenase (hUGDH) UDP-Glc zur Produktion von UDP-Glucuronsäure (UDP-GlcUA), welche wiederum als Substrat in der Synthese von UDP-Xylose (UDP-Xyl) durch UDP-Xyl-Synthase (hUXS) fungiert. Die Produkte dieser nicotinamidadenindinukleotid (NAD^+)-abhängigen komplexen mehrstufigen Umwandlungen sind im Aufbau von Proteoglykanen in der extrazellulären Matrix unerlässlich.

Um die Interaktion zwischen hUGDH und einem Thiohemiacetalintermediat zu untersuchen, wurden *in situ* ^{1}H-NMR-Messungen verwendet. Im Fall von hUXS diente eine Kombination aus strukturellen Studien, Analyse des Reaktionsverlaufs und Moleküldynamiksimulationen dazu, die drei Schritte der enzymkatalysierten oxidativen Decarboxylierung aufzuklären. Die Ergebnisse zeigten, dass eine Verformung des Pyranosidrings durch eine hochkonservierte Aminosäuresequenz im aktiven Zentrum von hUXS die Katalyse durch die optimale Orientierung von reaktiven Seitengruppen des Liganden mit dem Enzym fördert und führten zu einem detaillierten mechanistischen Vorschlag für die hUXS-katalysierte Reaktion. Die Bedeutung der Aminosäuresequenzkonservierung in hUXS wurde durch Mutationsstudien, welche Einblicke in Struktur-Funktions-Beziehungen im Enzym gaben, weitererforscht.

Synthetische Wege zu UDP-GlcUA und UDP-Xyl sind trotz deren hoher biologischer Bedeutung kaum vorhanden, weshalb eine enzymatische Redoxkaskadenreaktion mit hUGDH und hUXS zur Herstellung dieser Verbindungen entwickelt wurde. Um eine Inhibierung durch reduziertes NAD^+ zu verhindern und hohe Erträge zu erzielen, war es entscheidend, die biosynthetische Reaktion mit einer dreistufigen chemoenzymatischen Kaskade zur Coenzymregenerierung mittels Xylosereduktase aus *Candida tenuis* und Rinderleberkatalase zu koppeln.

Die Herstellung von ^2H- und ^{13}C-markierter sowie deoxygenierter UDP-GlcUA stellte die Voraussetzung für die nachfolgende Untersuchung von UDP-Apiose (UDP-Api)/UDP-Xyl-Synthase (UAXS) dar. D-Apiose (Api) ist ein nur in Pflanzen vorkommender verzweigter Zucker, der der Quervernetzung verschiedener Polysaccharidketten in Glykokonjugaten in der Zellwand dient. UAXS katalysiert die chemisch interessante Decarboxylierung-Pyranosidringkontraktion von UDP-GlcUA zum Api-Vorläufer UDP-Api. Eine umfassende Untersuchung der enzymatischen Reaktion mithilfe der erzeugten Stoffe ermöglichte, den bemerkenswerten Mechanismus von UAXS zu entschlüsseln und zeigte, wie das Enzym die Pyranosid-zu-Furanosid-Reorganisation des Kohlenstoffgerüsts chemisch realisiert.

Table of contents

Catalytic mechanism of human UDP-glucose 6-dehydrogenase: *in situ* proton NMR studies reveal that the *C*-5 hydrogen of UDP-glucose is not exchanged with bulk water during the enzymatic reaction

Catalytic mechanism of human UDP-glucose 6-dehydrogenase: *in situ* proton NMR studies reveal that the *C*-5 hydrogen of UDP-glucose is not exchanged with bulk water during the enzymatic reaction

Carbohydrate Research 356 (2012) 209–214

Contents lists available at SciVerse ScienceDirect

Carbohydrate Research

journal homepage: www.elsevier.com/locate/carres

Catalytic mechanism of human UDP-glucose 6-dehydrogenase: in situ proton NMR studies reveal that the C-5 hydrogen of UDP-glucose is not exchanged with bulk water during the enzymatic reaction

Thomas Eixelsberger [a], Lothar Brecker [b], Bernd Nidetzky [a,*]

[a] Institute of Biotechnology and Biochemical Engineering, Graz University of Technology, Petersgasse 12/1, A-8010 Graz, Austria
[b] Institute of Organic Chemistry, University of Vienna, Währingerstraße 38, A-1090 Vienna, Austria

ARTICLE INFO

Article history:
Received 1 February 2012
Received in revised form 23 March 2012
Accepted 24 March 2012
Available online 2 April 2012

Keywords:
UDP-glucose dehydrogenase
Thiohemiacetal and thioester intermediates
Catalytic mechanism
Deuterium incorporation
UDP-*gluco*-hexodialdose

ABSTRACT

Human UDP-glucose 6-dehydrogenase (hUGDH) catalyzes the biosynthetic oxidation of UDP-glucose into UDP-glucuronic acid. The catalytic reaction proceeds in two NAD^+-dependent steps via covalent thiohemiacetal and thioester enzyme intermediates. Formation of the thiohemiacetal adduct occurs through attack of Cys^{276} on C-6 of the UDP-*gluco*-hexodialdose produced in the first oxidation step. Because previous studies of the related enzyme from bovine liver had suggested loss of the C-5 hydrogen from UDP-*gluco*-hexodialdose due to keto-enol tautomerism, we examined incorporation of solvent deuterium into product(s) of UDP-glucose oxidation by hUGDH. We used wild-type enzyme and a slow-reacting Glu^{161}→Gln mutant that accumulates the thioester adduct at steady state. In situ proton NMR measurements showed that UDP-glucuronic acid was the sole detectable product of both enzymatic transformations. The product contained no deuterium at C-5 within the detection limit (⩽2%). The results are consistent with the proposed mechanistic idea for hUGDH that incipient UDP-*gluco*-hexodialdose is immediately trapped by thiohemiacetal adduct formation.

UDP-glucuronic acid (UDP-GlcUA) is an important metabolite of cellular physiology. It also serves a role in tissue development, because biosynthesis of extracellular matrix glycosaminoglycans in vertebrates requires UDP-GlcUA as precursor.[1] UDP-GlcUA is derived from UDP-glucose (UDP-Glc) by two-step NAD^+-dependent oxidation of the C-6 alcohol, catalyzed by UDP-glucose 6-dehydrogenase (UGDH).[2] Genes encoding UGDH are present throughout all domains of life. Analysis of UGDH amino acid sequences reveals that enzymes from different lineages clearly share common ancestry.[2] Basic elements of structure and function are therefore conserved among the different UGDHs.[3,4] All known UGDHs fold into oligomers.[2] The homodimeric quaternary structure adopted by bacterial enzymes appears to be the basic unit of UGDH enzyme function.[3,5,6] Enzymes from eukaryotic origin form more complex ring-shaped homohexameric assemblies.[4,7–10] The role of the particular structural architecture of UGDH from higher organisms is not entirely clear, but it could confer certain features of allosteric regulation.[7,8] Residues of the active site are highly conserved among the different UGDHs, with only few exceptions.[2] The catalytic mechanism of UGDH therefore seems to be highly conserved. Enzymatic oxidation of UDP-Glc occurs in three catalytic steps via covalent thiohemiacetal and thioester intermediates, as shown in Scheme 1 and Fig. 1.[3,4,10–16] The proposed basic mechanism of UGDH is well supported by evidence from crystal structures and biochemical data for the wild-type enzyme and relevant mutants thereof.

Mechanistic proposals for UGDH differ in an important detail that is the kinetic significance of the enzyme-bound product of the first oxidation step, namely UDP-*gluco*-hexodialdose.[12,13] Studies of UGDH from different sources concur that not even traces of UDP-*gluco*-hexodialdose are released from the enzyme during the reaction. One possibility considered was that the incipient UDP-*gluco*-hexodialdose is immediately trapped at the active site as a covalent thiohemiacetal adduct (Scheme 1).[4] Hydride transfer oxidation by NAD^+ and nucleophilic addition of the thiolate side chain of cysteine to the reactive C-6 of substrate would therefore take place in a kinetically coupled fashion, effectively reducing the lifetime of any UDP-*gluco*-hexodialdose formed in the reaction. We refer to this mechanism as *concerted* throughout the paper. The mechanistic idea is supported by kinetic data for human UGDH (hUGDH) from this laboratory, demonstrating that enzyme deprotonation, presumably at the active-site cysteine (Cys^{276}), occurs kinetically in parallel with the initial substrate oxidation.[4] Moreover, total disruption of covalent catalysis by Cys^{276} in a Cys→Ala mutant resulted in the massive impairment of already the *first* oxidation step.[4,10] If the cysteine was required only in the *second* oxidation step, one would expect that a Cys→Ala mutant accumulates

* Corresponding author. Tel.: +43 316 873 8400; fax: +43 316 873 8434.
E-mail address: bernd.nidetzky@tugraz.at (B. Nidetzky).

0008-6215 © 2012 Elsevier Ltd. Open access under CC BY-NC-ND license.
http://dx.doi.org/10.1016/j.carres.2012.03.028

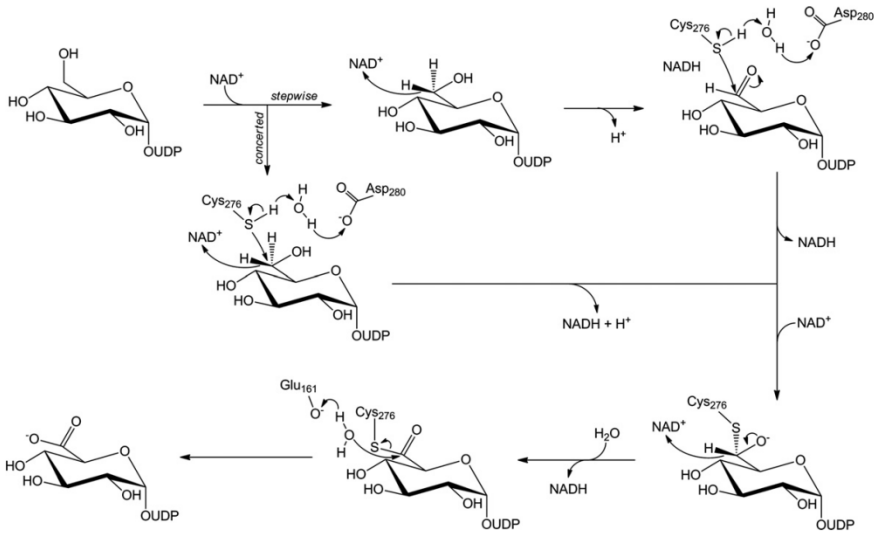

Scheme 1. Proposed course of the catalytic reaction of UGDH. For clarity reasons, only the herein relevant amino acids of the active site of hUGDH are shown. The concerted mechanism would be inconsistent with exchange of the proton at glucosyl C-5 with solvent. The stepwise mechanism *might* allow proton exchange due to accumulation of enzyme-bound UDP-*gluco*-hexodialdose. Unless UDP-*gluco*-hexodialdose was released from the active site (which probably does not happen as shown later), exchange reaction would have to take place at the active site of the enzyme.

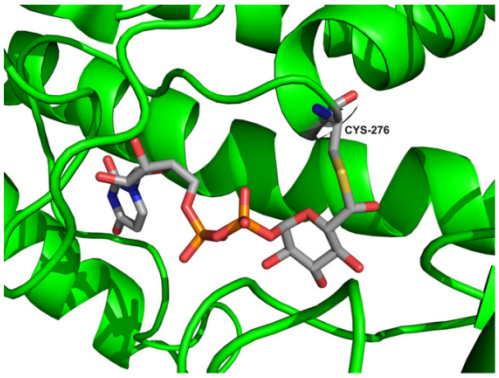

Figure 1. Close-up representation of the active site of E161Q in a trapped thiohemiacetal enzyme intermediate. Cys^{276} is the site of covalent modification. The PDB code of the structure is 3KHU.

a detectable amount of NADH in a pre-steady burst, which results due to the relatively fast conversion of UDP-Glc to UDP-*gluco*-hexodialdose. Even though alcohol oxidation by NAD^+ proceeds thermodynamically uphill, the non-favorable position of the reaction equilibrium would not prevent the formation of the aldehyde product as long as NAD^+ and UDP-Glc are present in excess. Note that aldehyde reductases readily oxidize primary alcohols by NAD^+ or $NADP^+$.[17] It is also relevant that trapping of the UDP-*gluco*-hexodialdose by chemical reduction with $NaBH_4$ proved fruitless unless the active-site cysteine (of bovine liver UGDH) had been inactivated by chemical modification with cyanide.[14]

The alternative possibility is that substrate aldehyde and covalent thiohemiacetal adduct are formed in two sequential kinetic steps (*stepwise mechanism*). Release of UDP-*gluco*-hexodialdose from the enzyme complex with NADH may not be possible due to the (closed) protein conformation adopted at this point of the reaction.[3,4] In support of this mechanistic view, chemically synthesized UDP-*gluco*-hexodialdose was a fairly good substrate for oxidation (with NAD^+) or reduction (with NADH) by UGDH.[12,13,15,18] Working with UGDH from the bacterium *Streptococcus pyogenes*, Tanner and co-workers showed that the wild-type enzyme, but also a mutated variant that had the key cysteine (Cys^{260}) replaced by Ala, catalyzed oxidation and reduction of UDP-*gluco*-hexodialdose.[12] These authors therefore concluded that the cysteine had no catalytic role in the first oxidation step.[12] They also proposed that NADH was released from the enzyme complex with UDP-*gluco*-hexodialdose only after formation of the covalent thiohemiacetal adduct (Scheme 1). In their mechanistic studies of bovine liver UGDH, Feingold and colleagues observed that tritium label from C-5 of UDP-Glc was partly 'washed out' to solvent during the enzymatic reaction.[19] Loss of label (30% of the original tritium) was explained by an enolization of the C-6 aldehyde in UDP-*gluco*-hexodialdose prior to covalent adduct formation (Scheme 2). No exchange of tritium was thought to occur in the thiohemiacetal and thioester intermediates. The proposed keto-enol tautomerism at the UGDH active site requires the C-6 aldehyde to become a rather long-lived intermediate of the enzymatic reaction and therefore, it would be clearly inconsistent with the idea of a strong kinetic coupling between substrate oxidation and thiohemiacetal formation. Utilization of UDP-*gluco*-hexodialdose as substrate for oxidation and reduction, by contrast, could be reconciled with the concerted mechanism, because the observed activities may not reflect exactly the steps that occur in the normal reaction pathway. Using UDP-*galacto*-hexodialdose (prepared from UDP-galactose by oxidation with galactose oxidase) as surrogate of UDP-*gluco*-hexodialdose, the authors demonstrated that the C-5 tritium readily exchanges with the solvent proton in a spontaneous (non-enzymatic) reaction.[19] In contrast, chemically synthesized UDP-*gluco*-hexodialdose forms

Catalytic mechanism of human UDP-glucose 6-dehydrogenase: *in situ* proton NMR studies reveal that the *C*-5 hydrogen of UDP-glucose is not exchanged with bulk water during the enzymatic reaction

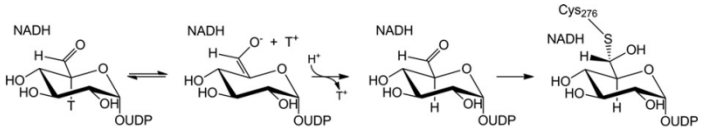

Scheme 2. Enolization and proton exchange at C-5 of UDP-*gluco*-hexodialdose. If the aldehyde enolized prior to covalent intermediate formation, tritium label at C-5 could be replaced by hydrogen through label 'wash-out' to solvent. Similarly, deuterium could be incorporated ('washed in') if the reaction was performed in D_2O.

a hydrate upon contact with water, as shown by Campbell and Tanner.[18] No enolization or C-5 proton exchange was observed in their study.

Considering the mechanistic significance of the problem, and the partially contradictive results published so far, we decided to re-examine in this work the reported hydrogen exchange at C-5 during enzymatic oxidation of UDP-Glc. We took an approach distinct from that of Feingold and co-workers[19] in that we measured incorporation of solvent deuterium by the UDP-GlcUA product. In situ proton NMR spectroscopy was employed to observe the enzymatic transformations in real time. We performed experiments with two forms of hUGDH, the wild-type enzyme and a point mutant that had Glu^{161} replaced by Gln (E161Q). Reason to compare the two enzymes was that each represented a distinct rate-determining step.[4,10] Glu^{161} is the general catalytic base for hydrolysis of the thioester intermediate in the proposed mechanism of hUGDH (Scheme 1). The E161Q mutant is particularly impaired in the hydrolysis step and therefore accumulates the thioester adduct at steady state. The mutant is about 600 times less reactive in terms of turnover number (k_{cat}) than wild-type hUGDH.[10] In the wild-type enzyme at non-saturating concentration of NAD^+ (0.5 mM), the thiohemiacetal intermediate accumulates at a steady state because the overall exchange of NADH by NAD^+ becomes rate limiting.[4] At saturating concentration of NAD^+, none of the different catalytic steps in Scheme 1 appears to be distinctly rate determining in wild-type hUGDH. We considered that if hydrogen/deuterium exchange at C-5 of enzyme-bound UDP-*gluco*-hexodialdose took place at all in hUGDH, we should be able to accumulate sufficient amounts of the relevant intermediate in one of the two enzymes to make the exchange reaction eventually observable in the experiment. We performed in situ NMR experiments at pD 7.5 (wild type) and 8.3 (E161Q), because hUGDH is active and stable under these conditions. The previous work with bovine liver UGDH was done at a higher pH of 8.7.[19] We therefore analyzed deuterium incorporation into the UDP-GlcUA product at different pD values in the range 5.9–8.8, using NMR measurement at a single time point of the reaction.

Figure 2 shows time-resolved proton NMR data recorded for oxidation of UDP-Glc by wild-type hUGDH (panel A) and E161Q (panel B). Results are presented in stack plots of seven selected spectra acquired over a reaction time of 12 h. Some selected signals from the UDP-Glc, UDP-GlcUA and NADH were assigned according to the literature and allow unambiguous identification of the reaction products. No intermediate UDP-*gluco*-hexodialdose was observed within detection limit, as expected. The presumed stoichiometry of the enzymatic transformation that two NADH and one UDP-GlcUA are produced for each UDP-Glc oxidized was confirmed in a quantitative analysis of the NMR data, as shown in Figure 3 (panels A and C). The rather low conversion of UDP-Glc observed in our experiments can be explained by a large solvent isotope effect on k_{cat} for the respective enzyme used, resulting in a fourfold decreased reaction rate in D_2O as compared to the corresponding reaction rate in water under the conditions applied. This large solvent isotope effect could deserve further attention in future mechanistic studies of hUGDH. The intrinsical low activity of E161Q combines with the isotope effect on k_{cat} to give a very low overall activity of the mutant in the experiment. Substrate conversion did not exceed 20% after extended incubation times. However, it was sufficient to characterize the stoichiometry of the reaction and to determine the relevant proton signals in the UDP-GlcUA product. No UDP-*gluco*-hexodialdose was detectable in the reaction of E161Q.

The ^1H NMR signal of proton H-4 in resulting UDP-GlcUA appears at 3.50 ppm. Although it is slightly overlapped (Fig. 2A), its doublet of doublet structure is well detectable and the $^3J_{H\text{-}H}$ coupling constants can be determined to be 10.2 Hz and 9.2 Hz, respectively. Such quite large couplings indicate H-4 as well as both neighbored protons H-3 and H-5 to be in axial positions. The H-5 is hence not exchanged by deuterium. Furthermore, no additional signal of H-4 with one $^3J_{H\text{-}H}$ to H-3 and a $^3J_{H\text{-}D}$ to H-5 can be detected. The concomitant slight isotope shift would cause such signal to be in the spectral region of ±0.015 ppm around that of H-4 in the fully protonated UDP-GlcUA. This region is not overlapped by signals of further protons and hence allows a detection even of small amounts of byproducts. The absence of such signal can hence be used to exclude possible H/D exchange in an extent of more than 1%, which is the detection limit.

We analyzed the development of signal intensity of selected protons from UDP-GlcUA (H-1, H-4, H-5) in dependence of the incubation time. The results are summarized in Figure 3 for the reaction of wild-type UGDH (panel B) and E161Q (panel D). There was no loss of H-5 signal within error limit of 2%, which also indicates that exchange with the solvent had not occurred. Additionally, we tested the effect of lowering the concentration of NAD^+ from 15 mM, which is completely saturating, to just 0.5 mM, which is limiting at the steady state, on H-5 signal evolution in product. It was shown in recent work that at 0.5 mM NAD^+ the overall oxidation of thiohemiacetal intermediate becomes rate determining.[4] We considered that under the conditions of limiting NAD^+ the proton exchange reaction might therefore be favored. The reaction was performed for that reason directly in the NMR tube and NAD^+ was supplemented in regular intervals to promote the conversion. NMR data showed that H-5 signal intensity was not affected as compared to reference proton signals.

We also examined the effect of pH on the protonation state of C-5 in UDP-GlcUA. Reactions were performed in D_2O at pD 5.9, 7.0, 7.9, and 8.8. Conversion of UDP-Glc substrate increased in response to a raise of pD, as one might expect from the known pH dependencies of k_{cat} for wild-type enzyme and E161Q (Fig. 4). Both enzymes show optimum activity at pH 8 or higher.[4,10] Under each of the conditions used, neither enzymatic transformation went along with a relative decrease in H-5 signal. We therefore conclude that incorporation of solvent deuterium at C-5 did not take place in the course of reactions catalyzed by wild-type enzyme and E161Q.

In summary, evidence from this work does not support the mechanistic proposal for UGDH (Scheme 2) that the UDP-*gluco*-hexodialdose intermediate of the enzymatic reaction partly exchanges its proton at C-5 with bulk solvent due to keto-enol tautomerism. The original observation made with bovine liver UGDH that tritium label at C-5 of UDP-Glc was partly washed out during reaction[19] was re-examined using an alternative, equally diagnostic approach in which deuterium uptake from

Catalytic mechanism of human UDP-glucose 6-dehydrogenase: *in situ* proton NMR studies reveal that the *C*-5 hydrogen of UDP-glucose is not exchanged with bulk water during the enzymatic reaction

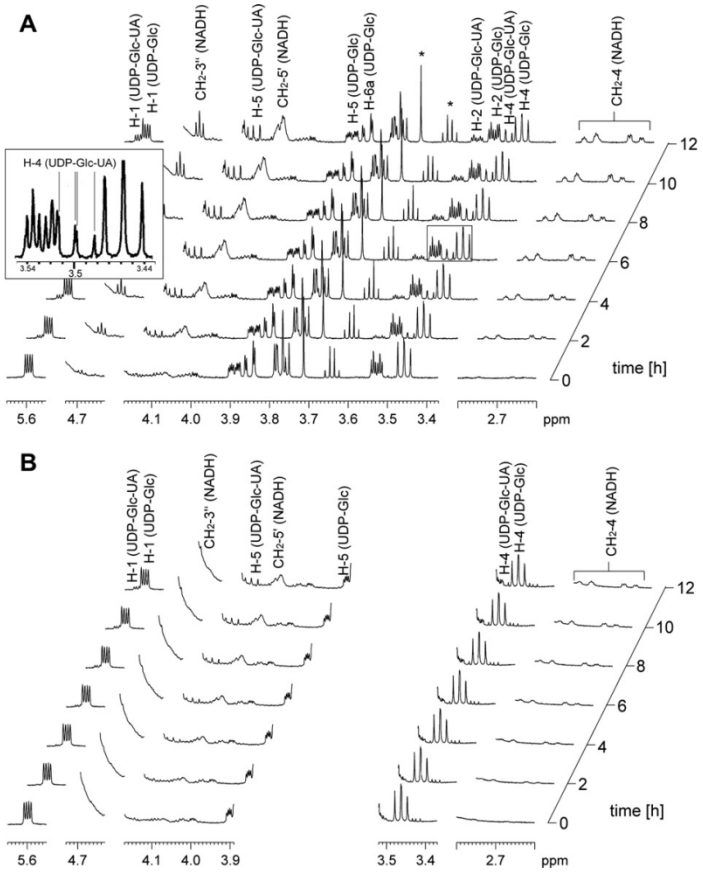

Figure 2. In situ NMR spectroscopic measurement of hUGDH catalyzed oxidation of UDP-Glc to UDP-GlcUA. The data are presented as stack plot of seven selected spectra in regular intervals of 2 h. Indicative signals of NADH, UDP-Glc, and UDP-Glc-UA are marked and assigned according to literature.[24] Signals of impurities (TRIS from enzyme preparations, ethanol from commercial NAD^+) are indicated with asterisks. No signals indicating presence of UDP-*gluco*-hexodialdose could be detected. Panels A and B show the reaction of wild-type hUGDH and E161Q, respectively. The spectral region from 3.89 ppm to 3.52 ppm is not shown in panel B due to presence of larger signals from impurities (glycerol). In panel A, the area of the spectrum showing the ^{1}H NMR signal of proton H-4 in UDP-GlcUA is also presented enlarged in a box.

solvent was measured. Instead of the bovine liver enzyme, the structurally and mechanistically well-characterized hUGDH, both in wild-type and Glu^{161}→Gln mutated form, was used. There was no deuterium incorporation, measured as relative H-5 signal loss, under a range of conditions (pH, NAD^+ concentration) that were chosen to involve change in rate-determining step of the enzymatic reaction. Our observations are therefore consistent with the idea of a concerted mechanism for the human enzyme (Scheme 1) that precludes proton exchange with solvent. They are however also consistent with a sequential mechanism in which the intermediary UDP-*gluco*-hexodialdose is sequestered at the binding site of the enzyme so that exchange with bulk solvent is prevented effectively. We note however that protons are released from the active site of hUGDH in the course of the first oxidation step, suggesting that there exists probably connection between the catalytic center and solvent during the reaction.[4] We also note that chemically, hydration of C-6 aldehyde might be a more likely outcome of contact of UDP-*gluco*-hexodialdose with water than fast enolization at around neutral pH. It is difficult to envision mechanistic differences between hUGDH and the enzyme from bovine liver that would reconcile the conflicting findings from deuterium incorporation and tritium 'wash out' experiments. Accumulation of UDP-*gluco*-hexodialdose as enzyme-bound intermediate in bovine liver UGDH is a possibility. This would be not consistent however with the proposed kinetic mechanism of the enzyme having thioester hydrolysis as the rate determining step.[20]

1. Experimental

1.1. Materials

UDP-Glc (sodium salt) was purchased at Carbosynth. UDP-GlcUA (ammonium salt; >98% purity), and NAD^+ (sodium salt; 98% purity) were obtained from Sigma–Aldrich.

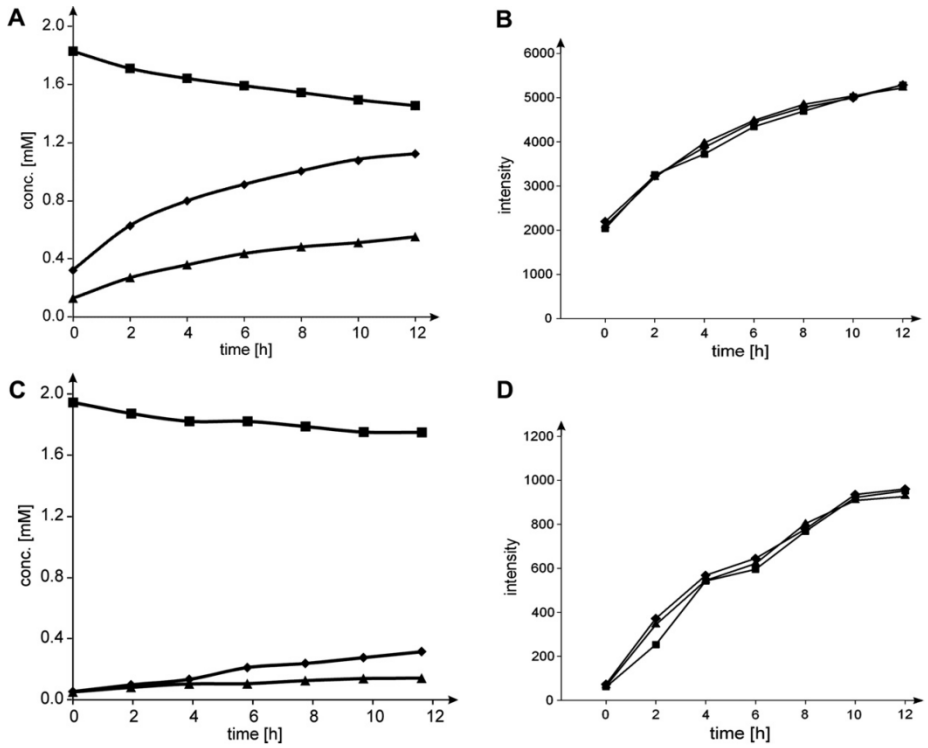

Figure 3. Time courses of enzymatic oxidations of UDP-Glc, and determination of the associated change of relative H-5 signal intensity in UDP-GlcUA product. Time courses are shown in panels A (wild-type) and C (E161Q), the symbols used are square (UDP-Glc), triangle (UDP-GlcUA), and diamond (NADH). The low conversion can be explained by a large solvent isotope effect on k_{cat} (see text). Two equivalents of NADH are formed per equivalent UDP-Glc utilized, as expected. Proton signal intensities in UDP-GlcUA are shown in panels B and D (square: H-1; triangle H-4; diamond: H-5) for reactions with wild-type enzyme and E161Q mutant, respectively. In case of deuterium incorporation at C-5, one would see a decrease of the respective proton signal compared to H-1 and H-4.

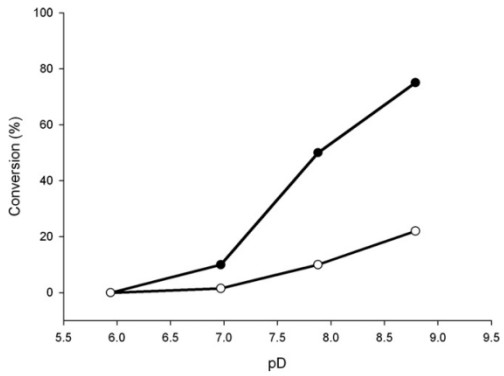

Figure 4. pH dependence of conversion of UDP-Glc by wild-type hUGDH and E161Q mutant. The symbols are filled circle (wild-type enzyme) and empty circle (mutant). The reaction time was 16 h at 25 °C.

1.2. Enzymes

Purified preparations of wild-type hUGDH and E161Q mutant were obtained using reported procedures.[4,10] Briefly, overexpression of the coding genes was done in *Escherichia coli* BL21(DE3)-R3. Both enzymes were produced as fusion proteins containing an N-terminal extension, which comprised a solubility enhancement tag, a streptavidin tag, and a tobacco etch virus protease cleavage site. Cell extracts were first purified by affinity chromatography. The N-terminal extension was then removed, and the enzymes were further purified by gel filtration and anion-exchange chromatography. Full details of the purification protocol are given elsewhere.[4,10]

1.3. Assays

Enzymatic assays were performed in 1 mL of D_2O. A 50 mM potassium phosphate buffer at pD 5.9, 7.0, 7.9 or 8.8 was used. The pD was determined as meter reading +0.4. Starting concentrations were 15 mM NAD^+, 2 mM UDP-Glc and 0.38 μM wild-type hUGDH or 15 μM E161Q. After addition of all components, the reactions were incubated at 25 °C for 16 h.

For determination of the solvent isotope effect, enzymatic conversions in H_2O or D_2O were performed in a Beckman Coulter

DU800 spectrophotometer using a 50 mM potassium phosphate buffer with pH/pD 7.5. Reaction velocity was measured by NADH absorption (λ = 340 nm).

1.4. In situ proton NMR spectroscopy

All spectra were recorded on a Bruker DRX-600 AVANCE spectrometer (Bruker, Rheinstetten, Germany) at 600.13 MHz (^{1}H). The ^{1}H NMR spectra were measured at 298.2 K with presaturation (1.0 s) and acquisition of 32k data points. After zero filling to 64k data points, spectra were performed with a range of 7200 Hz. Chemical shifts were referenced to external acetone (δ_H = 2.225 ppm). The reactions were directly made in a 5 mm high precision NMR sample tube (Promochem, Wesel, Germany) to measure in situ ^{1}H NMR spectra. Samples contained 2 mM UDP-Glc, 15 mM NAD^+, and 0.084 μM wild-type hUGDH or 33 μM E161Q, as well as 50 mM potassium phosphate buffer in D_2O (0.70 mL, 99.9% D, pD 7.5 or 8.3).[21,22] Reaction progress was monitored in situ over ca. 12 h in the magnet by recording up to 64 ^{1}H NMR spectra in regular intervals.[23]

1.5. Data analysis

The Topspin 3.0 software from Bruker was used for processing the NMR spectra after data acquisition. For quantitative analysis of the NMR data, a correction value was subtracted from the integral values of each proton to account for background noise.

Acknowledgement

Financial support from the Austrian Science Fund FWF (Project DK Molecular Enzymology W901-B05) is gratefully acknowledged.

References

1. Clarkin, C. E.; Allen, S.; Kuiper, N. J.; Wheeler, B. T.; Wheeler-Jones, C. P.; Pitsillides, A. A. *J. Cell. Physiol.* **2011**, *226*, 749–761.
2. Egger, S.; Chaikuad, A.; Kavanagh, K. L.; Oppermann, U.; Nidetzky, B. *Biochem. Soc. Trans.* **2010**, *38*, 1378–1385.
3. Campbell, R. E.; Mosimann, S. C.; van De Rijn, I.; Tanner, M. E.; Strynadka, N. C. *Biochemistry* **2000**, *39*, 7012–7023.
4. Egger, S.; Chaikuad, A.; Kavanagh, K. L.; Oppermann, U.; Nidetzky, B. *J. Biol. Chem.* **2011**, *286*, 23877–23887.
5. Rocha, J.; Popescu, A. O.; Borges, P.; Mil-Homens, D.; Moreira, L. M.; Sá-Correia, I.; Fialho, A. M.; Frazão, C. *J. Bacteriol.* **2011**, *193*, 3978–3987.
6. Chen, Y. Y.; Ko, T. P.; Lin, C. H.; Chen, W. H.; Wang, A. H. *J. Struct. Biol.* **2011**, *175*, 300–310.
7. Kadirvelraj, R.; Sennett, N. C.; Polizzi, S. J.; Weitzel, S.; Wood, Z. A. *Biochemistry* **2011**, *50*, 5780–5789.
8. Sennett, N. C.; Kadirvelraj, R.; Wood, Z. A. *Biochemistry* **2011**, *50*, 9651–9663.
9. Rajakannan, V.; Lee, H. S.; Chong, S. H.; Ryu, H. B.; Bae, J. Y.; Whang, E. Y.; Huh, J. W.; Cho, S. W.; Kang, L. W.; Choe, H.; Robinson, R. C. *PLoS One* **2011**, *6*, e25226.
10. Egger, S.; Chaikuad, A.; Klimacek, M.; Kavanagh, K. L.; Oppermann, U.; Nidetzky, B. *J. Biol. Chem.* **2012**, *287*, 2119–2129.
11. Ge, X.; Campbell, R. E.; van de Rijn, I.; Tanner, M. E. *J. Am. Chem. Soc.* **1998**, *120*, 6613–6614.
12. Ge, X.; Penney, L. C.; van de Rijn, I.; Tanner, M. E. *Eur. J. Biochem.* **2004**, *271*, 14–22.
13. Ridley, W. P.; Houchins, J. P.; Kirkwood, S. *J. Biol. Chem.* **1975**, *250*, 8761–8767.
14. Ordman, A. B.; Kirkwood, S. *J. Biol. Chem.* **1977**, *252*, 1320–1326.
15. Nelsestuen, G. L.; Kirkwood, S. *J. Biol. Chem.* **1971**, *246*, 3824–3834.
16. Schiller, J. G.; Bowser, A. M.; Feingold, D. S. *Carbohydr. Res.* **1972**, *21*, 249–253.
17. Pival, S. L.; Klimacek, M.; Kratzer, R.; Nidetzky, B. *FEBS Lett.* **2008**, *582*, 4095–4099.
18. Campbell, R. E.; Tanner, M. E. *Angew. Chem., Int. Ed.* **1997**, *36*, 1520–1522.
19. Prihar, H. S.; Feingold, D. S. *FEBS Lett.* **1979**, *99*, 106–108.
20. Ordman, A. B.; Kirkwood, S. *Biochim. Biophys. Acta* **1977**, *481*, 25–32.
21. Mussini, P. R.; Mussini, T.; Rondinini, S. *Pure Appl. Chem.* **1997**, *69*, 1007–1014.
22. Luo, D. *Huaxue Shijie* **1985**, *26*, 24–26.
23. Brecker, L.; Ribbons, D. W. *Trends Biotechnol.* **2000**, *18*, 197–202.
24. Gu, X.; Glushka, J.; Yin, Y.; Xu, Y.; Denny, T.; Smith, J.; Jiang, Y.; Bar-Peled, M. *J. Biol. Chem.* **2010**, *295*, 9030–9040.

Structure and mechanism of human UDP-xylose synthase: evidence for a promoting role of sugar ring distortion in a three-step catalytic conversion of UDP-glucuronic acid

Enzymology:

Structure and Mechanism of Human UDP-xylose Synthase: EVIDENCE FOR A PROMOTING ROLE OF SUGAR RING DISTORTION IN A THREE-STEP CATALYTIC CONVERSION OF UDP-GLUCURONIC ACID

Thomas Eixelsberger, Sabine Sykora, Sigrid Egger, Michael Brunsteiner, Kathryn L. Kavanagh, Udo Oppermann, Lothar Brecker and Bernd Nidetzky

J. Biol. Chem. 2012, 287:31349-31358.
doi: 10.1074/jbc.M112.386706 originally published online July 18, 2012

Structure and mechanism of human UDP-xylose synthase: evidence for a promoting role of sugar ring distortion in a three-step catalytic conversion of UDP-glucuronic acid

⌘ *Author's Choice*

THE JOURNAL OF BIOLOGICAL CHEMISTRY VOL. 287, NO. 37, pp. 31349–31358, September 7, 2012

Structure and Mechanism of Human UDP-xylose Synthase

EVIDENCE FOR A PROMOTING ROLE OF SUGAR RING DISTORTION IN A THREE-STEP CATALYTIC CONVERSION OF UDP-GLUCURONIC ACID[*][S]

Received for publication, May 30, 2012, and in revised form, July 17, 2012 Published, JBC Papers in Press, July 18, 2012, DOI 10.1074/jbc.M112.386706

Thomas Eixelsberger[‡1], **Sabine Sykora**[‡1], **Sigrid Egger**[‡§¶], **Michael Brunsteiner**[‡‖], **Kathryn L. Kavanagh**[§], **Udo Oppermann**[§**], **Lothar Brecker**[‡‡], **and Bernd Nidetzky**[‡¶‖2]

From the [‡]*Institute of Biotechnology and Biochemical Engineering, Graz University of Technology, A-8010 Graz, Austria, the* [§]*Structural Genomics Consortium, University of Oxford, Oxford OX3 7DQ, United Kingdom, the* [¶]*Austrian Centre of Industrial Biotechnology (ACIB), A-8010 Graz, Austria, the* [‖]*Research Center Pharmaceutical Engineering (RCPE), A-8010 Graz, Austria, the* [**]*Botnar Research Centre, NIHR Oxford Biomedical Research Unit, University of Oxford, Oxford OX3 7LD, United Kingdom, and the* [‡‡]*Institute of Organic Chemistry, University of Vienna, A-1090 Vienna, Austria*

Background: Human UDP-xylose synthase (hUXS1) is responsible for conversion of UDP-glucuronic acid to UDP-xylose.
Results: Crystal structure, molecular dynamics simulations, and reaction course analysis give conclusive insight into the enzymatic mechanism in three catalytic steps.
Conclusion: Distortion of sugar pyranose ring in bound substrate facilitates enzymatic reaction.
Significance: A detailed mechanism for catalysis by hUXS1 is proposed.

UDP-xylose synthase (UXS) catalyzes decarboxylation of UDP-D-glucuronic acid to UDP-xylose. In mammals, UDP-xylose serves to initiate glycosaminoglycan synthesis on the protein core of extracellular matrix proteoglycans. Lack of UXS activity leads to a defective extracellular matrix, resulting in strong interference with cell signaling pathways. We present comprehensive structural and mechanistic characterization of the human form of UXS. The 1.26-Å crystal structure of the enzyme bound with NAD^+ and UDP reveals a homodimeric short-chain dehydrogenase/reductase (SDR), belonging to the NDP-sugar epimerases/dehydratases subclass. We show that enzymatic reaction proceeds in three chemical steps via UDP-4-keto-D-glucuronic acid and UDP-4-keto-pentose intermediates. Molecular dynamics simulations reveal that the D-glucuronyl ring accommodated by UXS features a marked $^4C_1$ *chair* to $B_{O,3}$ *boat* distortion that facilitates catalysis in two different ways. It promotes oxidation at C_4 (step 1) by aligning the enzymatic base Tyr^{147} with the reactive substrate hydroxyl and it brings the carboxylate group at C_5 into an almost fully axial position, ideal for decarboxylation of UDP-4-keto-D-glucuronic acid in the second chemical step. The protonated side chain of Tyr^{147} stabilizes the enolate of decarboxylated C_4 keto species ($^2H_1$ *half-chair*) that is then protonated from the *Si* face at C_5, involving water coordinated by Glu^{120}. Arg^{277}, which is positioned by a salt-link interaction with Glu^{120}, closes up the catalytic site and prevents release of the UDP-4-keto-pentose and NADH intermediates. Hydrogenation of the C_4 keto group by NADH, assisted by Tyr^{147} as catalytic proton donor, yields UDP-xylose adopting the relaxed $^4C_1$ *chair* conformation (step 3).

Proteoglycans are complex assemblies between proteins and linear glycosaminoglycan polysaccharides such as heparan sulfate and chondroitin sulfate (1). They are found in all connective tissues of vertebrates, and on the surfaces of many cell types as components of the extracellular matrix or the glycocalix (1–3). Due to hydration of their glycosaminoglycan chains, proteoglycans impart hydrostatic and elastic properties to the extracellular matrix. As receptors, proteoglycans are critically involved in cell signaling, with consequent effects on tissue development in health or disease (*e.g.* cancer) (1–6). Association between glycosaminoglycan molecules and the protein core of the proteoglycan usually involves enzymatic transfer of a xylosyl residue from UDP-xylose to a protein serine (7). Covalent attachment of the xylosyl group is the first step in generating a functional tetrasaccharide linker on which glycosaminoglycan chain elongation takes place. The UDP-xylose precursor is derived from UDP-glucuronic acid through complex oxidoreductive decarboxylation catalyzed by UDP-xylose synthase (UXS; EC 4.1.1.35; other names: UDP-glucuronic acid decarboxylase; UDP-glucuronic acid carboxylyase) (8, 9). Adequate supply of UDP-xylose was shown in zebrafish to be essential for functional deposition of proteoglycans in the extracellular matrix (10). Defects in production and organization of the extracellular matrix resulting from insufficient UXS[3] activity were correlated with alterations in cell signaling pathways, mirrored in the impaired morphogenesis of various tissues, including the bone. The central and universal biological importance of UXS in vertebrates, including mammals, therefore raises considerable interest in structural and functional properties of

* This work was supported by the Austrian Science Fund DK Molecular Enzymology Grant W901-B05 and the SGC. The SGC is a registered charity (number 1097737) that receives funds from multiple sources.
⌘ *Author's Choice*—Final version full access.
[S] This article contains supplemental "Methods" and Figs. S1–S5.
[1] Both authors contributed equally to this work.
[2] To whom correspondence should be addressed: Institute of Biotechnology and Biochemical Engineering, Graz University of Technology, Petersgasse 12/I, 8010 Graz, Austria. Tel.: 43-316-873-8400; Fax: 43-316-873-108400; E-mail: bernd.nidetzky@tugraz.at.

[3] The abbreviations used are: UXS, UDP-xylose synthase; UDP-GlcUA, UDP-glucuronic acid; hUXS1, human form of UXS; SeMet, selenomethionine; SDR, short-chain dehydrogenase/reductase; MD, molecular dynamics.

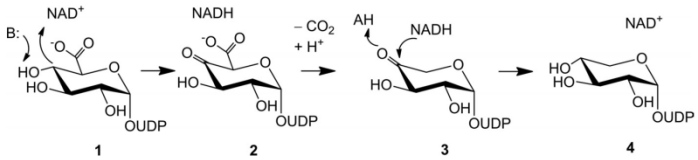

SCHEME 1. **Proposed course of the UXS-catalyzed reaction.** See text for further explanations.

the enzyme. In this work, we present a comprehensive characterization of the human form of UXS (hUXS1) that involved determination of a crystal structure at 1.26-Å resolution.

Phylogenetic analysis reveals that UXS is one of the most strongly conserved nonmitochondrial proteins in nature, with about 57% sequence identity shared between hUXS1 and various bacterial enzyme forms (10). The physiological involvement of UXS differs across the three domains of life, and besides the above described synthesis of protein-linked glycosaminoglycans (7), it also includes the formation of xylose-containing polysaccharides in plants (11) and microorganisms (12–15). Even though UXS activity has been reported in various organisms and cell types, there have only been a few studies of the isolated enzyme. Working with UXS from wheat germ and the fungus *Cryptococcus laurentii*, Feingold and colleagues (16) have developed an ingenious chemical proposal that is shown in Scheme 1. The reaction catalyzed by UXS starts with oxidation of the C_4 alcohol in UDP-glucuronic acid by enzyme-bound NAD^+. The resulting UDP-4-keto-glucuronic acid undergoes decarboxylation, followed by protonation to yield UDP-4-keto-pentose. Keto group reduction by the NADH still bound to the enzyme occurs with retention of the original stereochemistry at C_4, giving UDP-xylose as product. A recent NMR study of a bacterial UXS ortholog appears consistent with the proposed reaction course (17). These insights into the enzymatic transformation notwithstanding, the catalytic mechanism of UXS is fundamentally unknown. The mechanism merits a detailed investigation as it is both biologically very important and chemically intriguing (18–19).

Based on similarity at the primary structure level, hUXS1 is classified in the short-chain dehydrogenase/reductase (SDR) superfamily of proteins (20). hUXS1 is most closely related to the divergent group of so-called "extended SDRs" that include nucleotide-sugar epimerization and dehydration as their main activities (for reviews on enzyme mechanisms, see Refs. 18, 19, 21, and 22). Sequence alignment (supplemental Fig. S1) suggests that hUXS1 is equipped with the canonical SDR active site in which a highly conserved triad of residues (Thr^{118}, Tyr^{147}, Lys^{151}) is probably involved in catalytic oxidoreduction. However, there are also variable features (*e.g.* Glu^{120}, Arg^{277}) that could have a decisive role in the enzymatic conversion. Herein we report on results of structure determination, molecular dynamics (MD) simulation, and reaction course analysis for wild-type and mutated forms of hUXS1, which in combination give conclusive evidence on the enzyme mechanism, delineating how individual active site residues assist the reaction in each of its three catalytic steps. A significant feature of the mechanism is that the catalytic reaction course is underpinned by promoting conformational changes in the pyranose ring structure of the UDP-sugar substrate/intermediate. We have identified the protein residues responsible for the sugar ring distortion and clarified their role in catalysis.

EXPERIMENTAL PROCEDURES

Materials—Unless stated otherwise, all materials were of highest purity available from Roth (Karlsruhe, Germany). UDP-glucuronic acid (>98% purity) was obtained from Sigma and UDP-xylose (>95% purity) from Carbosynth (Compton, UK). D_2O (99.8% D) was purchased from ARMAR Chemicals (Döttingen, Switzerland).

Protein Preparation—We used a truncated form of hUXS1 (residues 85–402) that was optimized for crystallization. The construct was designed to encompass the entire Rossmann-fold and ordered regions at the C terminus. Regions predicted to encode a signal peptide and transmembrane helix were deleted from the N terminus, whereas a predicted random coil was deleted from the C terminus. The final construct contained a 23-amino acid long N-terminal peptide comprising the His_6 tag. We refer to this construct throughout when hUXS1 is mentioned. Experimental procedures used for recombinant protein preparation are described in full detail in the supplemental "Methods". Briefly, the enzyme was overexpressed in *Escherichia coli* Rosetta 2(DE3) using the pET-derived expression vector p11 (wild-type) or the pNIC28-Bsa4 plasmid (mutants). After high-pressure cell disruption (1500 psi), the enzyme was isolated from the crude extract using a Cu^{2+}-loaded IMAC-Sepharose High Performance column (GE Healthcare). Stepwise elution with imidazole was employed to yield highly pure hUXS1 (checked by SDS-PAGE). Imidazole was removed by buffer exchange to 50 mM Tris/HCl (pH 7.5) containing 5% glycerol and 1 mM DTT using a NAP-25 desalting column (GE Healthcare) or Vivaspin-20 centrifugal concentrator (Sartorius Stedim, Göttingen, Germany). Preparations of hUXS1 were stored at −70 °C. For crystallization experiments, SeMet-labeled enzyme was produced in *E. coli* B834(DE3) grown on SelenoMethionine Medium Base plus Nutrient Mix containing SeMet at 40 mg/liter (Molecular Dimensions, Newmarket, UK). Site-directed mutagenesis was performed using standard protocols. Mutants purified similarly as the wild-type enzyme.

Crystallization, Data Collection, and Refinement—SeMet-labeled hUXS1 containing 5 mM NAD^+ and 5 mM UDP was concentrated to 12 mg/ml (~0.3 mM). Crystals were obtained by vapor diffusion at 20 °C in 150-nl sitting drops, equilibrated against mother liquor containing 20% PEG 6000, 10% ethylene glycol, and 0.2 M NaCl in 0.1 M HEPES (pH 7). Diffraction data to 1.2 Å were collected at 100 K at the Swiss Light Source station X10SA using a MARMOSAIC 225 mm CCD detector at a single wavelength near the selenium absorption edge (λ = 0.9795 Å).

Data were indexed and integrated in MOSFLM (23) and scaled in SCALA (23). Merging of the data and analysis of systematic absences identified the space group as P121, with the following cell dimensions: a = 46 Å, b = 45 Å, c = 85 Å; α = 90°, β = 97°, γ = 90°. The program SHELXD (24) located 11 SeMet residues in hUXS1, indicating complete labeling of the protein. SHELXE was used for phasing and automated chain tracing was done with ARP/wARP. The hUXS1 structure was manually rebuilt in COOT (25), and restrained refinement was performed using REFMAC5 (26). When electron density showed the presence of NAD^+ and UDP in the active site as well as an additional UDP forming a crystal contact, the ligands were fitted to the density and included in the refinement. Although the full range of data to 1.2 Å was used in refinement, analysis of data completeness and signal to noise suggests that 1.26 Å is a more reasonable estimate of the resolution of the model. Data collection and refinement statistics are summarized in Table 1.

Molecular Dynamics Simulation—All MD simulations were performed using Gromacs (27). For the protein and water a variation of the Amber99sb (28) and the TIP3P (29) force fields was used. For NAD, substrate, intermediates, and product General Amber Force Field (GAFF) parameters (30) and Gromacs input files were generated using the Amber Antechamber suite of programs (31) together with the perl script amb2gmx (32). As starting structure for MD simulations the crystal structure of UXS (PDB code 2B69) was used, approximate pK_a values of ionizable residues were established using PROPKA (33), and ionizable residues were protonated accordingly. For the MD simulations the protein with substrate, product, or intermediates was positioned in the center of a cubic box with 6.7-nm side length and solvated in ~8,000 water molecules. The appropriate number of water molecules was replaced by sodium ions to neutralize the system. A leapfrog algorithm with a time step of 2 fs was used for integrating the equations of motion. The temperature was kept constant at 300 K using a Nosé-Hoover thermostat (34). Electrostatic long range interactions were accounted for using a particle mesh Ewald algorithm (35). A cut-off of 10 Å was used for the real space part of the Ewald summation and the van der Waals interactions. A constant pressure of 1 atm was maintained using a Berendsen thermostat (36). All bonds including hydrogens were constrained using a LINCS algorithm (37). Conformations were saved every 2 ps. The MD simulations covered a time between 4 and 6 ns. In each case the trajectories covering the last 2 ns were used to calculate hydrogen bonding and average structures. For visual inspection of trajectories and conformations Chimera was used. The trajectories were analyzed with various Gromacs tools and in-house scripts.

Analysis of the Enzymatic Reaction Course—Reactions were performed at 25 °C in 50 mM Tris/HCl buffer (pH 7.5). Substrate and enzyme concentrations as well as reaction times differed depending on the specific experimental setup and are therefore mentioned individually. Reactions were stopped by addition of acetonitrile in a 1:1 volume ratio to buffer. Precipitated protein was removed by centrifugation (10 min, 4 °C, 16,000 × g). Samples were analyzed with a reversed phase HPLC (see supplemental "Methods"). It was shown that consumption of UDP-GlcUA proceeded linearly in dependence of reaction time, so that measurements were suitable for calculation of initial rates. Data for kinetic analysis were obtained under conditions in which the concentration of NAD^+ or UDP-GlcUA was varied, whereas the concentration of the respective other substrate was constant (wild-type, 0.5 mM NAD^+ and 2 mM UDP-GlcUA; mutants, 10 mM NAD^+ and 10 mM UDP-GlcUA). V_{max} values were derived from nonlinear fits of the Michaelis-Menten equation. The molarity of enzyme active sites (E) was calculated from the protein concentration, assuming a molecular mass of 38,595 Da for the protein subunit. It was used to determine the turnover number, using the relationship $k_{cat} = V_{max}/E$. Experiments were performed in triplicate (S.D. ≤ 15%).

Transient Kinetic Studies—Experiments were performed at 25 °C with an Applied Photophysics (Leatherhead, UK) model SX.18 MV Stopped-flow Spectrometer. Enzyme was used in a limiting concentration (≤25 μM). A 50 mM Tris/HCl buffer (pH 7.5) was used. Enzyme solution was mixed in 1:1 ratio with substrate solution, yielding concentrations of 0.5 mM NAD^+ and 10 mM UDP-GlcUA, unless stated otherwise. The absorbance of enzyme-bound NADH was measured at 340 nm and converted to concentration using an extinction coefficient of 6,220 M^{-1} cm^{-1}. The stopped-flow instrument had a dead-time of 1.5 ms, and data were recorded up to 1,000 s. Slow reactions catalyzed by hUXS1 mutants were followed additionally in a conventional UV/visible spectrophotometer (Beckman Coulter DU 800), measuring the change in absorbance at 340 nm.

Solvent Kinetic Isotope Effect—For examination of the solvent kinetic isotope effect, a 20 mM potassium phosphate buffer (pH/pD 7.5) in H_2O or D_2O was prepared. The pD was determined as pH meter reading plus 0.4 (38). Concentrations of 10 mM UDP-GlcUA, 0.5 (wild type) or 1 (E120A) mM NAD^+, and 15 (wild type) or 36 (E120A) μM enzyme were used. Enzymes were gel-filtered three times employing deuterated phosphate buffer and equilibrated with solvent prior to the experiments in D_2O. Reactions were stopped after 8 min (wild-type) or 50 min (E120A) by addition of acetonitrile in 1:1 ratio and samples were analyzed on the HPLC. Solvent isotope effects were calculated from the ratio of k_{cat} values measured in H_2O and D_2O.

In Situ NMR Analysis—Enzymatic reactions were performed directly in a 5-mm high precision NMR sample tube (Promochem, Wesel, Germany) and monitored *in situ* over 12 h in the magnet, by recording up to 64 ^1H NMR spectra in regular intervals. For further measurements, samples were kept in a temperature-controlled water bath (30 °C) and measured in unsteady intervals over ~48 h. All spectra were obtained with a Bruker DRX-600 AVANCE spectrometer (Bruker, Rheinstetten, Germany) at 600.13 MHz (^1H) using the Bruker Topspin 1.3 software. Chemical shifts were referenced to external acetone (δH 2.225 ppm). Further details are provided under supplemental "Methods".

Other Methods—Force field tests, nondenaturing anionic PAGE, and HPLC analysis are described in supplemental "Methods" and Fig. S5.

RESULTS AND DISCUSSION

High-resolution Crystal Structure of hUXS1—We solved the crystal structure of hUXS1 in complex with NAD^+ and UDP to

Structure and mechanism of human UDP-xylose synthase: evidence for a promoting role of sugar ring distortion in a three-step catalytic conversion of UDP-glucuronic acid

TABLE 1
Crystallographic data collection and refinement statistics

Enzyme complex	hUXS1-UDP-NAD$^+$
PDB accession code	2B69
Synchrotron beamline	SLS, X10SA
Wavelength (Å)	0.9795
Space group	P121
Unit cell dimensions	$a = 46, b = 45, c = 85$ Å
	$\alpha = \gamma = 90.0°$
	$\beta = 97°$
Resolution range[a] (Å)	42–1.20 (1.26–1.20)
No. unique reflections[a]	93023 (8576)
Completeness[a] (%)	91.3 (58.1)
Mean I/sdI $\langle I/\sigma(I)\rangle$[a]	25.2 (1.3)
R_{merge}[a] (%)	6.5 (53.7)
Redundancy[a]	2.1 (1.3)
Refinement	
No. atoms P/L/O[b]	2439/94/353
R_{work}/R_{free} (%)	13.4/16.2
R.m.s. deviation bond length[c] (Å)	0.014
R.m.s. deviation bond angle (°)	1.506
B_{mean} P/L/O[b] (Å^2)	14/28/32

[a] Values in parentheses correspond to data in highest resolution shell.
[b] P/L/O refer to protein, ligand, and solvent atoms.
[c] R.m.s. deviation is root mean square deviation.

a resolution of 1.26 Å (PDB code 2B69; Table 1). The experimental structure consists of a single polypeptide chain of 312 amino acids and is composed of 12 α-helices (37%) and 17 β-strands (Fig. 1*A*, supplemental Fig. S1).[4] The N-terminal His tag in addition to 3 N-terminal residues and 5 C-terminal residues were not visible in electron density maps and were not modeled. Although the asymmetric unit contains a single hUXS1 subunit, analysis of the crystal packing by the program PISA (39) suggests the protein is dimeric. Similar to other dimeric SDRs, the dimer interface is composed of helices α5 and α7, forming a helical bundle as shown in Fig. 1*A*. The monomeric form of hUXS1 has a predicted molecular mass of 38.6 kDa, which was confirmed by SDS-PAGE (supplemental Fig. S2*A*). In nondenaturing anionic PAGE, the enzyme showed a migration behavior consistent with its presence as a homodimer (supplemental Fig. S2*B*). Furthermore, we used gel filtration to estimate an apparent molecular mass of about 70–75 kDa for hUXS1 in solution (data not shown). The structural and biochemical data therefore support the notion that the enzyme is a functional homodimer (calculated mass 77.2 kDa). Mutants of hUXS1 migrated similarly in nondenaturing PAGE, giving evidence that they are also present as dimers in solution (data not shown).

Functionally, hUXS1 can be split into two domains: a large NAD$^+$-binding domain (residues 4–181, 216–242, and 279–294) and a considerably smaller UDP-GlcUA binding domain (residues 182–215, 243–278, and 295–315). The large domain of hUXS1 is built of a seven-stranded parallel β-sheet sandwiched between two arrays of parallel helices with a small helix capping one end of the sheet, resulting in a modified version of the classic Rossmann fold. The UDP-GlcUA binding domain is composed of two small 2-stranded β-sheets (one parallel and one anti-parallel) and a 3-helix bundle. The active site of the enzyme is located in a cavity formed between the two domains (Fig. 1*B*). Fig. 1 shows how NAD$^+$ (*panel C*) and UDP (*panel D*) are accommodated in their respective binding sites on the enzyme. The NAD$^+$ is buried deeply in the protein structure, suggesting that coenzyme is bound tightly by the enzyme. This is consistent with biochemical data indicating that hUXS1 displays about 60% of its maximum activity under assay conditions where no external NAD$^+$ is added (supplemental Fig. S2*C*).

The Active Site of hUXS1—There are 6 highly conserved residues that make up the active site of hUXS1, as shown in Fig. 2. Thr^{118}, Tyr^{147}, and Lys^{151} form the characteristic signature of a typical SDR catalytic center. Ser^{119}, Glu^{120}, and Arg^{277} are distinct features of the UXS group of enzymes (Fig. 1*B*, supplemental Fig. S1). We analyzed binding of the substrate by carrying out an energy-minimized docking of UDP-GlcUA followed by MD simulation of the resulting ternary hUXS1·NAD$^+$·substrate complex. The protein-ligand structure readily converged into a stable conformation that was characterized by a root mean square deviation of ≤0.15 nm as compared with the experimental structure (supplemental Fig. S3*A*). Fig. 2 shows that in the modeled structure the D-glucuronyl pyranose ring of UDP-GlcUA was distorted from the expected low-energy $^4C_1$ *chair* conformation to $B_{O,3}$ *boat*. Sugar ring distortion is required for Tyr^{147} to become hydrogen bonded with the C_4 hydroxyl, thus positioning the reactive substrate group for general base catalysis by the tyrosine. The C_4 hydrogen was within plausible reaction distance (3.6 Å) to the NAD$^+$ nicotinamide C_4, suggesting that the modeled complex would be catalytically competent. Hydride transfer would therefore take place with pro-*S* stereospecificity, fully consistent with expectations for a member of the SDR superfamily. Our model further suggests that Thr^{118} contributes to the sugar ring distortion by forming a strong hydrogen bond with the carboxylate group at C_5. In the experimental structure of hUXS1 bound with UDP, Thr^{118} is bonded to a water molecule (Fig. 1*C*). Tyr^{147} and Lys^{151} were hydrogen bonded to the hydroxyls at C_2 and C_3 of the nicotinamide ribose (Fig. 1*C*), respectively, thus facilitating precise relative positioning of reactive parts of substrate and coenzyme at the enzyme active site, as also seen in classical SDR enzymes (40).

Fig. 2 also shows that Ser^{119} is strongly hydrogen bonded with the substrate carboxylate group. The interaction between Glu^{120} and Arg^{277} fastens together two long loops (residues 119–144 and 268–277), thus closing up the active site (Fig. 2, supplemental Fig. S4, *C* and *D*). This loop closing is conducive to catalysis because it brings both Thr^{118} and Ser^{119} into their reactive positions. In the closed conformation of hUXS1, the glucuronyl moiety of the substrate is buried deeply inside the protein structure, whereas the UDP portion is partially solvent exposed (Fig. 1*B*, supplemental Fig. S4, *A* and *B*).

One of the closest structural neighbors of hUXS1 is the decarboxylase domain of ArnA, a bifunctional enzyme from *E. coli* that catalyzes conversion of UDP-GlcUA into UDP-4-amino-4-deoxy-L-arabinose (41–43) (supplemental Fig. S4*E*). Reactions of hUXS1 and ArnA probably proceed on identical paths up to the UDP-4-keto-pentose intermediate, with the exception that ArnA releases the NADH produced. The transformylase domain of ArnA then utilizes UDP-4-keto-pentose in a stereospecific transaminase reaction to give UDP-4-amino-4-deoxy-L-arabinose as the product. A structure of a nonpro-

[4] Amino acid numbering for hUXS1 within the manuscript corresponds to PDB structure 2B69. There is an offset of −85 compared with the gene-derived sequence.

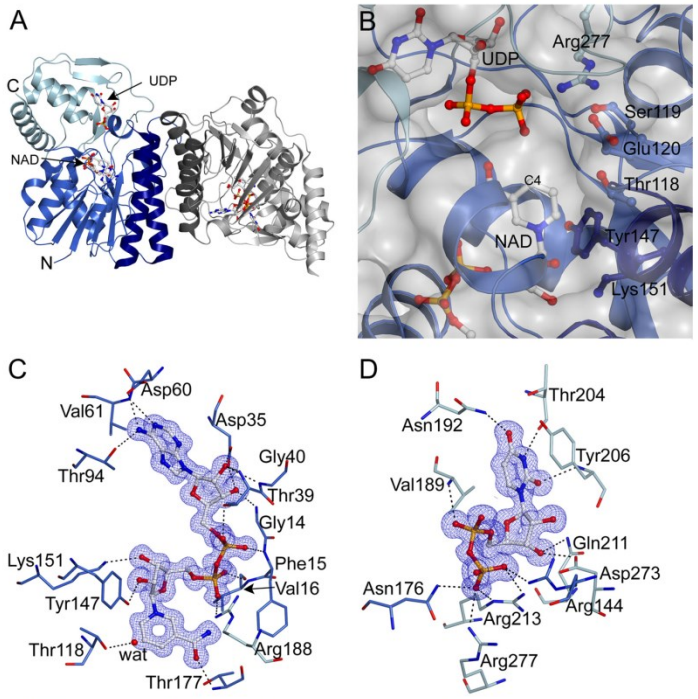

FIGURE 1. **X-ray structure of hUXS1 bound with NAD$^+$ and UDP.** *A*, α-carbon trace of the hUXS1 crystallographic dimer. The single molecule in the asymmetric unit is colored *blue* with the UDP-GlcUA binding domain shown *lighter blue* and the helices at the dimeric interface *darker blue*. A symmetry-related molecule is shown in *gray*. *B*, surface representation of the hUXS1 active site. The NAD$^+$ is buried with C_4 14 Å from the surface at the interface between the two domains. Conserved residues are labeled. *C* and *D*, electron density ($2F_o - F_c$ contoured at 1σ) and hydrogen-bonding interactions ≤3.2 Å for bound ligands NAD$^+$ (*C*) and UDP (*D*). A water molecule coordinated to Thr^{118} is shown as a *red sphere*.

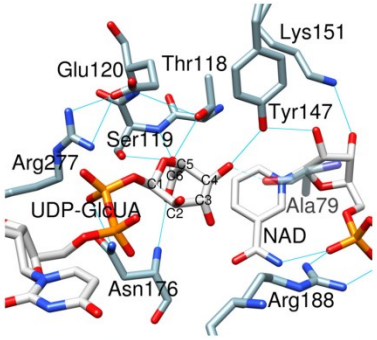

FIGURE 2. **Active site of hUXS1 with the D-glucuronyl ring of UDP-GlcUA accommodated in a distorted $B_{O,3}$ conformation.** Substrate binding mode was obtained by MD simulation. Hydrogen bonds are indicated by *blue lines*. The interaction between Ala^{79} and sugar C_4 oxygen only occurred in <60% of structures during simulation (supplemental Fig. S3*B*) and is therefore shown transparently.

ductive ternary complex of full-length ArnA that has UDP-GlcUA and ATP (as NAD$^+$ surrogate) bound to the decarboxylase domain was solved at 3.0-Å resolution (PDB code 1Z7E). The active sites of hUXS1 and the ArnA decarboxylase domain are similar and the binding sites for substrate and coenzyme appear to be also largely conserved. Interestingly, therefore, the D-glucuronyl ring of substrate bound to ArnA was in the undistorted $^4C_1$ *chair* conformation (42) (supplemental Fig. S4*F*). This may be due to the lack of a reactive nicotinamide moiety on ATP (compared with NAD$^+$), preventing the sugar ring distortion from taking place. In ArnA, Thr^{432} formed a hydrogen bond with the hydroxyl at C_4, whereas Tyr^{463} adopted a position about 5 Å away from the reactive site of the substrate, inconsistent with a direct participation of the tyrosine in catalysis (see later). Our docking experiments reveal that it is possible to accommodate UDP-GlcUA in an "ArnA-like binding mode" in hUXS1. However, under molecular dynamics conditions the enzyme complex structure relaxed immediately to the time-averaged conformation depicted in Fig. 2. Mutagenesis experiments described below strongly support the $B_{O,3}$ *boat* model, which therefore constitutes a highly probable representation of the productive hUXS1 ternary complex.

Reaction Course for Wild-type and Mutated Forms of hUXS1—The course of conversion of UDP-GlcUA by wild-type hUXS1 was recorded using HPLC and *in situ* proton NMR (Fig. 3). The absorbance of NADH was also measured, serving as an on-enzyme spectroscopic probe of the reaction at steady state and under conditions of rapid mixing in a stopped-flow analyzer. Table 2 summarizes the results. UDP-xylose was the sole prod-

uct of the enzymatic reaction. Traces of UDP-4-keto-pentose were detectable by NMR. Because NADH was also formed in roughly corresponding amounts (≤0.001-fold the molar equivalent of substrate converted) and the relevant NMR signals were relatively broad, it is probable that the enzyme-bound form of the UDP-4-keto-pentose intermediate was observed. Looking at the time domain from milliseconds to about 10 s, in which according to its k_{cat} value the wild-type enzyme would have undergone one full turnover, there was no accumulation of NADH above the steady-state level (Fig. 4*A*). These results immediately imply that in native hUXS1 the decarboxylation of UDP-4-keto-GlcUA and the reduction of UDP-4-keto-pentose are both substantially faster than the initial oxidation of UDP-GlcUA, which is therefore identified as the rate-determining chemistry in the overall reaction. The NMR data also reveal that during reaction in D_2O, the UDP-xylose became deuterium-labeled at the C_5 and the incorporation was stereospecific. The relative small $^3J_{H\text{-}H}$ coupling constant (~5.7 Hz) between the remaining proton at C_5 and the proton at C_4 of the pyranose ring indicate the chiral center at C_5 to be in *S*-configuration and suggest that the deuterium was most probably incorporated at the axial position (Fig. 3, *traces A* and *B*).

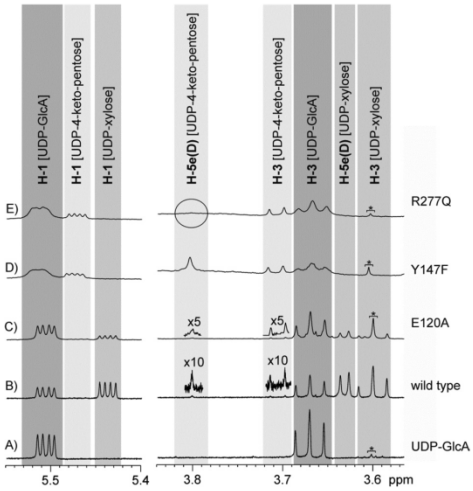

FIGURE 3. **Results from *in situ* NMR experiments with hUXS1.** *Trace A* shows some signals of the substrate UDP-GlcUA at the beginning of the transformations. In *trace B*, additional signals of the final product UDP-xylose are visible. This product is formed during the wild-type catalyzed reaction and contains one deuterium atom in position H-5_{ax}. A further tiny amount of the UDP-4-keto-pentose is detectable, which also carries a deuterium atom in position H-5_{ax}. Transformations catalyzed by the E120A mutant lead to comparable results, as shown in *trace C*. Here also mainly UDP-xylose is accumulated, whereas UDP-4-keto-pentose is undetectable or present only in very tiny concentrations, respectively. Transformations catalyzed by the Y147F mutant exclusively accumulate the intermediate UDP-4-keto-pentose with one deuterium atom in position H-5_{ax} (*trace D*). Transformations with the R277Q mutant (*trace E*) also lead to the same intermediate, which, however, is deuterated twice in position 5. In none of the transformations have any hints for accumulation of the UDP-4-keto-GlcUA been detected. An impurity (TRIS) causes the additional singlet at 3.605 ppm, which is indicated with an *asterisk*.

We suggests that Glu^{120}, Tyr^{147}, and Arg^{277} could be catalytically important, and we examined their roles through characterization of E120A, Y147F, and R277Q mutants. All mutants were less active in terms of k_{cat} than the wild-type enzyme (Table 2). Y147F had completely lost the ability to form UDP-xylose as a product of UDP-GlcUA conversion; R277Q produced only traces of UDP-xylose. Therefore, these two mutants accumulated NADH in amounts corresponding to the molar equivalent of UDP-GlcUA used (Table 2). Reactions of the Y147F and R277Q mutants became stalled at the level of UDP-4-keto-pentose. The product made by Y147F in D_2O contained a single deuterium at C_5, whereas the corresponding product of the reaction of R277Q was doubly deuterated at this position (Table 2 and Fig. 3, *traces D* and *E*). NMR data show that deuterium incorporation by Y147F occurred with the same stereoselectivity as in the wild-type enzyme.

We determined that there was no spontaneous H/D exchange at the C_5 of UDP-GlcUA, UDP-xylose, and UDP-4-keto-pentose in the time span of our experiments. Therefore, a double incorporation of deuterium label into the UDP-4-keto-pentose product necessitates that in the course of the reaction catalyzed by R277Q, the proton initially present at C_5 must have become sufficiently acidic to undergo complete exchange with bulk solvent. Based on chemical considerations, the C_5 proton of UDP-4-keto-GlcUA would be a strong candidate. Consider-

TABLE 2
Kinetic characterization of wild-type and mutated forms of hUXS1

Enzyme	k_{cat}/limiting reaction[a]	K_m UDP-GlcUA	Reaction product[b]	NADH formation[c]	Deuterium incorporation in product at C_5[d]
	s^{-1}	mM			
Wild-type	0.2/oxidation[e]	5.1	**4**, traces of **3**	≤0.001	Axial[f]
E120A	1.7×10^{-3}/reduction[e]	0.7	**4**, traces of **3**[g] (**3** and **4**)	~0.05[g] (~0.5)	Axial[f]
Y147F	1.3×10^{-4}/NA	>30[h]	**3**	~1	Axial[i]
R277Q	1.5×10^{-4}/NA	0.1	**3**, traces of **4**	~1	Double deuteration

[a] Determined from the rate of conversion of UDP-GlcUA.
[b] Notation: **3**, UDP-4-keto-pentose; **4**, UDP-xylose.
[c] Molar ratio of NADH formed and UDP-GlcUA converted; data have S.D. of about 15%.
[d] Determined by ^{1}H NMR.
[e] Determined by comparing the rate of NADH formation under conditions of rapid mixing in a stopped-flow apparatus to the steady-state rate of formation of UDP-xylose. Note that *reduction* is meant here to involve all reaction steps after formation of UDP-4-keto-GlcUA (**2**), including the decarboxylation. NA, not applicable.
[f] Stereochemical assignment is made for **4**. It follows from the proposed enzymatic reaction that **3** will have deuterium incorporated at C_5 with the same stereochemistry as **4**.
[g] The molar ratio of **4** and **3** decreased in response to increase of UDP-GlcUA (**1**) concentration, from the shown value at 10 mM of **1** to the value in parentheses at 50 mM of **1**.
[h] No exact determination possible, as no substrate saturation could be reached.
[i] Inferred from equivalence of ^{1}H spectra of **3** formed by Y147F mutant and wild-type enzyme.

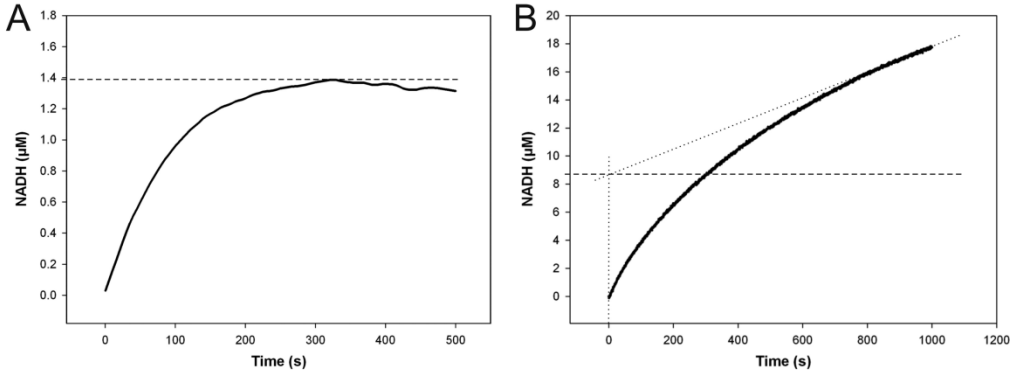

FIGURE 4. **Stopped-flow progress curves of NADH formation in reactions catalyzed by wild-type hUXS1 (*A*) and E120A mutant (*B*).** Reactions were performed using 0.5 mM NAD^+ and 10 mM UDP-GlcUA. *A*, reaction with 25 μM wild-type enzyme. There was no accumulation of NADH above 0.055 mol enzyme equivalents (1.4 μM; *dashed line*). *B*, the E120A mutant (15 μM) accumulated up to 0.58 mol enzyme equivalents (8.7 μM; *dashed line*) of NADH in the pre-steady state, indicating a shift in the rate-determining step from NADH formation to NADH consumption.

ing that the R277Q mutant did not produce UDP-4-keto-GlcUA in detectable amounts (Fig. 3), we conclude that the H/D exchange must have taken place at the active site of the mutant. Occurrence of this exchange was not primarily determined by intermediate lifetime, as we could show that the formation of NADH did not proceed ahead of production of UDP-4-keto-pentose during the first turnover. This would be the case if decarboxylation of UDP-4-keto-GlcUA had become the slowest step of the overall reaction of the mutant. Enhanced readiness of R277Q-bound UDP-4-keto-GlcUA to undergo H/D exchange must therefore be ascribed to a direct effect of the mutation on the solvent accessibility of the intermediate, reinforced by results of MD simulations to be described below.

Product distribution of the E120A-catalyzed reaction was dependent on the UDP-GlcUA concentration used, whereupon UDP-4-keto-pentose formation was promoted at high substrate levels. Unlike wild-type enzyme, E120A accumulated substantial amounts of NADH (up to 0.58 molar enzyme equivalents) in the pre-steady state of their reactions (Fig. 4*B*). Therefore, rate limitation was shifted from NADH formation (substrate oxidation) in wild-type enzyme to NADH consumption (substrate reduction including decarboxylation) in the mutant. Interestingly, the k_{cat} for E120A displayed a solvent kinetic isotope effect of 4.4 ($= k_{cat}(H_2O)/k_{cat}(D_2O)$), whereas that of wild-type enzyme was just 1.4.[5]

Sugar Ring Distortions at the Active Site and Their Role in Promoting Catalysis—Fig. 2 suggests that substrate binding involves considerable strain on the D-glucuronyl pyranose ring. We therefore performed MD simulations on all complexes of the proposed enzymatic reaction (Scheme 1). Results indicate a trajectory of the pyranose ring pucker that moves from the relaxed $^4C_1$ *chair* in free substrate via $B_{O,3}$ *boat* in Michaelis complex (Fig. 5*A*) to a ^2S_O *skew-boat* conformation in the UDP-4-keto-GlcUA intermediate (Fig. 5*B*). This trajectory, which is plausible as it contains only conformations accessible to the D-glucuronyl ring in solution (44, 45), appears to be highly conducive to UXS catalysis in each step. The $^4C_1 \rightarrow B_{O,3}$ transition serves to align the catalytic groups for NAD^+-dependent oxidation at C_4, however, already in expectation of the subsequent decarboxylation because the carboxylate group at C_5 is brought into an axial position that makes it an excellent leaving group. The $B_{O,3} \rightarrow {}^2S_O$ transition, which accompanies substrate oxidation, additionally involves a slight tilt of the pyranose ring at the active site (*cf.* Fig. 5, *A* and *B*), resulting in distinctly altered hydrogen bonding of the 4-keto-GlcUA moiety with the enzyme as compared with substrate. In particular, contact between Thr^{118} and the carboxylate group is disrupted and the threonine now interacts with the 4-keto group of the intermediate. This new arrangement of hydrogen bonds (involving Thr^{118} and Ser^{119}) would provide excellent stabilization for β-keto acid decarboxylation (46). Generating the E120A mutant *in silico*, we find that due to loss of hydrogen bonding capability in the mutant as compared with wild-type enzyme, substrate distortion in the Michaelis complex is decreased substantially and equatorial-to-axial reorientation of the carboxylate group of the substrate does not occur (Fig. 5*E*). Therefore, these findings could explain the dual effect of the $Glu^{120} \rightarrow$ Ala substitution that reaction is slowed already at the substrate oxidation step, whereas at the same time rate limitation is shifted to the following steps of the catalytic cycle.

MD simulation of the substrate complex of the R277Q mutant revealed an even larger pyranoside ring distortion than in wild-type enzyme, involving a different way of accommodating the carboxylate at C_5 in which Thr^{118} has no role (Fig. 5*F*). Reactive carbons on substrate and NAD^+ appear to be better aligned for hydride transfer in the wild-type complex as compared with the R277Q complex, providing a tentative explanation for the low reactivity of the mutant in the initial oxidation step of the catalytic reaction. The modeled UDP-4-keto-GlcUA complex of R277Q (Fig. 5*G*) differs from the corresponding wild-type complex (Fig. 5*B*) in that the pyranose ring of the 4-keto-GlcUA moiety adopts a $^1C_4$ (rather than ^2S_O) conforma-

[5] Reaction conditions were used where E120A mutant forms UDP-xylose and only trace amounts of UDP-4-keto-pentose upon conversion of UDP-GlcUA.

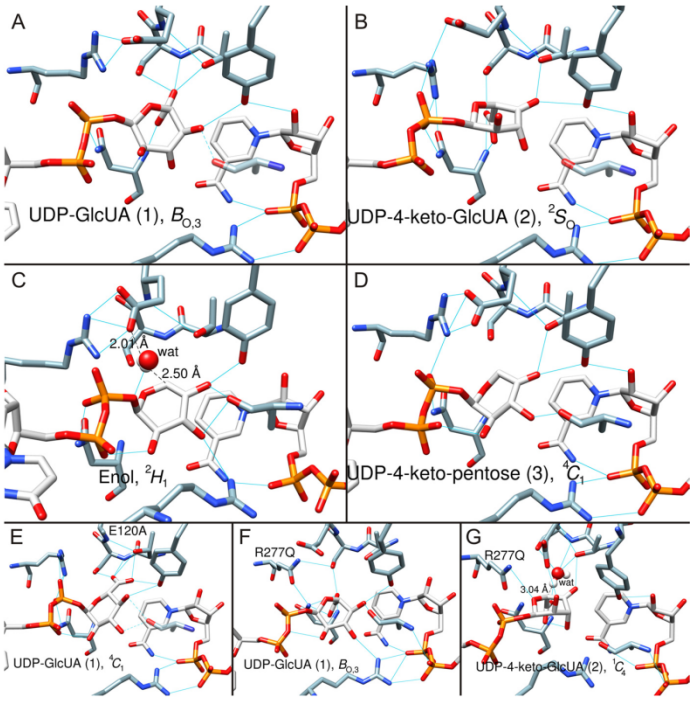

FIGURE 5. **Trajectory of sugar ring conformation along the hUXS1 reaction coordinate determined by MD simulation.** Numbering of substrate/intermediate corresponds to the designation shown in Schemes 1 and 2. *Blue lines* indicate hydrogen bonds. Amino acid residues (except mutations) are not labeled here for better clarity (refer to Fig. 2). *A,* substrate UDP-GlcUA, **1**, is in $B_{O,3}$ *boat* conformation. *B,* UDP-4-keto-GlcUA intermediate, **2**, in ^2S_O *skew-boat* conformation. *C,* UDP-4-keto-pentose, enol form, in $^2H_1$ *half-chair* conformation. The water that protonates C_5 is shown in *white/red*. *D,* UDP-4-keto-pentose intermediate, **3**, in $^4C_1$ *chair* conformation. *E,* mutant complex E120A·NAD$^+$·UDP-GlcUA. The substrate, **1**, is in the $^4C_1$ *chair* conformation. *F,* mutant complex R277Q·NAD$^+$·UDP-GlcUA. The substrate, **1**, is in the $B_{O,3}$ *boat* conformation. *G,* mutant complex R277Q·NADH·UDP-4-keto-GlcUA. The 4-keto-D-glucuronyl ring of UDP-4-keto-GlcUA, **2**, is in a $^1C_4$ *chair* conformation. MD simulation revealed a water molecule possibly involved in hydrogen/deuterium exchange at C_5 of UDP-4-keto-GlcUA in the R277Q mutant. The water is shown in *white/red*. Note that the modeled structure of the corresponding NADH·UDP-4-keto-GlcUA complex of the wild-type enzyme (*panel B*) lacked water in a position suitable for hydrogen/deuterium exchange, consistent with only a single deuterium being incorporated during reaction in D_2O.

tion. However, the carboxylate group of the substrate is still oriented axial, consistent with experimental observation that R277Q forms decarboxylated product exclusively. Interestingly, the mutant complex shows a water molecule in the immediate proximity to the C_5 proton of UDP-4-keto-GlcUA, suggesting how H/D exchange could occur at this point (Fig. 5*G*). Space restriction due to the Arg^{277} side chain and a different local network of hydrogen bonds presumably exclude water in the corresponding wild-type complex (Fig. 5*B*).

Proceeding with analysis of the wild-type enzyme, we find that the enol/enolate produced by decarboxylation adopts a $^2H_1$ *half-chair* conformation that is strained by the presence of the endocyclic double bond (Fig. 5*C*). We carefully examined the simulated structures for candidate groups involved in stereospecific protonation of the enolate at C_5. There are no protein residues close enough to adopt this role. However, a water molecule bonded to Glu^{120} is found in all structures in a position optimally suited for stereospecific protonation from below the sugar ring through a *Si* side attack on C_5 (Fig. 5*C*). Solvent deuterium would thus be incorporated in axial position at C_5 of UDP-xylose, in agreement with our NMR data and consistent with stereochemical analysis of the UXS reaction by Schutzbach and Feingold (16) using C_5 tritium-labeled UDP-GlcUA as substrate. The large solvent isotope effect on k_{cat} for E120A would be consistent with the proposed role for Glu^{120}. The resulting UDP-4-keto-pentose adopts a flattened $^4C_1$ *chair* (Fig. 5*D*). The reactive 4-keto group is placed suitably for stereospecific hydride transfer from NADH under general acid catalytic assistance from Tyr^{147}. The UDP-xylose product is in a relaxed $^4C_1$ conformation (data not shown), similar as in Fig. 5*D*.

The Catalytic Mechanism of hUXS1 and Its Biological Implications—A detailed proposal for the catalytic mechanism of hUXS1 is supported (Scheme 2). Having captured the relevant (stable) intermediates of the enzymatic reaction, we present here the first direct observation that conversion of UDP-GlcUA by UXS proceeds in three discrete catalytic steps. We further assign catalytic functions to the individual active site groups in each reaction step, thus revealing how the classical SDR catalytic center is expanded in UXS to accommodate the specific task of oxidative decarboxylation. Tyr^{147} is the Brøn-

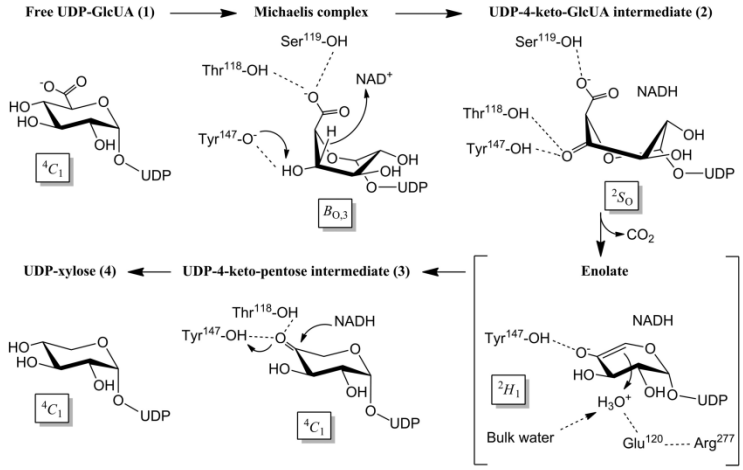

SCHEME 2. **Proposed catalytic mechanism of hUXS1.**

sted acid-base for catalytic oxidation and reduction. Mutation of the tyrosine to the incompetent phenylalanine was strongly disruptive for activity in substrate dehydrogenation and, not unexpectedly, it completely eliminated reductase activity toward the unactivated keto group in UDP-4-keto-pentose. Thr^{118} has a key role in positioning the substrate for oxidative decarboxylation by forming a strong hydrogen bond with the carboxylate group at C_5. This role differs from the canonical catalytic function of homologous threonine/serine residues in SDR active sites that is in the orientation of the reactive alcohol group on the substrate (20, 40). Arg^{277} indirectly contributes to catalysis by bonding with Glu^{120} from the neighboring loop in the structure. Thus, the binding pocket for the carboxylate group of the substrate is created, and the active site is closed up. This prevents escape of UDP-4-keto-pentose during reaction. Glu^{120} is furthermore important for stereospecific protonation of the enolate formed in the decarboxylation step. A particular component of significance of the hUXS1 mechanism is that the sugar ring pucker in the substrate/intermediates changes along the reaction coordinate to optimally underpin the chemical steps. Glu^{120} is important for the binding site to exercise strain on the enzyme-bound substrate. Destabilization of substrate is an important general mechanism of enzyme catalysis and hUXS1 appears to have found an ingenious way to apply it. Our findings furthermore provide an explanation for the interesting pattern of residue conservation in extended SDRs that Glu^{120} and Arg^{277} of hUXS1 are invariant within the UXS group of enzymes, whereas the same residues are not present in "counterpart" epimerases that prevent decarboxylation at C_5 in a highly similar transformation of UDP-GlcUA via oxidation and reduction at C_4 (11, 47) (supplemental Fig. S1). Of note, Glu^{120} and Arg^{277} of UXS are replaced, respectively, by a serine and a threonine in the epimerases. We predict that in epimerases, the pyranose ring pucker for enzyme-bound substrate and oxidized intermediate will not be the same as in UXS, thus preventing the decarboxylation. Enzymes utilizing UDP-4-keto-pentose as a key intermediate for making products other than UDP-xylose are expected to employ a mechanism of oxidative decarboxylation analogous to that of hUXS1. Molecular strategies for diversification at the level of UDP-4-keto-pentose involve "early" release of NADH as in ArnA (41–43) or catalytic pyranoside ring contraction as in UDP-α-D-apiose synthase (48, 49). The high-resolution structure of hUXS1 provides a valuable basis to further explore these alternative enzymatic reaction mechanisms. Considering the essential role of the enzyme in human extracellular matrix glycobiology, the hUXS1 structure will furthermore be of great interest for exploitation in the design of small-molecule effectors or inhibitors of the enzyme. Evidence from our MD simulations provides useful guidance to such efforts.

REFERENCES

1. Theocharis, A. D., Skandalis, S. S., Tzanakakis, G. N., and Karamanos, N. K. (2010) Proteoglycans in health and disease. Novel roles for proteoglycans in malignancy and their pharmacological targeting. *FEBS J.* **277,** 3904–3923
2. Bernfield, M., Götte, M., Park, P. W., Reizes, O., Fitzgerald, M. L., Lincecum, J., and Zako, M. (1999) Functions of cell surface heparan sulfate proteoglycans. *Annu. Rev. Biochem.* **68,** 729–777
3. Bishop, J. R., Schuksz, M., and Esko, J. D. (2007) Heparan sulfate proteoglycans fine-tune mammalian physiology. *Nature* **446,** 1030–1037
4. Iozzo, R. V. (1998) Matrix proteoglycans. From molecular design to cellular function. *Annu. Rev. Biochem.* **67,** 609–652
5. Lander, A. D., and Selleck, S. B. (2000) The elusive functions of proteoglycans. *In vivo* veritas. *J. Cell Biol.* **148,** 227–232
6. Schaefer, L., and Schaefer, R. M. (2010) Proteoglycans. From structural compounds to signaling molecules. *Cell Tissue Res.* **339,** 237–246
7. Prydz, K., and Dalen, K. T. (2000) Synthesis and sorting of proteoglycans. Commentary. *J. Cell Sci.* **113,** 193–205
8. Kearns, A. E., Vertel, B. M., and Schwartz, N. B. (1993) Topography of glycosylation and UDP-xylose production. *J. Biol. Chem.* **268,** 11097–11104
9. Moriarity, J. L., Hurt, K. J., Resnick, A. C., Storm, P. B., Laroy, W., Schnaar, R. L., and Snyder, S. H. (2002) UDP-glucuronate decarboxylase, a key enzyme in proteoglycan synthesis. Cloning, characterization, and localization. *J. Biol. Chem.* **277,** 16968–16975

10. Eames, B. F., Singer, A., Smith, G. A., Wood, Z. A., Yan, Y. L., He, X., Polizzi, S. J., Catchen, J. M., Rodriguez-Mari, A., Linbo, T., Raible, D. W., and Postlethwait, J. H. (2010) UDP xylose synthase 1 is required for morphogenesis and histogenesis of the craniofacial skeleton. *Dev. Biol.* **341,** 400–415
11. Bar-Peled, M., and O'Neill, M. A. (2011) Plant nucleotide sugar formation, interconversion, and salvage by sugar recycling. *Annu. Rev. Plant Biol.* **62,** 127–155
12. Bar-Peled, M., Griffith, C. L., and Doering, T. L. (2001) Functional cloning and characterization of a UDP-glucuronic acid decarboxylase. The pathogenic fungus *Cryptococcus neoformans* elucidates UDP-xylose synthesis. *Proc. Natl. Acad. Sci. U.S.A.* **98,** 12003–12008
13. Coyne, M. J., Fletcher, C. M., Reinap, B., and Comstock, L. E. (2011) UDP-glucuronic acid decarboxylases of *Bacteroides fragilis* and their prevalence in bacteria. *J. Bacteriol.* **193,** 5252–5259
14. Gu, X., Lee, S. G., and Bar-Peled, M. (2011) Biosynthesis of UDP-xylose and UDP-arabinose in *Sinorhizobium meliloti* 1021. First characterization of a bacterial UDP-xylose synthase, and UDP-xylose 4-epimerase. *Microbiology* **157,** 260–269
15. Rosenberger, A. F., Hangelmann, L., Hofinger, A., and Wilson, I. B. (2012) UDP-xylose and UDP-galactose synthesis in *Trichomonas vaginalis*. *Mol. Biochem. Parasitol.* **181,** 53–56
16. Schutzbach, J. S., and Feingold, D. S. (1970) Biosynthesis of uridine diphosphate D-xylose IV. Mechanism of action of uridine diphosphoglucuronate carboxylyase. *J. Biol. Chem.* **245,** 2476–2482
17. Gu, X., Glushka, J., Yin, Y., Xu, Y., Denny, T., Smith, J., Jiang, Y., and Bar-Peled, M. (2010) Identification of a bifunctional UDP-4-keto-pentose/UDP-xylose synthase in the plant pathogenic bacterium *Ralstonia solanacearum* strain GMI1000, a distinct member of the 4,6-dehydratase and decarboxylase family. *J. Biol. Chem.* **285,** 9030–9040
18. He, X. M., and Liu, H. W. (2002) Formation of unusual sugars. Mechanistic studies and biosynthetic applications. *Annu. Rev. Biochem.* **71,** 701–754
19. Tanner, M. E. (2008) Transient oxidation as a mechanistic strategy in enzymatic catalysis. *Curr. Opin. Chem. Biol.* **12,** 532–538
20. Kavanagh, K. L., Jörnvall, H., Persson, B., and Oppermann, U. (2008) The SDR superfamily. Functional and structural diversity within a family of metabolic and regulatory enzymes. *Cell Mol. Life Sci.* **65,** 3895–3906
21. Frey, P. A. (1996) The Leloir pathway. A mechanistic imperative for three enzymes to change the stereochemical configuration of a single carbon in galactose. *FASEB J.* **10,** 461–470
22. Thibodeaux, C. J., Melançon, C. E., and Liu, H. W. (2007) Unusual sugar biosynthesis and natural product glycodiversification. *Nature* **446,** 1008–1016
23. Collaborative Computational Project (1994) The CCP4 Suite. Programs for protein crystallography. *Acta Crystallogr. Sect. D Biol. Crystallogr.* **50,** 760–763
24. Sheldrick, G. M., and Schneider, T. R. (1997) SHELXL. High-resolution refinement. *Methods Enzymol.* **277,** 319–343
25. Emsley, P., and Cowtan, K. (2004) COOT. Model-building tools for molecular graphics. *Acta Crystallogr. Sect. D Biol. Crystallogr.* **60,** 2126–2132
26. Murshudov, G. N., Vagin, A. A., and Dodson, E. J. (1997) Refinement of macromolecular structures by the maximum-likelihood method. *Acta Crystallogr. Sect. D Biol. Crystallogr.* **53,** 240–255
27. Hess, B., Kutzner, C., van der Spoel, D., and Lindahl, E. (2008) GROMACS 4. Algorithms for highly efficient, load-balanced, and scalable molecular simulation. *J. Chem. Theory Comput.* **4,** 435–447
28. Hornak, V., Abel, R., Okur, A., Strockbine, B., Roitberg, A., and Simmerling, C. (2006) Comparison of multiple amber force fields and development of improved protein backbone parameters. *Proteins* **65,** 712–725
29. Jorgensen, W. L., Chandrasekhar, J., Madura, J. D., Impey, R. W., and Klein, M. L. (1983) Comparison of simple potential functions for simulating liquid water. *J. Chem. Phys.* **79,** 926
30. Wang, J., Wolf, R. M., Caldwell, J. W., Kollman, P. A., and Case, D. A. (2004) Development and testing of a general amber force field. *J. Comput. Chem.* **25,** 1157–1174
31. Wang, J., Wang, W., Kollman, P. A., and Case, D. A. (2006) Automatic atom-type and bond-type perception in molecular mechanical calculations. *J. Mol. Graph. Model.* **25,** 247–260
32. Mobley, D. L., Chodera, J. D., and Dill, K. A. (2006) On the use of orientational restraints and symmetry corrections in alchemical free energy calculations. *J. Chem. Phys.* **125,** 084902
33. Olsson, M. H. M., Søndergaard, C. R., Rostkowski, M., and Jensen, J. H. (2011) PROPKA3. Consistent treatment of internal and surface residues in empirical pK_a predictions. *J. Chem. Theory Comput.* **7,** 525–537
34. Hoover, W. G. (1985) Canonical dynamics. Equilibrium phase-space distributions. *Phys. Rev. A* **31,** 1695–1697
35. Essmann, U., Perera, L., Berkowitz, M. L., Darden, T., Lee, H., and Pedersen, L. G. (1995) A smooth particle mesh Ewald potential. *J. Chem. Phys.* **103,** 8577–8592
36. Berendsen, H. J. C., Postma, J. P. M., Van Gunsteren, W. F., DiNola, A., and Haak, J. R. (1984) Molecular dynamics with coupling to an external bath. *J. Chem. Phys.* **81,** 3684
37. Hess, B., Bekker, H., Berendsen, H. J., and Fraaije, J. G. (1997) LINCS. A linear constraint solver for molecular simulations. *J. Comput. Chem.* **18,** 1463–1472
38. Krezel, A., and Bal, W. (2004) A formula for correlating pK_a values determined in D_2O and H_2O. *J. Inorg. Biochem.* **98,** 161–166
39. Krissinel, E., and Henrick, K. (2007) Inference of macromolecular assemblies from crystalline state. *J. Mol. Biol.* **372,** 774–797
40. Filling, C., Berndt, K. D., Benach, J., Knapp, S., Prozorovski, T., Nordling, E., Ladenstein, R., Jörnvall, H., and Oppermann, U. (2002) Critical residues for structure and catalysis in short-chain dehydrogenases/reductases. *J. Biol. Chem.* **277,** 25677–25684
41. Gatzeva-Topalova, P. Z., May, A. P., and Sousa, M. C. (2004) Crystal structure of *Escherichia coli* ArnA (PmrI) decarboxylase domain. A key enzyme for lipid a modification with 4-amino-4-deoxy-L-arabinose and polymyxin resistance. *Biochemistry* **43,** 13370–13379
42. Gatzeva-Topalova, P. Z., May, A. P., and Sousa, M. C. (2005) Structure and mechanism of ArnA. Conformational change implies ordered dehydrogenase mechanism in key enzyme for polymyxin resistance. *Structure* **13,** 929–942
43. Williams, G. J., Breazeale, S. D., Raetz, C. R., and Naismith, J. H. (2005) Structure and function of both domains of ArnA, a dual function decarboxylase and a formyltransferase, involved in 4-amino-4-deoxy-L-arabinose biosynthesis. *J. Biol. Chem.* **280,** 23000–23008
44. Mikhailov, D., Mayo, K. H., Vlahov, I. R., Toida, T., Pervin, A., and Linhardt, R. J. (1996) NMR solution conformation of heparin-derived tetrasaccharide. *Biochem. J.* **318,** 93–102
45. Ochsenbein, P., Bonin, M., Schenk-Joss, K., and El-Hajji, M. (2011) The ^2S_O *skew-boat* conformation in L-iduronic acid. *Angew. Chem. Int. Ed.* **50,** 11637–11639
46. Pan, Y., Kee, C. W., Jiang, Z., Ma, T., Zhao, Y., Yang, Y., Xue, H., and Tan, C. H. (2011) Expanding the utility of bronsted base catalysis. Biomimetic enantioselective decarboxylative reactions. *Chem. Eur. J.* **17,** 8363–8370
47. Broach, B., Gu, X., and Bar-Peled, M. (2012) Biosynthesis of UDP-glucuronic acid and UDP-galacturonic acid in *Bacillus cereus* subsp. *cytotoxis* NVH 391–98. *FEBS J.* **279,** 100–112
48. Choi, S. H., Ruszczycky, M. W., Zhang, H., and Liu, H. W. (2011) A fluoro analogue of UDP-α-D-glucuronic acid is an inhibitor of UDP-α-D-apiose/UDP-α-D-xylose synthase. *Chem. Commun.* **47,** 10130–10132
49. Gebb, C., Baron, D., and Grisebach, H. (1975) Spectroscopic evidence for formation of a 4-keto intermediate in UDP-apiose UDP-xylose synthase reaction. *Eur. J. Biochem.* **54,** 493–498

SUPPLEMENTAL METHODS

Expression and purification of hUXS1—For crystallization experiments, a synthetic hUXS1 gene (ORF NM_025076) that was codon-optimized for high-level expression in *E. coli* was inserted into the pET-derived expression vector p11. The expression plasmid encoded a truncated hUXS1 (AA 85-402) fused to a 23 amino acid-long N-terminal peptide that consisted of the His_6 tag and a tobacco etch virus (TEV) protease cleavage site. The Met auxotroph *E. coli* strain B834(DE3) cells were transformed with the hUXS1 plasmid and a single colony was used to start a 5mL overnight culture in LB medium supplemented with 100 µg/mL ampicillin. The overnight culture (1 mL) was used to inoculate 50 mL of LB/AMP medium and grown at 37 °C to an OD_{600} of 1.0. The cells were harvested by centrifugation, washed four times and inoculated in 1 L of SelenoMethionine Medium Base plus Nutrient Mix containing Se-Met at 40 mg/L (Molecular Dimensions, Newmarket, U.K.), and grown at 37 °C to an OD_{600} of 0.6. The culture was induced by the addition of isopropyl-β-D-thiogalactopyranoside (IPTG) to a final concentration of 1 mM, cultured overnight at 25 °C, and collected by centrifugation. Pellets were resuspended in 20 mL lysis buffer (5 mM Imidazole, 500 mM NaCl, 50 mM HEPES, pH 7.5, 5% glycerol) including Protease inhibitor (complete; Roche, Basel, Switzerland), lysed by French Press, and the solution was centrifuged (30 min, 4 °C, 20000 x g). The supernatant was loaded onto a 2 mL gravity flow Ni-NTA column (Sigma-Aldrich, St. Louis, MO, U.S.A.), washed with 10 column volumes lysis buffer containing 30 mM imidazole and eluted in lysis buffer plus 250 mM imidazole. The protein was further purified by gel filtration using a Superdex S200 column (GE Healthcare, Little Chalfont, U.K.) developed with 10 mM HEPES, pH 7.5, 500 mM NaCl, 5% glycerol, 1 mM TCEP.

Wild-type hUXS1 for kinetic analysis was prepared in an analogous manner, except that the protein was produced in the *E. coli* strain Rosetta 2(DE3). Cells were grown in LB medium supplemented with 34 µg/mL chloramphenicol and 100 µg/mL ampicillin. For mutants of hUXS1, the pNIC28-Bsa4 expression vector (GenBank ID: EF198106) was used and ampicillin was replaced by kanamycin (50 µg/mL). Bacterial cultures (250 mL) were inoculated from an overnight pre-culture and first grown at 37 °C to an OD_{600} of ~0.8. After cooling to 18 °C, recombinant protein production took place overnight using induction with 0.5 mM isopropyl-β-D-thiogalactopyranoside (IPTG). Cells were recovered by centrifugation (20 min, 4 °C, 4400 x g), and the pellet was resuspended 1:1 in 50mM Tris/HCl buffer (pH 7.5) containing glycerol (5%, by volume). The cell extract obtained by high-pressure cell disruption (2 passes at 1500 psi) was fractionated on a Cu^{2+} loaded IMAC Sepharose High Performance column (GE Healthcare) using stepwise elution with imidazole. hUXS1 eluted at a concentration of 120 mM imidazole, and, after pooling the fractions containing UXS1 activity, imidazole was removed with a NAP-25 desalting column (GE Healthcare) or Vivaspin-20 centrifugal concentrator (Sartorius Stedim, Göttingen, Germany). Preparations of hUXS1 were brought to a concentration of 15-20 mg/mL and stored at -70 °C in the above Tris/HCl buffer supplemented with 1 mM DTT. The protein concentration was obtained from absorbance at 280 nm,

applying a molar extinction coefficient of 37360 $M^{-1}cm^{-1}$. Purity of wild-type and mutated enzymes was checked by SDS PAGE.

Force Field Test—GAFF is a widely used and well established force field for organic compounds. However, it has not been tested extensively for sugar molecules. Therefore, we performed test calculations comparing structures of the sugar moieties in the substrate and intermediate-1 compounds minimized at the DFT-level of theory to the same compounds modeled with Gromacs and the GAFF force field parameters. Starting from the relaxed chair conformation the substrate sugar was minimized using GAFF and Gromacs with a quasi-Newtonian minimization algorithm (1). For intermediate-1, the average structure from the MD simulation was used as conformation representing the classical force field. Both structures were then optimized using GAMESS-US (2). Here the DFT level of theory was combined with the B3LYP functional and a 6-31+G(d,p) basis set. The structures minimized with DFT and modeled with the classical force field are very close with an RMSD, including all non-hydrogen atoms, of 0.25 Å and 0.30 Å for the substrate and intermediate-1, respectively. The fact that the DFT optimized structure of intermediate-1 is very close to the average structure from the MD simulation suggests that this conformation corresponds to local minimum of the sugar ring. These two calculations can of course not serve as a comprehensive test of GAFFs ability to model sugars, but doing so would be beyond the scope of this work. Given these two results together with the extensive effort put into the development of GAFF as a force field for general organic molecules (3), we conclude that the force fields accuracy is sufficient for our purposes.

HPLC analysis—Samples were analyzed on an Agilent 1200 HPLC system equipped with a 5µm Zorbax SAX Analytical HPLC Column (4.6 × 250 mm; Agilent, Santa Clara, CA, U.S.A.) and a UV detector (λ = 254 nm). After 5 min elution with 5 mM potassium phosphate buffer (pH 3.2), a linear gradient of potassium phosphate buffer (pH 3.2) between 5 mM and 360 mM was used over 20 min. The column was washed (15 min each) with 600 mM and 5 mM potassium phosphate buffer (pH 3.2) after each analysis. The flow rate was 1.5 mL/min. Authentic standards were used for calibration. Note that the applied conditions were carefully optimized for reaction and analysis. Under the conditions used, UDP-GlcUA, UDP-xylose, and UDP-4-keto-pentose were baseline separated (Fig. S5).

In situ NMR analysis—Samples contained 1 mM UDP-GlcUA, 0.5 mM NAD^+ and 7 µM enzyme in case of the wild type. For reactions with mutants, 1 mM UDP-GlcUA, 1 mM NAD^+ and 15 µM enzyme (E120A) or 10 mM UDP-GlcUA, 1 mM NAD^+ and 100 µM enzyme (Y147F, R277Q) were used. All experiments were made in a 20 mM Tris/HCl buffer prepared in D_2O (0.70 mL, 99.9 % deuterium, pD 7.9). The ^1H NMR spectra were recorded at 303.2 K with presaturation (1 s) and acquisition of 32k data points. After zero filling to 64k data points, spectra were performed with a range of 7200 Hz.

Non-denaturing anionic PAGE—Protein samples were mixed with a 1:1 mixture of glycerol and 20mM Tris/HCl buffer (pH 7.4), containing 1% Triton X-100 and 0.9 g/L bromophenol blue. Separation was done on a 10% polyacrylamide gel according to the instructions of the supplier (Bio-

Rad Laboratories, Hercules, CA, U.S.A.), using a Tris-glycine native running buffer (24 mM Tris and 188 mM glycine) and a voltage of 100 V. Buffers and gel were prepared without SDS. After electrophoresis, the proteins were visualized by Coomassie blue staining.

References

1. Shanno, D. F. (1970) Conditioning of quasi-Newton methods for function minimization. *Math. Comp.* **24**, 647-656
2. Gordon, M. S., and Schmidt, M. W. (2005) Advances in electronic structure theory: GAMESS a decade later. in *Theory and Applications of Computational Chemistry: the first forty years* (C. E. Dykstra, Frenking, G., Kim, K. S., and Scuseria, G. E. eds.), Elsevier, Amsterdam. pp 1167-1189
3. Wang, J., Wolf, R. M., Caldwell, J. W., Kollman, P. A., and Case, D. A. (2004) Development and testing of a general amber force field. *J. Comput. Chem.* **25**, 1157-1174

SUPPLEMENTAL FIGURE LEGENDS

FIGURE S1. Protein sequence alignment of human UXS and similar proteins from other species. Protein sequences of *Homo sapiens* UDP-glucuronic acid decarboxylase 1 (UXS_human; NP_079352.2), *Oryza sativa subs. japonica* UDP-glucuronic acid decarboxylase (UXS_rize; Q75PK6), *Cryptococcus neoformans var. neoformans JEC21* UDP-glucuronic acid decarboxylase (UXS_fungus; XP_572003.1), *Escherichia coli K12* bifunctional polymyxin resistance protein ArnA (ArnA; P77398.1, AA 151-693 shown), *Solanum tuberosum* UDP-apiose/xylose synthase (UAXS; ABC75032.1), and *Bacillus cytotoxicus NVH 391-98* UDP-glucuronic acid 4-epimerase (UGlcAE; HM581979.1) were aligned with PRALINE using the BLOSUM62 scoring matrix. Secondary structure motifs in UXS_human were obtained with STRIDE from PDB entry 2B69. Residues of the catalytic triad are marked with black boxes in the numbering row; other residues of the active site are marked with grey boxes in the numbering row.

FIGURE S2. Biochemical characterization of hUXS1. A. SDS-PAGE used to determine the molecular mass of the monomeric form of hUXS1. 10 µg of purified hUXS1 were loaded on the gel and visualized by Coomassie blue staining after electrophoresis. The standard used (left lane) is a low molecular weight marker (masses in kDa) from GE Healthcare (Little Chalfont, U.K.). B**.** Native gel electrophoresis. 6 µg aliquots of purified hUXS1 were loaded on the gel. Lane 1 and 2 are wild-type hUXS1; lane 3 is a high molecular weight marker for native gel electrophoresis (GE Healthcare; masses in kDa). Although the exact molecular mass cannot be determined by native PAGE (4), the position of the hUXS1 bands (between the markers for 66 kDa and 140 kDa) indicates the presence of a dimer (77.2 kDa). C. Evidence for partial saturation of hUXS1 with NAD^+ after isolation. NAD^+ is very tightly bound by the enzyme (K_m = 4 µM), therefore hUXS1 shows about 60% of its maximum activity under conditions where no external NAD^+ is added (2 mM UDP-GlcUA; 10 µM hUXS1).

FIGURE S3. MD simulations. A. Convergence of MD simulations, shown as RMSD between all protein non-hydrogen atoms in the simulation and in the initial structure (based on coordinates in PDB 2B69). B. Hydrogen bonds between the substrate sugar moiety and the protein. Donors and acceptors of the protein are drawn on the x-axes, sugar oxygens on the y-axes. For each combination, the relative time during which an H-bond is established between the two atoms is indicated by a square in gray-scale: black 100% simulation time, white 0% simulation time.

FIGURE S4. Surface model of hUXS1 with substrate and NAD^+ bound and comparison with ArnA. A and B. Front view of hUXS1 (A: closed, B: in section), showing the accommodation of UDP-glucuronic acid (green) and NAD^+ (yellow) in the active site. C and D. Two back views of the UXS active site, C: long shot, D: close up. For residues E120 and R277 the protein surface is not shown to

demonstrate that removal of the two side chains can potentially open a channel allowing access to the active site; also shown are the substrate (green) and NAD^+ (yellow). E. Overlay of hUXS1 and ArnA structures, showing the high similarity between the two enzymes. F. Accommodation of UDP-GlcUA in the active site of ArnA. In contrast to hUXS1, the sugar ring is in the undistorted $^4C_1$ *chair* conformation.

FIGURE S5. HPLC chromatogram showing the separation of UDP-glucuronic acid, UDP-xylose and NAD^+ signals (reaction of wild-type hUXS1). The insert shows an overlay with a chromatogram of Y147F reaction, illustrating separation of UDP-xylose and UDP-4-keto-pentose.

References

4. Razandi, M., Pedram, A., Merchenthaler, I., Greene, G. L., and Levin, E. R. (2004) Plasma membrane estrogen receptors exist and function as dimers. *Mol. Endocrinol.* **18**, 2854-2865

Figure S1

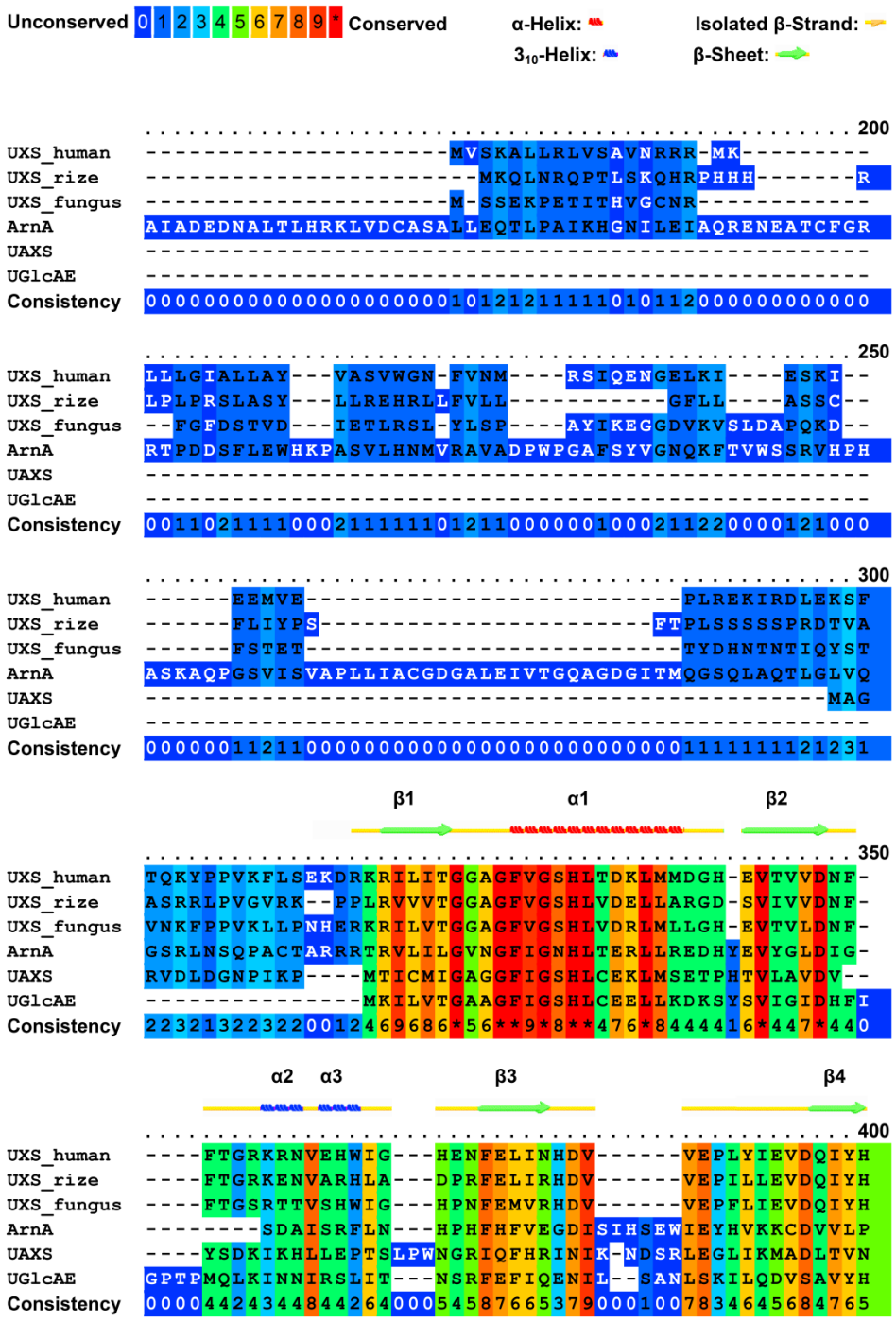
Unconserved 0 1 2 3 4 5 6 7 8 9 * Conserved
α-Helix:
3₁₀-Helix:
Isolated β-Strand:
β-Sheet:
UXS_human
UXS_rize
UXS_fungus
ArnA
UAXS
UGlcAE
Consistency
β1
α1
β2
α2
α3
β3
β4

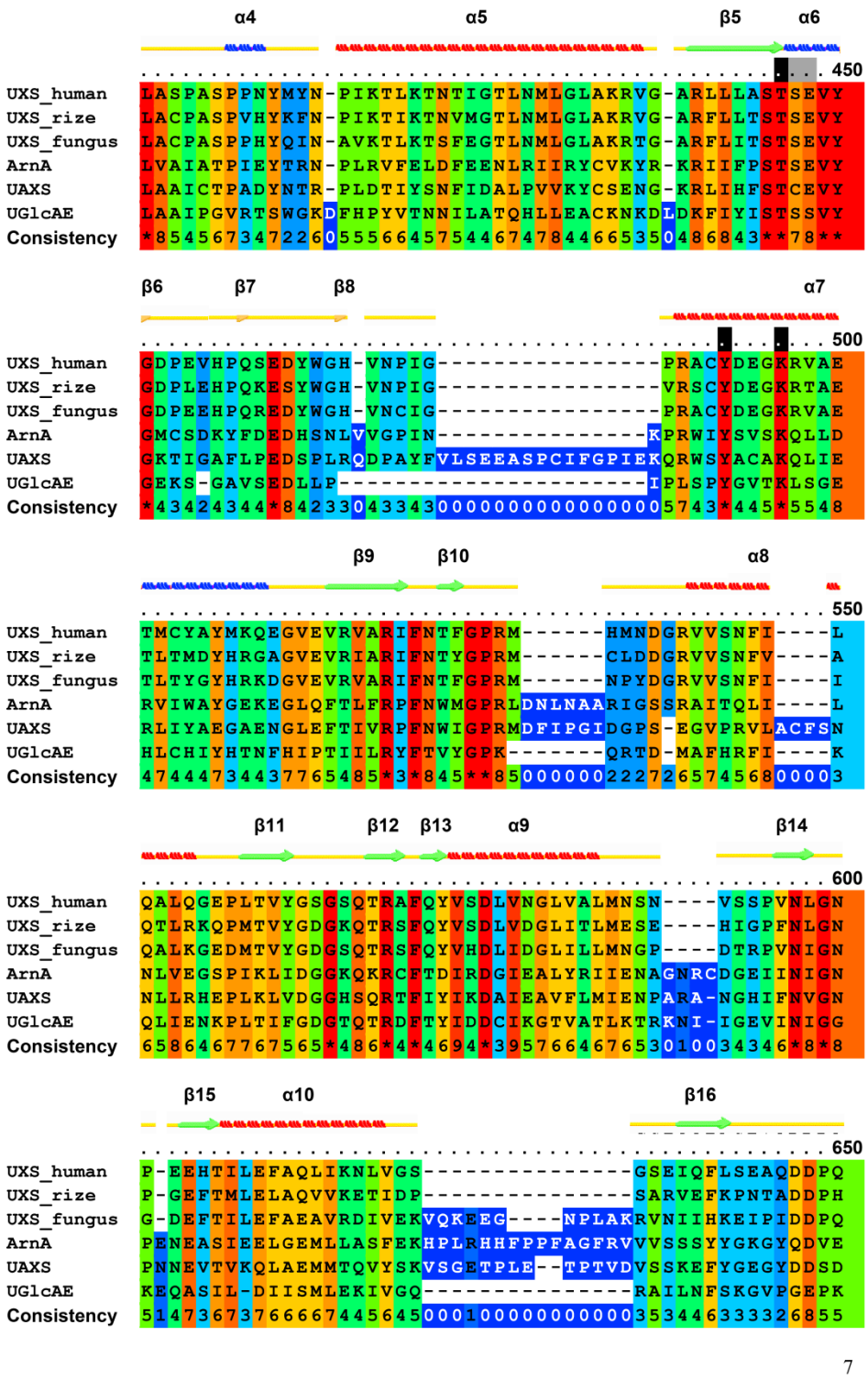
α4 α5 β5 α6
450
UXS_human LASPASPPNYMYN-PIKTLKTNTIGTLNMLGLAKRVG-ARLLLASTSEVY
UXS_rize LACPASPVHYKFN-PIKTIKTNVMGTLNMLGLAKRVG-ARFLLTSTSEVY
UXS_fungus LACPASPPHYQIN-AVKTLKTSFEGTLNMLGLAKRTG-ARFLITSTSEVY
ArnA LVAIATPIEYTRN-PLRVFELDFEENLRIIRYCVKYR-KRIIFPSTSEVY
UAXS LAAICTPADYNTR-PLDTIYSNFIDALPVVKYCSENG-KRLIHFSTCEVY
UGlcAE LAAIPGVRTSWGKDFHPYVTNNILATQHLLEACKNKDLDKFIYISTSSVY
Consistency *8545673472260555664575446747844665350486843**78**
β6 β7 β8 α7
500
UXS_human GDPEVHPQSEDYWGH-VNPIG----------PRACYDEGKRVAE
UXS_rize GDPLEHPQKESYWGH-VNPIG----------VRSCYDEGKRTAE
UXS_fungus GDPEEHPQREDYWGH-VNCIG----------PRACYDEGKRVAE
ArnA GMCSDKYFDEDHSNLVVGPIN----------KPRWIYSVSKQLLD
UAXS GKTIGAFLPEDSPLRQDPAYFVLSEEASPCIFGPIEKQRWSYACAKQLIE
UGlcAE GEKS-GAVSEDLLP----------IPLSPYGVTKLSGE
Consistency *434243 44*842330433430000000000000005743*445*5548
β9 β10 α8
550
UXS_human TMCYAYMKQEGVEVRVARIFNTFGPRM------HMNDGRVVSNFI----L
UXS_rize TLTMDYHRGAGVEVRIARIFNTYGPRM------CLDDGRVVSNFV----A
UXS_fungus TLTYGYHRKDGVEVRVARIFNTFGPRM------NPYDGRVVSNFI----I
ArnA RVIWAYGEKEGLQFTLFRPFNWMGPRLDNLNAARIGSSRAITQLI----L
UAXS RLIYAEGAENGLEFTIVRPFNWIGPRMDFIPGIDGPS-EGVPRVLACFSN
UGlcAE HLCHIYHTNFHIPTIILRYFTVYGPK-------QRTD-MAFHRFI----K
Consistency 474447344377654 85*3*845**850000002227265745680000 3
β11 β12 β13 α9 β14
600
UXS_human QALQGEPLTVYGSGSQTRAFQYVSDLVNGLVALMNSN----VSSPVNLGN
UXS_rize QTLRKQPMTVYGDGKQTRSFQYVSDLVDGLITLMESE----HIGPFNLGN
UXS_fungus QALKGEDMTVYGDGSQTRSFQYVHDLIDGLILLMNGP----DTRPVNIGN
ArnA NLVEGSPIKLIDGGKQKRCFTDIRDGIEALYRIIENAGNRCDGEIINIGN
UAXS NLLRHEPLKLVDGGHSQRTFIYIKDAIEAVFLMIENPARA-NGHIFNVGN
UGlcAE QLIENKPLTIFGDGTQTRDFTYIDDCIKGTVATLKTRKNI-IGEVINIGG
Consistency 658646776756 5*486*4*4694*39576646765301003434 6*8*8
β15 α10 β16
650
UXS_human P-EEHTILEFAQLIKNLVGS----------GSEIQFLSEAQDDPQ
UXS_rize P-GEFTMLELAQVVKETIDP----------SARVEFKPNTADDPH
UXS_fungus G-DEFTILEFAEAVRDIVEKVQKEEG----NPLAKRVNIIHKEIPIDDPQ
ArnA PENEASIEELGEMLLASFEKHPLRHHFPPFAGFRVVVSSSYYGKGYQDVE
UAXS PNNEVTVKQLAEMMTQVYSKVSGETPLE--TPTVDVSSKEFYGEGYDDSD
UGlcAE KEQASIL-DIISMLEKIVGQ----------RAILNFSKGVPGEPK
Consistency 5147367376666744564500010000000000035344633332 6855
7

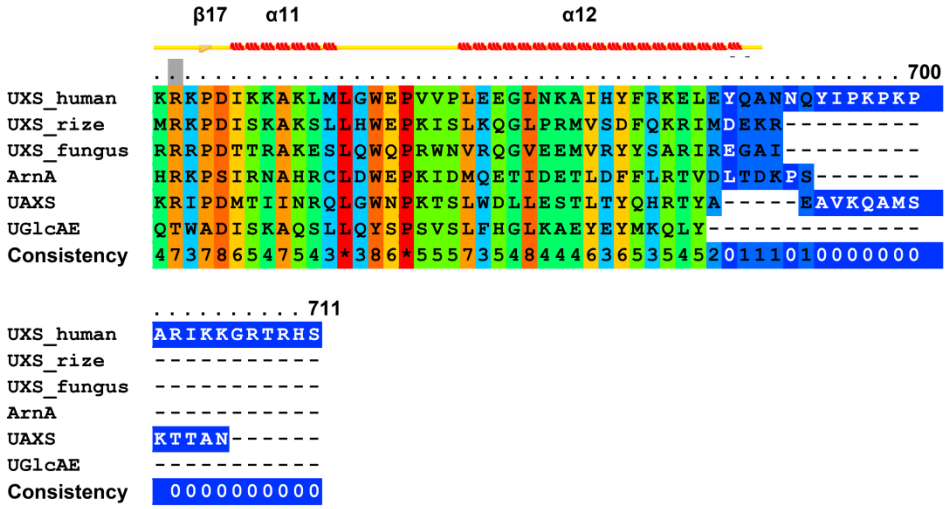
β17
α11
α12
700
UXS_human KRKPDIKKAKLMLGWEPVVPLEEGLNKAIHYFRKELEYQANNQYIPKPKP
UXS_rize MRKPDISKAKSLLHWEPKISLKQGLPRMVSDFQKRIMDEKR---------
UXS_fungus RRRPDTTRAKESLQWQPRWNVRQGVEEMVRYYSARIREGAI---------
ArnA HRKPSIRNAHRCLDWEPKIDMQETIDETLDFFLRTVDLTDKPS-------
UAXS KRIPDMTIINRQLGWNPKTSLWDLLESTLTYQHRTYA-----EAVKQAMS
UGlcAE QTWADISKAQSLLQYSPSVSLFHGLKAEYEYMKQLY----------
Consistency 4737865475 43*386*5557354844463653545201110100000 00
711
UXS_human ARIKKGRTRHS
UXS_rize ----------
UXS_fungus ----------
ArnA ----------
UAXS KTTAN------
UGlcAE ----------
Consistency 0000000000

8

Figure S2

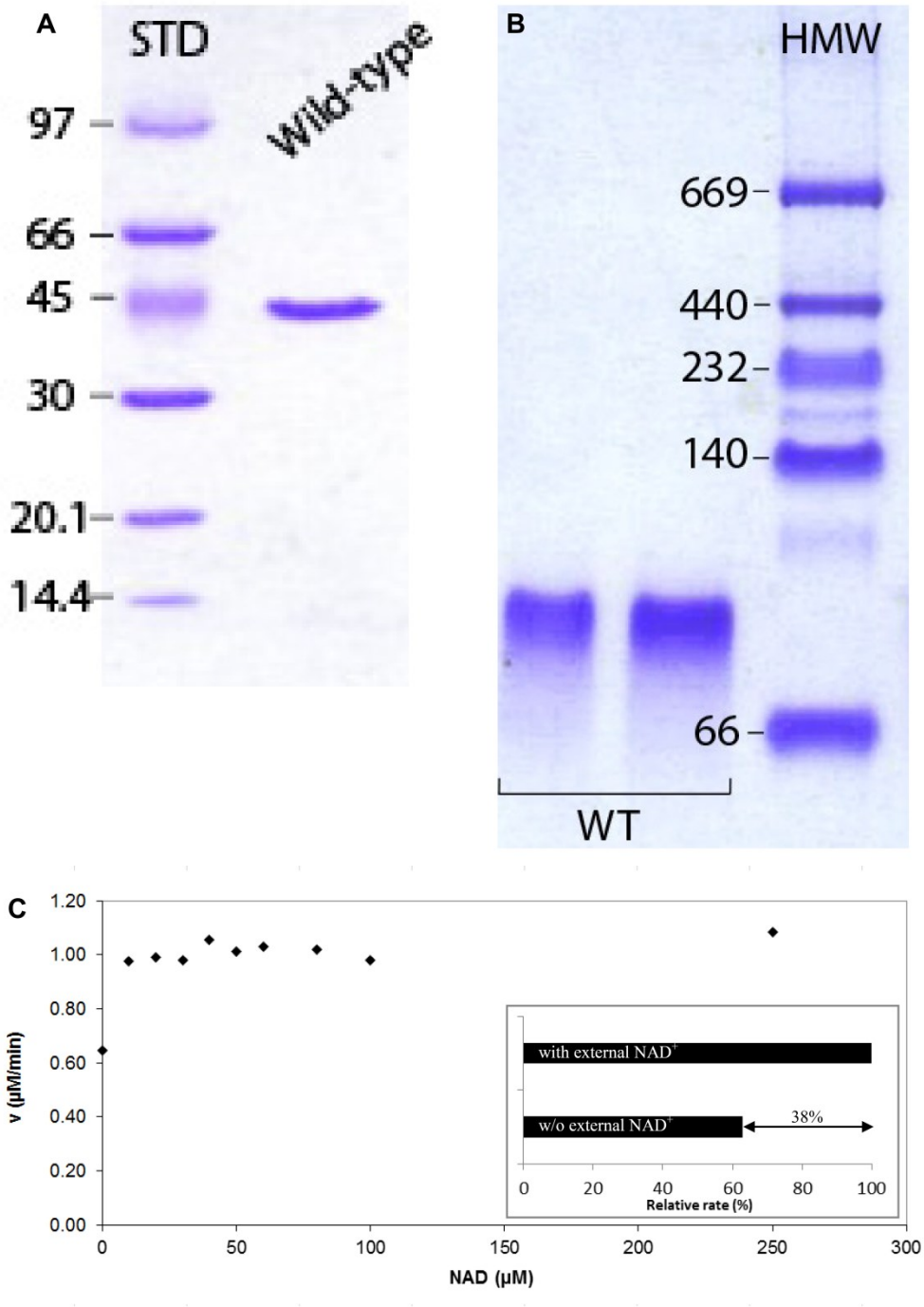
A
STD
Wild-type
97
66
45
30
20.1
14.4
B
HMW
669
440
232
140
66
WT
C
v (μM/min)
NAD (μM)
with external NAD+
w/o external NAD+
38%
Relative rate (%)

9

Figure S3

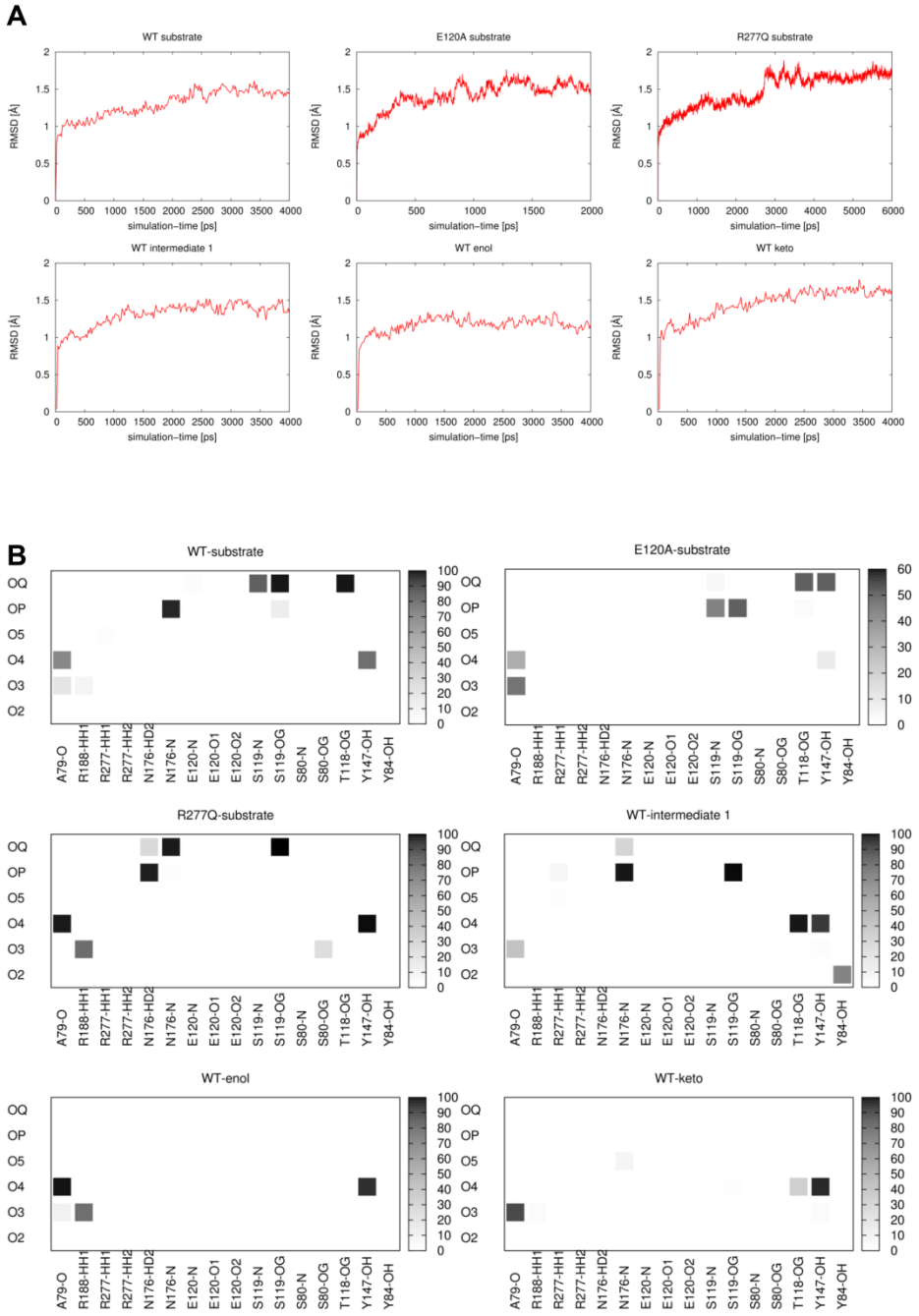
A
WT substrate
E120A substrate
R277Q substrate
WT intermediate 1
WT enol
WT keto
RMSD [Å]
simulation−time [ps]
B
WT-substrate
E120A-substrate
R277Q-substrate
WT-intermediate 1
WT-enol
WT-keto
OQ
OP
O5
O4
O3
O2
A79-O
R188-HH1
R277-HH1
R277-HH2
N176-HD2
N176-N
E120-N
E120-O1
E120-O2
S119-N
S119-OG
S80-N
S80-OG
T118-OG
Y147-OH
Y84-OH

10

Figure S4

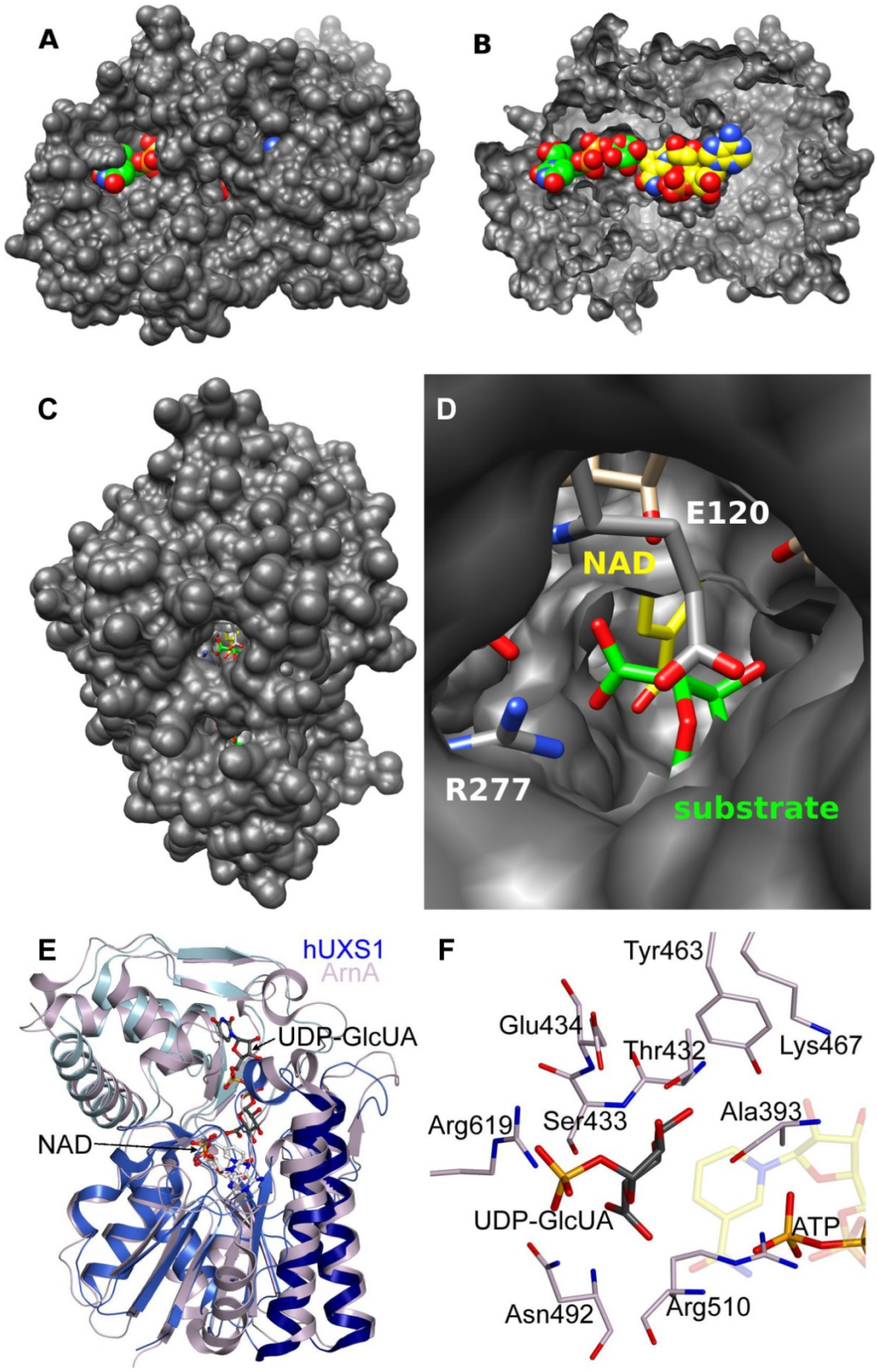
A
B
C
D
E120
NAD
R277
substrate
E
hUXS1
ArnA
UDP-GlcUA
NAD
F
Tyr463
Glu434
Thr432
Lys467
Arg619
Ser433
Ala393
UDP-GlcUA
ATP
Asn492
Arg510

11

Figure S5

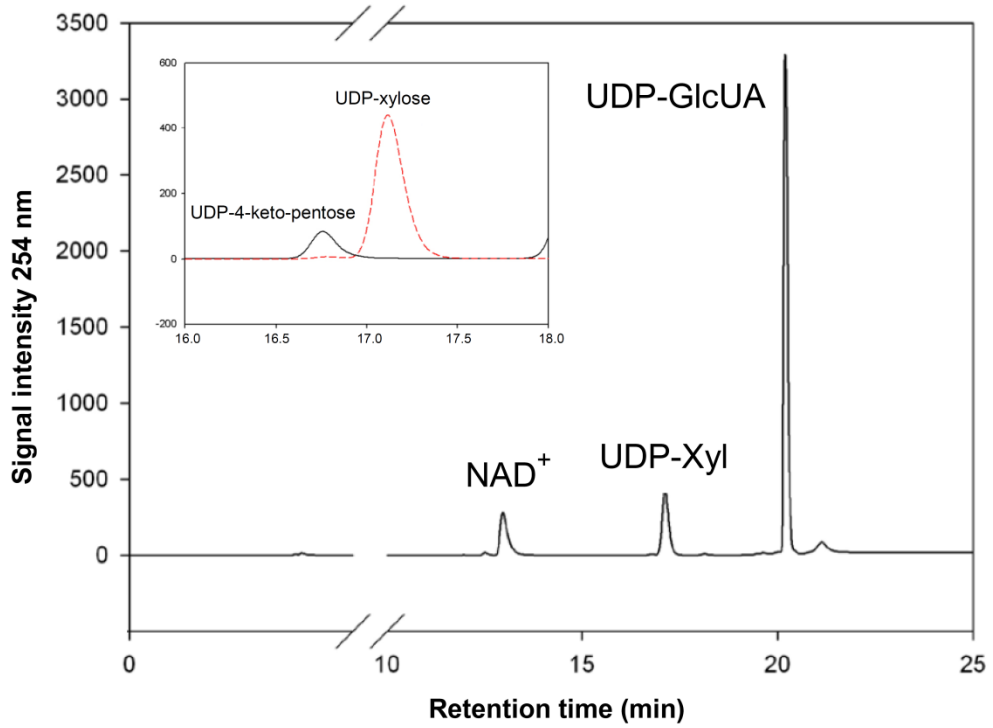
Signal intensity 254 nm
3500
3000
2500
2000
1500
1000
500
0
UDP-xylose
UDP-4-keto-pentose
600
400
200
0
-200
16.0
16.5
17.0
17.5
18.0
UDP-GlcUA
NAD+
UDP-Xyl
0
10
15
20
25
Retention time (min)

12

Catalytic mechanism of human UDP-xylose synthase: significance of conserved residues in the active site

Note

Catalytic mechanism of human UDP-xylose synthase: significance of conserved residues in the active site

Thomas Eixelsberger[1], Hansjörg Weber[2], Bernd Nidetzky[1,3,*]

[1] Institute of Biotechnology and Biochemical Engineering, Graz University of Technology, NAWI Graz, Petersgasse 12/I, A-8010 Graz, Austria

[2] Institute of Organic Chemistry, Graz University of Technology, NAWI Graz, Stremayrgasse 9, A-8010 Graz, Austria

[3] Austrian Centre of Industrial Biotechnology, Petersgasse 14, A-8010 Graz, Austria

* Corresponding author; e-mail: bernd.nidetzky@tugraz.at, tel.: +43 316 873 8400, fax: +43 316 873 108400

Abstract

Uridine 5'-diphosphate (UDP)-xylose (UDP-Xyl) synthase (UXS) catalyzes the three-step oxidative decarboxylation of UDP-glucuronic acid (UDP-GlcUA) to UDP-Xyl. A remarkable feature of this transformation is distortion of the pyranoside ring by UXS during the reaction. The closely related UDP-glucuronic acid 4-epimerase (UGAE) interconverts UDP-GlcUA and UDP-galacturonic acid (UDP-GalUA) in a highly similar manner via oxidation and reduction at *C*-4 of the sugar ring, but is able to prevent decarboxylation of UDP-4-keto-GlcUA. Human UXS (hUXS) and UGAE from *Arabidopsis thaliana* exhibit high structural similarity in the active site, with the catalytic triad being conserved. Two other catalytically important residues in hUXS (Glu^{120} and Arg^{277}) are replaced by Ser and Thr in the UGAE group. Additionally, Asn^{176}, which participates in substrate binding, is changed to Thr. To evaluate the significance of these substitutions for product specificity, we analyzed mutants of hUXS for *C*-4 epimerization activity. Although the mutants did not produce UDP-GalUA, they gave interesting insights into structure-function relationships in UXS, suggesting that interaction between active site and overall enzyme structure rather than distinct conserved residues are decisive for product formation.

Keywords: UDP-xylose, UDP-galacturonic acid, epimerization, decarboxylation, UDP-xylose synthase

Uridine 5‘-diphosphate (UDP)-xylose (UDP-Xyl) synthase (UXS) is responsible for production of UDP-Xyl from UDP-glucuronic acid (UDP-GlcUA) in numerous organisms, from bacteria to mammals.[1] The UXS reaction is a complex oxidative decarboxylation in three distinct steps that proceeds via UDP-4-keto-GlcUA and UDP-4-keto-Xyl intermediates (Scheme 1).[2,3] Its product, UDP-Xyl, plays a central role in cell physiology.[4,5] In mammals, it is especially important in synthesis of extracellular matrix proteoglycans, as the glycosaminoglycan side chains of these macromolecules are attached to a core protein via a xylosyl residue in a common tetrasaccharide linker.[6,7] Loss of UXS activity leads to a defective extracellular matrix and malformation of various tissues, e.g. the bone.[8] The sequence of UXS is highly conserved and bacterial forms share 57% sequence identity with human UXS (hUXS).[8] The enzyme belongs to the diverse group of “extended short-chain dehydrogenases/reductases (SDR)” that have nucleotide sugar epimerization and dehydration as their main activities.[9] One remarkable feature of UXS is that the pyranoside ring of UDP-GlcUA is heavily distorted upon being bound by the enzyme ($^4C_1 \rightarrow B_{O,3}$), and adopts different conformations during the catalytic cycle (^2S_O, $^2H_1$, $^4C_1$), which is strongly conducive to catalysis (Scheme 1).[3] This is achieved through six residues in the active site that are almost invariant in the UXS group of enzymes. Three of these residues (Thr, Tyr and Lys) represent a typical SDR catalytic triad, while Ser, Glu and Arg are distinct features of UXS. Replacement of Tyr by Phe or Arg by Asn resulted in disruption of the catalytic cycle and release of UDP-4-keto-Xyl and NADH.[3]

Within the group of extended SDRs, UDP-glucuronic acid 4-epimerases (UGAEs) are closely related to UXS and catalyze the interconversion of UDP-GlcUA and UDP-galacturonic acid (UDP-GalUA) in a highly similar transformation via oxidation and reduction at *C*-4.[10-12] However, UGAE is able to prevent decarboxylation of UDP-4-keto-GlcUA, in contrast to UXS. Different accommodation of the glucuronic acid moiety in the active site was suggested as possible explanation, as the pattern of residue conservation in the active site of UGAE

differs from that of UXS.[3] While the catalytic triad is essentially unchanged, Glu is replaced by Ser and Arg by Thr in the UGAE group. Additionally, an Asn residue not directly involved in catalysis in UXS is altered to Thr. These changes are highly conserved among UGAE (Figure 1A), however, the impact of these differences on the product pattern has not yet been investigated. As a crystal structure of UGAE was not available, we used the Phyre2 suite to create a homology model of the enzyme from *Arabidopsis thaliana* (*At*UGAE).[13] Comparison with the crystal structure of hUXS revealed very high structural similarity in the active site (Figure 1B), although sequence identity between *At*UGAE and hUXS was only 22%. Therefore, it was suspected that replacement of Glu^{120}, Asn^{176} and/or Arg^{277} in the active site of hUXS by the respective amino acids found in *At*UGAE could result in the mutant enzymes producing UDP-GalUA or anther product with altered stereochemistry at *C*-4. Evidence gained from analysis of these mutants could thus be helpful in identifying the origin of the unique features of UXS and getting a better understanding of structure-function relationships in the enzyme. Additionally, knowledge about the interesting residue conservation pattern within different SDR subgroups could be enhanced.[14]

Starting from wild-type hUXS1, we created Glu^{120}→Ser (E120S) and Arg^{277}→Thr (R277T) single mutants, a Glu^{120}→Ser/Arg^{277}→Thr (E120S/R277T) double mutant and a Glu^{120}→Ser/Asn^{176}→Thr/Arg^{277}→Thr (E120S/N176T/R277T) triple mutant using established protocols.[15] Wild-type and mutant enzymes were expressed in *E. coli* BL21 Gold (DE3), and after His_6-tag affinity chromatography purification, SDS-PAGE showed one band at 39 kDa, in accordance with the expected molecular weight of 38.6 kDa.[3] Expression yields of the mutants were comparable to wild-type hUXS1, however, all mutants showed considerably lower initial activities (at least 1000-fold reduction). R277T, the double and the triple mutant showed formation of NADH upon incubation with UDP-GlcUA (Figure 2), in contrast to E120S and wild-type enzyme (data not shown). Measurement of absorption spectra in the end of the reaction confirmed that indeed NADH was present and the increase in absorption did

not only represent unspecific scattering, e.g. due to enzyme denaturation. As this result was indicative of a catalytic cycle that does not (or only partly) involve reduction of an intermediate, which is a prerequisite for formation of UDP-GalUA, a complete switch from oxidative decarboxylation to *C*-4 epimerization by exchange of the selected active site residues seemed unlikely. Analysis of the reactions by HPLC and capillary zone electrophoresis showed appearance of unknown peaks, but identification of the formed compounds was unsuccessful, as authentic standards for reaction intermediates and products were unavailable or could not be separated from the substrate, respectively.

^{1}H NMR analysis was therefore chosen to elucidate the product pattern of the mutant enzymes. Suspected compounds included UDP-GalUA, UDP-Xyl, UDP-4-keto-GlcUA and UDP-4-keto-Xyl. The results are summarized in Table 1. E120S exclusively produced UDP-Xyl, not even traces of UDP-4-keto-Xyl could be detected, in contrast to a Glu^{120}→Ala mutant investigated in previous studies (Figure 3).[3] Glu^{120}, although highly conserved in UXS, therefore does not seem to be an essential residue determining product specificity and is not necessary for formation of UDP-Xyl. Investigation of the R277T mutant showed that mainly UDP-4-keto-Xyl, but also small amounts of UDP-Xyl were formed, similar to an Arg^{277}→Asn (R277Q) mutant studied previously.[3] The products formed by R277T contained two deuterium atoms at *C*-5 when the reaction was done in D_2O (Figure 3), in contrast to the wild-type enzyme, which showed single deuteration (from protonation of the enolate intermediate; see Scheme 1). In the R277Q mutant, this effect was ascribed to a water molecule in the active site, allowing for D/H exchange, which was excluded in the wild-type through a different hydrogen bonding network and space restrictions due to the longer Arg^{277} side group.[3] Therefore, a similar impact of the R277T mutation likely seemed to be the reason for the observed effect. As mutation of Arg^{277} was previously shown to influence accommodation of UDP-4-keto-GlcUA in the active site, but this compound could not be detected in the R277T reaction mixture, we used *in situ* ^{1}H NMR measurement to check for

transient formation of this intermediate (Figures 4A and 4B). However, within 70 hrs of reaction, no hints for formation of a non-decarboxylated intermediate could be found. Thus, replacement of Arg^{277} by Thr did not aid in preventing decarboxylation. Interestingly, the E120S/R277T double mutant did not produce any UDP-Xyl, but only UDP-4-keto-Xyl (Figure 3). The E120S single mutant, in contrast, formed only UDP-Xyl (see above). The effect of the E120S substitution therefore seems to depend on the active site structure, and a direct catalytic effect of the second substitution is less likely than different accommodation of the pyranoside ring of substrate and intermediates in the active site of the double mutant. This could align it better for initial oxidation and decarboxylation, but worse for reduction of UDP-4-keto-Xyl by NADH and Tyr^{147}. This is strengthened by the fact that activity of E120S/R277T was considerably increased compared to R277T. Another remarkable effect is that only one deuterium is found at *C*-5 of UDP-4-keto-Xyl produced by the double mutant. This result indicates that space restriction due to Arg^{277} in wild-type hUXS1 cannot be the only reason for single deuteration, as in the double mutant one would expect even more space due to the smaller Ser^{120} side chain. However, it is possible that here water is excluded from the active site due to the different binding between the UDP-4-keto-GlcUA intermediate and the enzyme, which would support the finding of higher activity in the double mutant. However, unfortunately also E120S/R277T did not show formation of UDP-4-keto-GlcUA, UDP-GalUA or the corresponding decarboxylated analogue in an *in situ* ^{1}H NMR experiment over 90 hrs (Figures 4C and 4D). The E120S/N176T/R277T triple mutant only formed UDP-4-keto-Xyl with one deuterium at *C*-5 at a very low rate, indicating that substitution of Asn^{176} had no effect on product specificity (Figure 3). In both *in situ* experiments (R277T and E120S/R277T, respectively) rise of a small signal around 5.60 ppm could be detected (Figures 4A and 4C). However, two-dimensional NMR spectroscopy of an E120S/R277T reaction mixture showed small amounts of GlcUA 1-phosphate, e.g. degradation of UDP-GlcUA without formation of UDP-4-keto-Xyl or UDP-Xyl had occurred. This can be ascribed to a

low pyrophosphorylase activity that is not detectable in wild-type hUXS, as it was reported for other enzymes containing the Rossmann fold motif.[16,17]

Although the *in silico* determined differences between UXS and UGAE seemed suitable to explain the unique activities of the enzymes, it was not possible to detect any *C*-4 epimerization activity in the created hUXS1 mutants. Especially as the mode of accommodation of substrate/intermediate is an essential factor in catalysis, our data suggest that the complex transformations catalyzed by UXS and UGAE depend on carefully interrelated interactions between active site residues and the overall structure of the enzyme rather than on distinct amino acids alone.[18] This is in accordance with the reaction catalyzed by UDP-apiose/UDP-Xyl synthase (UAXS), whose active site also shows high similarity to UXS (or UGAE; respectively), but leads to a very different transformation involving decarboxylation and pyranoside ring contraction.[19]

1. Experimental

1.1 Chemicals and enzymes

UDP-D-glucuronic acid (> 98% purity) was purchased from Sigma-Aldrich (Vienna, Austria) and NAD^+ (> 98% purity) was obtained from Roth (Karlsruhe, Germany). All other chemicals were purchased either from Sigma-Aldrich or Roth and were of the highest purity available. Site-directed mutagenesis of hUXS1 was done using a reported two-stage PCR protocol in which a pET-derived expression vector (p11) encoding the wild-type enzyme was used as template.[15] An expression strain was created by transformation of electro-competent *E. coli* BL21 Gold (DE3) after the gene had been sequenced to confirm introduction of the desired mutations. Expression and purification of wild-type and mutant hUXS1 were done as described previously.[3] Purified enzymes were stored at -70° C.

1.2 Enzymatic assays

Reactions were performed at 37 °C on a Thermomixer Comfort (Eppendorf, Hamburg, Germany) without agitation. If not stated otherwise, 2 mM UDP-GlcUA and 2.5 mM NAD^+ in 50 mM potassium phosphate buffer (PPB) pH 7.5 were used. The hUXS1 concentration varied depending on the experiment and is mentioned individually. Samples were taken in regular intervals, as indicated. For stopping the reaction, samples were heated to 99 °C for 5 min or mixed with acetonitrile (1:1 ratio). Online NADH measurements and UV-Vis spectra were recorded using a Beckman Coulter DU800 spectrophotometer (Beckman Coulter GmbH, Vienna, Austria) with temperature-controlled sample holder (λ = 340 nm, T = 37 °C).

1.3 High performance liquid chromatography

Samples were analyzed on an Agilent 1200 HPLC system equipped with a 5 mm Zorbax SAX analytical HPLC column (4.6 × 250 mm; Agilent, Santa Clara, CA, USA) and a UV detector (λ = 262 nm). An injection volume of 30 µL, a temperature of 25 °C and a flow rate of 1.5 mL min^{-1} were used in analysis. For elution, an isocratic flow with 5 mM PPB (pH 3.2) over 5 min was followed by a linear gradient up to 360 mM PPB over 20 min. The column was washed (15 min each) with 600 mM and 5 mM PPB after each analysis. Authentic standards were used for calibration.

1.4 Capillary zone electrophoresis

Capillary zone electrophoresis analyses were performed at 18 °C on an HP 3D CE system (Hewlett Packard, Palo Alto, CA, USA) equipped with an extended light path fused silica capillary (5.6 mm × 56 cm) from Agilent and a diode array detector (λ = 262 nm). The electrophoresis buffer was 20 mM sodium tetraborate (pH 9.3). Prior to each sample, the capillary was pre-conditioned with 2 min H_2O, 2 min NaOH 0.1 M, 3 min H_2O and 10 min electrophoresis buffer. Samples were injected by pressure (50 mbar, 5 s or 10 s) and analyzed

with a voltage of up to 30 kV for 20 min. Preparation of the samples was done according to HPLC analysis except that caffeine was added as internal standard.

1.5 NMR spectroscopy

A Varian (Agilent) INOVA 500-MHz NMR spectrometer and the VNMRJ 2.2D software were used for all measurements. ^{1}H NMR spectra (499.89 MHz) were measured on a 5 mm indirect detection PFG-probe. Enzymatic *in situ* reactions were performed at 37 °C in a total volume of 600 µL potassium phosphate buffer 50 mM pD 7.5 in D_2O containing 2 mM UDP-GlcUA, 2.5 mM NAD^+ and 100 µM mutant hUXS1. The pD was determined as pH meter reading plus 0.4.[20] ^{1}H NMR spectra were recorded with pre-saturation of the water signal by a shaped pulse. Standard pre-saturation sequence was used: relaxation delay 2 s; 90° proton pulse; 2.048 s acquisition time; spectral width 8 kHz; number of points 32 k. Arrayed spectra were acquired with an array of pre-acquisition delay of 120 min. ACD/NMR Processor Academic Edition 12.0 (Advanced Chemistry Development Inc., Toronto, Canada) was used for evaluation of spectra.

Acknowledgement

Financial support from the Austrian Science Fund FWF (Project W901-B05 DK Molecular Enzymology) is gratefully acknowledged. We thank Prof. Klaus Zangger from the Institute of Chemistry at the University of Graz for performing two-dimensional NMR analysis.

References

1 Moriarity, J. L.; Hurt, K. J.; Resnick, A. C.; Storm, P. B.; Laroy, W.; Schnaar, R. L.; Snyder, S. H. *J. Biol. Chem.* **2002**, 277, 16968-16975.

2 Schutzbach, J. S., Feingold, D. S. *J. Biol. Chem.* **1970**, 245, 2476-2482.

3 Eixelsberger, T.; Sykora, S.; Egger, S.; Brunsteiner, M.; Kavanagh, K. L.; Oppermann, U.; Brecker, L.; Nidetzky, B. *J. Biol. Chem.* **2012**, 287, 31349-31358.

4 Schaefer, L.; Schaefer, R. M. *Cell Tissue Res.* **2010**, 339, 237-246.

5 Theocharis, A. D.; Skandalis, S. S.; Tzanakakis, G. N.; Karamanos, N. K. *FEBS J.* **2010**, 277, 3904-3923.

6 Prydz, K.; Dalen, K. T. *J. Cell Sci.* **2000**, 113, 193-205.

7 Silbert, J. E.; Sugumaran, G. *IUBMB Life* **2002**, 54, 177-186.

8 Eames, B. F.; Singer, A.; Smith, G. A.; Wood, Z. A.; Yan, Y.-L.; He, X.; Polizzi, S. J.; Catchen, J. M.; Rodriguez-Mari, A.; Linbo, T.; Raible, D. W.; Postlethwait, J. H. *Dev. Biol.* **2010**, 341, 400-415.

9 Kavanagh, K. L.; Jörnvall, H.; Persson, B.; Oppermann, U. *Cell. Mol. Life Sci.* **2008**, 65, 3895-3906.

10 Broach, B.; Gu, X.; Bar-Peled, M. *FEBS J.* **2012**, 279, 100-112.

11 Gu, X.; Bar-Peled, M. *Plant Physiol.* **2004**, 136, 4256-4264.

12 Mølhøj, M.; Verma, R.; Reiter, W.-D. *Plant Physiol.* **2004**, 135, 1221-1230.

13 Kelley, L. A.; Mezulis, S.; Yates, C. M.; Wass, M. N.; Sternberg, M. J. E. *Nat. Protoc.* **2015**, 10, 845-858.

14 Tiwari, P.; Singh, N.; Dixit, A.; Choudhury, D. *Proteins: Struct., Funct., Bioinf.* **2014**, 82, 2842-2856.

15 Wang, W. Y.; Malcolm, B. A. *BioTechniques* **1999**, 26, 680-682.

16 Urbaniak, M. D.; Collie, L. T.; Fang, W. X.; Aristotelous, T.; Eskilsson, S.; Raimi, O. G.; Harrison, J.; Navratilova, I. H.; Frearson, J. A.; van Aalten, D. M. F.; Ferguson, M. A. J. *ACS Chem. Biol.* **2013**, 8, 1981-1987.

17 Kleczkowski, L. A.; Decker, D.; Wilczynska, M. *Plant Physiol.* **2011**, 156, 3-10.

18 Polizzi, S. J.; Walsh Jr., R. M.; Peeples, W.B.; Lim, J.-M.; Wells, L.; Wood, Z. A. *Biochemistry* **2012**, 51, 8844-8855.

19 Mølhøj, M.; Verma, R.; Reiter, W.-D. *Plant J.* **2003**, 35, 693-703.

20 Krężel, A.; Bal, W. *J. Inorg. Biochem.* **2004**, 98, 161-166.

21 Simossis, V. A.; Heringa, J. *Nucleic Acids Res.* **2005**, 33, W289-W294.

22 Bar-Peled, M.; Griffith, C. L.; Doering, T. L. *Proc. Natl. Acad. Sci. U. S. A.* **2001**, 98, 12003-12008.

Figure legends

Scheme 1: Catalytic mechanism of hUXS. Distortion of the pyranoside ring during transformation strongly promotes catalysis by optimally aligning the reactive side groups of substrate/intermediate with the active site residues. In wild-type hUXS, deuterium incorporation at *C*-5 of UDP-Xyl originates from protonation of the enolate intermediate by a water molecule present in the active site.

Figure 1: Comparison of hUXS and *At*UGAE. **A**. Multiple sequence alignment (PRALINE[21]) of hUXS and UGAEs from different organisms. It is visible that residues of the catalytic triad are conserved among UXS and UGAE, but distinct UXS features are not present in UGAE and replaced by other conserved residues, respectively. Colored boxes indicate enzymes used for structural comparison. **B**. Alignment of the crystal structure of hUXS with bound UDP and NAD^+ (grey; PDB code 2B69) and a Phyre2-predicted homology model of *At*UGAE (turquoise).[13] The catalytic triad is labeled in green, distinct UXS features that were suspected to be decisive for product formation are labeled in blue.

Figure 2: NADH formation profiles of hUXS mutants (5 µM). **A**. R277T. **B**. E120S/R277T. **C**. E120S/N176T/R277T.

Figure 3: ^{1}H NMR spectra after 19 hrs reaction time. 2 mM UDP-GlcUA and 2.5 mM NAD^+ in 50 mM PPB pH 7.5 in D_2O were incubated with 46 µM E120S (red), 60 µM R277T (green), 80 µM E120S/R277T (blue) or 100 µM E120S/N176T/R277T (orange). Enzyme concentrations were chosen based on expected activity. References containing UDP-GlcUA (grey) and UDP-Xyl (black) produced by 100 µM wild-type hUXS were used for comparison. Consumption of UDP-GlcUA (G) and formation of UDP-4-keto-Xyl (K) and UDP-Xyl (X) are shown by means of the anomeric proton signal.[22] In the area between 3.60 ppm and 4.00 ppm, signals of *H*-5 of UDP-4-keto-Xyl and UDP-Xyl, respectively, indicate single or double deuterium incorporation at *C*-5 (in the reactions of E120S/R277T and

E120S/N176T/R277T a singlet is visible at 3.83 ppm, which is not present in the R277T reaction).

Figure 4: *In situ* ^{1}H NMR measurement of UDP-GlcUA conversion by R277T (**A**) and E120S/R277T (**C**). Signals of UDP-GlcUA (G), UDP-4-keto-Xyl (K), UDP-Xyl (X) and a degradation product (D) are indicated.[22] Time between two spectra is 14 hrs. In case of the double mutant, the first spectrum shown is after 21 hrs. The corresponding progress curves are depicted in Panels **B** (R277T) and **D** (E120S/R277T), with filled circles representing UDP-GlcUA, empty circles UDP-4-keto-Xyl, filled rectangles UDP-Xyl and filled triangles the degradation product.

Tables

Table 1: Comparison of product formation by hUXS1 wild-type and mutants

UXS	UDP-Xyl	UDP-4-keto-Xyl	Degradation	*C*-5 deuteration
wild-type	●	-	n.d.	Single
E120S	●	-	n.d.	Single
R277T	●	●	●	Double
E120S/R277T	-	●	●	Single
E120S/N176T/R277T	-	●	n.d.	Single

n.d.: not determined

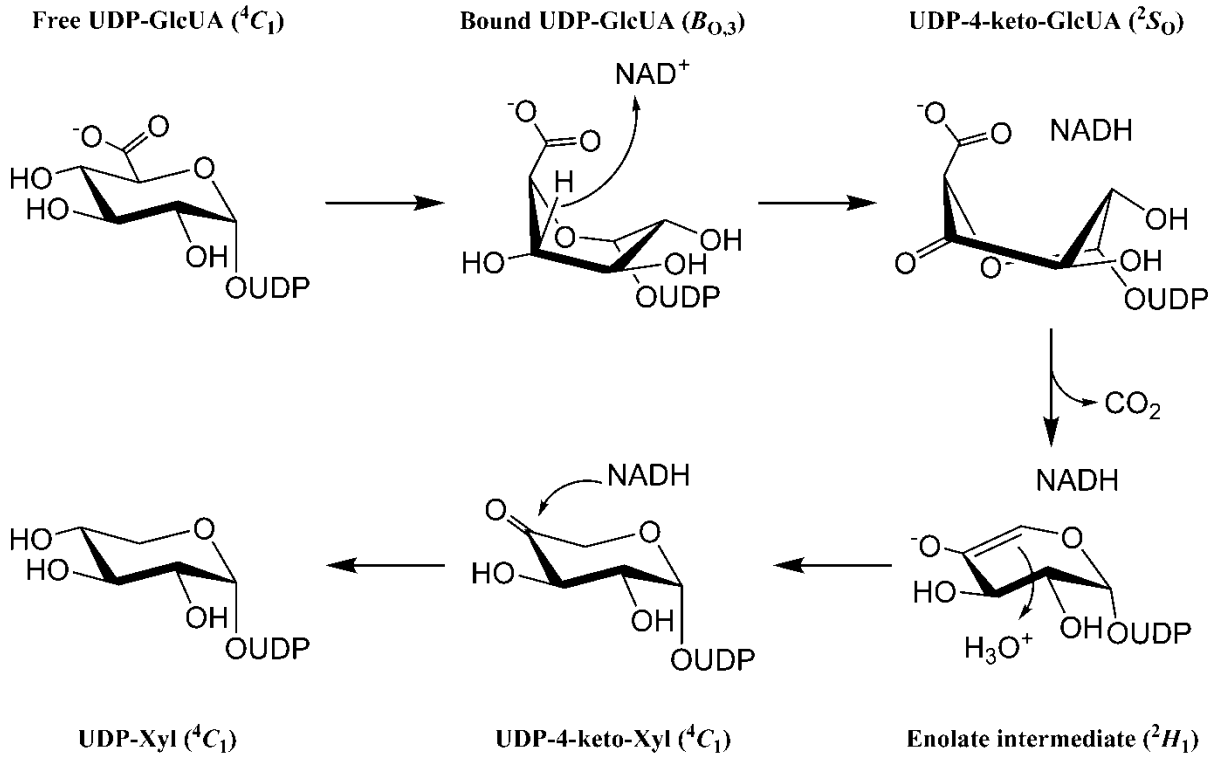
Free UDP-GlcUA ($^4C_1$)
Bound UDP-GlcUA ($B_{O,3}$)
UDP-4-keto-GlcUA (^2S_O)
NAD+
NADH
CO2
NADH
NADH
H3O+
UDP-Xyl ($^4C_1$)
UDP-4-keto-Xyl ($^4C_1$)
Enolate intermediate ($^2H_1$)

Scheme 1.

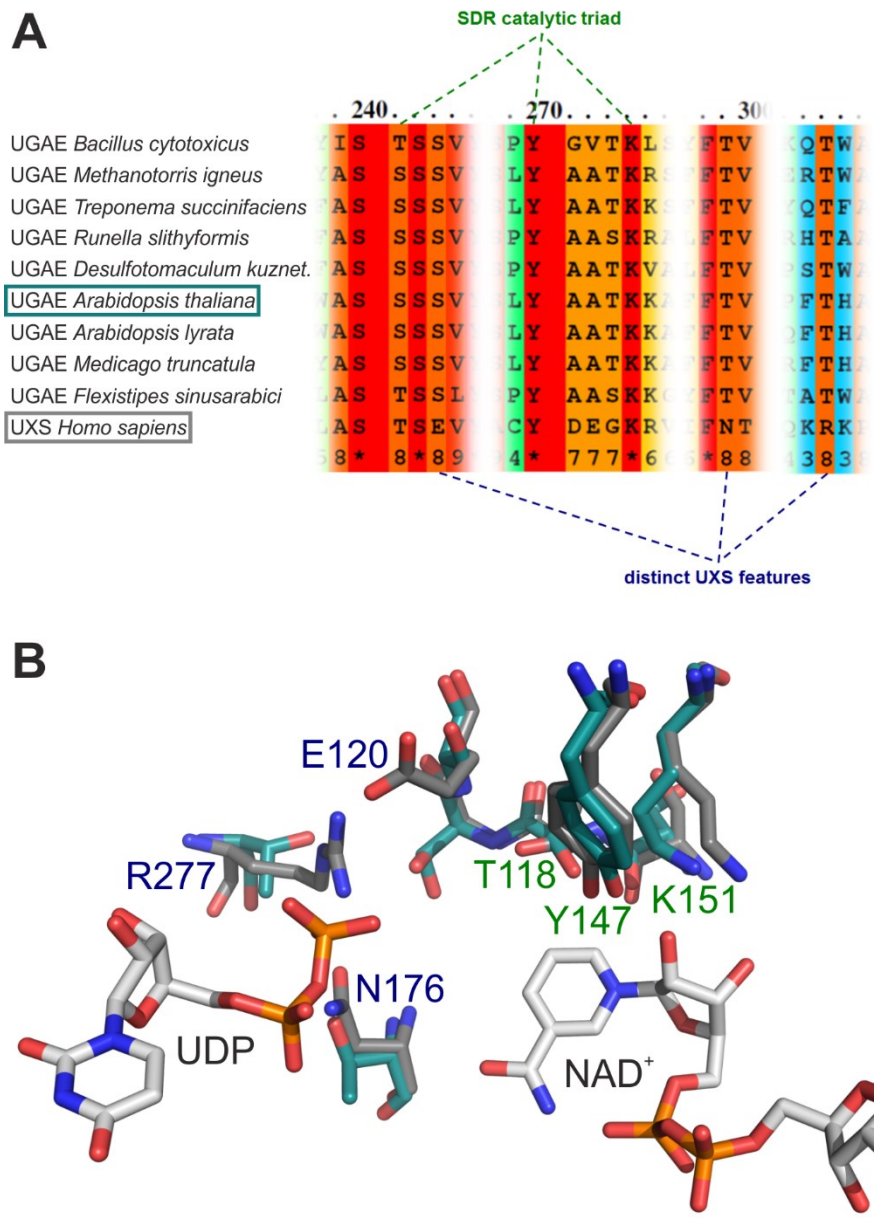
A
SDR catalytic triad
240
270
300
UGAE Bacillus cytotoxicus
UGAE Methanotorris igneus
UGAE Treponema succinifaciens
UGAE Runella slithyformis
UGAE Desulfotomaculum kuznet.
UGAE Arabidopsis thaliana
UGAE Arabidopsis lyrata
UGAE Medicago truncatula
UGAE Flexistipes sinusarabici
UXS Homo sapiens
distinct UXS features
B
E120
R277
T118
Y147
K151
N176
UDP
NAD+

Figure 1.

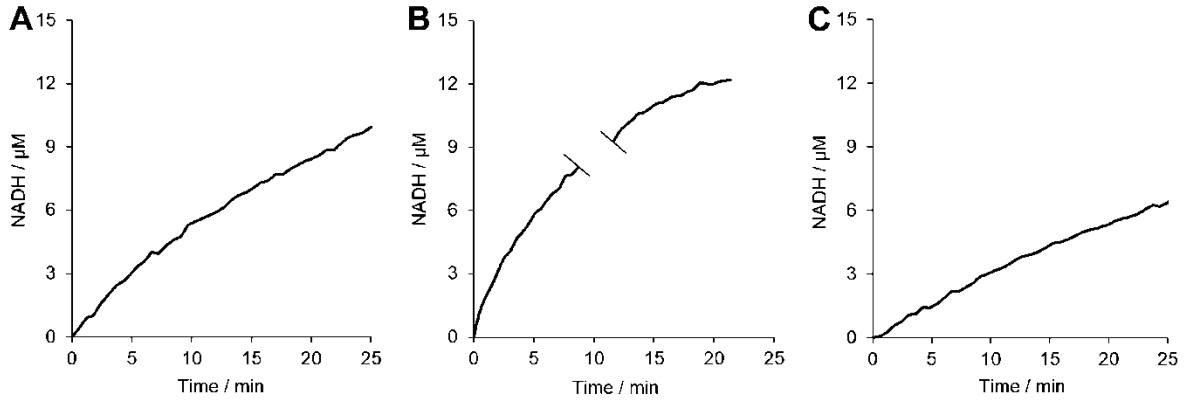

Figure 2.

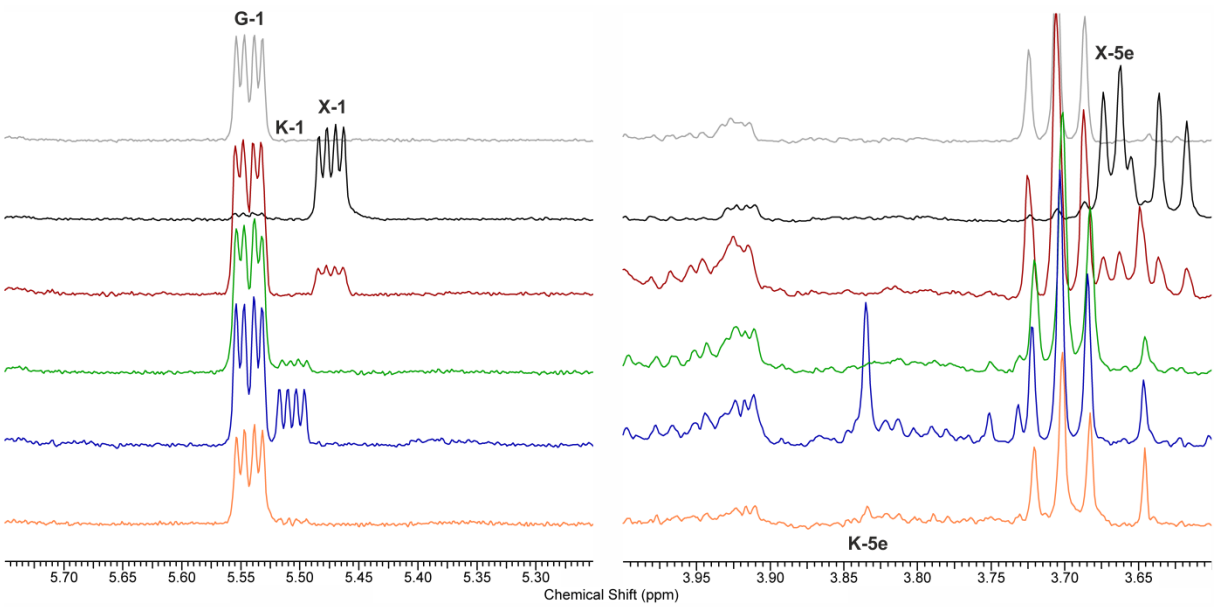
G-1
K-1
X-1
X-5e
K-5e
5.70
5.65
5.60
5.55
5.50
5.45
5.40
5.35
5.30
3.95
3.90
3.85
3.80
3.75
3.70
3.65
Chemical Shift (ppm)

Figure 3.

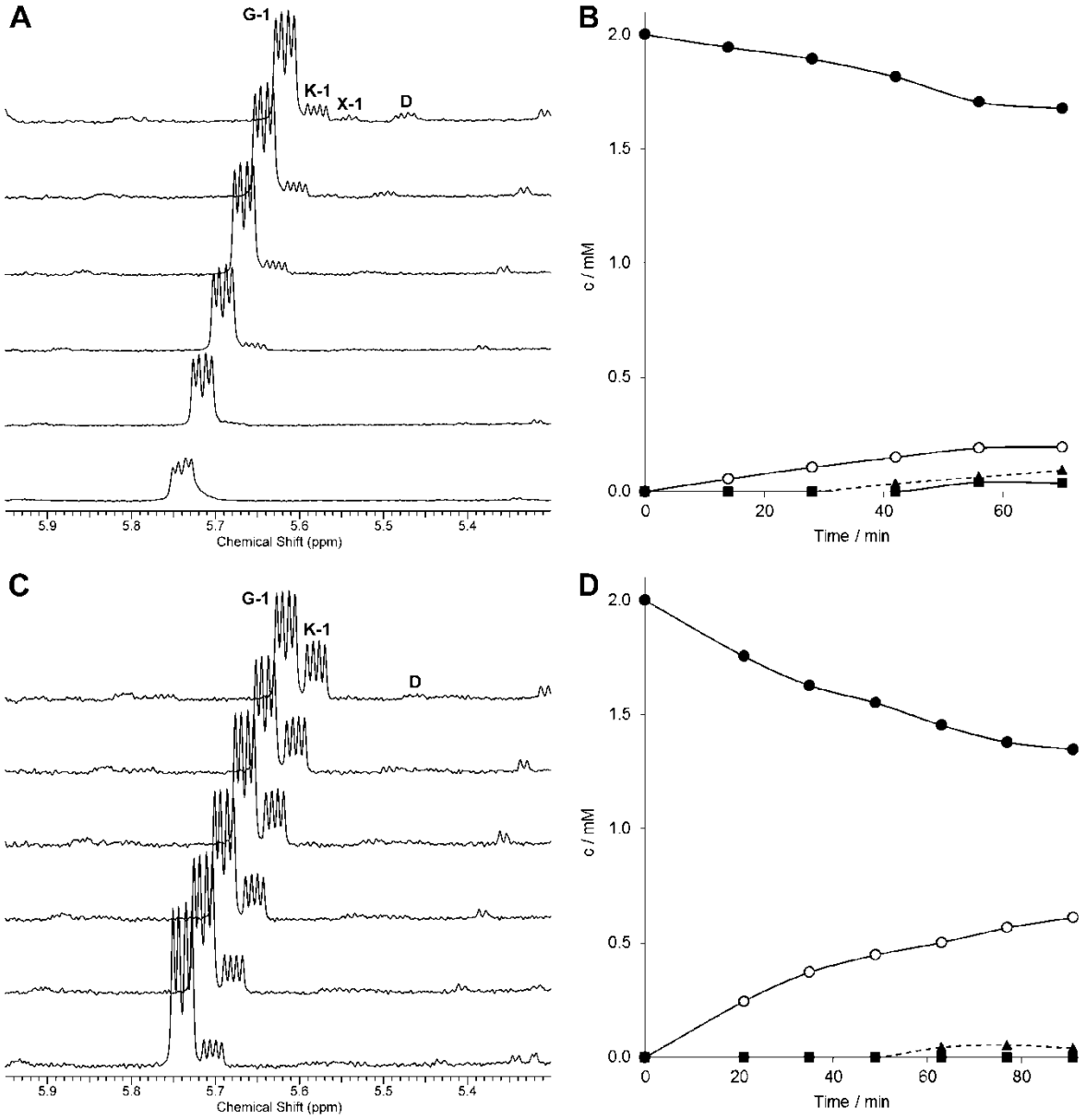
A
G-1
K-1
X-1
D
5.9
5.8
5.7
5.6
5.5
5.4
Chemical Shift (ppm)
B
2.0
1.5
1.0
0.5
0.0
c / mM
0
20
40
60
Time / min
C
G-1
K-1
D
5.9
5.8
5.7
5.6
5.5
5.4
Chemical Shift (ppm)
D
2.0
1.5
1.0
0.5
0.0
c / mM
0
20
40
60
80
Time / min

Figure 4.

Enzymatic redox cascade for one-pot synthesis of uridine 5'-diphosphate xylose from uridine 5'-diphosphate glucose

FULL PAPERS

Advanced Synthesis & Catalysis

DOI: 10.1002/adsc.201400766

Enzymatic Redox Cascade for One-Pot Synthesis of Uridine 5′-Diphosphate Xylose from Uridine 5′-Diphosphate Glucose

Thomas Eixelsberger[a] and Bernd Nidetzky[a,b,*]

[a] Institute of Biotechnology and Biochemical Engineering, Graz University of Technology, NAWI Graz, Petersgasse 12/I, A-8010 Graz, Austria
[b] Austrian Centre of Industrial Biotechnology, Petersgasse 14, A-8010 Graz, Austria
Fax: (+43)-316-873-108400; phone: (+43)-316-873-8400; e-mail: bernd.nidetzky@tugraz.at

Received: August 3, 2014; Published online: November 5, 2014

Supporting information for this article is available on the WWW under http://dx.doi.org/10.1002/adsc.201400766.

Abstract: Synthetic ways towards uridine 5′-diphosphate (UDP)-xylose are scarce and not well established, although this compound plays an important role in the glycobiology of various organisms and cell types. We show here how UDP-glucose 6-dehydrogenase (hUGDH) and UDP-xylose synthase 1 (hUXS) from *Homo sapiens* can be used for the efficient production of pure UDP-α-xylose from UDP-glucose. In a mimic of the natural biosynthetic route, UDP-glucose is converted to UDP-glucuronic acid by hUGDH, followed by subsequent formation of UDP-xylose by hUXS. The nicotinamide adenine dinucleotide (NAD^+) required in the hUGDH reaction is continuously regenerated in a three-step chemo-enzymatic cascade. In the first step, reduced NAD^+ (NADH) is recycled by xylose reductase from *Candida tenuis via* reduction of 9,10-phenanthrenequinone (PQ). Radical chemical re-oxidation of this mediator in the second step reduces molecular oxygen to hydrogen peroxide (H_2O_2) that is cleaved by bovine liver catalase in the last step. A comprehensive analysis of the coupled chemo-enzymatic reactions revealed pronounced inhibition of hUGDH by NADH and UDP-xylose as well as an adequate oxygen supply for PQ re-oxidation as major bottlenecks of effective performance of the overall multi-step reaction system. Net oxidation of UDP-glucose to UDP-xylose by hydrogen peroxide (H_2O_2) could thus be achieved when using an *in situ* oxygen supply through periodic external feed of H_2O_2 during the reaction. Engineering of the interrelated reaction parameters finally enabled production of 19.5 mM (10.5 g L^{-1}) UDP-α-xylose. After two-step chromatographic purification the compound was obtained in high purity (>98%) and good overall yield (46%). The results provide a strong case for application of multi-step redox cascades in the synthesis of nucleotide sugar products.

Keywords: biosynthetic cascade; carbohydrates; multi-enzyme catalysis; nucleotide sugars; UDP-glucose dehydrogenase; UDP-xylose synthase; uridine 5′-diphosphate (UDP)

Introduction

Uridine 5′-diphosphate D-xylose (UDP-xylose; UDP-Xyl) is the donor substrate of xylosyltransferases (XylT) that transfer a xylosyl moiety to different acceptor molecules in the biosynthesis of glycoconjugates. Proteoglycan biosynthesis, for example, is initiated through transfer of a xylosyl residue to the protein acceptor. Xylosyl-containing glycoconjugates play central roles in different cellular processes including signalling, virulence or build-up of the cell wall and the extracellular matrix.[1] In nature, UDP-Xyl is produced by UDP-xylose synthase (UXS; EC 4.1.1.35) *via* oxidative decarboxylation of UDP-glucuronic acid (UDP-GlcUA).[2] UDP-glucose dehydrogenase (UGDH; EC 1.1.1.22) synthesizes UDP-GlcUA in

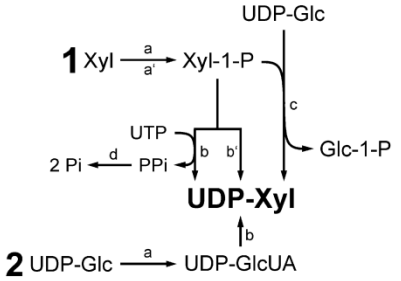

Scheme 1. Generic methods of nucleotide sugar synthesis, exemplified for UDP-Xyl preparation (Xyl-1-P: α-D-xylose 1-phosphate, Glc-1-P: α-D-glucose 1-phosphate).

a NAD^+-dependent two-step oxidation of UDP-glucose (UDP-Glc).[3] UDP-Glc is ultimately derived from glucose *via* the glycolytic intermediate glucose 6-phosphate and glucose 1-phosphate.[4]

Besides its important biological function, UDP-Xyl is a valuable chemical that finds use as substrate for XylT in different research applications. UDP-Xyl is needed for enzyme activity profiling and *in vitro* enzyme characterization. It is also used for *in vivo* studies of XylT function in cell biology and tissue development. UDP-Xyl is an important ligand and inhibitor of enzymes other than XylT, UGDH, for example.[5] To support the different fields in glycobiology research with UDP-Xyl, therefore, an efficient supply of anomerically pure compound would be desirable.[6] However, while synthesis methods for some nucleotide sugars (e.g., UDP-Glc) are well established, synthetic routes or pathways to UDP-Xyl are rare.[4c,7] Although several research groups have enzymatically prepared UDP-Xyl *in vitro*, the resulting product was rarely purified and/or isolated.[7,8]

Generic ways of nucleotide sugar synthesis are shown in Scheme 1.[7] Starting from a monosaccharide as in route (**1**), the product is synthesized enzymatically in two steps, where in the first step (a) a diastereoselective kinase forms an α-configured sugar 1-phosphate using a nucleoside triphosphate donor. The sugar 1-phosphate is then converted into the desired nucleotide sugar *via* step (b) or (c). Catalytic reaction (b) involves a nucleotidyltransferase where nucleoside triphosphate (here: UTP) is the second substrate. However, use of the nucleotidyltransferase reaction constitutes a potentially critical issue in the overall synthetic route, because transformations are often characterized by a highly unfavorable reaction equilibrium, as well as inhibition by pyrophosphate released from nucleoside triphosphate.[9] Provision of thermodynamic "pull" from a coupled reaction where pyrophosphatase (d) is used to catalyze hydrolysis of the pyrophosphate presents a possible solution, but further enhances complexity of the reaction system. Glycosyl exchange with a nucleotide sugar (c) is another approach, but also depends on a nucleotidyltransferase exhibiting a back reaction.

The same synthetic route (**1**) is also pursued with purely chemical methods (a′–b′)[10] or chemo-enzymatically (e.g., a′–c). A recent example for chemical UDP-Xyl synthesis following route (b) is the strategy by Ishimizu et al.[6] where pure UDP-α-Xyl was prepared from activated UMP and xylose 1-phosphate. A yield of 35% after a relatively long reaction time of five days was reported. Errey et al. showed a chemoenzymatic method for production of UDP-Xyl and also of other UDP sugars according to route (a′–c).[8h] UDP-Xyl was enzymatically prepared from chemically synthesized xylose 1-phosphate on a small 500 μL scale (37.5 $g\,L^{-1}$). Chemical methods for UDP-Xyl synthesis starting from D-xylose have also been established, but they often lead to anomeric mixtures of the product.[11] Additionally, *in vivo* enzymatic approaches starting from D-glucose have been reported. For example, Yang et al. used engineered *Escherichia coli* cells for production of various NDP sugars, including UDP-Xyl.[8g]

When an already available nucleotide sugar is used as substrate for UDP-Xyl synthesis, the target molecule is formed either by direct conversion (e.g., sugar oxidation) or in several steps, as shown in route (**2**).[7] Oka et al. established route (**2**) in the yeast *Saccharomyces cerevisiae* where engineered cells synthesized UDP-Xyl from the naturally present UDP-Glc.[8i] From the very limited number of reports about pure UDP-Xyl preparation, the need for an efficient and convenient synthesis is evident. In particular, the preparation of anomerically pure UDP-Xyl is a problem requiring special attention. We present herein a new enzymatic *in vitro* approach according to route (**2**) in Scheme 1. In analogy to the natural biosynthetic pathway, UDP-Glc is converted to UDP-Xyl by UGDH and UXS. Both enzymes exhibit no observable back reaction, which presents a clear advantage in having eliminated thermodynamic restrictions of the nucleotidyltransferase-catalyzed conversion. Comprehensive step-by-step reaction analysis and optimization enabled us to set up an effective biocatalytic system for the production of pure UDP-α-Xyl. The results provide a strong case for synthetic use of multi-step redox cascades in the preparation of nucleotide sugar products.

Results and Discussion

The herein presented system consists of a two-step conversion of UDP-Glc to UDP-Xyl *via* UDP-GlcUA catalyzed by UGDH and UXS, as shown in Scheme 2. Human enzymes (hUGDH and hUXS) were used to

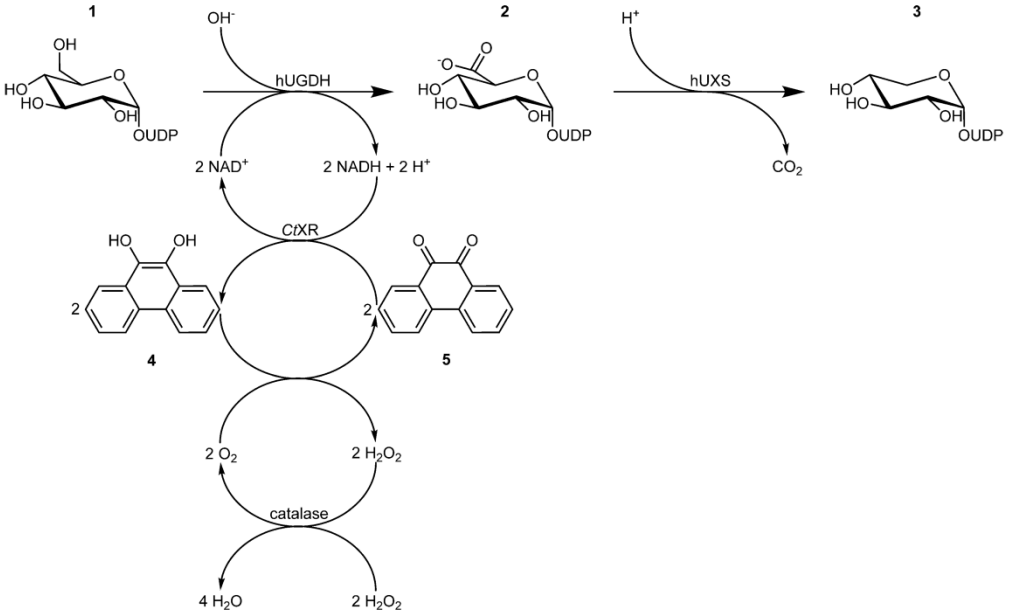

Scheme 2. Chemo-enzymatic cascade transformation employed for synthesis of UDP-Xyl (**3**) from UDP-Glc (**1**) *via* UDP-GlcUA (**2**) through the combined action of hUGDH, hUXS, *Ct*XR and bovine catalase. The coupling of the hUGDH reaction to *Ct*XR-based NAD^+ regeneration strongly improves efficiency of the system. Oxidation of PQH_2 (**4**) to PQ (**5**) is coupled to H_2O_2 decomposition for *in situ* O_2 supply, leading formally to oxidative decarboxylation of UDP-Glc to UDP-Xyl by H_2O_2.

accomplish this task. We coupled the hUGDH reaction to a coenzyme regeneration cascade making use of *Candida tenuis* xylose reductase (*Ct*XR) and bovine liver catalase.[12] Thermodynamic and kinetic requirements as well as cost considerations had to be taken into account, as regeneration of NAD^+ is not well established, compared to NADH.[13] We applied a system originally described by Pival et al., in which *Ct*XR reduces 9,10-phenanthrenequinone (PQ) to 9,10-phenanthrene hydroquinone (PQH_2).[12] The NADH produced in UDP-Glc oxidation is recycled to NAD^+ during PQ reduction. PQH_2 is spontaneously re-oxidized by molecular oxygen in a fast radical chain reaction. Finally, catalase cleaves the thus produced hydrogen peroxide. The thermodynamically highly favorable reduction of oxygen provides a strong driving force that keeps the cycle running.[12] For that purpose, the development of an effective oxygen supply method was crucial.

The second main task in developing this multi-enzyme multi-reaction system of UDP-Xyl synthesis in one pot was the optimization of various interrelated reaction parameters. Comprehensive analysis of thermodynamic, kinetic and stability effects on each reaction of the overall system was necessary, and it turned out that overcoming inhibition effects was especially important. UXS is inhibited by UDP-Xyl, UGDH is inhibited by UDP-Xyl and also by NADH.[7,14] Till now, these inhibitions constituted a major restriction in enzymatic *in vitro* synthesis of not only UDP-Xyl, but also UDP-GlcUA.[7]

Engineering of Reaction Parameters

The initial idea was to perform the synthesis as a "one-pot one-step" conversion, where all enzymes are present right from the beginning. However, conversion of 20 mM UDP-Glc stopped after production of only 2 mM UDP-Xyl (data not shown). The most likely cause for the low yield was inhibition of hUGDH, as it has been reported that full inhibition of UGDH can be accomplished by only 50 μM UDP-Xyl.[5] Therefore, we switched to a "one-pot two-step" reaction and separated UDP-GlcUA and UDP-Xyl production by adding hUXS only after UDP-Glc was fully consumed.

The first step (UDP-Glc→UDP-GlcUA) depends on the combined action of hUGDH, *Ct*XR and bovine catalase. It was therefore crucial to find condi-

tions suited for all three enzymes in order to establish an efficient synthetic system. As catalase activity is invariant over a large pH range (4.0–8.5) and the enzyme was employed in large excess, it was readily used in the synthesis without further testing or optimization.[15] Therefore, it was primarily necessary to match hUGDH and *Ct*XR reactions, which was done by adaption of buffer, temperature and pH conditions.

Because potassium phosphate buffer was known to be compatible with both hUGDH and *Ct*XR,[3,12] it was used in the synthesis experiments. Next, we determined the influence of different temperatures on UDP-Glc conversion. The *Ct*XR-based coenzyme recycling system had previously been developed at 25 °C, and stability of the reductase enzyme decreases above 30–35 °C.[11,16] However, an increase in reaction temperature from 25 °C to 37 °C during multi-enzymatic UDP-Glc conversion improved both reaction time and yield (data not shown). Based on these results, 37 °C was used in the UDP-Glc→UDP-GlcUA step.

Last, pH-activity dependencies of hUGDH and *Ct*XR at synthesis temperature were examined. We tested activities of both enzymes in the pH range 6.0 to 8.5 at 37 °C (Figure 1A). Although the pH optimum of hUGDH was distinctly higher than that of *Ct*XR, at pH 7.5 both enzymes exhibited sufficiently high activity for the coupled enzymatic conversion.

Investigation of hUXS, the only enzyme involved in the second step (UDP-GlcUA→UDP-Xyl), revealed that the enzyme also showed faster conversion and higher yield at 37 °C than at 25 °C using potassium phosphate buffer (Figure 1B). We thus chose to not change the reaction conditions prior to hUXS addition in the complete reaction system.

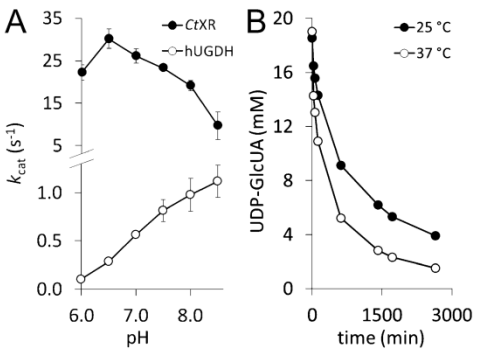

Figure 1. A) pH-activity dependencies of *Ct*XR and hUGDH. At pH 7.5 both enzymes show satisfactory activity. **B**) Comparison of UDP-GlcUA conversion by hUXS (30 μM) at 25 °C and 37 °C, showing the beneficial effect of the higher reaction temperature.

Engineering of UDP-Glc Conversion

Without efficient regeneration of the coenzyme, the conversion of UDP-Glc to UDP-GlcUA would be unfavorable for synthetic purposes (see Scheme 2). One commonly chosen group of enzymes to accomplish this task are water-forming NADH oxidases that use molecular oxygen to convert NADH to NAD^+.[17] However, their operational stability can be an issue under conditions of coenzyme recycling, for example, they are prone to inactivation by oxidizing agents.[12,18] We therefore used a modification of the method described by Pival et al. (Scheme 2), who used an enzymatic cascade to mimic the NADH oxidase reaction, and thus circumvented the known stability problems.[12] In this cascade reaction, the most critical point is an adequate oxygen supply for radical oxidation of PQH_2 to PQ (see Scheme 2) that was previously achieved by membrane gassing.[12] We investigated a new approach of oxygenation that is based on the "chemical oxygen source" H_2O_2. Underlying rationale was to achieve higher efficiency and easier parallelization and handling of the system. High catalase activity (100 U/mL) in combination with periodic feeding of H_2O_2 was used to realize fast *in situ* oxygen production (Scheme 2). Fast turnover of H_2O_2 was also necessary to prevent instability of hUGDH. 20 mM H_2O_2 led to a 50% reduction in initial activity and inactivation of the enzyme after only 1 min. In contrast, *Ct*XR was not affected by the oxidant, as already described previously.[12]

Initially, we investigated the use of 250 μM NAD^+ for conversion of 20 mM UDP-Glc. However, with these parameters substrate conversion was below 50%. As the UGDH reaction is considered irreversible in the UDP-GlcUA direction,[7] this effect was not due to equilibrium, but rather due to the K_i of 27 μM for NADH.[14] The low conversion was therefore ascribed tentatively to accumulation of NADH. Inactivation of *Ct*XR during the synthetic reaction (Figure 2A) was a plausible reason for the gradual increase in NADH during the reaction. In combination with the low initial NAD^+ concentration, the reaction would quickly come to a halt. However, *Ct*XR was already employed in high excess over hUGDH (12 U/mL *vs.* 0.9 U/mL initial activity). Therefore, a further increase in *Ct*XR concentration did not seem meaningful and we rather evaluated the influence of higher NAD^+ concentrations on overall UDP-Glc conversion to overcome the problem of enzyme inhibition. The use of 1 mM NAD^+ still resulted in progressive slowdown of the reaction and incomplete conversion even after 5 h. At 2 mM NAD^+, by contrast, UDP-Glc was fully converted after only 3 h (Figure 2B). Therefore, the latter concentration of was used in subsequent syntheses.

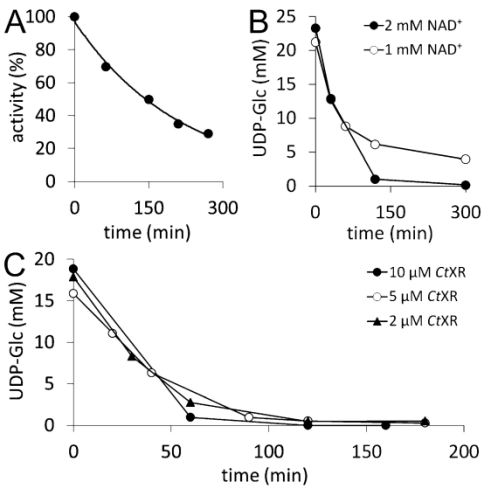

Figure 2. A) *Ct*XR inactivation during biocatalytic synthesis of UDP-GlcUA ($t_{1/2}$ = 150 min). **B**) Effect of NAD^+ concentration on conversion of UDP-Glc when 10 μM hUGDH were used. Full conversion was only achieved with 2 mM NAD^+, not with 1 mM. **C**) Effect of *Ct*XR concentration on conversion. No change in UDP-Glc conversion (10 μM hUGDH) was observed regardless of whether 10 μM, 5 μM or 2 μM *Ct*XR were used. The NAD^+ concentration was 2 mM.

However, the high excess of *Ct*XR was considered economically unfavorable, and, as shown above, the use of a higher NAD^+ concentration seemed more likely to be beneficial for UDP-GlcUA yield. We thus investigated the effect of lowering *Ct*XR concentration with regard to reaction time and completeness of conversion. No significant change in UDP-Glc conversion was noticed upon decreasing the *Ct*XR concentration from 10 μM to 2 μM (Figure 2C). In contrast, lowering the hUGDH concentration by 50% led to incomplete conversion of UDP-Glc (60%) and was not considered in further experiments (Supporting Information, Figure S1).

In all experiments, a UDP-Glc concentration of 20 mM was used. Attempts to use a higher concentration (e.g., 40 mM) failed and only about 50% conversion were reached (Supporting Information, Figure S2). This effect occurred most probably due to a large pH drop during UDP-GlcUA production (about one pH unit per 20 mM UDP-Glc converted), strongly decreasing hUGDH activity (see Figure 1A). Using a higher buffer concentration to maintain a stable pH interfered with activities of both hUGDH and *Ct*XR and was not further pursued (Supporting Information, Figure S3). Automated pH control would constitute a solution when working with larger reaction volumes; however, in the low volume of 1 mL used herein, the approach was not considered to be practical.

Engineering of UDP-GlcUA Conversion

The second part of the biosynthetic reaction consisted of direct conversion of UDP-GlcUA to UDP-Xyl, with the only by-product being CO_2 (Scheme 2). The hUXS reaction was not affected by the pH drop from 7.5 to about 6.5–6.7 during UDP-GlcUA synthesis. Even without adjusting the pH prior to addition of the enzyme, UDP-Xyl yield was approximately 90% at the end of the reaction (data not shown). The incomplete UDP-GlcUA conversion was most probably caused by a combination of hUXS inhibition by UDP-Xyl, as already reported for UXS,[7] and enzyme inactivation. We therefore doubled hUXS concentration to 30 μM, which indeed led to full conversion of UDP-GlcUA to UDP-Xyl within 24 h (see the next section).

Preparative UDP-Xyl Synthesis

Using the previously optimized parameters and conditions, a highly efficient biocatalytic reaction system for UDP-Xyl production could be set up. The time course of the reaction is depicted in Figure 3, reaction conditions are summarized in Table 1. Twenty millimoles of UDP-Glc/L were nearly fully (> 97.5%) and highly reproducibly (standard deviation in triplicate experiment < 3%) converted to UDP-Xyl within 29 h. Already after 3.5 h, residual UDP-Glc concentration was < 1% (0.23 ± 0.04 mM), and the UDP-GlcUA produced was readily transformed to UDP-Xyl after addition of hUXS.

H_2O_2 was added batch-wise, as shown in Figure 3. A total amount corresponding to 100 mM H_2O_2 was added for full conversion of 20 mM substrate, indicating that 40% of the generated oxygen were consumed in the reaction. Most likely gaseous oxygen was lost through the polypropylene (PP) reaction tube, as PP is highly oxygen permeable.[19] Usage of a tightly sealed, less oxygen permeable reaction vessel (e.g., PVC, PET) could be used to improve efficiency.[19] However, H_2O_2 does not contribute significantly to UDP-Xyl production costs due to its low price compared to the product (> 45 US $/mg).[20] In Figure 3 it is also visible that the hUXS reaction slowed down considerably after reaching about 50% conversion (see before), but still gained 98% conversion within a reasonable time. With this system, a total amount of 10.5 mg UDP-Xyl could be produced in one reaction batch and, due to the simple process set up, numbering up would easily be accomplishable.

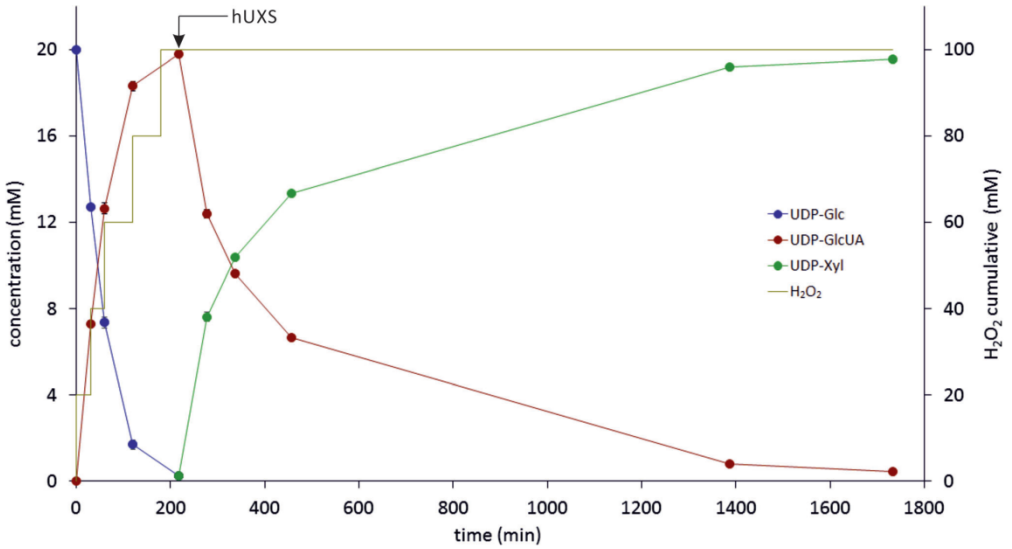

Figure 3. Time course of biocatalytic UDP-Xyl production (data from triplicate experiments). Concentrations of UDP-Glc, UDP-GlcUA and UDP-Xyl are shown (left ordinate). The yellow line depicts the total amount of H_2O_2 added to the reaction mixture. hUXS was added at the time indicated, after UDP-Glc was consumed.

Table 1. Reaction conditions of UDP-Xyl production.

UDP-Glc [mM]	NAD^+ [mM]	PQ [μM]	H_2O_2[a] [mM]	BSA [$g L^{-1}$]	hUGDH [μM]	hUXS [μM]	CtXR [μM]	Catalase [U]	V [mL]	T [°C]	pH
20	2	25	20	1	10	30	2	100	1	37	7.5

[a] Concentration in reaction tube after feeding H_2O_2 (see text).

We also determined total turnover numbers (TTN) of different compounds in the reaction to facilitate evaluation of the system (Table 2). Pival et al. reached a TTN_{PQ} of 1000 in conversion of 25 mM substrate, which fits well to the value obtained here (TTN_{PQ} = 780, $c_{substrate}$ = 20 mM).[12] Therefore, this indicates that the approach of feeding H_2O_2 is at least equally effective as membrane gassing. TTN values for NAD^+ and *Ct*XR are lower than those reported by Pival et al. due to the aforementioned inhibitory effects that occur during reaction. Nevertheless, the system provides a significant improvement over the use of stoichiometric amounts of the coenzyme.

Table 2. Characteristics of UDP-Xyl production.

hUGDH TTN[a]	hUXS TTN	*Ct*XR TTN	NAD^+ TTN	Re[b]	PQ TTN	Re
1950	650	9750	10	40	780	40

[a] Total turnover number (mM UDP-Xyl produced per mM of compound consumed).
[b] Number of regeneration cycles

Purification and Isolation of UDP-Xyl

After biocatalytic synthesis, a two-step chromatographic protocol was used to purify UDP-Xyl. In the first step, anion exchange chromatography (AEX) was employed to separate UDP-Xyl from other compounds of the reaction mixture. Subsequently, the salt used for elution was removed by size exclusion chromatography (SEC). To minimize total loading on the column and thereby improve separation and sugar binding capacity, proteins (hUGDH, hUXS, *Ct*XR, BSA and catalase) were removed by membrane filtration prior to AEX, as described in the Experimental Section.

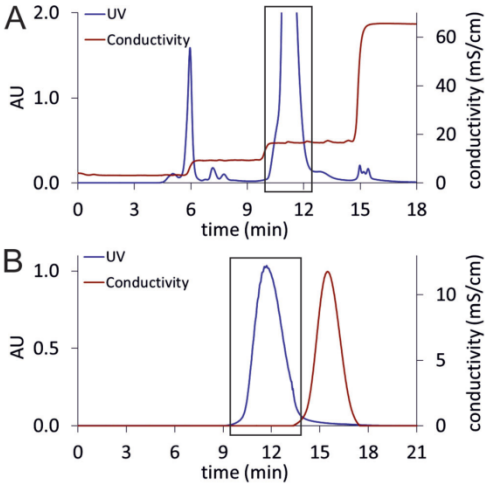

Figure 4. A) Anion exchange chromatography. The reaction mixture was loaded on a Resource Q column and eluted using a NH_4HCO_2 gradient. The peak inside the black box is UDP-Xyl. **B**) Size exclusion chromatography: UDP-Xyl-containing fractions from AEX were concentrated and applied to a Sephadex G-10 column. Elution with deionized water led to pure UDP-Xyl (black box).

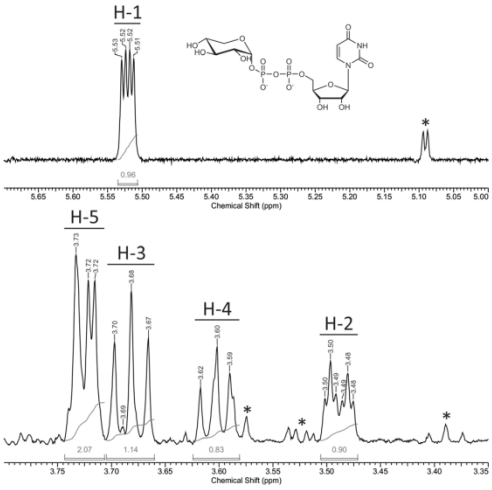

Figure 5. ^{1}H NMR spectrum of purified UDP-Xyl. Signals of sugar protons H-1 to H-5 were assigned according to the literature, impurities are indicated by an asterisk.[8a] Only a small formate signal is visible at 8.43 ppm,[22] indicating nearly complete removal of NH_4HCO_2 during purification (Supporting Information, Figure S7).

In AEX an ammonium formate (NH_4HCO_2) buffer (pH 4.2) was used as mobile phase. By applying a step-wise gradient between 20 mM and 500 mM NH_4HCO_2, resolution of the reaction mixture was possible within 18 min (Figure 4A). UDP-Xyl eluted separately from other compounds at 105 mM NH_4HCO_2 ($\sigma = 17$ mS·cm^{-1}).

For removal of NH_4HCO_2 and water in one step, lyophilization can be used. However, it is reported that nucleotide sugars are prone to decomposition under such conditions.[21] Therefore, we used SEC to separate NH_4HCO_2 from UDP-Xyl and evaluated different SEC stationary phases (Bio-Gel P-2 from Bio-Rad; Sephadex G-25 and Sephadex G-10 from GE Healthcare) in combination with elution by deionized water. As UDP-Xyl seemed to adsorb to Bio-Gel P-2 (polyacrylamide), this resin was unsuitable. Sephadex G-25 (dextran) led to good separation, however with some overlap between UDP-Xyl and NH_4HCO_2 (Supporting Information, Figure S4). In order to improve product recovery, the finer Sephadex G-10 material (exclusion limit = 700 Da *vs.* 1000 Da for G-25) was chosen. With this method, nearly full separation of UDP-Xyl and NH_4HCO_2 could be achieved (Figure 4B).

UDP-Xyl was finally isolated from the aqueous solution by removal of water under reduced pressure. It was previously confirmed that the chosen conditions do not lead to decomposition of the product. Within some hours, UDP-α-Xyl was obtained as its ammonium salt (white to yellow powder, see Supporting Information, Figure S5). Identity of the product was confirmed by ^{1}H NMR (Figure 5), and capillary zone electrophoresis (Supporting Information, Figure S6) showed a purity of 98%. The total amount obtained from one reaction batch was 5.3 mg, corresponding to an isolated yield of 46% (compared to the end of biocatalytic synthesis).

Conclusions

We have established a highly efficient multi-enzyme multi-step transformation for the synthesis of the rare and also expensive UDP-Xyl from the well available and comparably expedient substrate UDP-Glc. Conversion of UDP-Glc was achieved by coupling a two-step synthetic reaction cascade to a chemo-enzymatic coenzyme regeneration cascade, as shown in Scheme 2. We show that in-depth analysis of each individual reaction in combination with careful optimization work was important to bring the complex multi-component system to the point of truly effective performance. One key feature of conversion efficiency was *in situ* O_2 production from H_2O_2 as the actual chemical oxidant supplied to the overall reaction.

Separation in time of the catalytic action of hUXS from that of hUGDH was also critical for high synthesis rates and complete conversion. Fast chromatographic work-up of the reaction mixture lead to highly pure UDP-Xyl in good yield.

As there exist several well established systems for UDP-Glc synthesis based on assembly of UDP-Glc from glucose and UTP,[23] our system could be expanded by coupling one of these methods to the herein described UDP-Xyl synthesis. This would reduce the costs of UDP-Xyl synthesis even further. Additionally, our system also offers an efficient way to UDP-GlcUA, a compound whose synthesis was equally difficult to achieve till now.[7] We also believe that synthesis of UDP-Xyl provides a strong case supporting the use of multi-step enzymatic cascades in the preparation of high-value products such as nucleotide sugars.

Experimental Section

Chemicals and Strains

UDP-glucose (>90% purity) was purchased from Carbosynth (Compton, UK), UDP-glucuronic acid (>98% purity), 9,10-phenanthrenequinone (>99% purity), bovine serum album (BSA; >98% purity) and bovine catalase (3809 U/mg) from Sigma–Aldrich (Vienna, Austria). NAD^+ (>98% purity) was obtained from Roth (Karlsruhe, Germany). *Aspergillus niger* glucose oxidase type VII-S (GOD; 246 U/mg) and horseradish peroxidase type II (POD; 181 U/mg) were purchased from Sigma–Aldrich. All other chemicals were purchased either from Sigma–Aldrich or Roth and were of the highest purity available.

Design and assembly of the recombinant *Escherichia coli* strains for hUGDH, hUXS and *Ct*XR expression are described elsewhere.[2,3,12]

Enzyme Expression and Purification

Expression and purification of the recombinant hUGDH, hUXS and *Ct*XR are described in full detail elsewhere.[2,3,12] Briefly, the enzymes were overexpressed in *E. coli* Rosetta 2(DE3) using a pBEN- (hUGDH), p11- (hUXS) or pQE-30- (*Ct*XR) derived expression vector. After high-pressure cell disruption, His-tagged hUXS and *Ct*XR were isolated from the crude extract using a Cu^{2+}-loaded IMAC sepharose column (GE Healthcare, Vienna, Austria), while a Strep-Tactin sepharose column (QIAGEN, Hilden, Germany) was used for Strep-tagged hUGDH. Elution with imidazole (His-tag) or desthiobiotin (Strep-tag) yielded highly pure enzymes (checked by SDS-PAGE). Buffer exchange to remove imidazole or desthiobiotin was done using Vivaspin centrifugal concentrators (Sartorius Stedim, Göttingen, Germany). Enzyme preparations were stored at −70 °C.

Enzymatic Assays

Activities of hUGDH and *Ct*XR were determined by monitoring NADH formation (hUGDH) or consumption (*Ct*XR) on a Beckman-Coulter DU800 spectrophotometer (λ = 340 nm) with temperature-controlled sample holder (37 °C). Assays for hUGDH contained 0.1 μM enzyme, 0.5 or 1 mM UDP-Glc and 5 or 10 mM NAD^+ in 50 mM potassium phosphate buffer (PPB) (pH 7.5), for *Ct*XR 0.05 μM enzyme, 50 μM PQ and 250 μM NADH in the same buffer were used. hUXS was assayed using 5 μM enzyme, 5 mM UDP-GlcUA and 0.5 mM NAD^+ in 50 mM PPB (pH 7.5). In this case, results were obtained by measuring UDP-GlcUA consumption on HPLC or CE.

Enzyme activities during biocatalytic synthesis were measured by diluting a sample 1:100 (hUGDH) or 1:200 (*Ct*XR) in 50 mM PPB (pH 7.5) containing 5 mM NAD^+ (hUGDH) or 50 μM PQ (*Ct*XR). Reactions were started by addition of 1 mM UDP-Glc (hUGDH) or 250 μM NADH (*Ct*XR) and followed by monitoring the change in NADH concentration as described above.

The pH-activity dependencies of hUGDH and *Ct*XR were determined by measuring activity as described above using 50 mM PPB in the pH range 6.0–8.5.

Biocatalytic Synthesis

Unless otherwise stated, reaction mixtures for UDP-Xyl biosynthesis contained 20 mM UDP-Glc, 2 mM NAD^+, 25 μM PQ, and 0.1% (w/v) BSA in 50 mM PPB (pH 7.5). Enzymes were added in the following order: 100 U/mL bovine liver catalase, 2 μM *Ct*XR. All experiments were done on a Thermomixer Comfort (Eppendorf, Hamburg, Germany) at 37 °C without agitation. The reaction mixture was incubated for several minutes before reaction was started by addition of 10 μM hUGDH followed by immediate addition of 20 mM H_2O_2, mixing, and closing of the 1.5-mL Eppendorf reaction tube cap. Total reaction volume was 1 mL.

20 μL samples were taken at the beginning and the indicated time points. After each sample, H_2O_2 was added to a concentration of 20 mM, until UDP-Glc was fully consumed. 30 μM hUXS were added to the mixture afterwards and the reaction was allowed to proceed to completeness.

High Performance Liquid Chromatography

Samples were analyzed on an Agilent 1200 HPLC system equipped with a 5 μm Zorbax SAX analytical HPLC column (4.6 × 250 mm; Agilent, Santa Clara, CA, USA) and a UV detector (λ = 262 nm). Reactions were stopped by heating the samples to 99 °C for 5 min and precipitated enzymes were removed by centrifugation (16000 *g* for 5 min). The supernatant was diluted 1:20 with 50 mM PPB (pH 7.5) and measured using an injection volume of 10 μL, a temperature of 25 °C and a flow rate of 1.5 mL min^{-1}. Elution was performed with a linear gradient from 5 mM to 300 mM PPB (pH 3.2) over 10 min. The column was washed (3 min each) with 600 mM and 5 mM PPB (pH 3.2) after each analysis. Authentic standards were used for calibration.

Capillary Zone Electrophoresis

Capillary zone electrophoresis analyses were performed at 18 °C on an HP 3D CE system (Hewlett Packard, Palo Alto, CA, USA) equipped with an extended light path fused silica capillary (5.6 μm × 56 cm) from Agilent and a diode array detector (λ = 262 nm). The electrophoresis buffer was

20 mM sodium tetraborate (pH 9.3). The capillary was conditioned each day using the following protocol: 10 min NaOH 1 M, 10 min NaOH 0.1 M, 10 min H_2O, 15 min electrophoresis buffer. Prior to each sample, the capillary was pre-conditioned with 2 min H_2O, 2 min NaOH 0.1 M, 3 min H_2O and 10 min electrophoresis buffer. Samples were injected by pressure (50 mbar, 5 s) and measured using a protocol with a voltage of 30 kV for 10 min, 15 kV for 3 min and 30 kV for 8 min. Preparation of the samples was done according to HPLC analysis except that caffeine was added as internal standard. Authentic standards were used for calibration.

Proton NMR Spectroscopy

Spectra were recorded on a Bruker DRX-600 AVANCE spectrometer (Bruker, Rheinstetten, Germany) at 600.13 MHz (^{1}H). The ^{1}H NMR spectra were measured at 298.2 K with acquisition of 32 k data points. After zero filling to 64 k data points, spectra were performed with a range of 7200 Hz. 32 ^{1}H NMR spectra were recorded in one measurement, using a 5 mm high precision NMR sample tube (Promochem, Wesel, Germany). For evaluation of the spectra ACD/NMR Processor Academic Edition 12.0 (Advanced Chemistry Development Inc., Toronto, Canada) was used.

Photometric Nucleotide Sugar Determination

Assays for UDP-Glc, UDP-GlcUA and UDP-Xyl were linear up to 500 μM of the respective compound, and samples were diluted accordingly prior to analysis.

UDP-Glc was detected using a coupled enzymatic assay of GOD and POD.[24] UDP-Glc was hydrolyzed by addition of glacial acetic acid to the samples, yielding a final concentration of 28.5%, and heating to 99 °C for 10 min. Afterwards, the assay was performed using the hydrolyzed samples containing free glucose. Absorption at $\lambda = 420$ nm was measured on a Beckman-Coulter DU800 spectrophotometer.

Concentration of UDP-GlcUA was determined using a colorimetric assay described elsewhere.[25] Absorption ($\lambda =$ 525 nm) was measured on a Beckman-Coulter DU800 spectrophotometer.

UDP-Xyl was determined according to the method of Roe and Rice.[26] A hydrolysis step to allow detection of the UDP sugar was performed prior to the colorimetric assay, as described for UDP-Glc. Measurement was done using the same settings as described for UDP-GlcUA.

Preparative Anion Exchange Chromatography

Purification of the produced sugar nucleotide was done using a cooled (4 °C) BioLogic DuoFlow system (Bio-Rad, Vienna, Austria) equipped with a 6-mL Resource Q anion exchange column. A step-wise gradient of 6 mL min^{-1} NH_4HCO_2 (buffer A: 20 mM and buffer B: 500 mM) was used for elution of bound compounds. The steps were as follows: 24 mL NH_4HCO_2 58 mM, 30 mL NH_4HCO_2 106 mM, 24 mL NH_4HCO_2 500 mM. Prior to each run, the column was regenerated by flushing with three column volumes buffer B and buffer A, respectively. UV absorption ($\lambda =$ 254 nm) was used to detect the compounds, which were collected in 6 mL fractions.

The total volume of UDP-Xyl-containing fractions was 48 mL from one reaction batch, which was concentrated to 2 mL on a rotary evaporator (40 °C, 20 mbar) before proceeding with size exclusion chromatography.

Preparative Size Exclusion Chromatography

NH_4HCO_2 was removed from concentrated UDP-Xyl fractions on a BioLogic DuoFlow system (Bio-Rad) using a self-packed Sephadex G-10 (GE Healthcare) column (bed volume = 53 mL, H/D ratio = 3.8). Elution was performed with deionized water using a flow rate of 2 mL min^{-1}. UDP-Xyl was detected by UV absorption ($\lambda = 254$ nm), while conductivity measurement was used for NH_4HCO_2 detection. Automated fraction collection was used to collect 10.5 mL of pure UDP-Xyl solution. The water was finally removed on a rotary evaporator (40 °C, 3 mbar).

Acknowledgements

Financial support from the Austrian Science Fund FWF (Project W901-B05 DK Molecular Enzymology) is gratefully acknowledged. We thank Regina Kratzer from the Institute of Biotechnology and Biochemical Engineering at Graz University of Technology for xylose reductase. We also thank Prof. Lothar Brecker and Claudia Puchner from the Institute of Organic Chemistry at the University of Vienna for NMR analysis. Special thanks go to Silvia Maitz for her contributions to development of the biocatalytic system.

References

[1] a) T. Mega, *Biosci. Biotechnol. Biochem.* **2007**, *71*, 2893–2904; b) H. Mulder, F. Dideberg, H. Schachter, B. A. Spronk, M. De Jong-Brink, J. P. Kamerling, J. F. G. Vliegenthart, *Eur. J. Biochem.* **1995**, *232*, 272–283; c) J.-N. Park, D.-J. Lee, O. Kwon, D.-B. Oh, Y.-S. Bahn, H. A. Kang, *J. Biol. Chem.* **2012**, *287*, 19501–19515; d) C. J. Paul, E. A. Lyle, T. J. Beveridge, R. I. Tapping, A. M. Kropinski, E. Vinogradov, *Glycoconjugate J.* **2009**, *26*, 1097–1108; e) B. F. Eames, A. Singer, G. A. Smith, Z. A. Wood, Y.-L. Yan, X. He, S. J. Polizzi, J. M. Catchen, A. Rodriguez-Mari, T. Linbo, D. W. Raible, J. H. Postlethwait, *Dev. Biol.* **2010**, *341*, 400–415.

[2] T. Eixelsberger, S. Sykora, S. Egger, M. Brunsteiner, K. L. Kavanagh, U. Oppermann, L. Brecker, B. Nidetzky, *J. Biol. Chem.* **2012**, *287*, 31349–31358.

[3] S. Egger, A. Chaikuad, K. L. Kavanagh, U. Oppermann, B. Nidetzky, *J. Biol. Chem.* **2011**, *286*, 23877–23887.

[4] a) D. Voet, J. G. Voet, *Biochemistry* 3rd edn., Wiley-VCH, Weinheim, **2004**; b) C. J. Thibodeaux, C. E. Melançon III, H.-w. Liu, *Angew. Chem.* **2008**, *120*, 9960–10007; *Angew. Chem. Int. Ed.* **2008**, *47*, 9814–9859; c) T. Bülter, L. Elling, *Glycoconjugate J.* **1999**, *16*, 147–159.

[5] E. F. Neufeld, C. W. Hall, *Biochem. Biophys. Res. Commun.* **1965**, *19*, 456–461.

[6] T. Ishimizu, T. Uchida, K. Sano, S. Hase, *Tetrahedron: Asymmetry* **2005**, *16*, 309–311.
[7] L. Cai, *J. Carbohydr. Chem.* **2012**, *31*, 535–552.
[8] a) M. Bar-Peled, C. L. Griffith, T. L. Doering, *Proc. Natl. Acad. Sci. USA* **2001**, *98*, 12003–12008; b) S. J. Polizzi, R. M. Walsh Jr, P. Le Magueres, A. R. Criswell, Z. A. Wood, *Biochemistry* **2013**, *52*, 3888–3898; c) P. Guyett, J. Glushka, X. Gu, M. Bar-Peled, *Carbohydr. Res.* **2009**, *344*, 1072–1078; d) D.-F. Fan, D. S. Feingold, *Arch. Biochem. Biophys.* **1972**, *148*, 576–580; e) M. Mølhøj, R. Verma, W.-D. Reiter, *Plant J.* **2003**, *35*, 693–703; f) R. W. Gantt, P. Peltier-Pain, J. S. Thorson, *Nat. Prod. Rep.* **2011**, *28*, 1811–1853; g) T. Yang, Y. Bar-Peled, J. A. Smith, J. Glushka, M. Bar-Peled, *Anal. Biochem.* **2012**, *421*, 691–698; h) J. C. Errey, B. Mukhopadhyay, K. P. Ravindranathan Kartha, R. A. Field, *Chem. Commun.* **2004**, 2706–2707; i) T. Oka, Y. Jigami, *FEBS J.* **2006**, *273*, 2645–2657.
[9] a) T. Kotake, D. Yamaguchi, H. Ohzono, S. Hojo, S. Kaneko, H.-k. Ishida, Y. Tsumuraya, *J. Biol. Chem.* **2004**, *279*, 45728–45736; b) T. Ohashi, N. Cramer, T. Ishimizu, S. Hase, *Anal. Biochem.* **2006**, *352*, 182–187.
[10] H. Tanaka, Y. Yoshimura, M. R. Jørgensen, J. A. Cuesta-Seijo, O. Hindsgaul, *Angew. Chem.* **2012**, *124*, 11699–11702; *Angew. Chem. Int. Ed.* **2012**, *51*, 11531–11534.
[11] a) M. Arlt, O. Hindsgaul, *J. Org. Chem.* **1995**, *60*, 14–15; b) G. K. Wagner, T. Pesnot, R. A. Field, *Nat. Prod. Rep.* **2009**, *26*, 1172–1194; c) C. Ernst, W. Klaffke, *J. Org. Chem.* **2003**, *68*, 5780–5783.
[12] S. L. Pival, M. Klimacek, B. Nidetzky, *Adv. Synth. Catal.* **2008**, *350*, 2305–2312.
[13] B. Petschacher, N. Staunig, M. Müller, M. Schürmann, D. Mink, S. De Wildeman, K. Gruber, A. Glieder, *Comput. Struc. Biotechnol. J.* **2014**, *9*, e201402005.
[14] R. Kadirvelraj, N. C. Sennett, G. S. Custer, R. S. Phillips, Z. A. Wood, *Biochemistry* **2013**, *52*, 1456–1465.
[15] B. Chance, *J. Biol. Chem.* **1952**, *194*, 471–481.
[16] W. Neuhauser, D. Haltrich, K. D. Kulbe, B. Nidetzky, *Biochem. J.* **1997**, *326*, 683–692.
[17] a) H. Wu, C. Tian, X. Song, C. Liu, D. Yang, Z. Jiang, *Green Chem.* **2013**, *15*, 1773–1789; b) B. R. Riebel, P. R. Gibbs, W. B. Wellborn, A. S. Bommarius, *Adv. Synth. Catal.* **2002**, *344*, 1156–1168; c) B. Geueke, B. Riebel, W. Hummel, *Enzyme Microb. Technol.* **2003**, *32*, 205–211.
[18] Z. Findrik, A. V. Presečki, Đ. Vasić-Rački, *J. Biosci. Bioeng.* **2007**, *104*, 275–280.
[19] J. Lange, Y. Wyser, *Packag. Technol. Sci.* **2003**, *16*, 149–158.
[20] Complex Carbohydrate Research Center, CarboSource Services product list, **2014**.
[21] U. B. Gokhale, O. Hindsgaul, M. M. Palcic, *Can. J. Chem.* **1990**, *68*, 1063–1071.
[22] H. E. Gottlieb, V. Kotlyar, A. Nudelman, *J. Org. Chem.* **1997**, *62*, 7512–7515.
[23] X. Ma, J. Stöckigt, *Carbohydr. Res.* **2001**, *333*, 159–163.
[24] P. Wildberger, C. Luley-Goedl, B. Nidetzky, *FEBS Lett.* **2011**, *585*, 499–504.
[25] T. M. C. C. Filisetti-Cozzi, N. C. Carpita, *Anal. Biochem.* **1991**, *197*, 157–162.
[26] J. H. Roe, E. W. Rice, *J. Biol. Chem.* **1948**, *173*, 507–512.

Advanced Synthesis & Catalysis

Supporting Information

SUPPORTING INFORMATION

Enzymatic redox cascade for one-pot synthesis of uridine 5'-diphosphate xylose from uridine 5'-diphosphate glucose

Thomas Eixelsberger[a] and Bernd Nidetzky[a,b]*

[a] Institute of Biotechnology and Biochemical Engineering, Graz University of Technology, NAWI Graz, Petersgasse 12/I, A-8010 Graz, Austria
[b] Austrian Centre of Industrial Biotechnology, Petersgasse 14, A-8010 Graz, Austria
Phone: +43 316 873 8400, Fax: +43 316 873 108400; E-Mail: bernd.nidetzky@tugraz.at

Table of contents

1 Results and Discussion

1.1 Engineering of UDP-Glc conversion

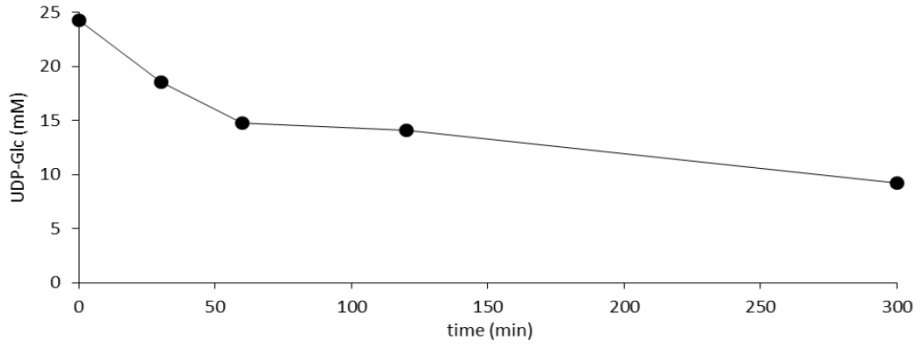

Figure S1. Conversion of UDP-Glc with 5 µM hUXS led to slow and incomplete conversion even after 300 min.

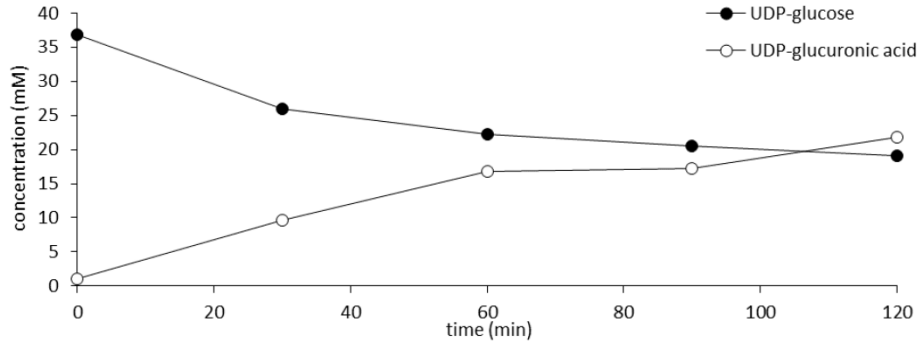

Figure S2. Conversion of 40 mM UDP-Glc to UDP-GlcUA led to only about 50% substrate conversion and was therefore not considered meaningful.

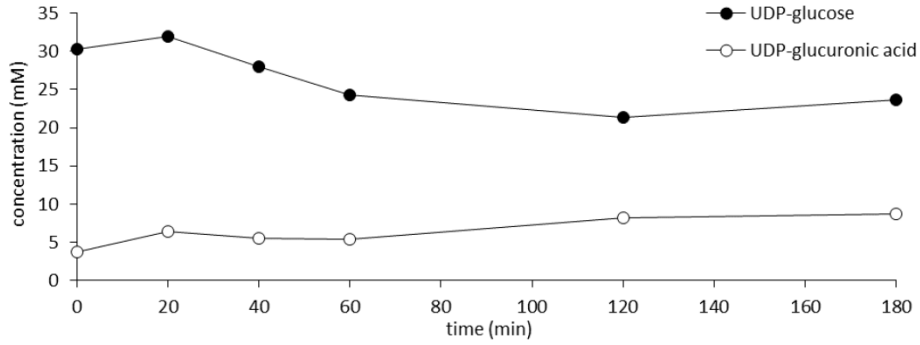

Figure S3. A higher buffer concentration (100 mM PPB instead of 50 mM PPB) showed no positive effect on conversion of 40 mM UDP-Glc to UDP-GlcUA.

1.2 Purification and isolation of UDP-Xyl

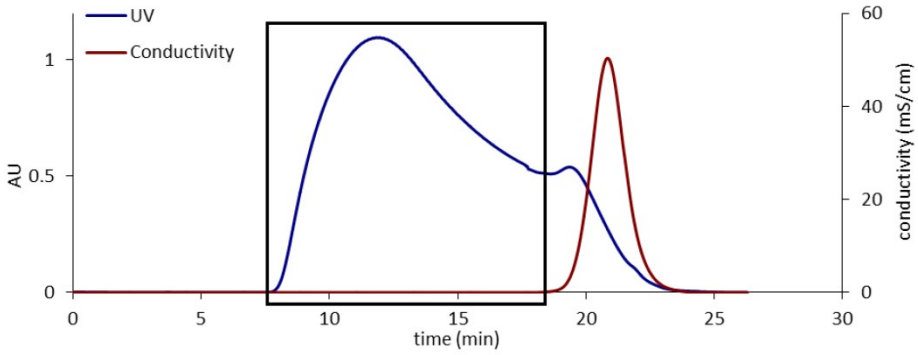

Figure S4. Removal of NH_4HCO_2 on a Sephadex G-25 SEC column. UV and conductivity traces are shown, UDP-Xyl is marked by the black box.

Figure S5. UDP-Xyl as obtained after purification and desalting (black box). For better clarity, black background was removed and image digitally optimized.

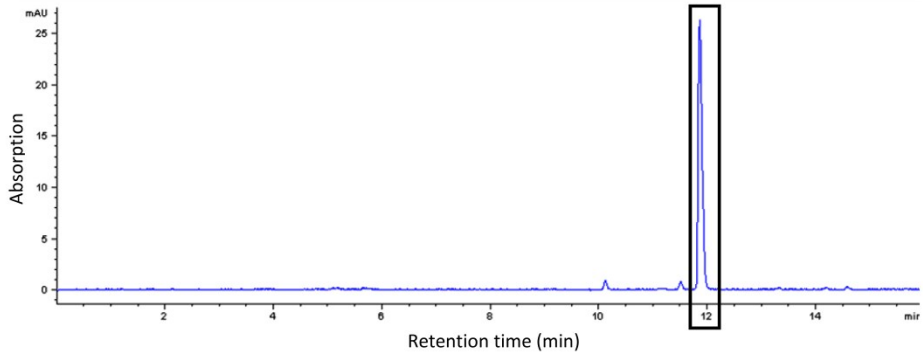

Figure S6. CE electropherogram of purified UDP-Xyl (black box).

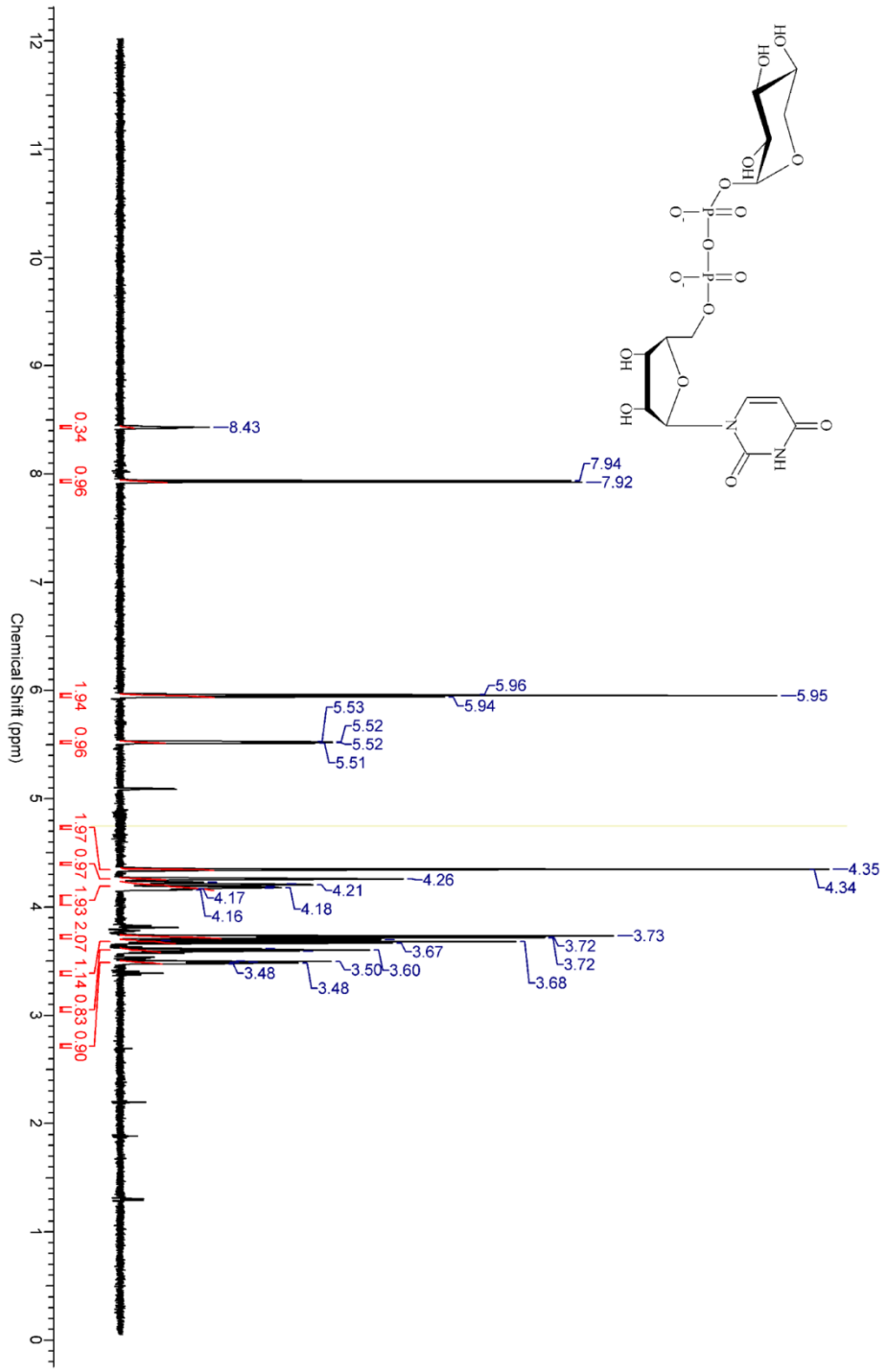

Figure S7. Full ^{1}H NMR spectrum of purified UDP-Xyl.

S4

The mechanism of UDP-apiose/UDP-xylose synthase reveals *C*-branched sugar biosynthesis in plants

The mechanism of UDP-apiose/UDP-xylose synthase reveals *C*-branched sugar biosynthesis in plants

Thomas Eixelsberger[1], Doroteja Horvat[1], Alexander Gutmann[1], Hansjörg Weber[2], Bernd Nidetzky[1,3,*]

[1] Institute of Biotechnology and Biochemical Engineering, Graz University of Technology, NAWI Graz, Petersgasse 12/I, A-8010 Graz, Austria

[2] Institute of Organic Chemistry, Graz University of Technology, NAWI Graz, Stremayrgasse 9, A-8010 Graz, Austria

[3] Austrian Centre of Industrial Biotechnology, Petersgasse 14, A-8010 Graz, Austria

* Corresponding author; e-mail: bernd.nidetzky@tugraz.at, tel.: +43 316 873 8400, fax: +43 316 873 108400

Abstract

D-Apiose (Api), a *C*-branched sugar unique to plants, plays an important role in cell wall development. An enzyme-catalysed, chemically intriguing decarboxylation/pyranoside ring contraction reaction leads from UDP-α-D-glucuronic acid (UDP-GlcUA) to the Api precursor UDP-α-D-apiose (UDP-Api). We deciphered the elusive mechanism of UDP-Api/UDP-α-D-xylose synthase (UAXS) through comprehensive probing of the reaction with site-selectively ^{13}C- or ^{2}H-labelled and deoxygenated substrates. Isotopic labelling delineated the carbon skeleton reorganization and revealed hydrogen transfer, via enzyme-bound NAD, from substrate *C*-4 to the exocyclic Api *C*-3'. Kinetic isotope effects (KIEs) from intermolecular competition between ^{1}H-3/^{2}H-3 substrates support a retroaldol-aldol mechanism of pyranoside-to-furanoside ring conversion. The analogue UDP-2-deoxy-GlcUA, which prevents the *C*-2/*C*-3 retroaldol cleavage, was completely inactive, indicating strong coupling between oxidative decarboxylation and sugar ring opening. Rearrangement and ring-contracting aldol addition in an open-chain intermediate gives UDP-Api aldehyde, which is intercepted via reduction by enzyme-NADH. KIEs from ^{2}H-4 in substrate show that this reduction step is pulling the aldehyde from a highly unfavourable equilibrium towards UDP-Api. The UAXS reaction pathway presents a mechanistic paradigm for biosynthesis of *C*-branched carbohydrates.

Uridine 5'-diphosphate (UDP)-α-D-apiose (**1**) is the precursor of D-apiose in the plant cell wall polysaccharides rhamnogalacturonan II and apiogalacturonan.[1] The biological importance of D-apiose residues lies in their ability to crosslink the polysaccharide chains through formation of a borate tetraester.[2,3] It has been shown that the absence of such crosslinks heavily interferes with growth and morphogenesis of the plant.[4] Nucleotide sugar **1** is derived from UDP-α-D-glucuronic acid (**2**) in a decarboxylation/pyranoside ring contraction reaction catalysed by UDP-α-D-apiose/UDP-α-D-xylose synthase (UAXS).[1] This chemically intriguing biotransformation has attracted considerable interest for a long time. It is thought to proceed via nicotinamide adenine dinucleotide (NAD^+)-assisted oxidation at *C*-4 of substrate **2**, followed by decarboxylation of the resulting UDP-4-keto-α-D-glucuronic acid (**3**) and formation of UDP-4-keto-α-D-xylose (**4**).[1] Several research groups have conducted studies on selected aspects of the reaction using ^{3}*H*- and ^{14}*C*-labelled substrates that gave an idea how intermediate **4** might be converted to product **1** (Figure 1a).[5-11] Rearrangement of the carbon skeleton would start with bond cleavage between *C*-2/*C*-3 of **4** in a retroaldol reaction, yielding intermediates **5** and **6**. Re-cyclization by aldol addition between *C*-2/*C*-4 of **6** would result in UDP-α-D-apiose 3'-aldehyde (**7**) that is then converted to product **1** by the reduced NAD^+ (NADH) formed in the initial reaction step.[5-13] In aqueous solutions, α-D-apiofuranosyl-1,2-cyclic phosphate (**8**) is spontaneously formed from **1** due to its instability.[11,14] More recently, Liu and co-workers suggested the possibility of a different mechanism, where aldehyde **7** would be formed directly out of intermediate **4** in a 1,2-bond shift mechanism.[12,13] UDP-α-D-xylose (**9**) could be formed from intermediate **4** through reduction of the 4-keto function by NADH prior to the ring contraction step(s), as done by the related UDP-xylose synthase (UXS), or from intermediate **5** via aldol addition between *C*-2/*C*-3 followed by reduction.[12,13,15] UAXS was able to convert a phosphonate analogue of **1** to the corresponding xylosyl compound, however, no conversion of product **9** to product **1** was observed.[1,13,16] This finding was explained by **9** adopting two stable chair conformations, of

which the more favourable one is inhibiting the enzyme.[13] UDP-2-deoxy-2-fluoro-α-D-glucuronic acid was shown to be an inhibitor of UAXS, too.[12]

Despite the development of these mechanistic concepts, core features of the UAXS-catalysed transformation, such as the way aldehyde **7** is formed (retroaldol-aldol vs. bond-shift mechanism), remain fundamentally elusive. Comprehensive analysis of the reaction's multiple steps, including dissection of the ring rearrangement through tracking of the individual atoms from substrate **2** to products **1** and **9**, has not been performed. The mechanistic options considered for UAXS should therefore be substantiated more rigorously to obtain definite evidence about the chemistry of this enzymatic transformation. The UAXS mechanism, although highly specialized, possesses fundamental significance, as other *C*-branched carbohydrates, like D-streptose, are thought to be formed via mechanistically highly similar transformations.[17-19] Furthermore, a reductoisomerase-catalysed *C*-branching rearrangement comparable to that of UAXS initiates the biosynthetic diversion of 1-deoxy-D-xylulose 5-phosphate into isoprenes in plants and certain microbial taxa.[20] The reductoisomerase mechanism was investigated using kinetic isotope effect (KIE) measurements, however, results from different studies were non-conclusive.[20-22] Elucidation of the mechanistic principles employed by UAXS is therefore of broad relevance in enzymology of nucleotide sugar biosynthesis and even beyond. UAXS expands the fascinating diversity of complex multi-step NAD^+/NADH-dependent enzymatic reactivities (e.g. oxidoreductive epimerization, oxidative decarboxylation with and without reduction) that evolved within the superfamily of short-chain dehydrogenases-reductases from the ancestral reactivity of a simple single-step NAD^+/NADH-dependent oxidation/reduction.[15,23]

We present here direct observation of the carbon skeleton rearrangement promoted by UAXS, which was made possible by employing site-selectively ^{13}C-2-, ^{13}C-3-, ^{2}H-3- and ^{2}H-4-labelled substrates combined with NMR-spectroscopic analysis (Figures 1b and 1c). The substrate analogue UDP-2-deoxy-GlcUA (**10**) and KIEs from intermolecular competition

between ^{1}H-3 and ^{2}H-3 substrates served to target the question of retroaldol-aldol or bond-shift mechanism.[24] Crucial steps were the development of multi-step chemo-enzymatic cascades for synthesis of isotope-labelled **2** from D-glucose (**11**) as well as compound **10** from D-glucal (**12**).[25-28]

Results

Synthesis of UDP-α-D-glucuronic acid (2) and UDP-2-deoxy-α-D-glucuronic acid (10)

The biocatalytic synthesis route leading to substrate **2** is depicted in Supplementary Fig. S1.[25-27] One-pot enzymatic transformation of monosaccharide **11** and uridine 5'-triphosphate (UTP) to UDP-α-D-glucose (**13**) had a yield of 85-99% after 24 hrs (Supplementary Fig. S2). Addition of inorganic pyrophosphatase (PPase) was necessary to avoid inhibition of UDP-glucose pyrophosphorylase (UGPase) and enzymatic hydrolysis of **13**.[29,30] Conversion of intermediate **13** to final product **2** was initiated when synthesis of **13** had finished. The applied chemo-enzymatic coenzyme regeneration cascade ensured full conversion by avoiding inhibition of UDP-glucose dehydrogenase (UGDH) by NADH, and after three hours, the reaction was complete (> 99% yield; Supplementary Fig. S3).[25,31] After anion exchange and size exclusion chromatography, compound **2** was obtained as sodium salt (isolated yield > 60%; Supplementary Fig. S4 and S5). ^{1}H and ^{13}C NMR spectroscopy were used to show identity and purity (> 90%) of the produced substrates (Supplementary Fig. S6-S11).[32] Substrate analogue **10** was produced as shown in Supplementary Figure S12.[28] Here, one-pot-transformation of **12**, phosphate and UTP to UDP-2-deoxy-α-D-glucose (**14**) had a yield of 41% after 70 hrs. Conversion of intermediate **14** to compound **10** was done as described above, however, the yield was lower (47%), which was explained by **14** being structurally different from the native substrate of UGDH (Supplementary Fig. S13). Compound **10** was obtained as sodium salt (12% isolated yield) in a purity of 86% using anion exchange and size exclusion chromatography (Supplementary Fig. S14-S19).

Reaction course analysis with ^{13}*C*-labelled substrates

UAXS from *Arabidopsis thaliana* (gene AXS1) was used.[1] Recombinant production of the enzyme resulted in good yields (32 mg/L culture medium) of highly pure UAXS (Supplementary Fig. S20). As activity and ratio of products **1** and **9** formed during conversion of substrate **2** were strongly pH-dependent, with both being highest at pH 8.5 (Supplementary Table T1), this pH was used in all experiments.

In Figure 2, consumption of ^{13}*C*-2 (Figure 2a) and ^{13}*C*-3 (Figure 2c) substrate **2** and formation of products **8** and **9** during *in situ* ^{13}C NMR measurements are shown. Due to the applied short acquisition time, signals of non-labelled carbons were not visible. Heteronuclear correlation spectroscopy (HETCOR; Figure 2b) was used to assign the ^{13}C NMR signals to the respective carbons in case of ^{13}*C*-2 substrate **2** (see Supplementary Fig. S21-S23 for product reference spectra).[14] The detected correlation signal at ^{13}C, ^{1}H = 78.85, 4.51 ppm confirmed that the labelled carbon in **8** is bound to *H*-2 of the compound, *i.e.* the ^{13}*C*-2 product **8** was obtained. Although no correlation signal for the very small doublet at 71.65 ppm could be observed, from ^{1}H NMR spectroscopy (Supplementary Fig. S24) and the proposed mechanism(s) it can be assumed that ^{13}*C*-2 product **9** was obtained (see Figure 1b). Interestingly, the phosphorus coupling of ^{13}*C*-2 seen in **2** and **9** was not observed in **8**, most probably due to a different spatial geometry of this compound.[33]

In case of the ^{13}*C*-3 substrate, heteronuclear single quantum coherence (HSQC) spectroscopy revealed the presence of the ^{13}*C* label at positions *C*-3' of product **8** and *C*-3 of product **9** (Figure 2d). The chemical shifts of the protons attached to the observed carbons (^{13}C, ^{1}H = 63.14, 3.51 ppm and 72.98, 3.63 ppm) were in accordance with the references for *H*-3' of **8** (3.53 ppm) and *H*-3 of **9** (3.65 ppm), respectively.[14,34] Furthermore, the negative phase of the signal of product **8** (blue colour) indicated a CH_2 group at *C*-3', in accordance with the structure of **8** (see Figure 1a).

Reaction course analysis with ^{2}*H*-labelled substrates

The ^{1}H NMR spectrum after conversion of the ^{2}*H*-3 substrate is shown in Figure 3a. Only signals of products **8** and **9** are visible, as expected. The ratio **8**:**9** was approximately 1.9:1, which is in line with the value obtained for conversion of unlabelled substrate (Supplementary Table T2). While in unlabelled cyclic phosphate **8** the *H*-3' protons appear as two doublets (Supplementary Fig. S21), there is only one singlet visible in the spectrum of the labelled compound, in accordance with presence of a $C^{2}H^{1}H$ group at position 3'. Binding between this proton and *C*-3' of **8** was confirmed by HSQC (Figure 3b). The absence of a second *H*-3' signal proved that no incorporation of hydrogen had occurred during catalytic ring rearrangement. No signal of product **9** *H*-3 was visible, as expected.

Product **8** obtained from conversion of ^{2}*H*-4 substrate **2** also contained a $C^{2}H^{1}H$ group at position 3' (Figures 3c and 3d), however, the hydrogen replaced by deuterium differed from that in reaction with the ^{2}*H*-3 substrate (cf. Figures 3a, 3c and Supplementary Fig. S21: in 3a, the singlet is located at 3.55 ppm, while it is at 3.51 ppm in 3c). This is consistent with transfer of the deuteride at *C*-4 of substrate **2** to NAD^{+} in the initial oxidation step and stereospecific re-transfer to *C*-3' of intermediate **7** in reduction of the aldehyde function.[5] No loss of the label was observed, in accordance with previous results.[7] The **8:9** ratio was distinctly lower than in reactions with unlabelled substrate (1.5:1 vs. 1.8:1; Supplementary Table T2), and conversion of ^{2}*H*-4 substrate **2** was approximately 1.5-fold slower than conversion of unlabelled substrate. These findings indicate that due to ^{2}*H*-4 the reduction of aldehyde **7** became slightly rate-limiting during synthesis of product **1**, as the lower reaction rate can be explained with slower transfer of the deuteride to aldehyde **7**.[35] A lower rate in this step also led to increased formation of product **9** due to the reversibility of the ring contraction steps.[12] In product **9**, deuterium was found at *C*-4, as expected.

Secondary kinetic isotope effects from intermolecular competition between ^{1}H-3 and ^{2}H-3 substrates

In synthesis of product **1**, secondary KIEs on k_{cat}/K_m arising from the ^{2}H-3 label can result either from aldol cleavage in intermediate **4** ($sp^3 \rightarrow sp^2$ hybridization change at *C*-3) or from reduction of aldehyde **7** ($sp^2 \rightarrow sp^3$ hybridization change at *C*-3').[20] Formation of product **9**, by contrast, could only be affected if it proceeded via the retroaldol-aldol mechanism (Figure 1a). Table 1 summarizes the results of an intermolecular competition experiment with unlabelled and ^{2}H-3 substrate **2** (for references on methods and interpretation, see 20, 24, 36, 37). After full conversion, there was no elevated hydrogen level detectable at position 3' of product **8**. However, at 50% conversion ^{1}H was enriched by 21% in product **8** and by 19% in product **9.** As shown in Table 1, the resulting KIEs are normal (≥ 1.00) and approach upper limits for a fully expressed secondary deuterium KIE, indicating rate limitation by the isotope-sensitive step or steps in the reaction. Considering the relatively small KIE resulting from ^{2}H-4 in substrate on the reduction of aldehyde **7**, the preferred incorporation of hydrogen in the apiosyl compound suggested that the rate-determining step in its synthesis was the aldol cleavage in intermediate **4**.[20] In combination with the lack of ^{1}H enrichment in product **8** after full conversion, these results were also conclusive in suggesting formation of the xylosyl compound via intermediate **5** rather than via direct reduction of intermediate **4**. In the latter case, one would expect hydrogen enrichment in product **8** and concomitant deuterium enrichment in product **9** after full conversion

Reaction course analysis with UDP-2-deoxy-α-D-glucuronic acid

Analogue **10** was investigated because formation of an apiosyl product from it would only be possible in the case of the bond-shift mechanism. In the retroaldol-aldol mechanism, by contrast, the missing hydroxyl group at *C*-2 would impede aldol cleavage. Consequently, also formation of UDP-2-deoxy-α-D-xylose (**15**) could only be achieved through direct reduction of UDP-2-deoxy-4-keto-α-D-xylose (**16**), without involvement of an open-chain intermediate

(Supplementary Fig. S25). To exclude that substrate analogue **10** was intrinsically unreactive to become transformed into the 4-keto compound in the initial oxidative decarboxylation step of the reaction, as it was observed for a 2-fluoro analogue of substrate **2**,[12] we also analysed conversion of **10** by UXS. The human form of UXS was used.[15]

HPLC analysis of a reaction mixture containing compound **10**, NAD^+ and UXS indeed showed formation of a nucleotide sugar, which was subsequently identified as product **15** by NMR spectroscopy (Supplementary Fig. S26-S28). Therefore, this clearly demonstrates the possibility of synthesis of **15** via intermediates UDP-2-deoxy-4-keto-α-D-glucuronic acid (**17**) and intermediate **16**. However, UAXS by contrast showed neither formation of UDP-2-deoxy-α-D-apiose (**18**) nor formation of product **15** or any intermediate from substrate analogue **10** under a range of conditions (different pH values, substrate, coenzyme and enzyme concentrations; see Supplementary Fig. S29-31). In accordance with the results from intermolecular competition experiments, these findings are consistent with the retroaldol-aldol mechanism and formation of product **9** from intermediate **5** rather than from **4**.

Discussion

The herein chosen research approach of probing the UAXS reaction with site-selectively labelled substrate variants and a deoxygenated analogue of substrate **2** proved fruitful in deciphering the multi-step mechanism of the enzyme. In particular, it revealed the elusive catalytic chemistry of pyranoside ring contraction. Development of efficient synthetic ways towards the critically required "substrate probes" was therefore a highly important part of this work. Considering that methodology for chemical and/or enzymatic synthesis of **2** is not well established, we think this *per se* is a significant result of broader interest from the current study.[38,39]

^{13}C-labelling of selected carbon atoms in the pyranoside ring of **2** provided a highly sensitive “on-molecule probe” for NMR spectroscopy, as the rearrangement of the carbon skeleton

could be monitored conveniently by the distinct ^{13}C chemical shifts of substrate and products.[40,41] In both suggested reaction routes to product **1**, *C*-2 of this product (as well as *C*-2 of product **9**) should originate from *C*-2 of substrate **2**, which was proven by our studies. *C*-3 of **2**, in contrast, would be shifted out of the sugar ring during catalytic rearrangement, which is why it should be present in an exocyclic CH_2 group in the apiosyl product (*C*-3'). Likewise, *H*-3 of substrate **2** should be part of this CH_2 group (*H*-3'). Indeed, both atoms could be tracked unambiguously from the substrate to their respective positions in product **1**, giving strong evidence that UAXS rebuilds the carbon skeleton by bond formation between *C*-2 and *C*-4 of intermediate **6**. We could also demonstrate that ^{2}H-4 from substrate **2** was stereospecifically transferred to *C*-3' in aldehyde reduction. These findings altogether give conclusive evidence for the pyranoside-to-furanoside ring rearrangement as shown in Figure 1a.

Preferred incorporation of hydrogen over deuterium originating from position 3 of substrate **2** in both the apiosyl and xylosyl product during the course of the reaction can be rationalized by the fact that the overall rate-determining step of the reaction involves aldol cleavage in the 4-keto-pentose species (**4**). However, this excludes direct formation of **9** prior to the ring opening, which could be confirmed as no product **15** was formed from substrate analogue **10** by UAXS, although its formation was possible using UXS. The bond-shift mechanism in formation of the apiosyl product could also be excluded, as no formation of product **18** was detectable. Combined evidence from intermolecular competition and substrate analogue experiments therefore strongly supported the retroaldol-aldol mechanism with formation of product **1** from aldol addition between *C*-2/*C*-4 of intermediate **6**. Product **9** is formed through aldol addition between *C*-2/*C*-3 of intermediate **5**. Interestingly, not even formation of the 4-keto intermediates **17** or **16** was visible when incubating UAXS with substrate analogue **10**. This finding is interpreted as evidence for a strong coupling between the initial oxidative decarboxylation and sugar ring opening, that is, the 4-keto intermediates are only formed in

detectable amounts when aldol cleavage in intermediate **4** is possible. As this is impeded in the *C*-2 deoxy intermediate **16**, no reaction at all occurs.

In summary, we present a comprehensive mechanistic characterization of the UAXS catalytic reaction. Retroaldol-aldol chemistry is suggested to underlie the enzymatic pyranoside ring contraction. Unexpectedly and contrary to previous proposals,[1,5-11,14] point of divergence of the UAXS and UXS pathway is probably early in the reaction, that is, prior to formation of **4** as *intermediate* of the enzymatic pathway. The final mechanistic proposal, which is formation of products **1** and **9** from different "exit points" in the retroaldol-aldol route where interception of intermediate **7** via reduction by enzyme-NADH is the decisive step towards product **1**, is developed to a degree that chemical enzymology can best achieve. Our results therefore elucidate biosynthesis of *C*-branched sugars that play important biological roles not only in plant cell wall development, but also, like D-streptose, in bacterial secondary metabolism.[4,18] Furthermore, the high potential of selective isotope labelling in dissection of chemical and enzymatic reaction mechanisms is emphasized.[20,24,26,40]

Methods

Chemicals and strains

Isotope-labelled D-glucose was acquired from Omicron Biochemicals (South Bend, Indiana, USA) and had purities of 99% (^{13}C-labelled) or 98% (^{2}H-labelled). UTP (> 99% purity) was purchased from Carbosynth (Compton, UK), UDP-α-D-glucuronic acid (> 98% purity), 9,10-phenanthrenequinone (> 99% purity) and bovine serum albumin (BSA; > 98% purity) were from Sigma-Aldrich (Vienna, Austria). NAD^+ (> 98% purity) was obtained from Roth (Karlsruhe, Germany). Deuterium oxide for NMR measurements (99.96% ^{2}H) was from Euriso-Top (Saint-Aubin Cedex, France). All other chemicals were purchased either from Sigma-Aldrich or Roth and were of the highest purity available.

Bovine liver catalase (3809 U/mg), *S. cerevisiae* hexokinase (25 U/mg), rabbit muscle phosphoglucomutase (≥ 100 U/mg) and *S. cerevisiae* inorganic pyrophosphatase (PPase; ≥ 500 U/mg) were purchased from Sigma-Aldrich. Expression and purification of the recombinant human UGDH, *Candida tenuis* xylose reductase (*Ct*XR), *Cellulomonas uda* cellobiose phosphorylase (*Cu*CPase) and human UXS are described elsewhere.[15,28,42,43] Gene BLLJ_1074 coding for UTP-glucose-1-phosphate uridylyltransferase (UGPase) from *Bifidobacterium longum* subsp. *longum* JCM 1217 (UniProt: E8MIY8), cloned into a pET-30a vector using *Nde*I and *Xho*I restriction sites for expression with a *C*-terminally fused His_6 tag, was kindly provided by Dr. Motomitsu Kitaoka (National Agriculture and Food Research Organization, Japan). The gene was sequenced before creating an expression strain by transformation of electrocompetent *E. coli* BL21 Gold (DE3) cells.

The sequence of gene AXS1 (GenBank: NM_128345) from *Arabidopsis thaliana*, coding for UAXS, was codon-optimized for expression in *E. coli* and a synthetic gene (Supplementary Fig. S32) was ordered from GenScript (Piscataway, New Jersey, USA). The gene was cloned in a pET-26b(+) vector by the supplier using *Nde*I and *Xho*I restriction sites, fusing it to a *C*-terminal His_6 tag. After transformation of electrocompetent *E. coli* BL21 Gold (DE3) cells, the construct was validated by sequencing (LGC Genomics, Berlin, Germany; Supplementary Fig. S33). For long-term storage, cells from a liquid culture (see below) were frozen with 40% (v/v) glycerol and stored at -70 °C.

Expression and purification of UAXS

Recombinant production of the enzyme was done according to established protocols.[15] A pre-culture containing 50 mL LB medium (50 mg/L kanamycin) in a 300 mL baffled flask was inoculated and grown overnight at 37 °C and 130 rpm. Main cultures contained 250 mL LB medium with kanamycin in 1 L baffled flasks and were inoculated to an OD_{600} of 0.01. The cultures were incubated at 37 °C and 130 rpm until the OD_{600} reached a value of 0.6-0.8, when 250 µM IPTG were added and the temperature was decreased to 18 °C. Afterwards,

expression of UAXS was performed overnight in a Certomat BS-1 incubator (Sartorius Stedim, Vienna, Austria).

Cells were harvested by centrifugation at 5000 rpm and 4 °C using a Sorvall Evolution RC centrifuge (Thermo Fisher Scientific, Waltham, Massachusetts, USA) equipped with a F10-S rotor and the pellet was stored at -20 °C. For purification, cells were disrupted by a French Pressure Cell Press (American Instrument Company, Silver Spring, Maryland, USA) and solid parts were removed by centrifugation (16000 g, 4 °C, 60 min) on an Eppendorf 5415 R centrifuge (Eppendorf, Hamburg, Germany). The supernatant was filtered through a 1.2 µm Minisart filter (Sartorius Stedim) and loaded on a self-packed Cu^{2+}-loaded IMAC sepharose column (GE Healthcare, Vienna, Austria) using a BioLogic DuoFlow liquid chromatograph (Bio-Rad, Vienna, Austria). Elution was done using 50 mM Tris/HCl pH 7.5 buffers containing 5% (v/v) glycerol (buffer A and B) and 400 mM imidazole (buffer B). UAXS started eluting at 120 mM imidazole. All enzyme-containing fractions were pooled and the buffer was exchanged to 50 mM Tris/HCl pH 7.5 containing 5% (v/v) glycerol and 1 mM dithiothreitol using Amicon Ultra-15 centrifugal concentrators (Millipore, Vienna, Austria). Enzyme preparations were stored at -70 °C. Purity of the enzyme was checked by SDS-PAGE (NuPAGE 4-12% Bis-Tris-Gel, Life Technologies, Vienna, Austria) and Silver Staining (Supplementary Fig. S20). UAXS concentrations were determined by UV spectroscopy (λ = 280 nm) on a DeNovix DS-11+ microvolume spectrophotometer (DeNovix, Wilmington, Delaware, USA) using a molar extinction coefficient ϵ of 48360 M^{-1} cm^{-1} and a molecular weight of 44703 Da (calculated by the ExPASy ProtParam web service).

Synthesis of UDP-α-D-glucuronic acid (2)

The method for enzymatic synthesis of intermediate **13** was adapted from literature.[26,27] The reaction mixture (3 mL) contained 15 mM (isotope-labelled) monosaccharide **11** (8.11 mg, 0.045 mmol), 40-50 mM UTP (58.1-72.6 mg, 0.120-0.150 mmol), 5 mM $MgCl_2$ (1.43 mg, 0.015 mmol), 10 µM α-D-glucose 1,6-bisphosphate and 0.13% (w/v) BSA (3.9 mg) dissolved

in 50 mM Tris/HCl buffer (pH 7.5). 12 U/mL hexokinase (36 U), 6 U/mL phosphoglucomutase (18 U), 1.2 U/mL UGPase (3.6 U) and 1.2 U/mL inorganic PPase (3.6 U) were added and the reaction was incubated at 30 °C for 24 hrs. Upon completion, the mixture was split in three 1-mL-batches and synthesis of compound **2** was started by increasing temperature to 37 °C and adding 2 mM NAD^+ (1.33 mg, 0.002 mmol), 25 µM 9,10-phenanthrenequinone (**19)**, 20 mM hydrogen peroxide (H_2O_2; 0.68 mg, 0.020 mmol), 2.4 U/mL *Ct*XR (2.4 U), 100 U/mL catalase (100 U) and 0.9 U/mL hUGDH (0.9 U) to each batch. The mixtures were incubated for 180 min and H_2O_2 was fed in regular intervals, as described previously.[25]

Prior to chromatographic purification of substrate **2**, enzymes were removed by ultrafiltration using Vivaspin-6 centrifugal concentrators (Sartorius Stedim). Purification of the produced nucleotide sugars was done using an ÄKTA FPLC liquid chromatograph (GE Healthcare) equipped with a 5 mL HiTrap Q HP (GE Healthcare) anion exchange column and a 2 mL sample loop. A step-wise gradient of 7.5 mL min^{-1} sodium chloride (buffer A: 20 mM and buffer B: 500 mM) in a 20 mM sodium acetate buffer (pH 4.2) was used for elution of bound compounds (Supplementary Fig. S4). The steps were as follows: 6 mL NaCl 0 mM, 36.5 mL NaCl 75 mM, 26 mL NaCl 125 mM, 15 mL NaCl 500 mM, 15 mL NaCl 0 mM. Prior to each run, the column was regenerated by flushing with at least three column volumes of buffer B and buffer A. UV absorption (λ = 254 nm) was used to detect the target compounds, which were collected. All product-containing fractions were pooled and concentrated on a Laborota 4000 rotary evaporator (Heidolph, Schwabach, Germany) at 45 °C and 20 mbar to a final volume of approximately 4 mL.

NaCl was removed from nucleotide sugar preparations using ÄKTA FPLC with a 2 mL sample loop and a Superdex Peptide 10/300 GL size exclusion column (GE Healthcare). Elution was performed with deionized water at a flow rate of 1 mL min^{-1}. The target compound was detected by UV absorption (λ = 254 nm; Supplementary Fig. S5). Product-

containing fractions were collected, pooled and concentrated on the Laborota 4000 at 45 °C and 20 mbar to a final volume of approximately 5-10 mL. Residual H_2O was removed by lyophilization on a Christ Alpha 1-4 lyophilizer (B. Braun Biotech International, Melsungen, Germany), after which nucleotide sugars were obtained as white powder.

Synthesis of UDP-2-deoxy-α-D-glucuronic acid (10)

Compound **12** was converted to 2-deoxy-α-D-glucose 1-phosphate (**20**) by *Cu*CPase using a modification of the method published by Wildberger *et al.*[28], and further on to intermediate **14** by UGPase, as described for synthesis of substrate **2**. The reaction mixture (3 × 1 mL) contained 40 mM compound **12** (17.5 mg, 0.120 mmol), 20 mM UTP (29.1 mg, 0.060 mmol), 5 mM $MgCl_2$ (1.43 mg, 0.015 mmol) and 0.13% (w/v) BSA (3.9 mg) dissolved in 31 mM potassium phosphate buffer (pH 7.0). After addition of 0.5 U/mL inorganic PPase (1.5 U), 84.5 U/mL UGPase (253.5 U) and 15 µM *Cu*CPase (0.045 µmol), the reaction was incubated at 30 °C for 70 hrs. For synthesis of substrate analogue **10**, the pH was set to 7.5 and temperature was increased to 37 °C. After addition of 2 mM NAD^+ (1.33 mg, 0.002 mmol), 25 µM compound **19**, 20 mM H_2O_2 (0.68 mg, 0.020 mmol), 2.64 U/mL *Ct*XR (2.64 U), 100 U/mL catalase (100 U) and 1.8 U/mL hUGDH (1.8 U) to each batch, the mixtures were incubated for 5.5 hrs. H_2O_2 was fed in regular intervals as described previously.[25] Purification was done according to substrate **2**, however, a 1 mL SuperQ 650M column (Tosoh Bioscience GmbH, Stuttgart, Germany), a flow rate of 3 mL min^{-1} and the following steps were used: 16 mL NaCl 0 mM, 92 mL NaCl 20 mM, 20 mL NaCl 150 mM, 17 mL NaCl 500 mM, 16 mL NaCl 0 mM (Supplementary Fig. S14). NaCl was separated from compound **10** as described for substrate **2** (Supplementary Fig. S15). Water was always removed under N_2 flow due to the instability of **10**.

UAXS enzymatic assays

Reactions were performed at 30 °C on a Thermomixer Comfort (Eppendorf) without agitation. If not stated otherwise, 2 mM of substrate were used and the buffer was 50 mM potassium phosphate pH 8.5. For measuring the pH profile, this buffer was used in the pH range 6.0-8.5 and 50 mM citrate was used between pH 5.0 and 6.0 as well as 50 mM Tris/HCl between pH 8.5 and 9.5. 20 µM UAXS were added to start the reaction and a sample was drawn immediately. Further samples were taken in regular intervals, as indicated. For stopping the reaction, samples were heated to 99 °C for 5 min or mixed with acetonitrile (1:1 ratio). Concentrations of substrate stock solutions were always confirmed by UV spectroscopy (λ = 262 nm) on a DeNovix DS-11+ microvolume spectrophotometer (DeNovix) using a molar extinction coefficient ϵ of 10 mM^{-1} cm^{-1}.[44]

KIEs from intermolecular competition experiments

Reaction conditions were the same as for standard enzymatic assays, except that 1 mM unlabelled substrate **2** and 1 mM ^{2}H-3 substrate **2** were mixed to yield the final substrate concentration. After the reaction had proceeded to the desired level, enzymes were removed by ultrafiltration, as described for synthesis of substrate **2**. Purification of the reaction products was done using an ÄKTA FPLC liquid chromatograph (GE Healthcare) equipped with a 5 mL HiTrap Q HP anion exchange column (GE Healthcare) and a 2 mL sample loop. A continuous gradient of 7.5 mL min^{-1} ammonium formate buffer (buffer A: 20 mM and buffer B: 500 mM; pH 4.2) was used for elution of bound compounds (Supplementary Fig. S34). Collected 5-mL-fractions were lyophilized and subjected to desalting on a Superdex Peptide 10/300 GL column (GE Healthcare), as described above. After lyophilization and dissolution in D_2O, all fractions were analysed by NMR spectroscopy.[37]

Evaluation of the spectra for determination of the $^{1}H/^{2}H$ ratio was done using ACD/NMR Processor Academic Edition NMR Processor Academic Edition 12.0 (Advanced Chemistry

Development Inc., Toronto, Canada). Peaks were fitted with a Gauss+Lorentz function and optimized using a Levenberg-Marquadt algorithm (starting Lorentz fraction: 0.5).

High performance liquid chromatography

Samples were analysed on a Shimadzu Prominence HPLC system (Shimadzu, Korneuburg, Austria) equipped with a 5 µm Kinetex C18 analytical HPLC column (4.6 × 50 mm; Phenomenex, Aschaffenburg, Germany) and a UV detector (λ = 262 nm). Precipitated protein was removed from samples by centrifugation (16000 g, 4 °C, 5 min) on an Eppendorf 5415 R centrifuge (Eppendorf), and after proper dilution, samples were measured using an injection volume of 5 µL, a temperature of 35 °C and a flow rate of 2 mL min^{-1}. Isocratic elution was performed using 87.5% 40 mM tetrabutylammonium bromide in 20 mM potassium phosphate buffer (pH 5.9) and 12.5% acetonitrile. Analysis time was 3.5 min (without UTP) or 4.5 min (with UTP). Authentic standards were used for calibration.

NMR spectroscopy

A Varian (Agilent) INOVA 500-MHz NMR spectrometer (Agilent Technologies, Santa Clara, California, USA) and the VNMRJ 2.2D software were used for all measurements. ^{1}H NMR spectra (499.98 MHz) were measured on a 5 mm indirect detection PFG-probe, while a 5 mm dual direct detection probe with z-gradients was used for ^{13}C NMR spectra (125.71 MHz). Enzymatic *in situ* reactions were performed at 30 °C in a total volume of 500 µL potassium phosphate buffer 50 mM (pD 8.5) in D_2O containing 2 mM of the respective substrate and 20 µM UAXS. The pD was determined as pH meter reading plus 0.4.[45] ^{1}H NMR spectra were recorded with pre-saturation of the water signal by a shaped pulse in case of *in situ* experiments. Standard pre-saturation sequence was used: relaxation delay 2 s; 90° proton pulse; 2.048 s acquisition time; spectral width 8 kHz; number of points 32 k. ^{13}C NMR spectra during *in situ* experiments were recorded with the following pulse sequence: standard ^{13}C pulse sequence with 45° carbon pulse, relaxation delay 2 s, Waltz decoupling during

acquisition, 2 s acquisition time. Up to 256 scans were accumulated in one measurement. Arrayed spectra were acquired with an array of pre-acquisition delay of 30 min or 60 min. HSQC spectra were measured with 128 scans per increment and adiabatic carbon 180° pulses. HETCOR spectra were recorded with 4 scans per increment and 256 increments. For KIE analysis, a standard proton experiment with relaxation delay of 25 s was used to record ^{1}H NMR spectra. ACD/NMR Processor Academic Edition 12.0 (Advanced Chemistry Development Inc.) was used for evaluation of spectra.

References

1 Mølhøj, M., Verma, R. & Reiter, W.-D. The biosynthesis of the branched-chain sugar D-apiose in plants: functional cloning and characterization of a UDP-D-apiose/UDP-D-xylose synthase from *Arabidopsis*. *Plant J.* **35**, 693-703 (2003).

2 McNeil, M., Darvill, A. G., Fry, S. C. & Albersheim, P. Structure and function of the primary cell walls of plants. *Annu. Rev. Biochem.* **53**, 625-663 (1984).

3 Longland, J. M., Fry, S. C. & Trewavas, A. J. Developmental control of apiogalacturonan biosynthesis and UDP-apiose production in a duckweed. *Plant Physiol.* **90**, 972-976 (1989).

4 O'Neill, M. A., Eberhard, S., Albersheim, P. & Darvill, A. G. Requirement of borate cross-linking of cell wall rhamnogalacturonan II for *Arabidopsis* growth. *Science* **294**, 846-849 (2001).

5 Baron, D. & Grisebach, H. Further studies on mechanism of action of UDP-apiose/UDP-xylose synthase from cell cultures of parsley. *Eur. J. Biochem.* **38**, 153-159 (1973).

6 Gebb, C., Baron, D. & Grisebach, H. Spectroscopic evidence for the formation of a 4-keto intermediate in the UDP-apiose/UDP-xylose synthase reaction. *Eur. J. Biochem.* **54**, 493-498 (1975).

7 Kelleher, W. J. & Grisebach, H. Hydride transfer in the biosynthesis of uridine diphospho-apiose from uridine diphospho-D-glucuronic acid with an enzyme preparation of *Lemna minor*. *Eur. J. Biochem.* **23**, 136-142 (1971).

8 Mendicino, J. & Abou-Issa, H. Conversion of UDP-D-glucuronic acid to UDP-D-apiose and UDP-D-xylose by an enzyme isolated from *Lemna minor*. *Biochim. Biophys. Acta* **364**, 159-172 (1974).

9 Picken, J. M. & Mendicino, J. The biosynthesis of D-apiose in *Lemna minor*. *J. Biol. Chem.* **242**, 1629-1634 (1967).

10 Sandermann, H., Tisue, G. T. & Grisebach, H. Biosynthesis of D-apiose IV. Formation of UDP-apiose from UDP-D-glucuronic acid in cell-free extracts of parsley (*Apium petroselinum* L.) and *Lemna minor*. *Biochim. Biophys. Acta* **165**, 550-552 (1968).

11 Sandermann, H. & Grisebach, H. Biosynthesis of D-apiose V. NAD^+-dependent biosynthesis of UDP-apiose and UDP-xylose from UDP-D-glucuronic acid with an enzyme preparation from *Lemna minor* L. *Biochim. Biophys. Acta* **208**, 173-180 (1970).

12 Choi, S.-h., Ruszczycky, M. W., Zhang, H. & Liu, H.-w. A fluoro analogue of UDP-α-D-glucuronic acid is an inhibitor of UDP-α-D-apiose/UDP-α-D-xylose synthase. *Chem. Commun.* **47**, 10130-10132 (2011).

13 Choi, S.-h., Mansoorabadi, S. O., Liu, Y.-n., Chien, T.-C. & Liu, H.-w. Analysis of UDP-D-apiose/UDP-D-xylose synthase-catalysed conversion of UDP-D-apiose phosphonate to UDP-D-xylose phosphonate: Implications for a retroaldol-aldol mechanism. *J. Am. Chem. Soc.* **134**, 13946-13949 (2012).

14 Guyett, P., Glushka, J., Gu, X. & Bar-Peled, M. Real-time NMR monitoring of intermediates and labile products of the bifunctional enzyme UDP-apiose/UDP-xylose synthase. *Carbohydr. Res.* **344**, 1072-1078 (2009).

15 Eixelsberger, T. *et al.* Structure and mechanism of human UDP-xylose synthase. Evidence for a promoting role of sugar ring distortion in a three-step catalytic conversion of UDP-glucuronic acid. *J. Biol. Chem.* **287**, 31349-31358 (2012).

16 Baron, D., Wellmann, E. & Grisebach, H. Purification and properties of an enzyme from cell suspension cultures of parsley catalyzing the synthesis of UDP-apiose and UDP-D-xylose from UDP-D-glucuronic acid. *Biochim. Biophys. Acta* **258**, 310-318 (1972).

17 He, X. M. & Liu, H.-w. Formation of unusual sugars: Mechanistic studies and biosynthetic applications. *Annu. Rev. Biochem.* **71**, 701-754 (2002).

18 Thibodeaux, C. J., Melançon III, C. E. & Liu, H.-w. Unusual sugar biosynthesis and natural product glycodiversification. *Nature* **446**, 1008-1016 (2007).

19 Thibodeaux, C. J., Melançon III, C. E. & Liu, H.-w. Natural-product sugar biosynthesis and enzymatic glycodiversification. *Angew. Chem., Int. Ed.* **47**, 9814-9859 (2008).

20 Munos, J. W., Pu, X., Mansoorabadi, S. O., Kim, H. J. & Liu, H.-w. A secondary kinetic isotope effect study of the 1-deoxy-D-xylulose-5-phosphate reductoisomerase-catalysed reaction: evidence for a retroaldol-aldol rearrangement. *J. Am. Chem. Soc.* **131**, 2048-2049 (2009).

21 Wong, U. & Cox, R. J. The chemical mechanism of D-1-deoxyxylulose-5-phosphate reductoisomerase from *Escherichia coli*. *Angew. Chem., Int. Ed.* **46**, 4926-4929 (2007).

22 Manning, K.A., Sathyamoorthy, B., Eletsky, A., Szyperski, T. & Murkin, A. S. Highly precise measurement of kinetic isotope effects using ^{1}H-detected 2D [^{13}C,^{1}H]-HSQC NMR spectroscopy. *J. Am. Chem. Soc.* **134**, 20589-20592 (2012).

23 Kavanagh, K. L., Jörnvall, H., Persson, B. & Oppermann, U. The SDR superfamily: functional and structural diversity within a family of metabolic and regulatory enzymes. *Cell. Mol. Life Sci.* **65**, 3895-3906 (2008).

24 Chan, J., Tang, A. & Bennet, A. J. A stepwise solvent-promoted S_Ni reaction of α-D-glucopyranosyl fluoride: mechanistic implications for retaining glycosyltransferases. *J. Am. Chem. Soc.* **134**, 1212-1220 (2012).

25 Eixelsberger, T. & Nidetzky, B. Enzymatic redox cascade for one-pot synthesis of uridine 5'-diphosphate xylose from uridine 5'-diphosphate glucose. *Adv. Synth. Catal.* **356**, 3575-3584 (2014).

26 Lee, S. S. *et al.* Mechanistic evidence for a front-side, S_Ni-type reaction in a retaining glycosyltransferase. *Nat. Chem. Biol.* **7**, 631-638 (2011).

27 Ma, X. & Stöckigt, J. High yielding one-pot enzyme-catalysed synthesis of UDP-glucose in gram scales. *Carbohydr. Res.* **333**, 159-163 (2001).

28 Wildberger, P., Brecker, L. & Nidetzky, B. Examining the role of phosphate in glycosyl transfer reactions of *Cellulomonas uda* cellobiose phosphorylase using D-glucal as donor substrate. *Carbohydr. Res.* **356**, 224-232 (2012).

29 Kotake, T. *et al.* UDP-sugar pyrophosphorylase with broad substrate specificity toward various monosaccharide 1-phosphates from pea sprouts. *J. Biol. Chem.* **279**, 45728-45736 (2004).

30 Ohashi, T., Cramer, N., Ishimizu, T. & Hase, S. Preparation of UDP-galacturonic acid using UDP-sugar pyrophosphorylase. *Anal. Biochem.* **352**, 182-187 (2006).

31 Kadirvelraj, R., Sennett, N. C., Custer, G. S., Phillips, R. S. & Wood, Z. A. Hysteresis and negative cooperativity in human UDP-glucose dehydrogenase. *Biochemistry* **52**, 1456-1465 (2013).

32 Gu, X. *et al.* Identification of a bifunctional UDP-4-keto-pentose/UDP-xylose synthase in the plant pathogenic bacterium *Ralstonia solanacearum* strain GMI1000, a distinct member of the 4,6-dehydratase and decarboxylase family. *J. Biol. Chem.* **285**, 9030-9040 (2010).

33 Karplus, M. Vicinal proton coupling in nuclear magnetic resonance. *J. Am. Chem. Soc.* **85**, 2870-2871 (1963).

34 Bar-Peled, M., Griffith, C. L. & Doering, T. L. Functional cloning and characterization of a UDP-glucuronic acid decarboxylase: The pathogenic fungus *Cryptococcus neoformans* elucidates UDP-xylose synthesis. *Proc. Natl. Acad. Sci. U.S.A* **98**, 12003-12008 (2001).

35 Northrop, D. B. The expression of isotope effects on enzyme-catalysed reactions. *Annu. Rev. Biochem.* **50**, 103-131 (1981).

36 Anslyn, E. V. & Dougherty, D. A. *Modern Physical Organic Chemistry* (University Science Books, Herndon, 2006).

37 Crich, D. & Chandrasekera, N. S. Mechanism of 4,6-*O*-benzylidene-directed β-mannosylation as determined by α-deuterium kinetic isotope effects. *Angew. Chem., Int. Ed.* **43**, 5386-5389 (2004).

38 Cai, L. Recent progress in enzymatic synthesis of sugar nucleotides. *J. Carbohydr. Chem.* **31**, 535-552 (2012).

39 Wagner, G. K., Pesnot, T. & Field, R. A. A survey of chemical methods for sugar-nucleotide synthesis. *Nat. Prod. Rep.* **26**, 1172-1194 (2009).

40 Huang, M. *et al.* Dissecting the mechanisms of a class of chemical glycosylation using primary ^{13}C kinetic isotope effects. *Nat. Chem.* **4**, 663-667 (2012).

41 Singh, S., Peltier-Pain, P., Tonelli, M. & Thorson, J. S. A general NMR-based strategy for the *in situ* characterization of sugar-nucleotide-dependent biosynthetic pathways. *Org. Lett.* **16**, 3220-3223 (2014).

42 Egger, S., Chaikuad, A., Kavanagh, K. L., Oppermann, U. & Nidetzky, B. Structure and mechanism of human UDP-glucose 6-dehydrogenase. *J. Biol. Chem.* **286**, 23877-23887 (2011).

43 Pival, S. L., Klimacek, M., Kratzer, R. & Nidetzky, B. Tyr-51 is the proton donoracceptor for NAD(H)-dependent interconversion of xylose and xylitol by *Candida tenuis* xylose reductase (AKR2B5). *FEBS Lett.* **582**, 4095-4099 (2008).

44 Cavaluzzi, M. J. & Borer, P. N. Revised UV extinction coefficients for nucleoside-5'-monophosphates and unpaired DNA and RNA. *Nucleic Acids Res.* **32**, e13 (2004).

45 Krężel, A. & Bal, W. A formula for correlating pK_a values determined in D_2O and H_2O. *J. Inorg. Biochem.* **98**, 161-166 (2004).

Acknowledgements

Financial support from the Austrian Science Fund FWF (Project W901-B05 DK Molecular Enzymology) is gratefully acknowledged. We thank Regina Kratzer from the Institute of Biotechnology and Biochemical Engineering at Graz University of Technology for xylose reductase.

Author contributions

T.E. and B.N. designed the research. T.E., D.H. and A.G. performed substrate syntheses. T.E. and H.W. performed NMR experiments. T.E. analysed data and wrote the paper with B.N.

Competing financial interests

The authors declare no competing financial interests.

Figure legends

Figure 1: Previous mechanistic suggestions for conversion of substrate **2** by UAXS and detailed proposal of the mechanism resulting from evidence obtained in this study. **a)** Depiction of possible ways for formation of products **1** and **9** via retroaldol-aldol or bond-shift mechanism (UMP = uridine 5'-monophosphate). Small coloured arrows indicate actions belonging to the respective pathway of the same colour. Dashed lines indicate possibilities for synthesis of products **1** and **9** directly from intermediate **4**. The framed steps of oxidative decarboxylation and ring opening appear to be strongly coupled in UAXS and involve rate limitation by retroaldol cleavage, as suggested by KIEs. **b)** Expected distribution of ^{13}C from substrate **2** to products **1** and **9** during enzymatic transformation. **c)** Expected distribution of ^{2}H from substrate **2** to products **1** and **9** during enzymatic transformation, assuming no $^{2}H/^{1}H$ exchange with the solvent.

Figure 2: Results of reaction course analysis with ^{13}C-labelled substrates. **a)** *In situ* ^{13}C NMR measurement of ^{13}C-2 substrate **2** conversion. Signals belonging to substrate **2** (G), product **8** (cA) and product **9** (X) are shown.[14] Time between two spectra is 150 min. **b)** HETCOR spectrum of the reaction mixture with ^{13}C-2 substrate **2** (F1 axis = ^{1}H, F2 axis = ^{13}C). The signal at 78.85, 4.51 ppm belongs to product **8** and shows binding of the ^{13}C label and *H*-2 of the compound. The signal at 71.41, 3.53 ppm belongs to the substrate. **c)** *In situ* ^{13}C NMR measurement of ^{13}C-3 substrate **2** conversion. Signals belonging to substrate **2** (G), product **8** (cA) and product **9** (X) are shown. Time between two spectra is 150 min. **d)** HSQC spectrum of the reaction mixture with ^{13}C-3 substrate **2** (F1 axis = ^{13}C, F2 axis = ^{1}H; blue = negative phase, orange = positive phase). The signal at 3.51, 63.14 ppm belongs to product **8** and shows binding of the ^{13}C label and *H*-3 of the compound. Binding between the ^{13}C label and *H*-3 of product **9** is confirmed by the signal at 3.63, 72.98 ppm. The signal at 3.70, 72.51 ppm belongs to the substrate.

Figure 3: Results of reaction course analysis with ^{2}H-labelled substrates. **a)** ^{1}H NMR spectrum after conversion of ^{2}H-3 substrate **2**. Signals belonging to substrate **2** (G), product **8** (cA) and product **9** (X) are shown. Only one proton is stereospecifically exchanged by deuterium originating from position 3 of substrate **2**. **b)** HSQC spectrum of the reaction mixture shown in panel 2a (F1 axis = ^{13}C, F2 axis = ^{1}H; blue = negative phase, orange = positive phase). The signal at 3.54, 63.06 ppm belongs to product **8** and shows binding of the ^{2}H label and *C*-3' of the compound. **c)** ^{1}H NMR spectrum after conversion of ^{2}H-4 substrate **2**. Signals belonging to substrate **2** (G), product **8** (cA) and product **9** (X) are shown. Only one proton is stereospecifically exchanged by deuterium originating from position 4 of substrate **2**. **d)** HSQC spectrum of the reaction mixture shown in panel 2c (F1 axis = ^{13}C, F2 axis = ^{1}H; blue = negative phase, orange = positive phase). The signal at 3.50, 62.92 ppm belongs to product **8** and shows binding of the ^{2}H label and *C*-3' of the compound.

Table 1: Results from intermolecular competition experiments using mixture of substrates containing ^{1}H-3 and ^{2}H-3. Products obtained from conversion of unlabelled substrate **2** were used to calculate relative signal areas. If no KIE occurred, values would be 100% for *H*-1, *H*-2 and *H*-4, 75% for *H*-3' and 50% for *H*-3. The values obtained in intermolecular competition experiments for *H*-3' and *H*-3 after partial substrate conversion are significantly higher (21% and 19%, respectively), indicating a KIE affecting formation of both products. See text for further explanations.

Product	Conv.	**Signal area (%) compared to unlabelled products**[a]					$k_{H\text{-}3}^{obs.}/k_{H\text{-}3}^{calc.}$
		H-1	*H*-2	*H*-3'a/b	*H*-3	*H*-4(a/b)[b]	
8	full	-[c]	102.0	75.5	-	100.4	**1.21 ± 0.01**[d]
	50%	-[c]	99.2	80.4	-	101.8	
9	full	98.0	-[c]	-	48.5	100.8	**1.19 ± 0.03**[d]
	50%	97.6	97.1	-	59.5	-[c]	

[a] Variability < 3%
[b] Product **9** only contains one proton at position 4.
[c] Not analysable due to signal overlap.
[d] Determined after 50% substrate conversion.

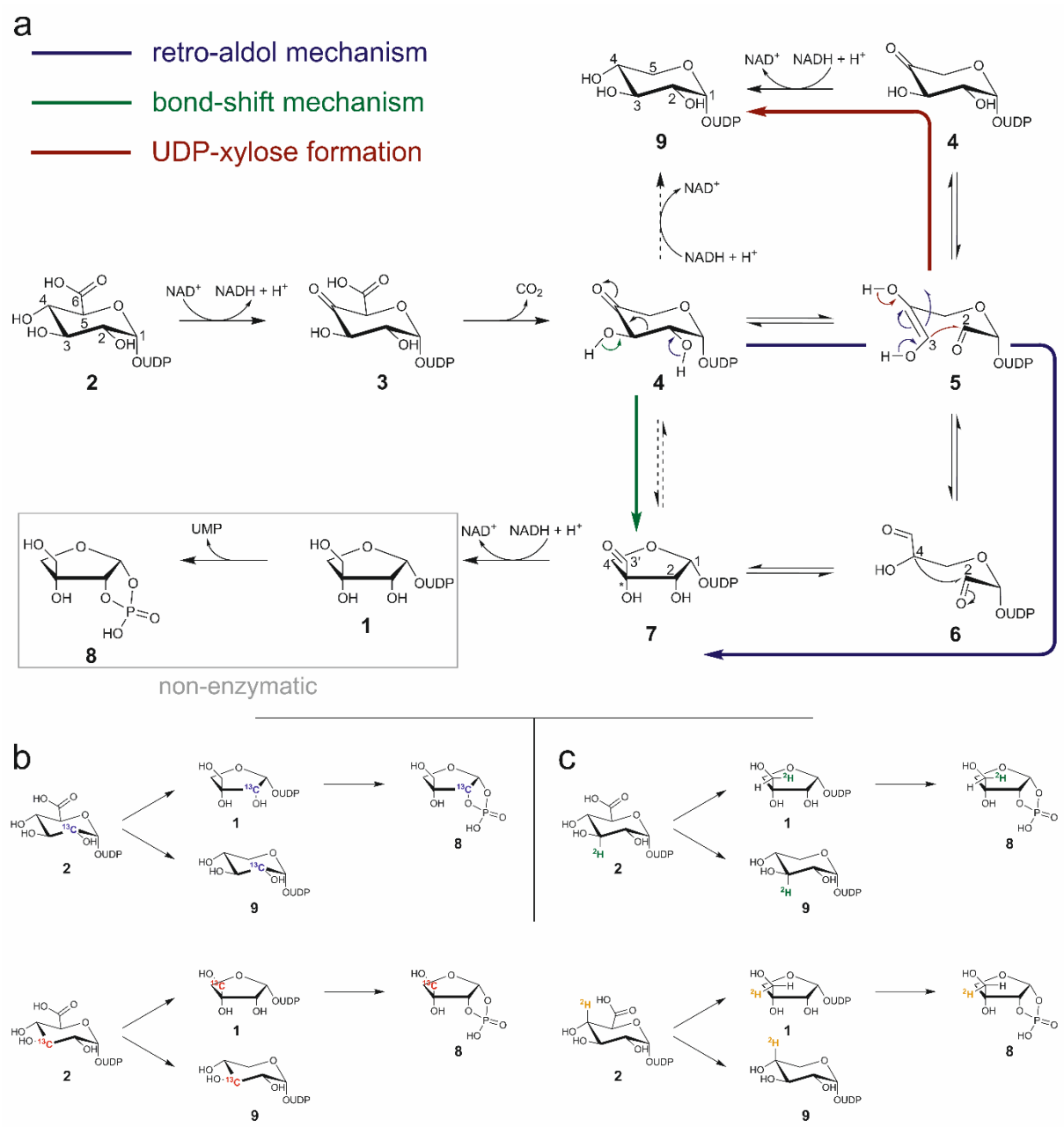
a
retro-aldol mechanism
bond-shift mechanism
UDP-xylose formation
NAD+
NADH + H+
CO2
UMP
OUDP
non-enzymatic
b
c

Figure 1.

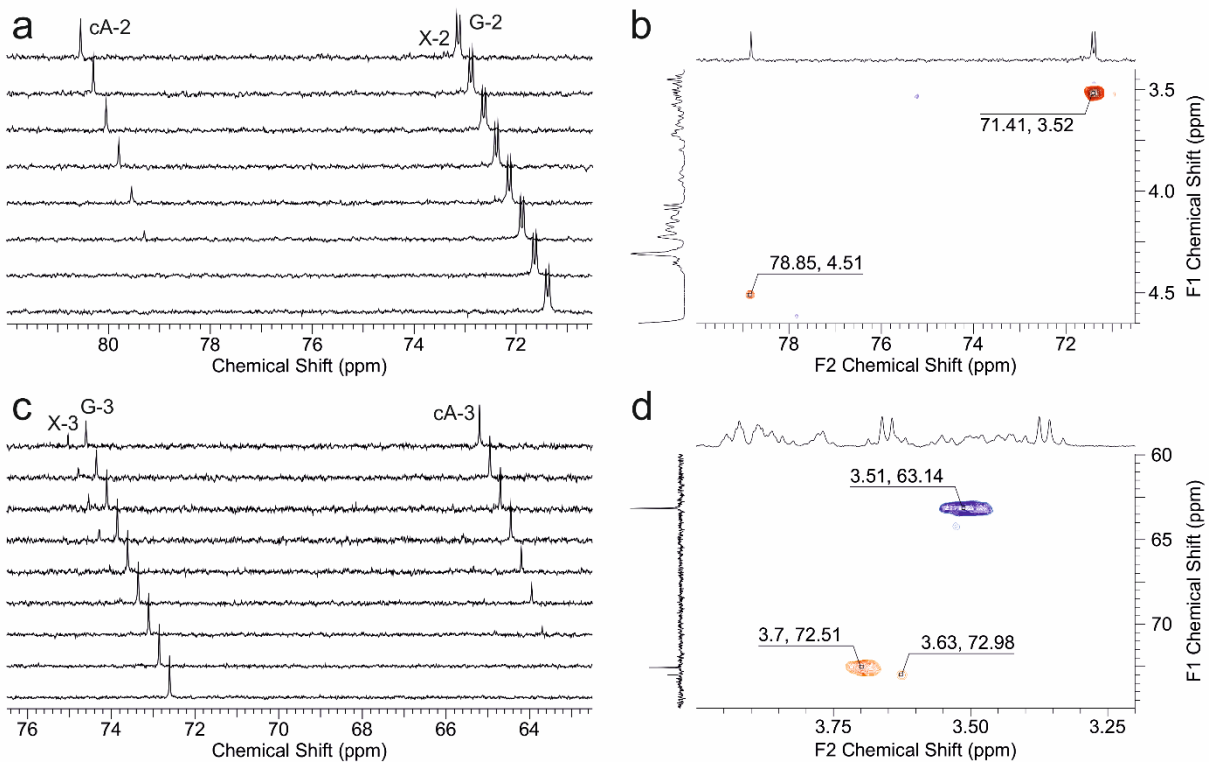
a
cA-2
X-2
G-2
80
78
76
74
72
Chemical Shift (ppm)
b
71.41, 3.52
78.85, 4.51
3.5
4.0
4.5
F1 Chemical Shift (ppm)
78
76
74
72
F2 Chemical Shift (ppm)
c
X-3
G-3
cA-3
76
74
72
70
68
66
64
Chemical Shift (ppm)
d
3.51, 63.14
3.7, 72.51
3.63, 72.98
60
65
70
F1 Chemical Shift (ppm)
3.75
3.50
3.25
F2 Chemical Shift (ppm)

Figure 2.

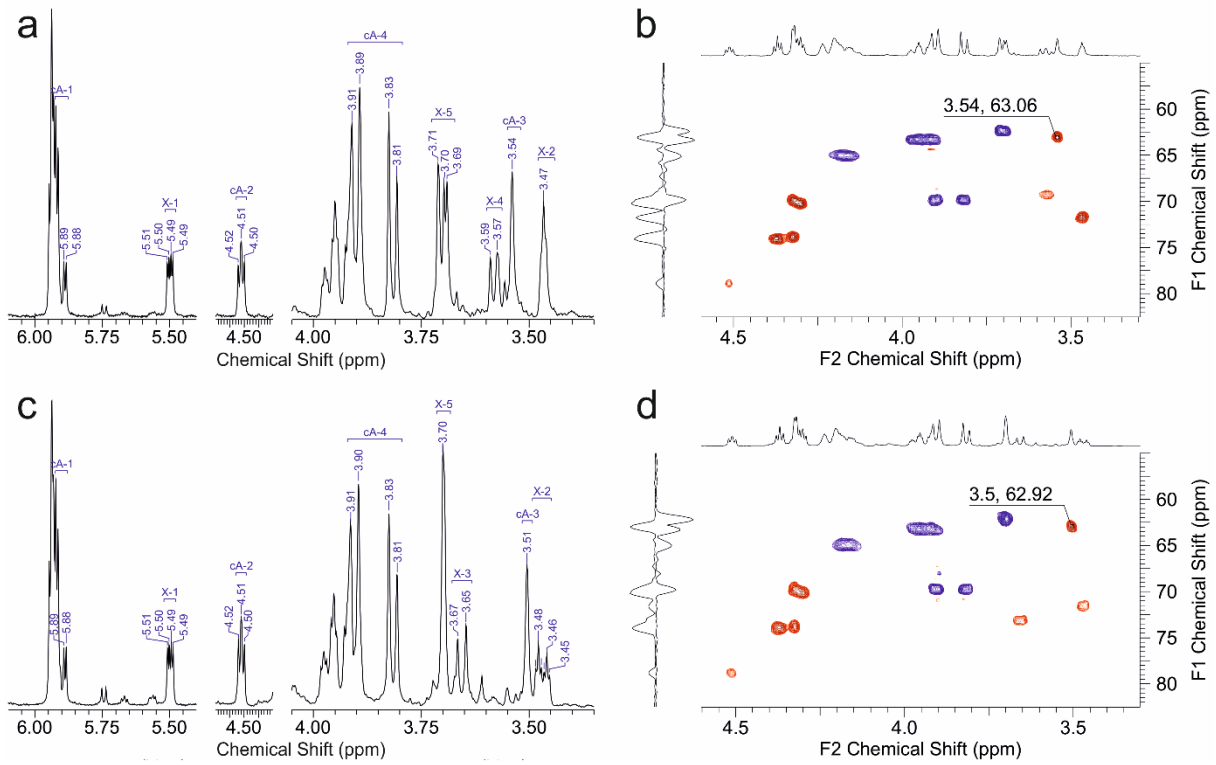
a
b
c
d
Chemical Shift (ppm)
F2 Chemical Shift (ppm)
F1 Chemical Shift (ppm)
3.54, 63.06
3.5, 62.92

Figure 3.

SUPPLEMENTARY INFORMATION

The mechanism of UDP-apiose/UDP-xylose synthase reveals *C*-branched sugar biosynthesis in plants

Thomas Eixelsberger[1], Doroteja Horvat[1], Alexander Gutmann[1], Hansjörg Weber[2], Bernd Nidetzky[1,3,*]

[1] Institute of Biotechnology and Biochemical Engineering, Graz University of Technology, NAWI Graz, Petersgasse 12/I, A-8010 Graz, Austria

[2] Institute of Organic Chemistry, Graz University of Technology, NAWI Graz, Stremayrgasse 9, A-8010 Graz, Austria

[3] Austrian Centre of Industrial Biotechnology (ACIB), Petersgasse 14, A-8010 Graz, Austria

* Corresponding author; e-mail: bernd.nidetzky@tugraz.at, tel.: +43 316 873 8400, fax: +43 316 873 108400

Table of contents

Supplementary Tables

Reaction course analysis with ^{13}C-labelled substrates

Supplementary Table T1: Kinetic properties of UAXS

pH value[a]	UAXS specific activity[b]		$\frac{[\text{Product 1}]^c}{[\text{Product 9}]}$	
	mU/mg	%	absolute	%
5.5	2.10	23.2	$7.61 \cdot 10^{-2}$	4.1
6.5	2.23	24.6	0.167	9.1
7.5	3.05	33.6	0.928	50.4
8.5	9.07	100	1.84	100
9.5	2.36	26.0	1.24	67.4

[a] Buffers used: 50 mM citrate (pH 5.5), 50 mM phosphate (pH 6.5-8.5), 50 mM Tris/HCl (pH 9.5)
[b] Measured under standard conditions (2 mM substrate, 20 µM enzyme)
[c] Measured as UMP

Reaction course analysis with ^{2}H-labelled substrates

Supplementary Table T2: Product ratios obtained from conversions of different substrates

Substrate	$\frac{[\text{Product 1}]^a}{[\text{Product 9}]}$
Unlabelled	1.84
^{2}H-3	1.92
^{2}H-4	1.48

[a] Measured as UMP

Supplementary Figures

Synthesis of UDP-α-D-glucuronic acid (2) and UDP-2-deoxy-α-D-glucuronic acid (10)

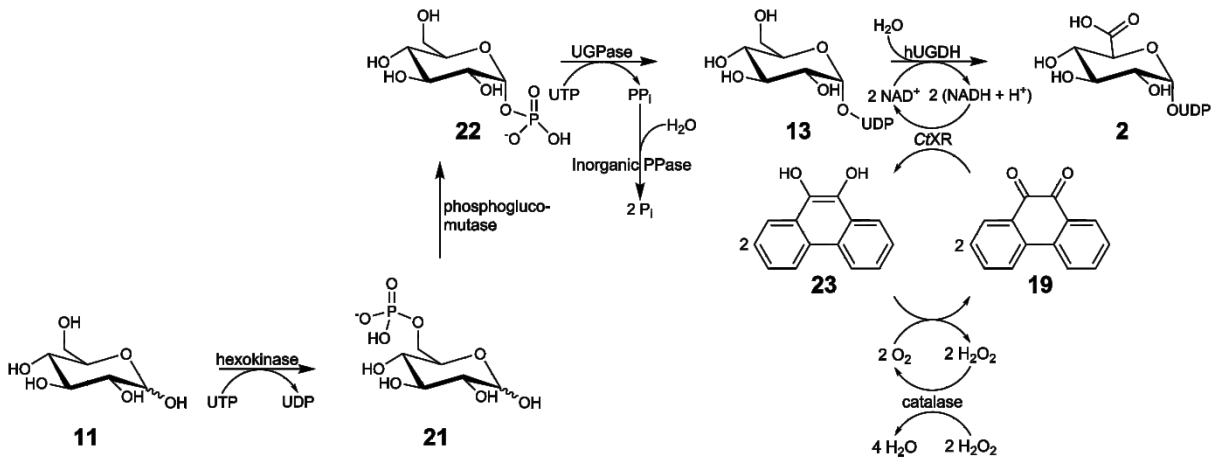

Supplementary Figure S1. Depiction of synthesis route for production of substrate **2** via intermediates D-glucose 6-phosphate (**21**), α-D-glucose 1-phosphate (**22**) and nucleotide sugar **13**. Phenanthrene hydroquinone (**23**) in the coenzyme regeneration cascade is non-enzymatically oxidized to **19**.

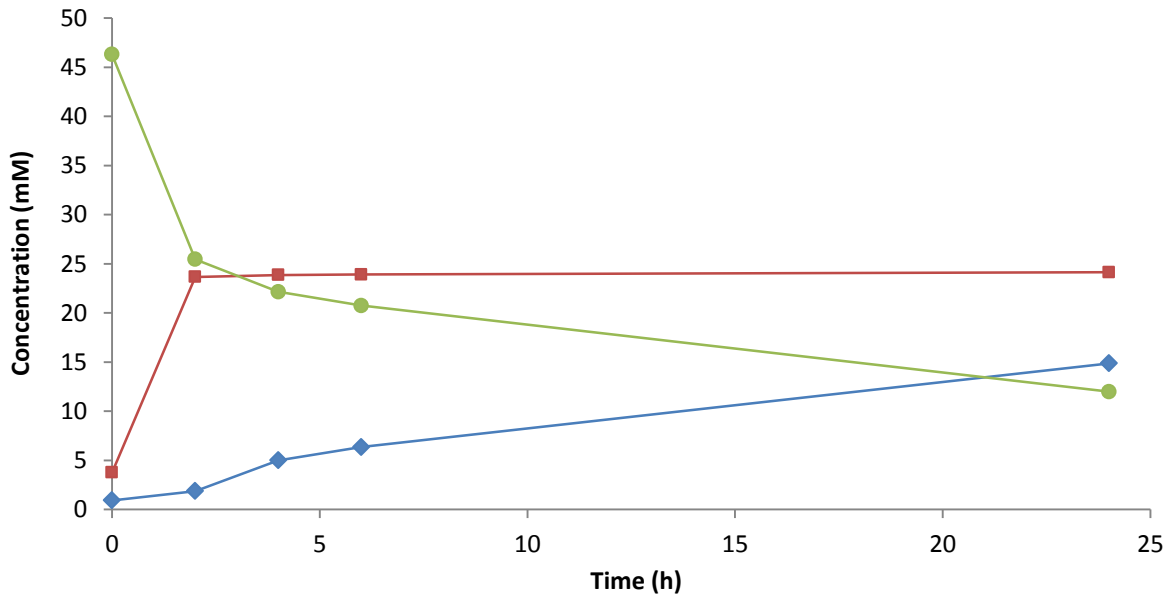

Supplementary Figure S2. Representative time course of synthesis of nucleotide sugar **13** from 15 mM monosaccharide **11** (blue: compound **13**, red: UDP, green: UTP).

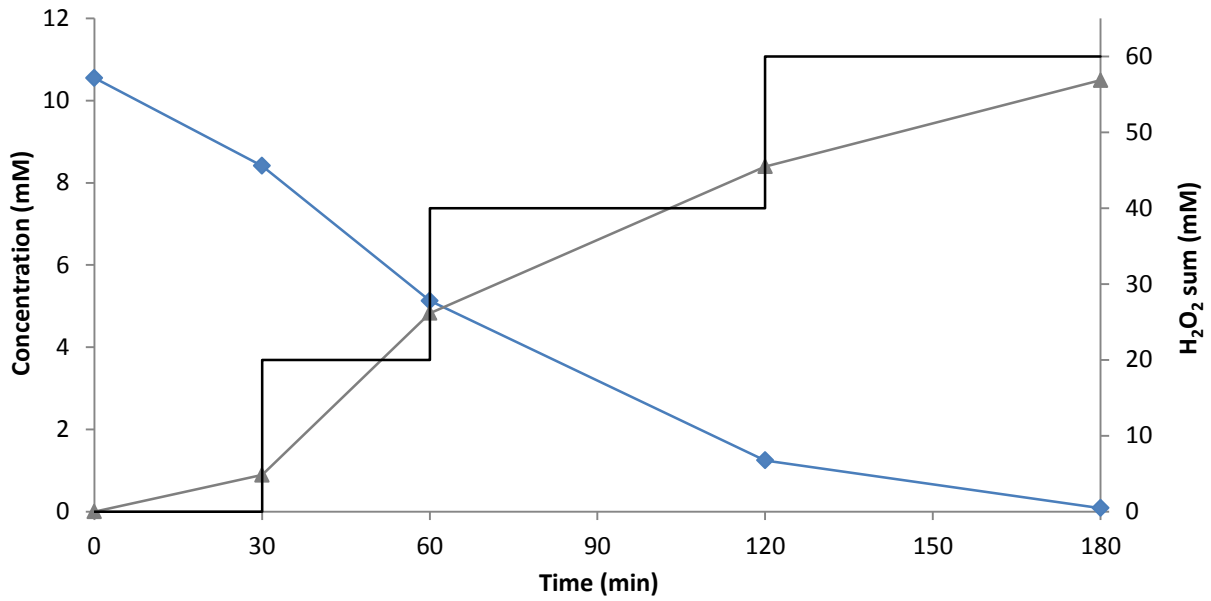

Supplementary Figure S3. Representative time course of synthesis of substrate **2** from nucleotide sugar **13** (blue: compound **13**, grey: substrate **2**, black: H_2O_2).

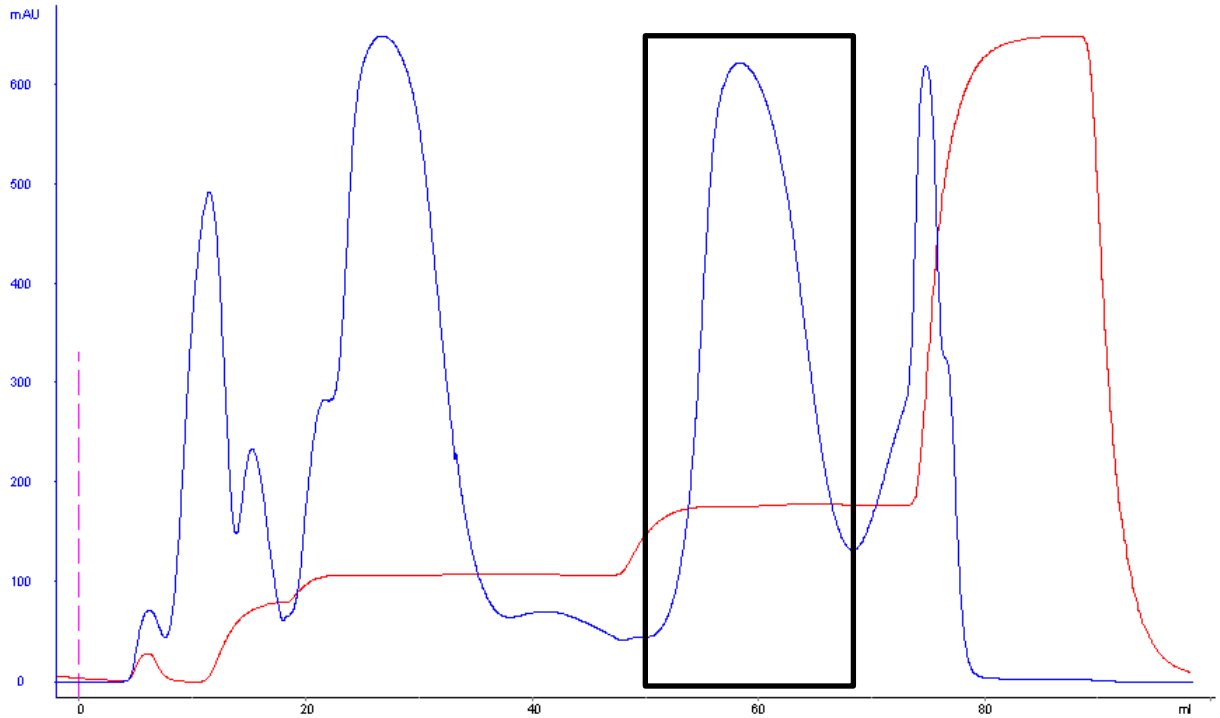

Supplementary Figure S4. Purification of substrate **2** (indicated by black box) using anion exchange chromatography (blue: UV signal, red: conductivity signal).

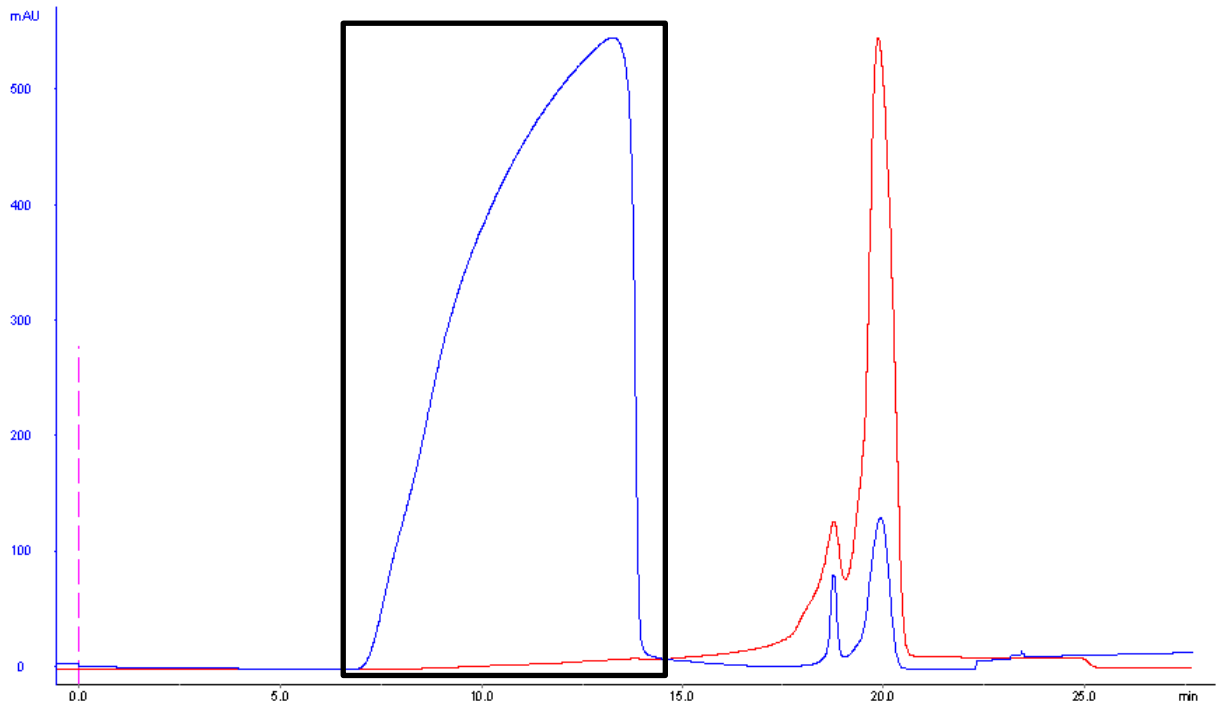

Supplementary Figure S5. Removal of salt by size exclusion chromatography. Substrate **2** (indicated by black box) could be separated from NaCl in one step (blue: UV signal, red: conductivity signal).

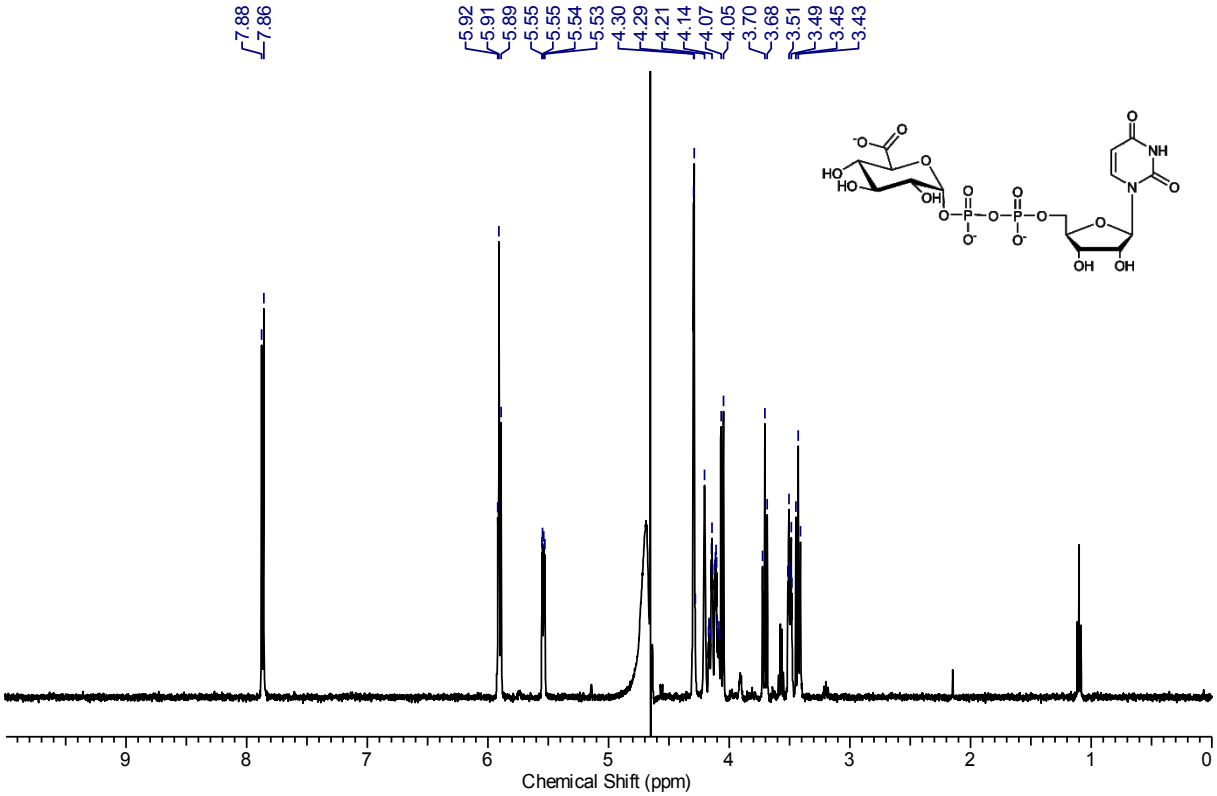

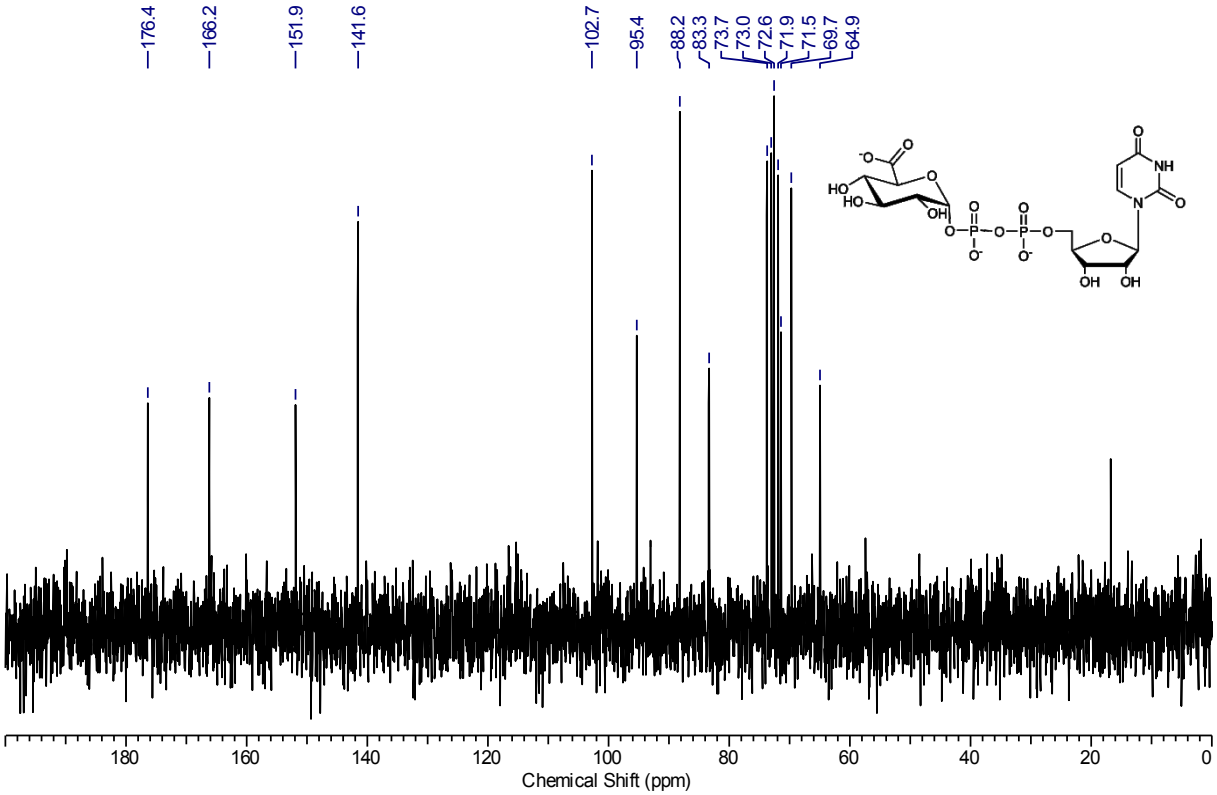

Supplementary Figure S6. Commercial substrate **2** (purchased from Sigma-Aldrich). ^{1}H NMR (500 MHz, D_2O) δ ppm 7.87 (d, *J*=8.30 Hz, 1 H), 5.88 - 5.93 (m, 2 H), 5.54 (dd, *J*=7.57, 3.66 Hz, 1 H), 4.27 - 4.31 (m, 2 H), 4.21 (br. s., 1 H), 4.08 - 4.18 (m, 2 H), 4.06 (d, *J*=9.76 Hz, 1 H), 3.71 (t, *J*=9.28 Hz, 1 H), 3.50 (dt, *J*=9.76, 3.17 Hz, 1 H), 3.43 (t, *J*=9.76 Hz, 1 H); ^{13}C NMR (125 MHz, D_2O) δ ppm 176.4, 166.2, 151.9, 141.6, 102.7, 95.4, 88.2, 83.3 (d, *J*=8.63 Hz), 73.7, 73.0, 72.6, 71.9, 71.4 (d, *J*=7.67 Hz), 69.7, 64.9

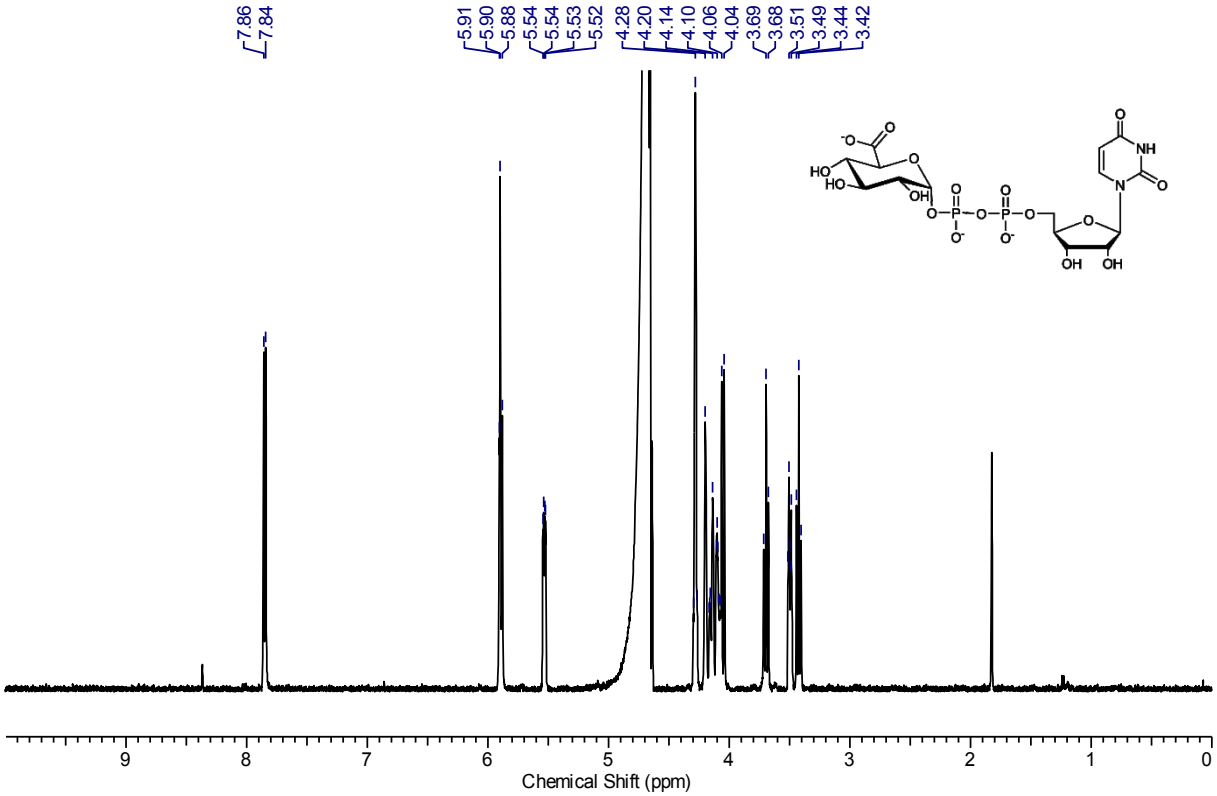

Supplementary Figure S7. Synthesized unlabelled substrate **2**. ^{1}H NMR (500 MHz, D_2O) δ ppm 7.85 (d, *J*=8.30 Hz, 1 H), 5.87 - 5.92 (m, 2 H), 5.53 (dd, *J*=7.32, 3.42 Hz, 1 H), 4.26 - 4.30 (m, 2 H), 4.20 (br. s., 1 H), 4.07 - 4.17 (m, 2 H), 4.05 (d, *J*=10.25 Hz, 1 H), 3.69 (t, *J*=9.28 Hz, 1 H), 3.50 (dt, *J*=9.76, 2.93 Hz, 1 H), 3.42 (t, *J*=9.76 Hz, 1 H)

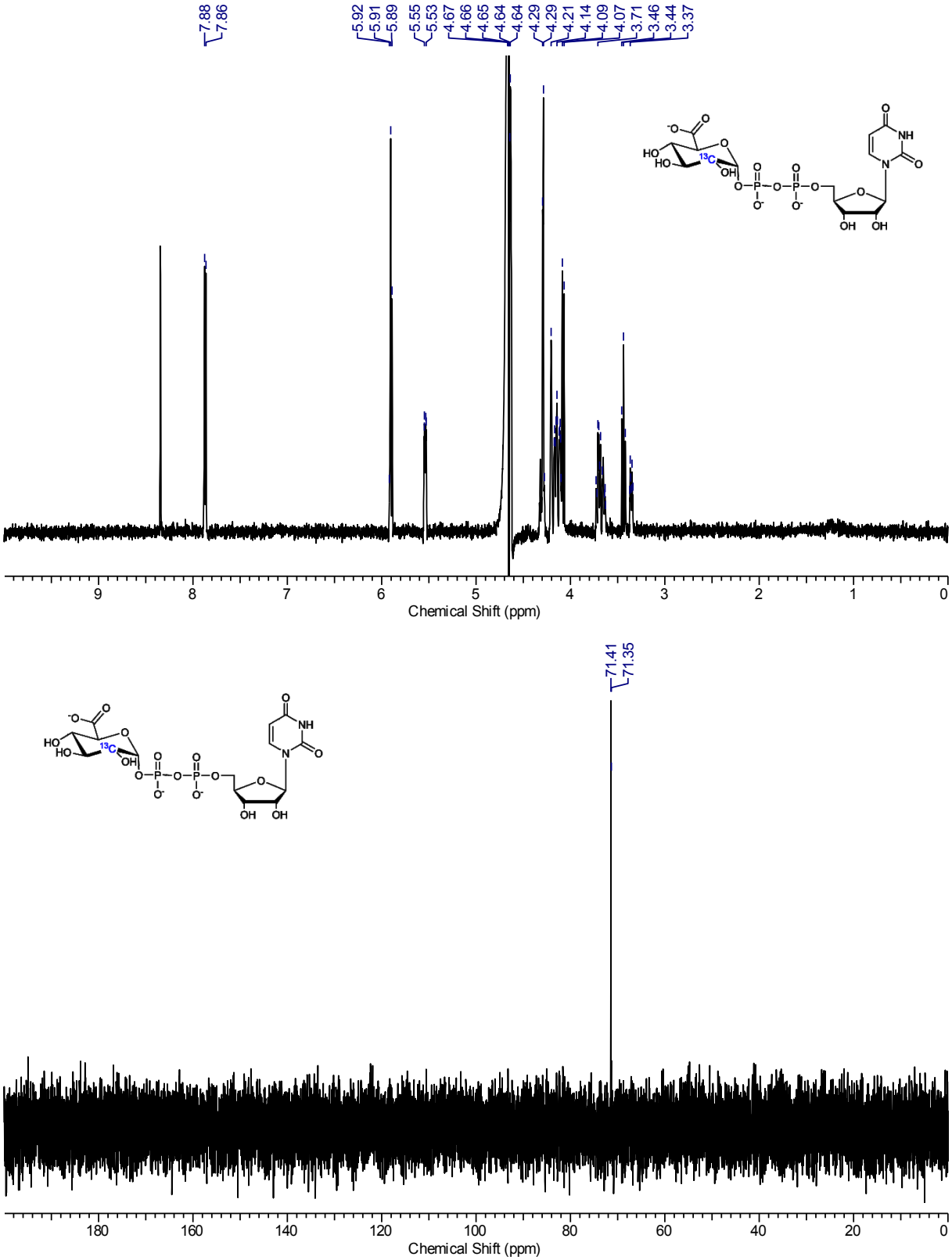

Supplementary Figure S8. Synthesized ^{13}C-2 substrate **2**. ^{1}H NMR (500 MHz, D_2O) δ ppm 7.87 (d, *J*=8.30 Hz, 1 H), 5.88 - 5.93 (m, 2 H), 5.54 (dd, *J*=7.57, 2.20 Hz, 1 H), 4.27 - 4.30 (m, 2 H), 4.21 (br. s., 1 H), 4.10 - 4.18 (m, 2 H), 4.08 (d, *J*=10.25 Hz, 1 H), 3.67 - 3.74 (m, 1 H), 3.64 (dt, *J*=9.76, 2.93 Hz, 0.5 H), 3.44 (t, *J*=9.52 Hz, 1 H), 3.36 (dt, *J*=9.76, 3.40 Hz, 0.5 H); ^{13}C NMR (125 MHz, D_2O) δ ppm 71.4 (d, *J*=8.63 Hz)

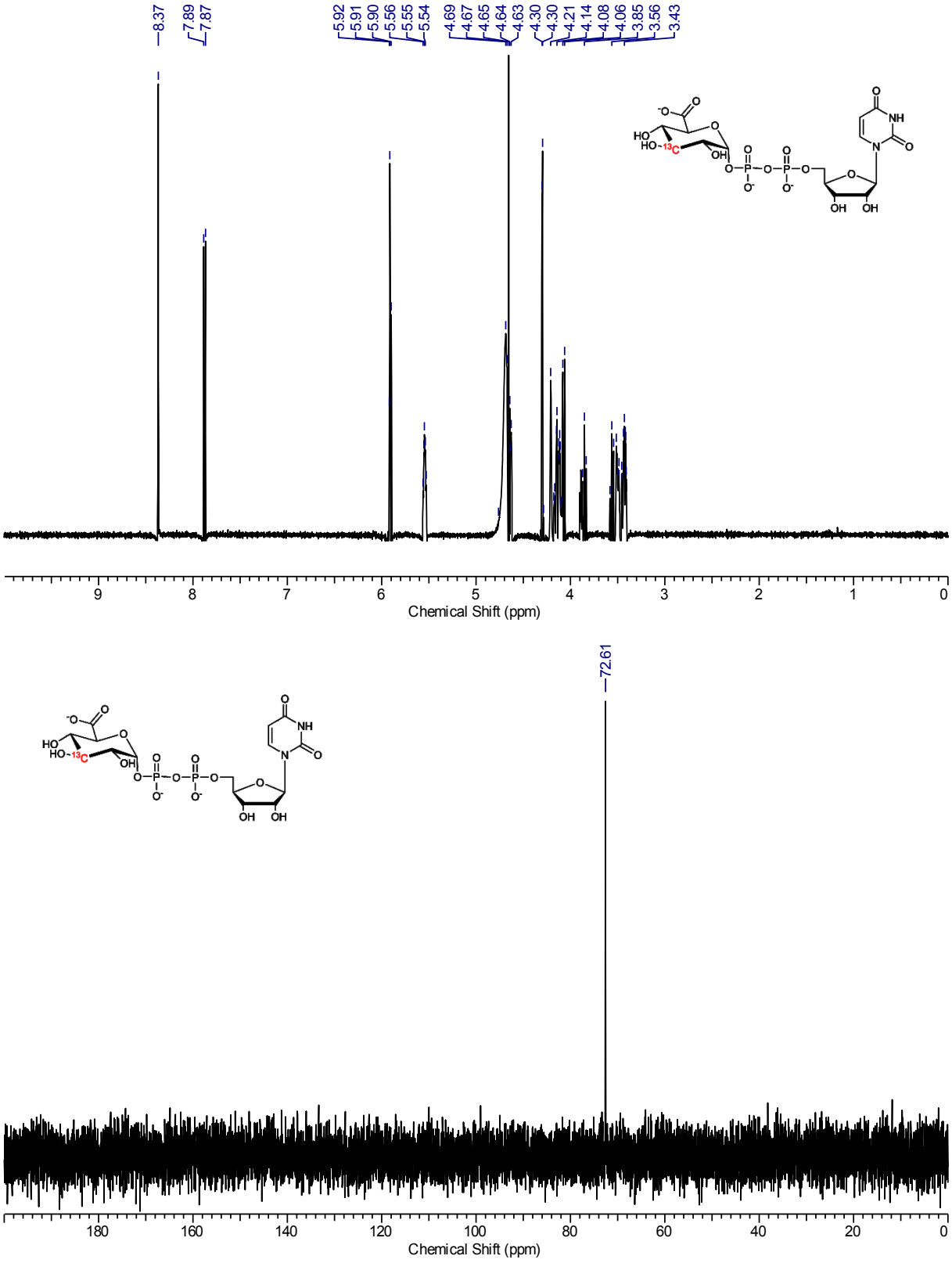

Supplementary Figure S9. Synthesized ^{13}C-3 substrate **2**. ^{1}H NMR (500 MHz, D_2O) δ ppm 7.88 (d, *J*=8.30 Hz, 1 H), 5.88 - 5.93 (m, 2 H), 5.52 - 5.57 (m, 1 H), 4.28 - 4.32 (m, 2 H), 4.21 (br. s., 1 H), 4.09 - 4.18 (m, 2 H), 4.07 (d, *J*=10.25 Hz, 1 H), 3.86 (t, *J*=9.76 Hz, 0.5 H), 3.56 (t, *J*=9.76 Hz, 0.5 H), 3.50 (dt, *J*=13.18, 3.42 Hz, 1 H), 3.40 - 3.47 (m, 1 H); ^{13}C NMR (125 MHz, D_2O) δ ppm 72.6

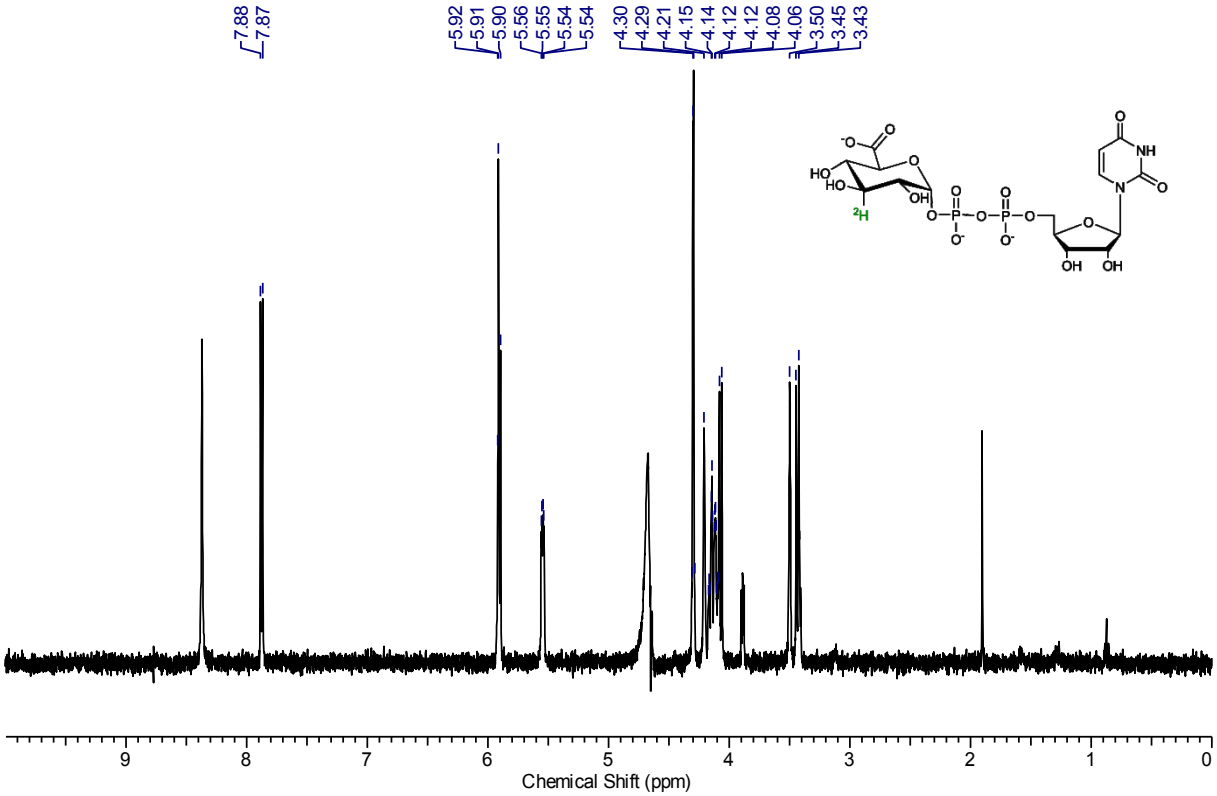

Supplementary Figure S10. Synthesized ^{2}H-3 substrate **2**. ^{1}H NMR (500 MHz, D_2O) δ ppm 7.88 (d, *J*=8.30 Hz, 1 H), 5.89 - 5.93 (m, 2 H), 5.55 (dd, *J*=7.81, 2.93 Hz, 1 H), 4.28 - 4.32 (m, 2 H), 4.21 (br. s., 1 H), 4.09 - 4.18 (m, 2 H), 4.07 (d, *J*=10.25 Hz, 1 H), 3.50 (br. s., 1 H), 3.44 (d, *J*=10.25 Hz, 1 H)

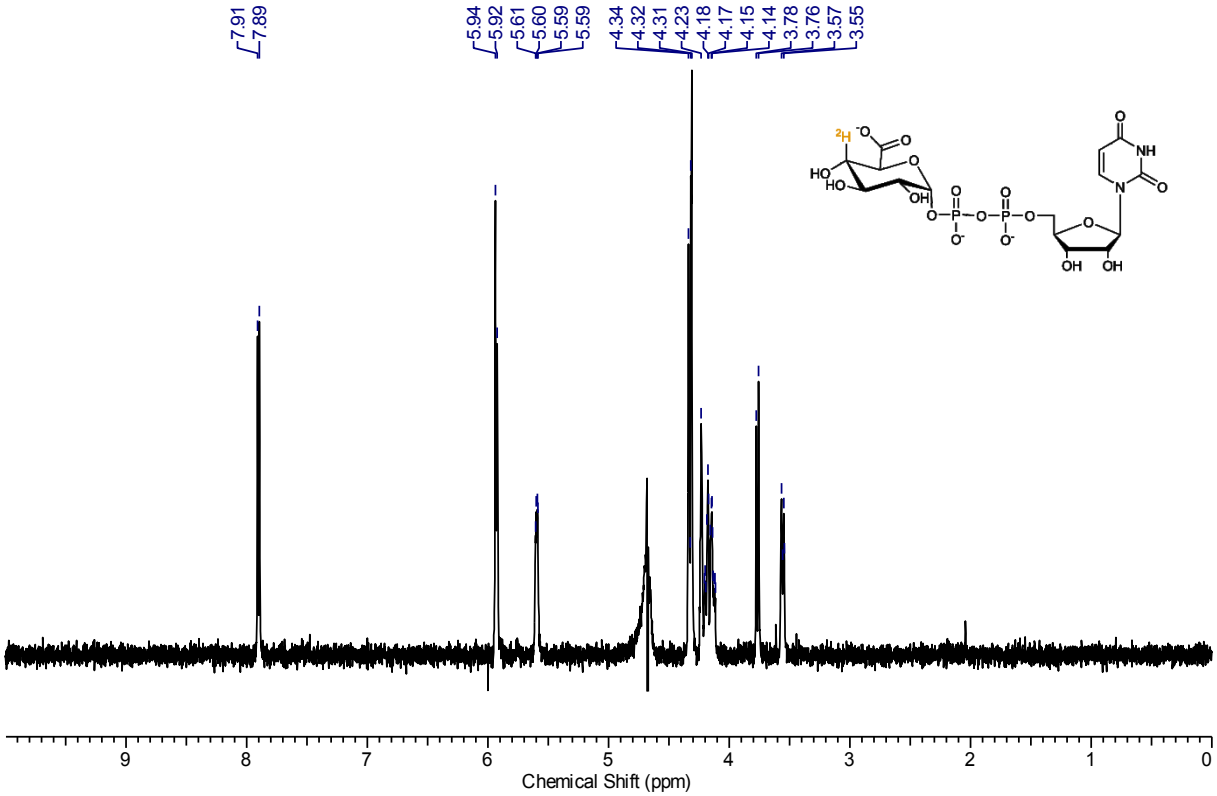

Supplementary Figure S11. Synthesized ^{2}H-4 substrate **2**. ^{1}H NMR (500 MHz, D_2O) δ ppm 7.90 (d, *J*=8.30 Hz, 1 H), 5.91 - 5.95 (m, 2 H), 5.60 (dd, *J*=6.59, 3.17 Hz, 1 H), 4.34 (s, 1 H), 4.29 - 4.33 (m, 2 H), 4.23 (br. s., 1 H), 4.11 - 4.21 (m, 2 H), 3.77 (d, *J*=9.76 Hz, 1 H), 3.55 (dt, *J*=9.28, 3.42 Hz, 1 H)

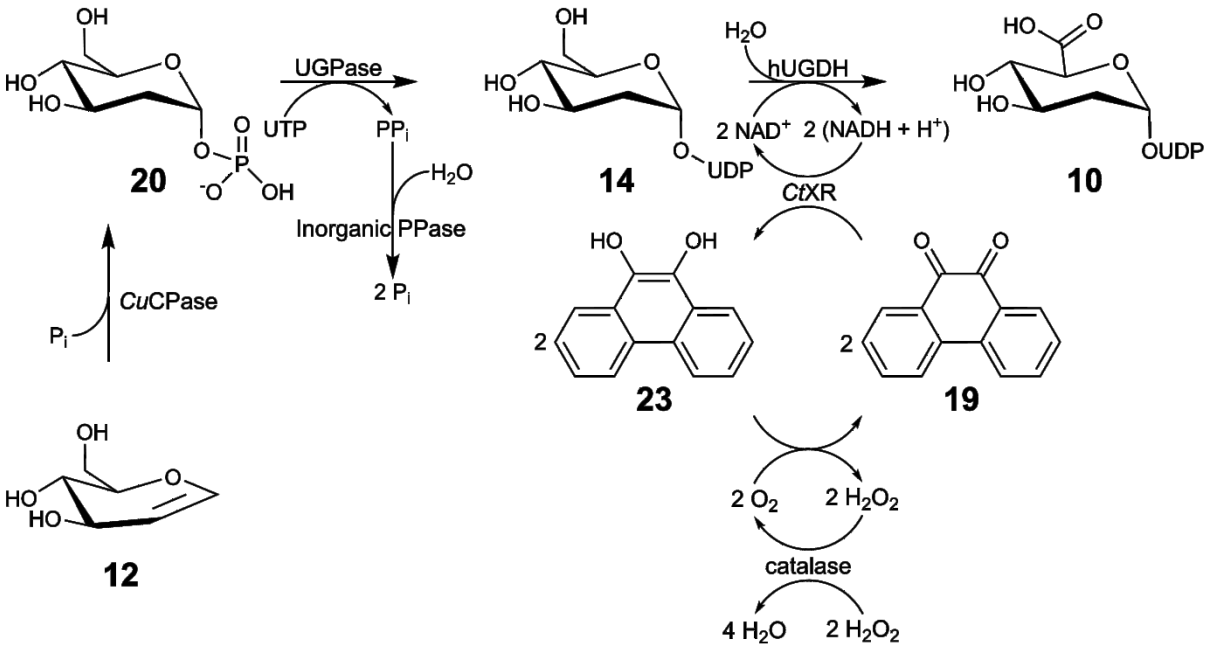

Supplementary Figure S12. Depiction of synthesis route for production of substrate analogue **10** via intermediate **20** and nucleotide sugar **14**.

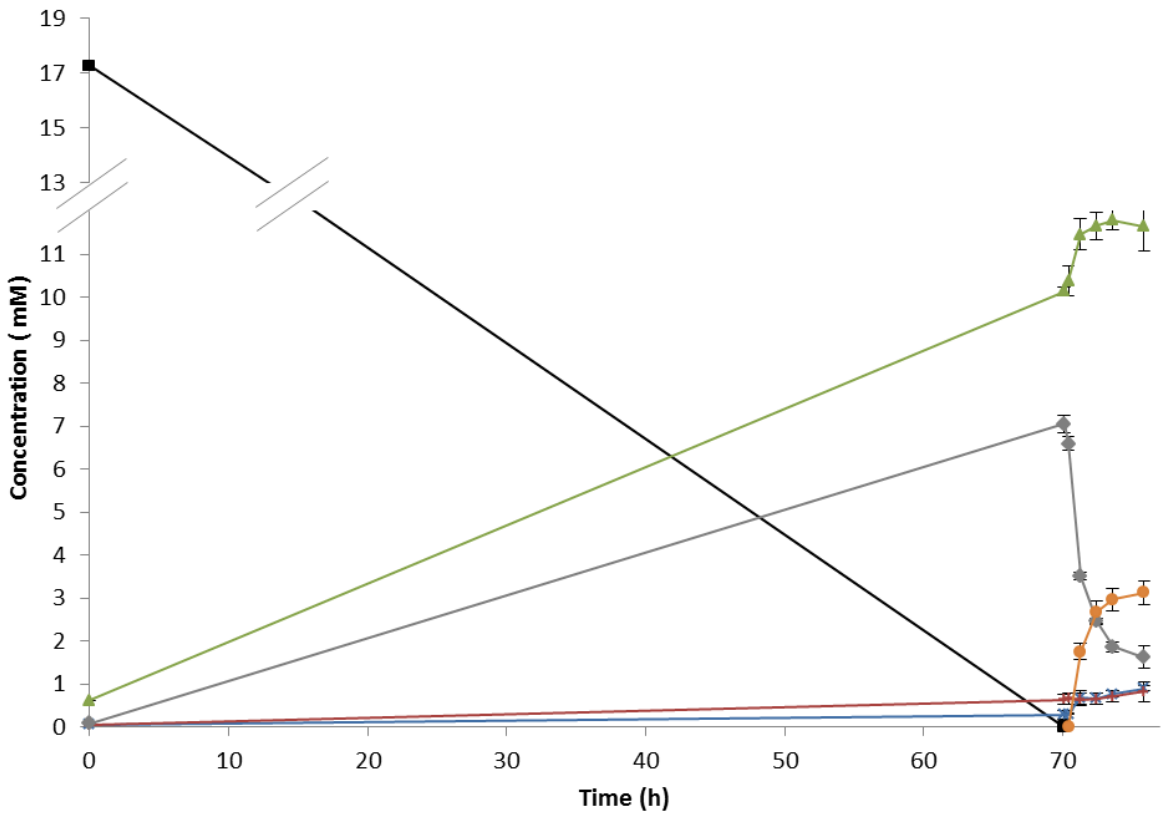

Supplementary Figure S13. Time course of synthesis of substrate analogue **10** from UTP and compound **12** (blue: uridine, red: UMP, green: UDP, black: UTP, grey: nucleotide sugar **14**, orange: substrate analogue **10**).

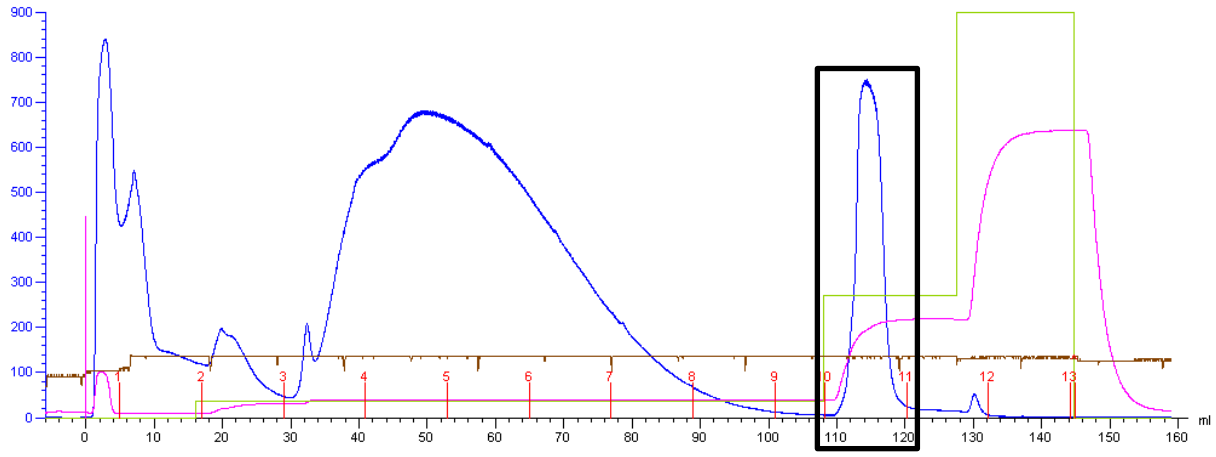

Supplementary Figure S14. Purification of substrate analogue **10** (indicated by black box) using anion exchange chromatography (blue: UV signal, pink: conductivity signal, green: concentration buffer B).

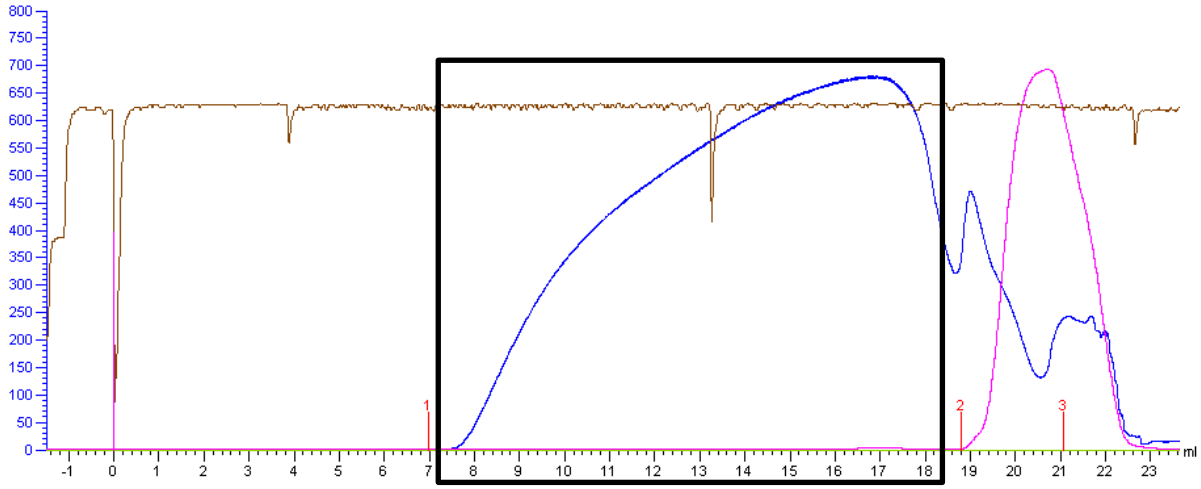

Supplementary Figure S15. Removal of NaCl from substrate analogue **10** (indicated by black box) by size exclusion chromatography (blue: UV signal, pink: conductivity signal).

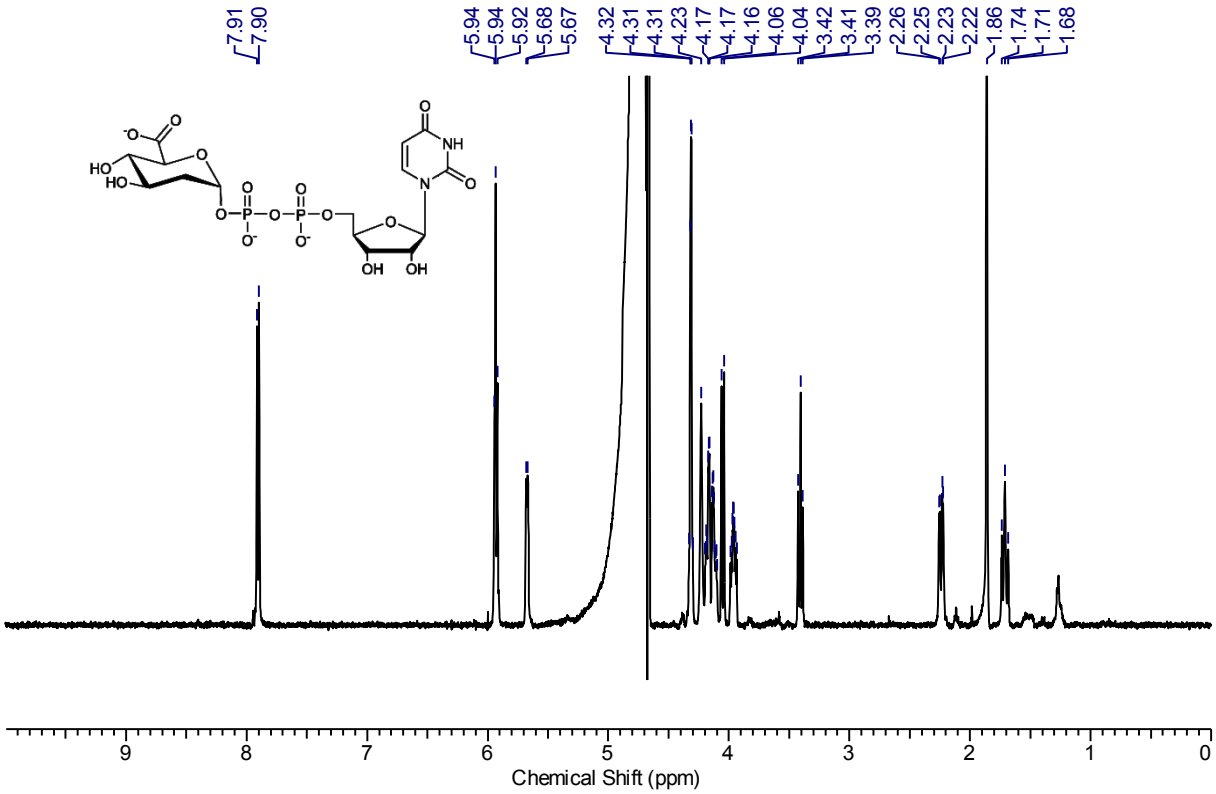

Supplementary Figure S16. Synthesized substrate analogue **10**. The singlet at 1.86 ppm is residual sodium acetate from purification. ^{1}H NMR (500 MHz, D_2O) δ ppm 7.91 (d, *J*=8.30 Hz, 1 H), 5.90 - 5.97 (m, 2 H), 5.67 (d, *J*=6.35 Hz, 1 H), 4.29 - 4.35 (m, 2 H), 4.23 (br. s., 1 H), 4.09 - 4.21 (m, 2 H), 4.05 (d, *J*=9.76 Hz, 1 H), 3.96 (ddd, *J*=11.35, 9.40, 5.13 Hz, 1 H), 3.41 (t, *J*=9.52 Hz, 1 H), 2.24 (dd, *J*=12.94, 4.64 Hz, 1 H), 1.71 (t, *J*=12.69 Hz, 1 H)

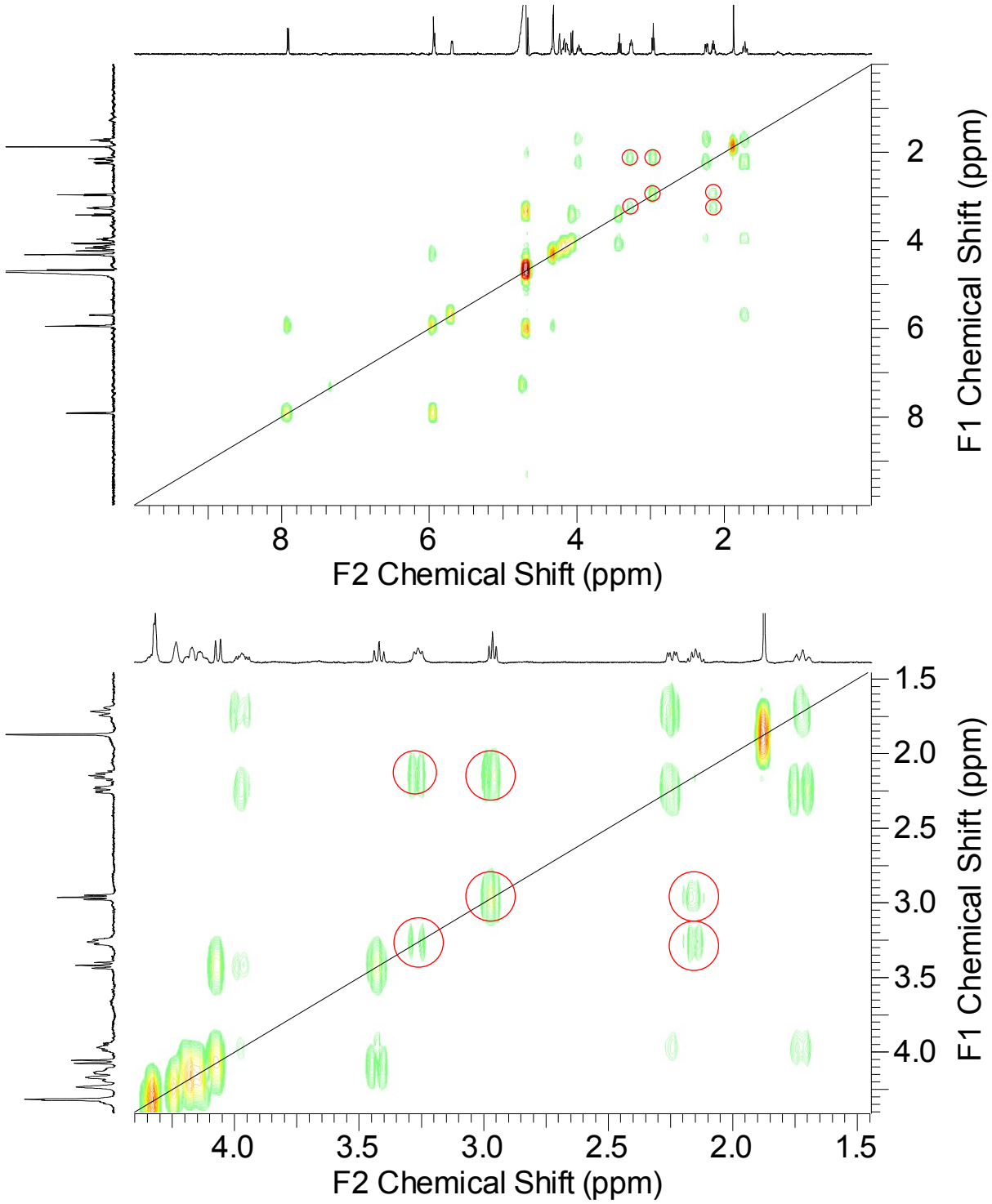

Supplementary Figure S17. Correlation spectroscopy (COSY) spectrum of synthesized substrate analogue **10**. Signals from solvent impurities are indicated with red circles.

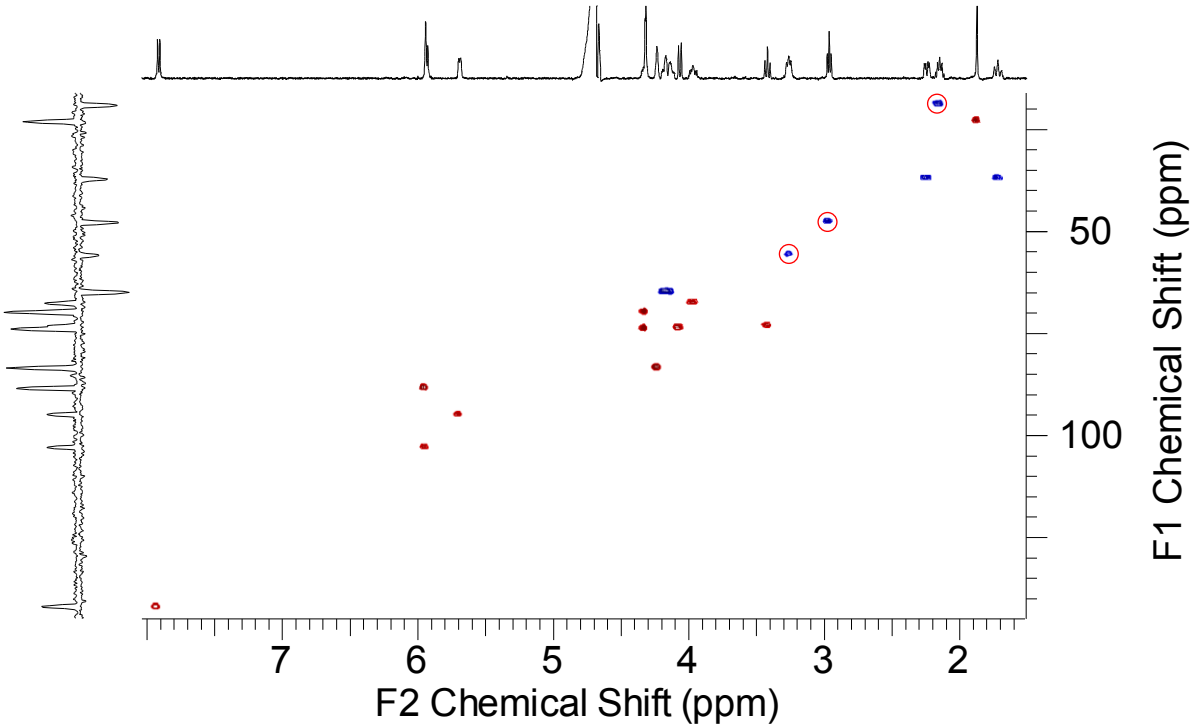

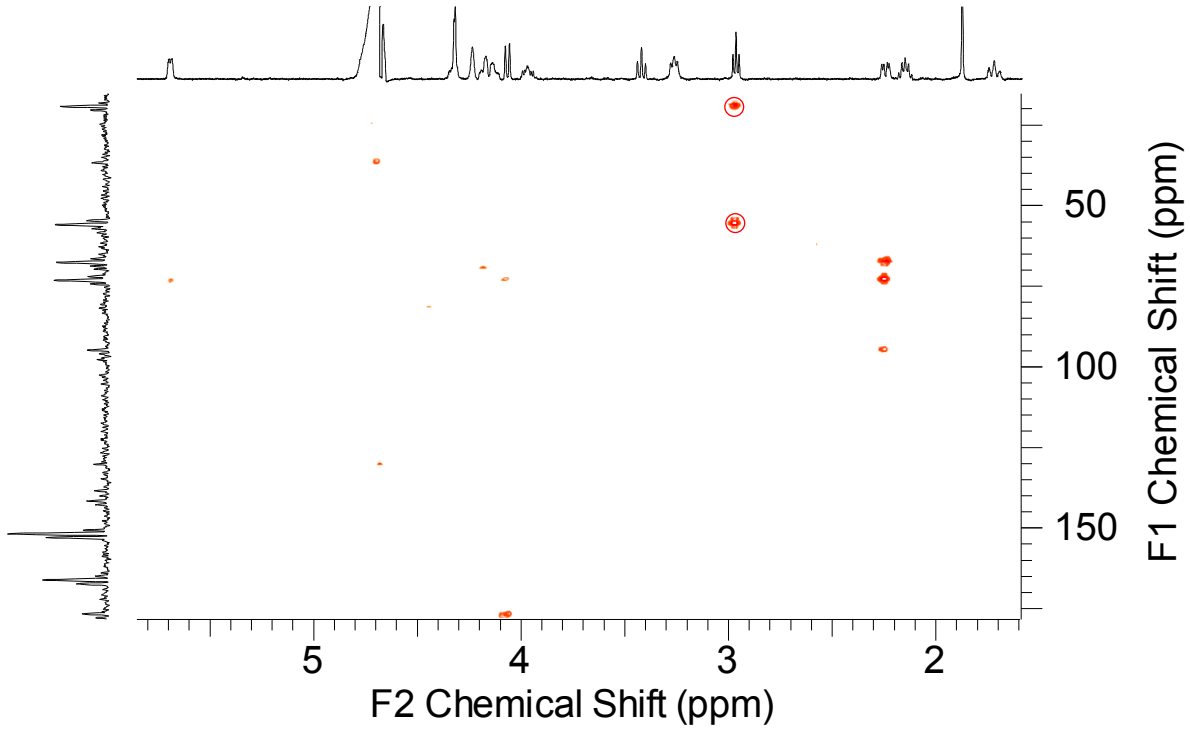

Supplementary Figure S18. HSQC (top) and heteronuclear multiple-bond correlation (HMBC; down) spectra of synthesized substrate analogue **10** (F1 axis = ^{13}C, F2 axis = ^{1}H). Signals from solvent impurities are indicated with red circles.

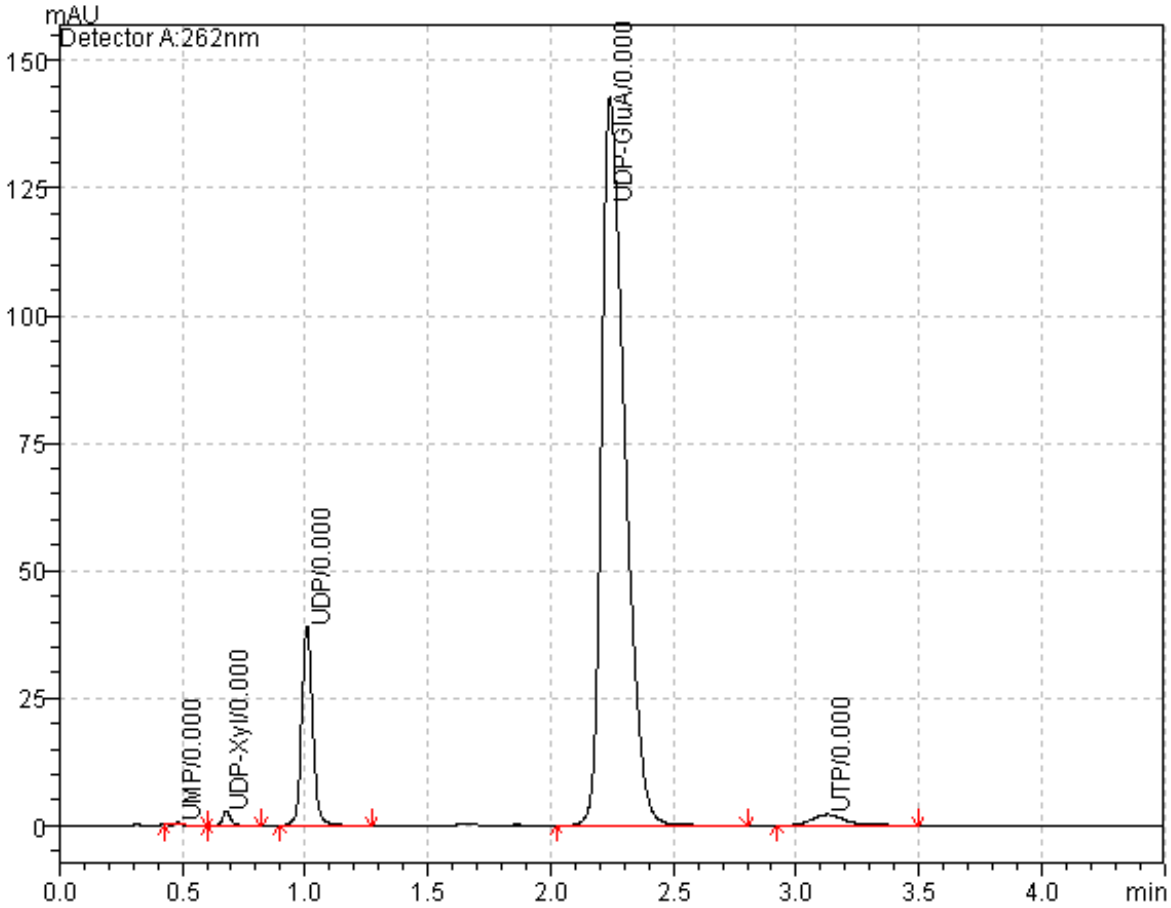

Supplementary Figure S19. HPLC trace (UV detection, λ = 262 nm) of synthesized substrate analogue **10**. UDP (< 15%) originates from partial decomposition during solvent removal.

Reaction course analysis with ^{13}*C*-labelled substrates

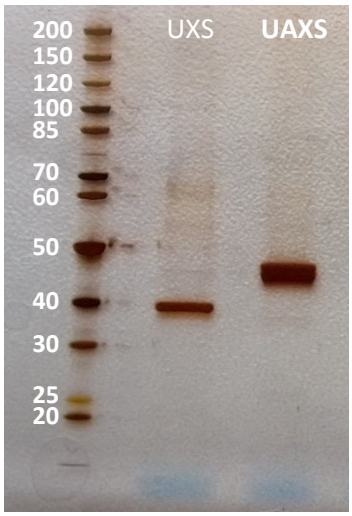

Supplementary Figure 20. SDS-PAGE of purified UAXS (44.7 kDa), compared to a molecular weight standard (masses in kDa) and UXS (38.6 kDa).

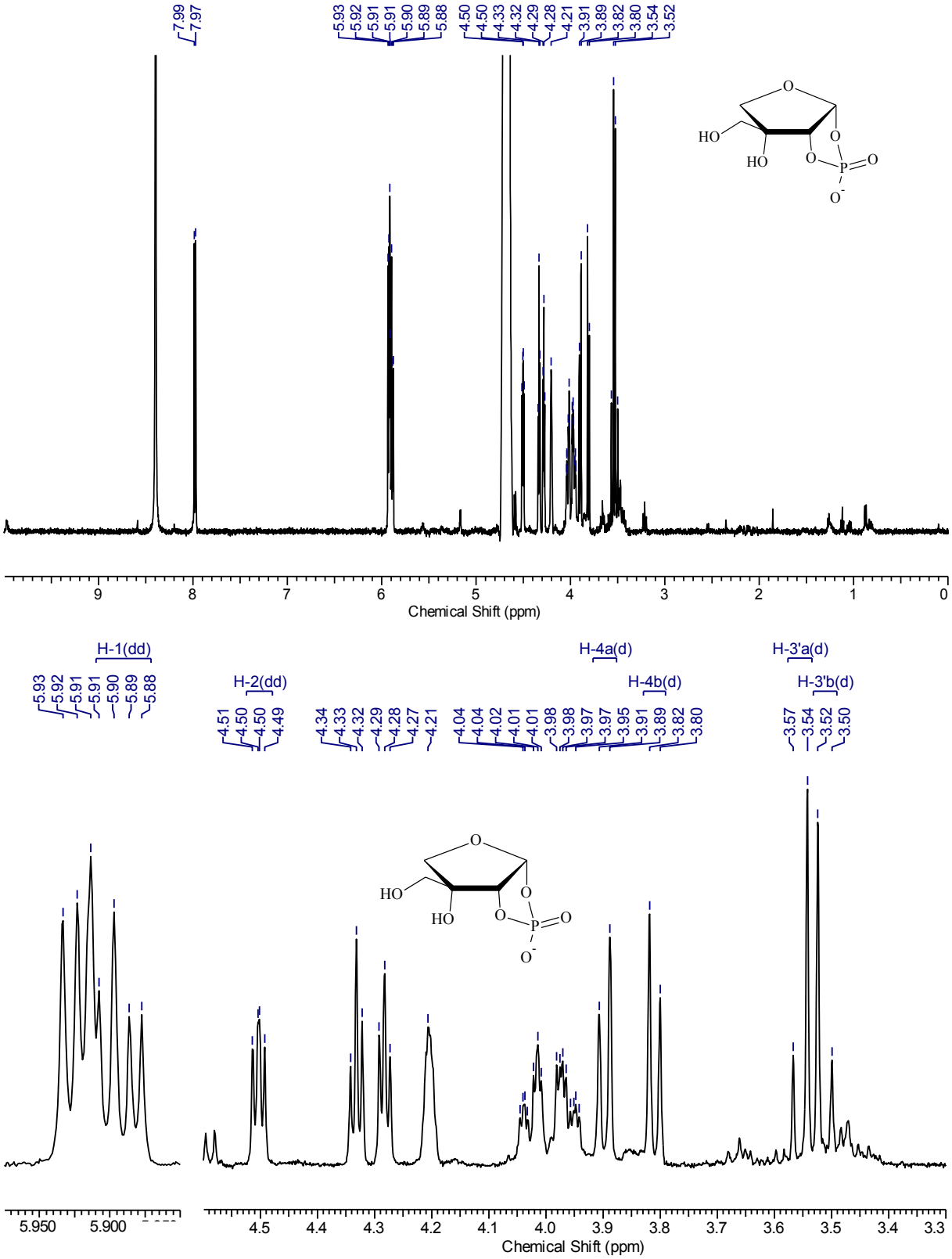

Supplementary Figure S21. Cyclic phosphate **8** (contaminated with co-eluting UMP). Signals of *H*-1, *H*-2, *H*-3' and *H*-4 are indicated.[1] The signal of *H*-1 partly overlaps with signals from UMP. ^{1}H NMR (500 MHz, D_2O) δ ppm 7.98 (d, *J*=8.30 Hz, 1 H), 5.86 - 5.95 (m, 3 H), 4.50 (dd, *J*=6.10, 4.64 Hz, 1 H), 4.33 (t, *J*=4.88 Hz, 1 H), 4.28 (t, *J*=4.88 Hz, 1 H), 4.21 (br. s., 1 H), 3.94 - 4.05 (m, 2 H), 3.90 (d, *J*=9.28 Hz, 1 H), 3.81 (d, *J*=9.28 Hz, 1 H), 3.55 (d, *J*=12.69 Hz, 1 H), 3.51 (d, *J*=12.69 Hz, 1 H)

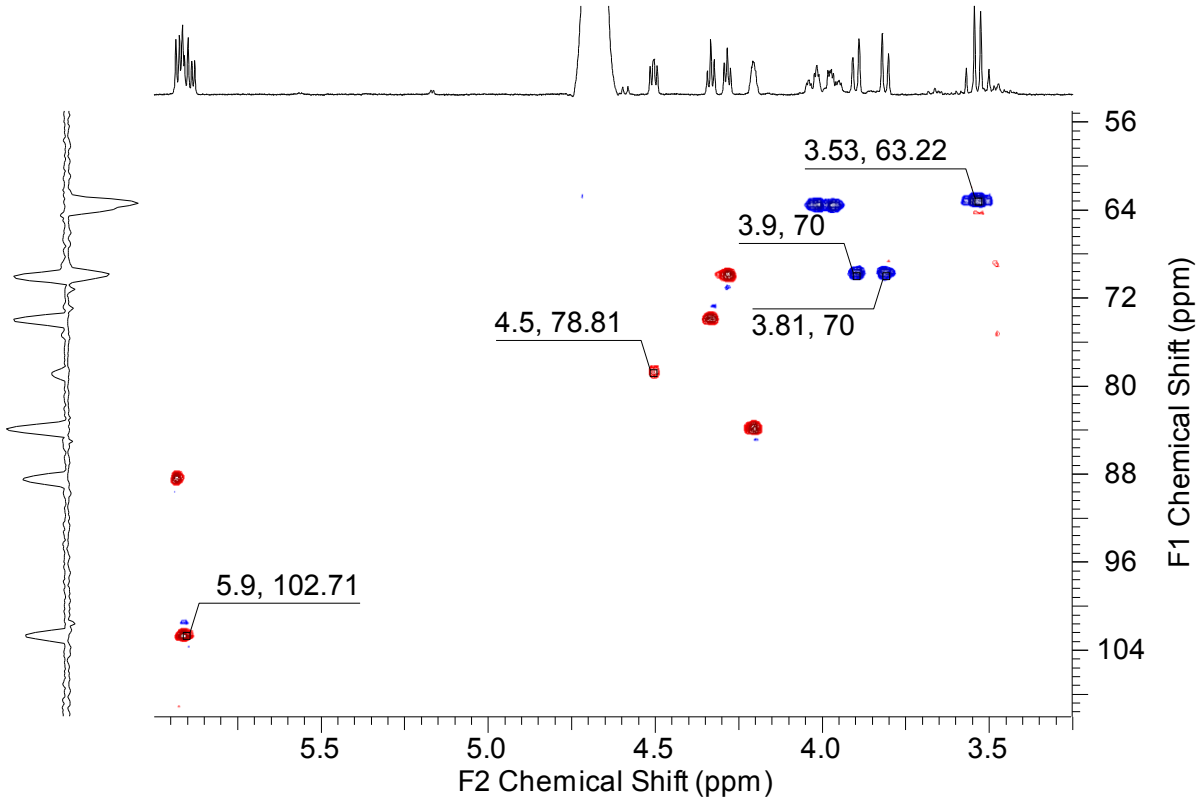

Supplementary Figure S22. HSQC (F1 axis = ^{13}C, F2 axis = ^{1}H) of cyclic phosphate **8** (contaminated with co-eluting UMP). Signals indicated are from position 1 (102.71, 5.9) position 2 (78.81, 4.5), position 3' (63.22, 3.53) and position 4 (70, 3.81 and 70, 3.9).[1]

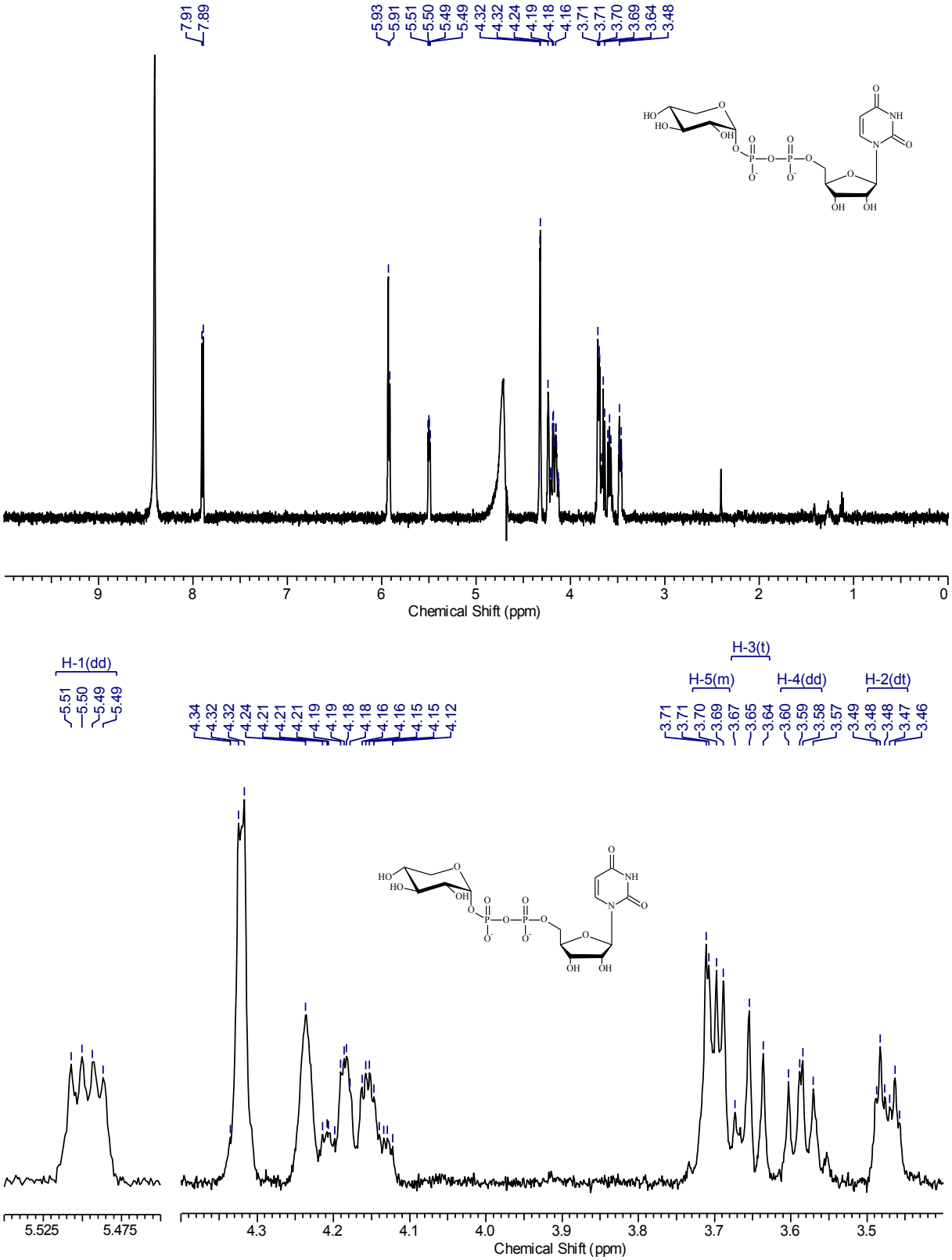

Supplementary Figure S23. Nucleotide sugar **9**. Signals of *H*-1, *H*-2, *H*-3, *H*-4 and *H*-5 are indicated.[2] ^{1}H NMR (500 MHz, D_2O) δ ppm 7.90 (d, *J*=8.30 Hz, 1 H), 5.90 - 5.95 (m, 2 H), 5.50 (dd, *J*=6.83, 3.42 Hz, 1 H), 4.30 - 4.35 (m, 2 H), 4.24 (br. s., 1 H), 4.12 - 4.22 (m, 2 H), 3.68 - 3.73 (m, 2 H), 3.65 (t, *J*=9.28 Hz, 1 H), 3.59 (dd, *J*=9.03, 7.08 Hz, 1 H), 3.47 (dt, *J*=9.52, 2.81 Hz, 1 H)

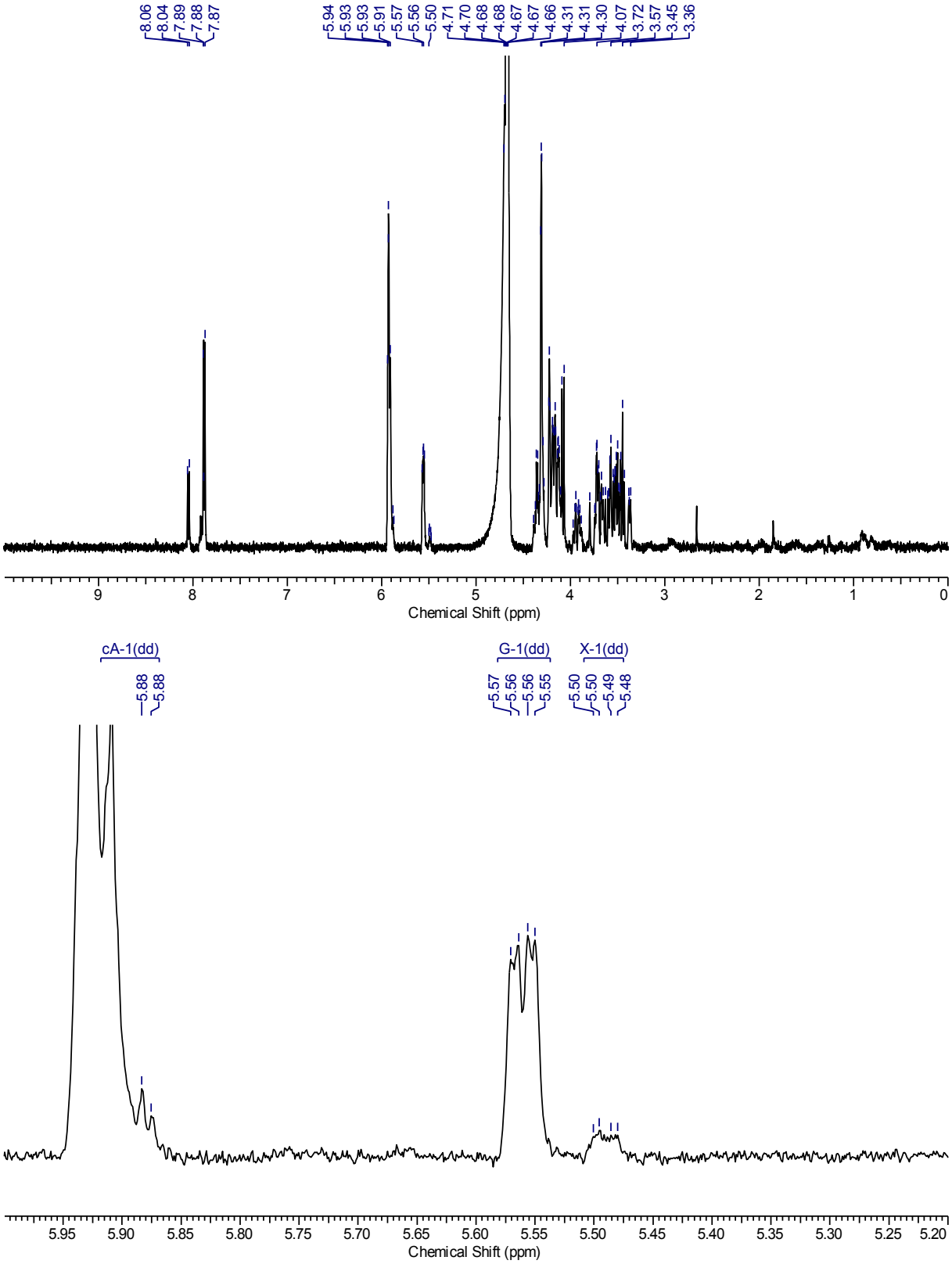

Supplementary Figure S24. ^{1}H NMR spectrum after conversion of ^{13}*C*-2 substrate **2** by UAXS in D_2O. Signals of the anomeric protons from substrate (G-1), product **8** (cA-1) and product **9** (X-1) are indicated.[1]

Reaction course analysis with UDP-2-deoxy-α-D-glucuronic acid

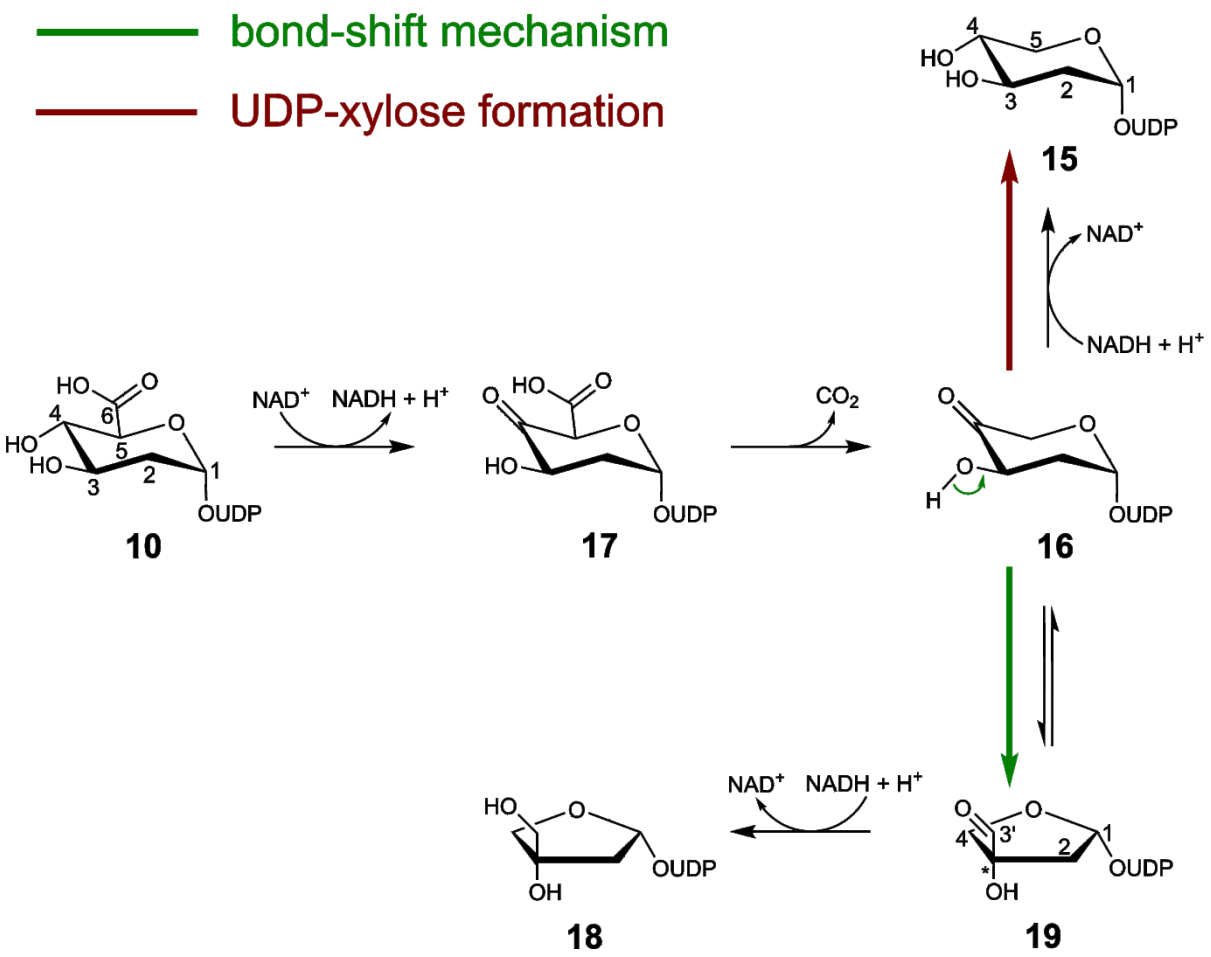

Supplementary Figure S25. Possible routes for conversion of substrate analogue **10** by UAXS. The retroaldol-aldol mechanism is not possible due to the missing hydroxyl group.

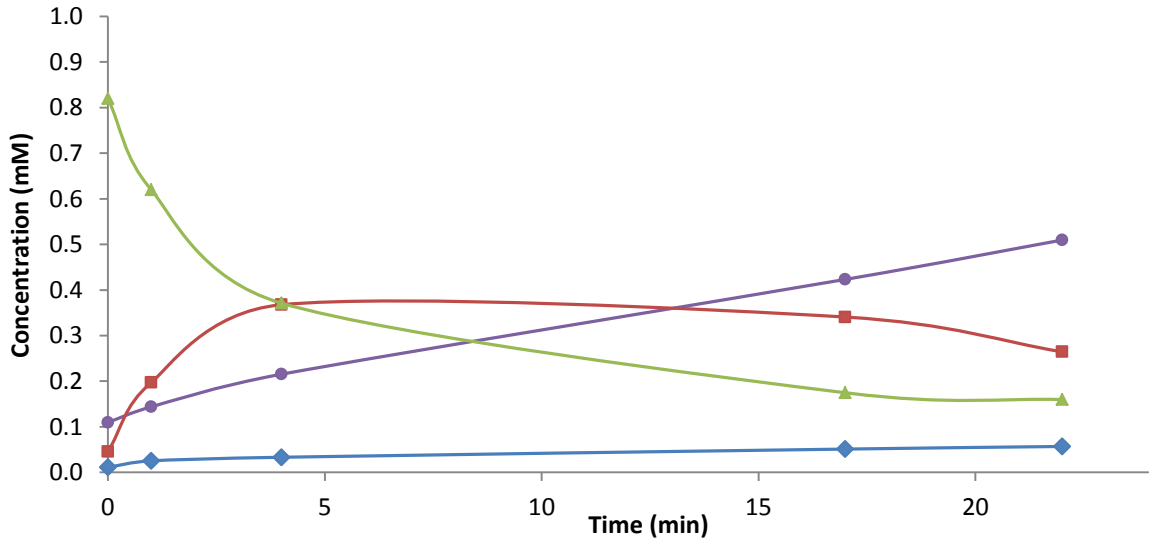

Supplementary Figure S26. Conversion of substrate analogue **10** by UXS (green: **10**, red: product **15**, blue: UMP, purple: UDP).

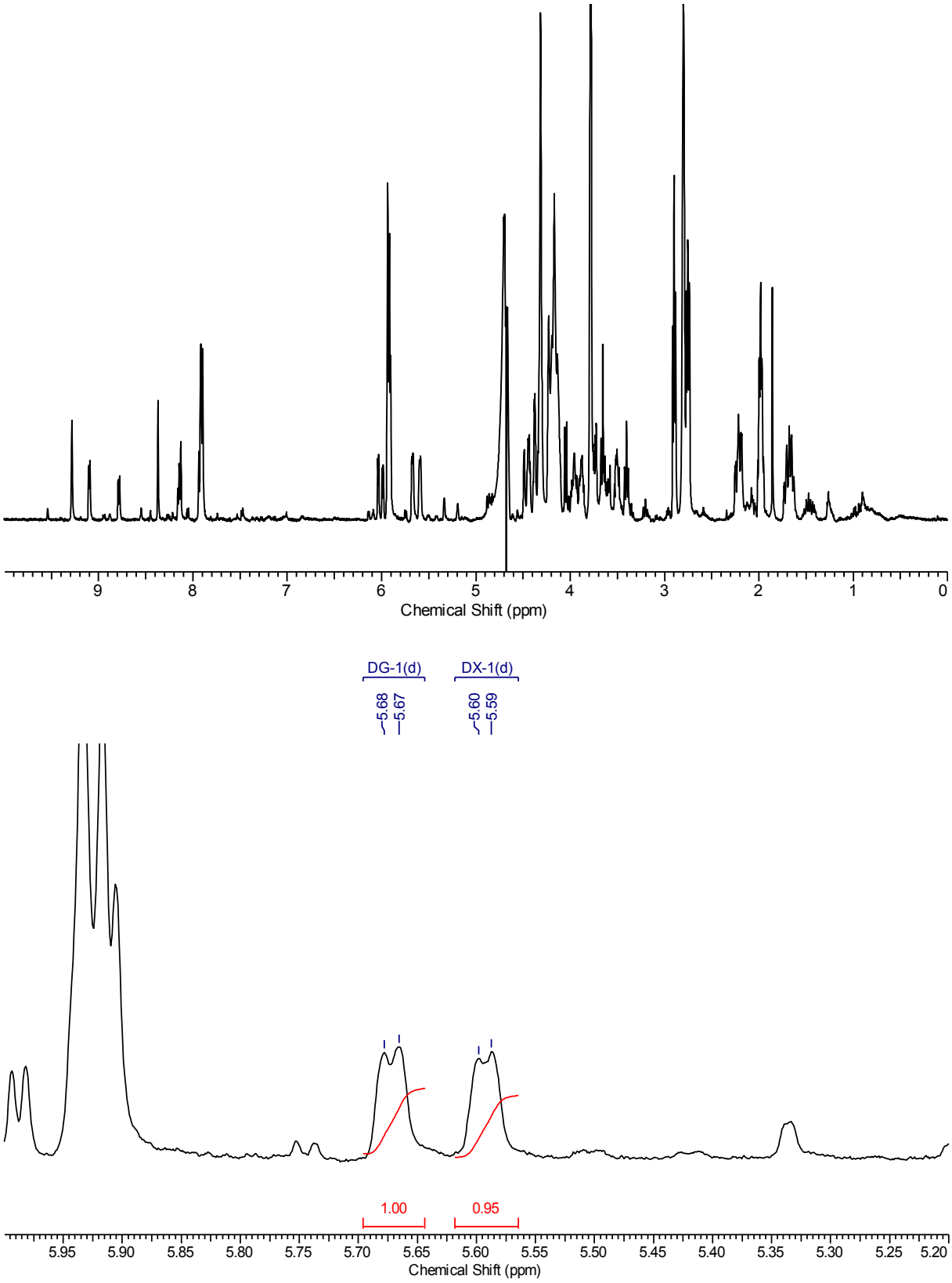

Supplementary Figure S27. ^{1}H NMR spectrum after conversion of substrate analogue **10** by UXS. Signals of the anomeric protons from substrate analogue **10** (DG-1) and product **15** (DX-1) are indicated.

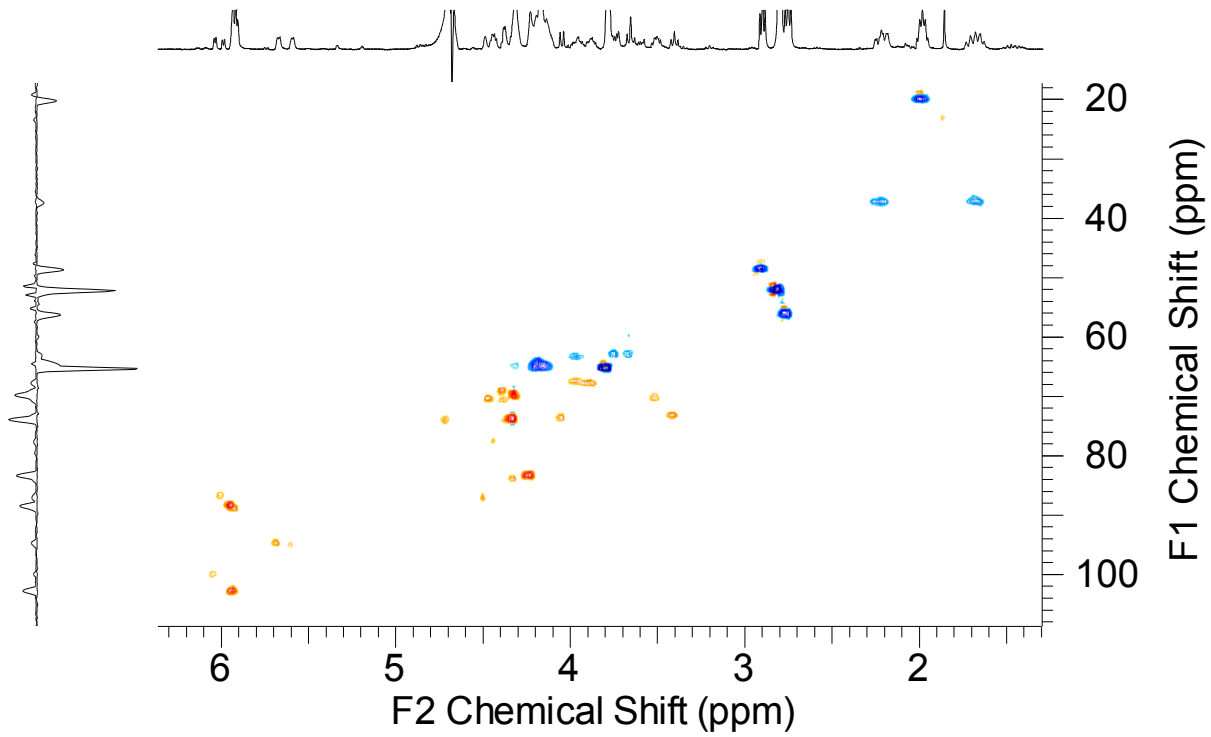

Supplementary Figure S28. HSQC spectrum (F1 axis = ^{13}C, F2 axis = ^{1}H) of reaction mixture containing substrate analogue **10**, NAD^{+} and UXS. Formation of product **15** is visible.

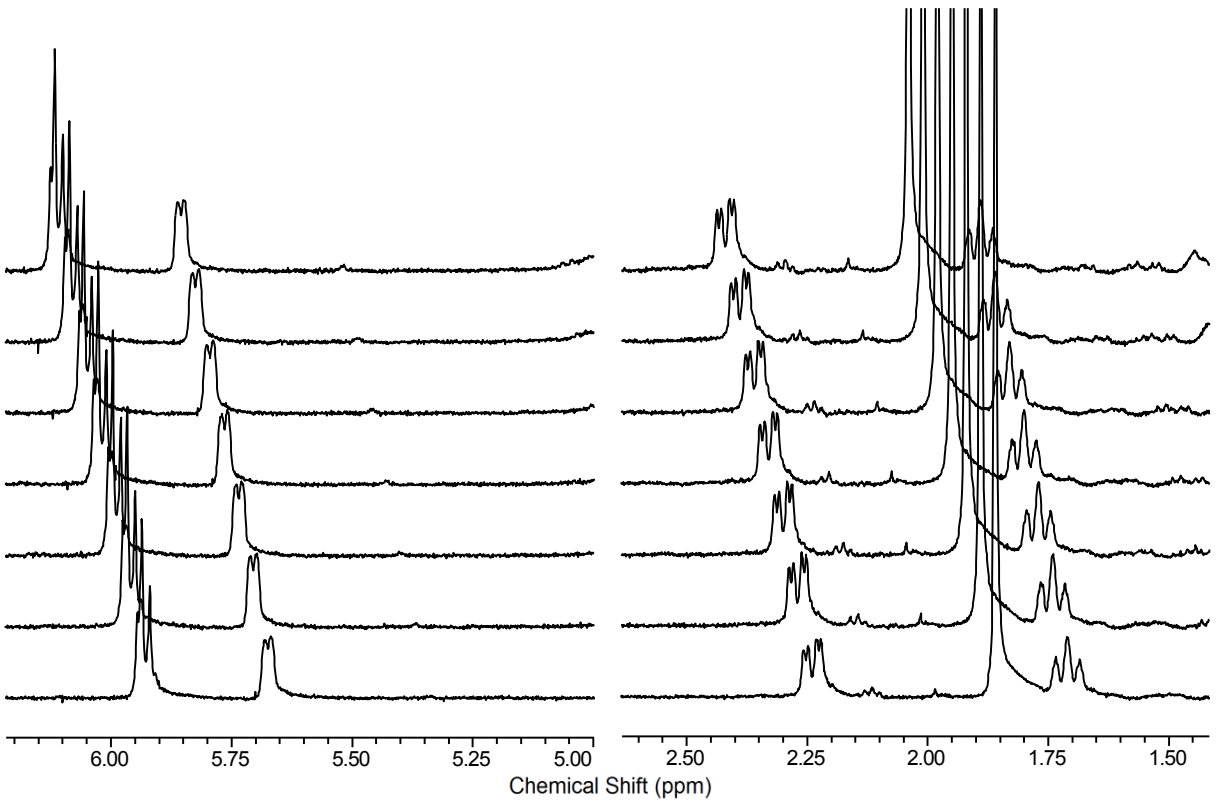

Supplementary Figure S29. *In situ* ^{1}H NMR experiment with 1 mM substrate analogue **10** and 20 µM UAXS (time between two spectra is 180 min). No product formation could be observed.

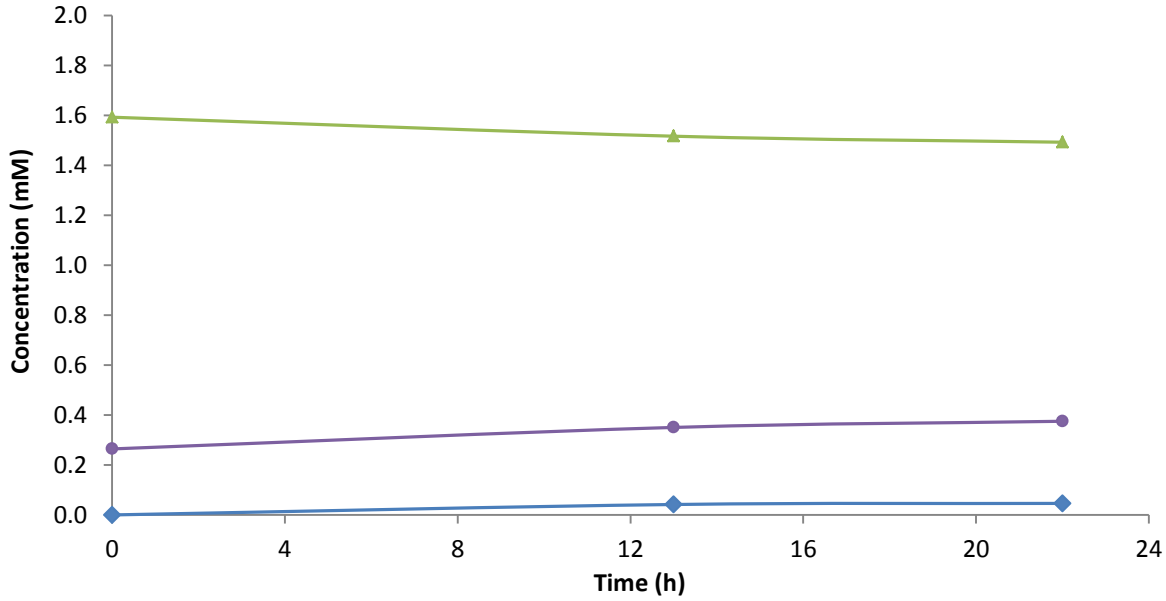

Supplementary Figure S30. Conversion of substrate analogue **10** by 50 µM UAXS. No product formation could be observed (green: substrate analogue **10**, blue: UMP, purple: UDP).

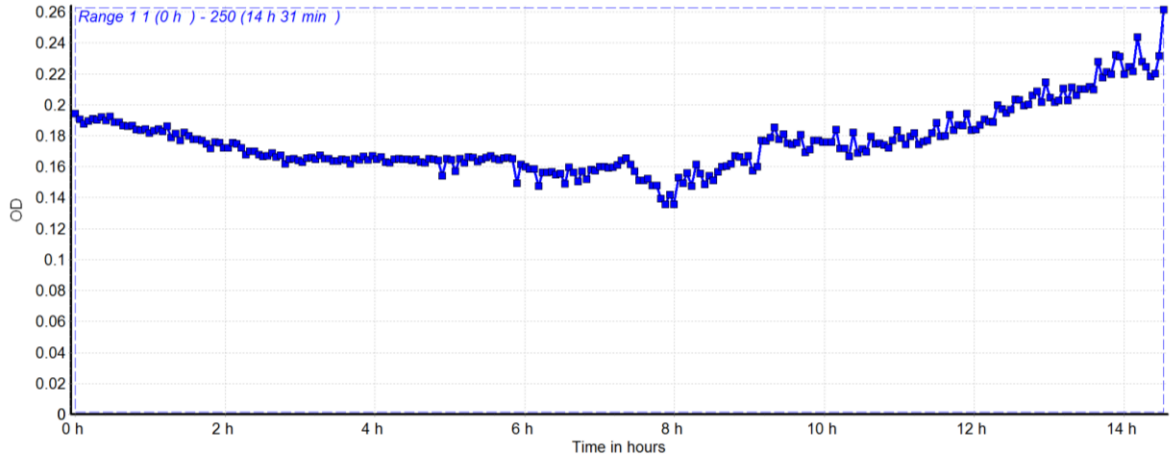

Supplementary Figure S31. Conversion of 1 mM substrate analogue **10** by 50 µM UAXS in presence of 2 mM NAD^+. No formation of NADH could be observed.

Methods

```
CLUSTAL O(1.2.1) multiple sequence alignment

GenBank             ---ATGGCGAATGGAGCTAATAGAGTGGATCTCGACGGGAAACCGATACAACCGTTGACA 57
Synthetic_gene      CATATGGCAAATGGTGCGAACCGTGTGGACCTGGACGGCAAACCGATTCAACCGCTGACG 60
                       ***** ***** ** **  * ***** ** ***** ******** ****** ****

GenBank             ATATGCATGATCGGCGCCGGAGGTTTCATCGGTTCACATCTCTGTGAAAAGCTCTTGACC 117
Synthetic_gene      ATCTGTATGATTGGTGCTGGCGGCTTTATTGGTAGTCATCTGTGCGAAAAACTGCTGACC 120
                    ** ** ***** ** ** ** ** ** ** ***   ***** ** ***** **  *****

GenBank             GAGACGCCACATAAGGTGCTTGCGCTCGATGTTTACAACGATAAGATCAAACACTTGCTT 177
Synthetic_gene      GAAACGCCGCACAAAGTTCTGGCCCTGGATGTCTATAACGACAAAATCAAACATCTGCTG 180
                    ** ***** ** ** ** ** ** ** ***** ** ***** ** ********  ****

GenBank             GAGCCTGATACCGTTGAATGGAGTGGTCGGATCCAGTTTCATCGTATCAATATTAAGCAT 237
Synthetic_gene      GAACCGGATACCGTTGAATGGAGCGGCCGTATTCAGTTTCATCGCATTAACATCAAACAC 240
                    ** ** ***************** ** ** ** *********** ** ** ** ** **

GenBank             GATTCGAGACTTGAAGGTCTTGTTAAGATGGCGGATCTGATTATAAATCTTGCTGCGATC 297
Synthetic_gene      GATTCTCGCCTGGAAGGTCTGGTCAAAATGGCAGACCTGATTATCAATCTGGCGGCCATT 300
                    *****  * ** ******** ** ** ***** ** ******** ***** ** ** **

GenBank             TGTACTCCAGCTGATTACAATACACGTCCTCTTGATACTATCTACAGCAATTTCATTGAT 357
Synthetic_gene      TGTACGCCGGCTGATTATAACACCCGTCCGCTGGACACGATCTACAGTAATTTCATTGAT 360
                    ***** ** ******** ** ** ***** ** ** ** ******** ************

GenBank             GCGCTTCCAGTTGTGAAATACTGTTCTGAGAACAACAAGCGTCTCATTCACTTTTCTACC 417
Synthetic_gene      GCACTGCCGGTGGTTAAATACTGCAGTGAAAACAACAAACGCCTGATCCATTTTTCCACC 420
                    ** ** ** ** ** ********   *** ******** ** ** ** ** ***** ***

GenBank             TGTGAAGTTTATGGAAAAACCATTGGAAGCTTTCTTCCTAAGGATCATCCTCTGCGTGAT 477
Synthetic_gene      TGTGAAGTGTACGGCAAAACGATTGGTTCCTTCCTGCCGAAAGATCACCCGCTGCGTGAT 480
                    ******** ** ** ***** *****   *** ** ** ** ***** ** *********

GenBank             GATCCTGCTTTCTATGTTCTTAAAGAAGATATTTCCCCTTGCATATTTGGTTCAATTGAG 537
Synthetic_gene      GACCCGGCTTTTTATGTTCTGAAAGAAGACATTAGTCCGTGCATCTTCGGCTCCATTGAA 540
                    ** ** ***** ******** ******** ***   ** ***** ** ** ** *****

GenBank             AAGCAGAGGTGGTCATATGCGTGTGCAAAGCAACTGATTGAGAGACTTGTTTACGCTGAG 597
Synthetic_gene      AAACAGCGTTGGTCTTATGCATGTGCTAAACAACTGATTGAACGCCTGGTCTACGCGGAA 600
                    ** *** * ***** ***** ***** ** ***********  * ** ** ***** **

GenBank             GGTGCTGAGAATGGGCTTGAGTTCACCATCGTACGACCTTTTAACTGGATTGGACCTAGG 657
Synthetic_gene      GGCGCCGAAAACGGTCTGGAATTTACCATCGTGCGTCCGTTCAATTGGATTGGCCCGCGC 660
                    ** ** ** ** ** ** ** ** ******** ** ** ** ** ******** **  *

GenBank             ATGGATTTCATCCCCGGCATTGATGGTCCTAGCGAAGGTGTCCCACGTGTCCTTGCCTGC 717
Synthetic_gene      ATGGATTTTATTCCGGGCATCGACGGTCCGTCAGAAGGTGTGCCGCGCGTTCTGGCGTGC 720
                    ******** ** ** ***** ** *****    ******** ** ** ** ** ** ***

GenBank             TTTAGTAACAATCTTCTACGTCGTGAGCCTCTCAAGCTTGTAGATGGTGGAGAATCACAG 777
Synthetic_gene      TTCTCGAACAATCTGCTGCGTCGCGAACCGCTGAAACTGGTGGATGGCGGTGAAAGCCAG 780
                    **    ******** ** ***** ** ** ** ** ** ** ***** ** ***   ***

GenBank             AGAACTTTCGTCTACATCAATGATGCTATTGAAGCTGTCCTTTTGATGATTGAAAACCCA 837
Synthetic_gene      CGTACCTTTGTGTATATCAATGACGCAATTGAAGCTGTTCTGCTGATGATCGAAAACCCG 840
                     * ** ** ** ** ******** ** *********** **  ******* ********

GenBank             GAGAGGGCAAATGGGCACATCTTCAACGTAGGCAACCCGAACAACGAAGTTACAGTAAGA 897
Synthetic_gene      GAACGTGCGAATGGCCACATTTTCAACGTTGGTAATCCGAACAATGAAGTCACCGTGCGC 900
                    **  * ** ***** ***** ******** ** ** ******** ***** ** **  *

GenBank             CAGCTCGCTGAAATGATGACCGAGGTTTACGCAAAAGTGAGTGGAGAAGGAGCCATTGAG 957
Synthetic_gene      CAACTGGCCGAAATGATGACGGAAGTCTACGCGAAAGTGTCAGGCGAAGGTGCCATCGAA 960
                    ** ** ** *********** ** ** ***** ******   ** ***** ***** **


GenBank             AGCCCAACGGTTGATGTTAGCTCCAAAGAGTTTTACGGGGAAGGTTATGATGACAGTGAC 1017
Synthetic_gene      TCGCCGACCGTTGATGTCAGCTCTAAAGAATTTTATGGCGAAGGTTACGATGACAGCGAT 1020
                       ** ** ******** ***** ***** ***** ** ******** ******** **
```

```
GenBank             AAGAGAATCCCAGACATGACCATCATTAACCGCCAACTCGGATGGAACCCGAAAACATCG 1077
Synthetic_gene      AAACGTATTCCGGACATGACCATTATCAACCGCCAACTGGGTTGGAATCCGAAAACGAGC 1080
                    **  * ** ** *********** ** *********** ** ***** ********

GenBank             CTATGGGACTTGCTCGAGTCGACCTTAACCTACCAGCACAGGACATACGCTGAAGCTGTG 1137
Synthetic_gene      CTGTGGGATCTGCTGGAATCTACCCTGACGTATCAACATCGCACCTATGCCGAAGCAGTG 1140
                    ** *****  **** ** ** *** * ** ** ** **  * ** ** ** ***** ***

GenBank             AAGAAGGCAACATCCAAACCAGTGGCTTCCTAA---       1170
Synthetic_gene      AAAAAAGCTACCAGCAAACCGGTCGCAAGCCTCGAG       1176
                    ** ** ** **   ****** ** **   *
```

Supplementary Figure S32. Sequence comparison of original AXS1 gene from GenBank and codon-optimized synthetic AXS1 gene used for recombinant UAXS production (green: restriction sites).

```
CLUSTAL O(1.2.1) multiple sequence alignment

Synthetic_gene      ----------------------------CATATGGCAAATGGTGCGAACCGTGTGGACC 31
Sequenced_gene      ATTTTGTTTAACTTTAAGAAGGAGATATACATATGGCAAATGGTGCGAACCGTGTGGACC 60
                                                ******************************

Synthetic_gene      TGGACGGCAAACCGATTCAACCGCTGACGATCTGTATGATTGGTGCTGGCGGCTTTATTG 91
Sequenced_gene      TGGACGGCAAACCGATTCAACCGCTGACGATCTGTATGATTGGTGCTGGCGGCTTTATTG 120
                    ************************************************************

Synthetic_gene      GTAGTCATCTGTGCGAAAAACTGCTGACCGAAACGCCGCACAAAGTTCTGGCCCTGGATG 151
Sequenced_gene      GTAGTCATCTGTGCGAAAAACTGCTGACCGAAACGCCGCACAAAGTTCTGGCCCTGGATG 180
                    ************************************************************

Synthetic_gene      TCTATAACGACAAAATCAAACATCTGCTGGAACCGGATACCGTTGAATGGAGCGGCCGTA 211
Sequenced_gene      TCTATAACGACAAAATCAAACATCTGCTGGAACCGGATACCGTTGAATGGAGCGGCCGTA 240
                    ************************************************************

Synthetic_gene      TTCAGTTTCATCGCATTAACATCAAACACGATTCTCGCCTGGAAGGTCTGGTCAAAATGG 271
Sequenced_gene      TTCAGTTTCATCGCATTAACATCAAACACGATTCTCGCCTGGAAGGTCTGGTCAAAATGG 300
                    ************************************************************

Synthetic_gene      CAGACCTGATTATCAATCTGGCGGCCATTTGTACGCCGGCTGATTATAACACCCGTCCGC 331
Sequenced_gene      CAGACCTGATTATCAATCTGGCGGCCATTTGTACGCCGGCTGATTATAACACCCGTCCGC 360
                    ************************************************************

Synthetic_gene      TGGACACGATCTACAGTAATTTCATTGATGCACTGCCGGTGGTTAAATACTGCAGTGAAA 391
Sequenced_gene      TGGACACGATCTACAGTAATTTCATTGATGCACTGCCGGTGGTTAAATACTGCAGTGAAA 420
                    ************************************************************

Synthetic_gene      ACAACAAACGCCTGATCCATTTTTCCACCTGTGAAGTGTACGGCAAAACGATTGGTTCCT 451
Sequenced_gene      ACAACAAACGCCTGATCCATTTTTCCACCTGTGAAGTGTACGGCAAAACGATTGGTTCCT 480
                    ************************************************************

Synthetic_gene      TCCTGCCGAAAGATCACCCGCTGCGTGATGACCCGGCTTTTTATGTTCTGAAAGAAGACA 511
Sequenced_gene      TCCTGCCGAAAGATCACCCGCTGCGTGATGACCCGGCTTTTTATGTTCTGAAAGAAGACA 540
                    ************************************************************

Synthetic_gene      TTAGTCCGTGCATCTTCGGCTCCATTGAAAAACAGCGTTGGTCTTATGCATGTGCTAAAC 571
Sequenced_gene      TTAGTCCGTGCATCTTCGGCTCCATTGAAAAACAGCGTTGGTCTTATGCATGTGCTAAAC 600
                    ************************************************************

Synthetic_gene      AACTGATTGAACGCCTGGTCTACGCGGAAGGCGCCGAAAACGGTCTGGAATTTACCATCG 631
Sequenced_gene      AACTGATTGAACGCCTGGTCTACGCGGAAGGCGCCGAAAACGGTCTGGAATTTACCATCG 660
                    ************************************************************

Synthetic_gene      TGCGTCCGTTCAATTGGATTGGCCCGCGCATGGATTTTATTCCGGGCATCGACGGTCCGT 691
Sequenced_gene      TGCGTCCGTTCAATTGGATTGGCCCGCGCATGGATTTTATTCCGGGCATCGACGGTCCGT 720
                    ************************************************************

Synthetic_gene      CAGAAGGTGTGCCGCGCGTTCTGGCGTGCTTCTCGAACAATCTGCTGCGTCGCGAACCGC 751
Sequenced_gene      CAGAAGGTGTGCCGCGCGTTCTGGCGTGCTTCTCGAACAATCTGCTGCGTCGCGAACCGC 780
                    ************************************************************
```

```
Synthetic_gene      TGAAACTGGTGGATGGCGGTGAAAGCCAGCGTACCTTTGTGTATATCAATGACGCAATTG 811
Sequenced_gene      TGAAACTGGTGGATGGCGGTGAAAGCCAGCGTACCTTTGTGTATATCAATGACGCAATTG 840
                    ************************************************************

Synthetic_gene      AAGCTGTTCTGCTGATGATCGAAAACCCGGAACGTGCGAATGGCCACATTTTCAACGTTG 871
Sequenced_gene      AAGCTGTTCTGCTGATGATCGAAAACCCGGAACGTGCGAATGGCCACATTTTCAACGTTG 900
                    ************************************************************

Synthetic_gene      GTAATCCGAACAATGAAGTCACCGTGCGCCAACTGGCCGAAATGATGACGGAAGTCTACG 931
Sequenced_gene      GTAATCCGAACAATGAAGTCACCGTGCGCCAACTGGCCGAAATGATGACGGAAGTCTACG 960
                    ************************************************************

Synthetic_gene      CGAAAGTGTCAGGCGAAGGTGCCATCGAATCGCCGACCGTTGATGTCAGCTCTAAAGAAT 991
Sequenced_gene      CGAAAGTGTCAGGCGAAGGTGCCATCGAATCGCCGACCGTTGATGTCAGCTCTAAAGAAT 1020
                    ************************************************************

Synthetic_gene      TTTATGGCGAAGGTTACGATGACAGCGATAAACGTATTCCGGACATGACCATTATCAACC 1051
Sequenced_gene      TTTATGGCGAAGGTTACGATGACAGCGATAAACGTATTCCGGACATGACCATTATCAACC 1080
                    ************************************************************

Synthetic_gene      GCCAACTGGGTTGGAATCCGAAAACGAGCCTGTGGGATCTGCTGGAATCTACCCTGACGT 1111
Sequenced_gene      GCCAACTGGGTTGGAATCCGAAAACGAGCCTGTGGGATCTGCTGGAATCTACCCTGACGT 1140
                    ************************************************************

Synthetic_gene      ATCAACATCGCACCTATGCCGAAGCAGTGAAAAAAGCTACCAGCAAACCGGTCGCAAGCC 1171
Sequenced_gene      ATCAACATCGCACCTATGCCGAAGCAGTGAAAAAAGCTACCAGCAAACCGGTCGCAAGCC 1200
                    ************************************************************

Synthetic_gene      TCGAG-------------------------------------------     1176
Sequenced_gene      TCGAGCACCACCACCACCACCACTGAGATCCGGCTGCTAACAAAGCC     1247
                    *****
```

Supplementary Figure S33. Sequence comparison of synthetic AXS1 gene as obtained by the supplier and sequencing results after plasmid isolation. The *C*-terminal His_6 tag is visible (blue).

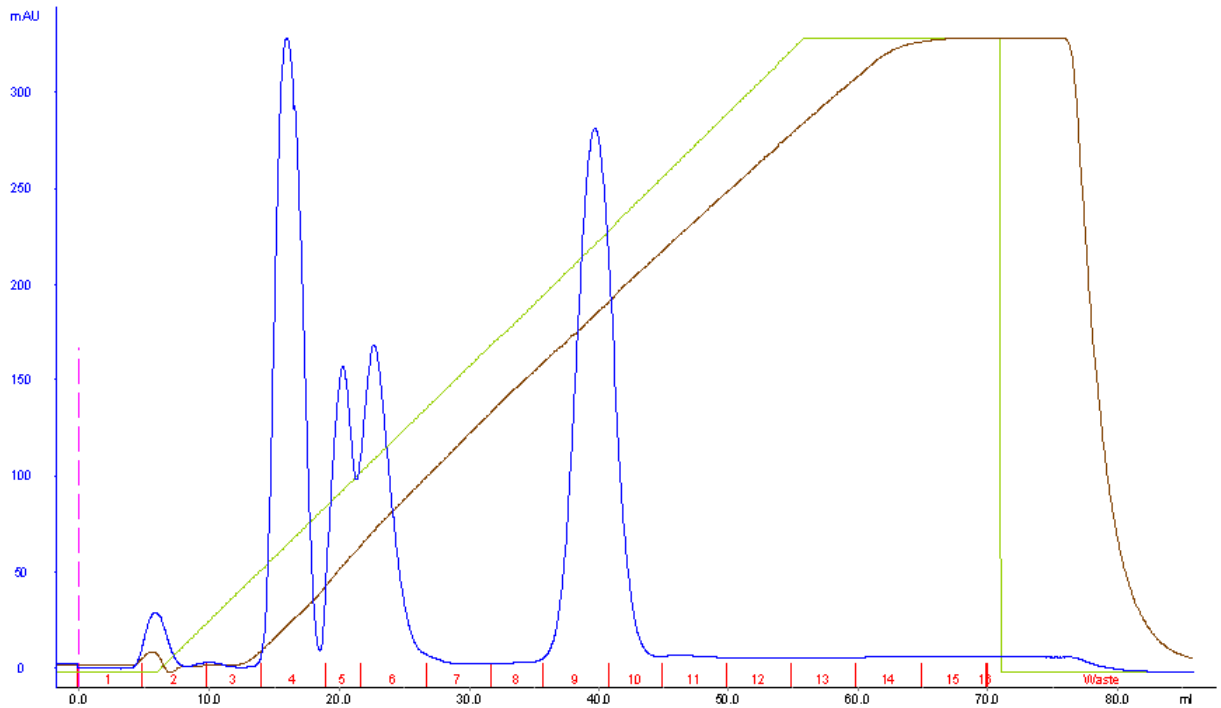

Supplementary Figure S34. Representative purification of UAXS reaction mixture for evaluation of intermolecular competition experiments (blue: UV signal, brown: conductivity signal, green: concentration buffer B).

References

1 Guyett, P., Glushka, J., Gu, X. & Bar-Peled, M. Real-time NMR monitoring of intermediates and labile products of the bifunctional enzyme UDP-apiose/UDP-xylose synthase. *Carbohydr. Res.* **344**, 1072-1078 (2009).

2 Bar-Peled, M., Griffith, C. L. & Doering, T. L. Functional cloning and characterization of a UDP-glucuronic acid decarboxylase: The pathogenic fungus *Cryptococcus neoformans* elucidates UDP-xylose synthesis. *Proc. Natl. Acad. Sci. U.S.A* **98**, 12003-12008 (2001).

Scientific record

Publications

Catalytic mechanism of human UDP-glucose 6-dehydrogenase: in situ proton NMR studies reveal that the C-5 hydrogen of UDP-glucose is not exchanged with bulk water during the enzymatic reaction
T. Eixelsberger, L. Brecker, B. Nidetzky, *Carbohydr. Res.* 356 (**2012**), 209-214

Structure and Mechanism of Human UDP-Xylose Synthase: EVIDENCE FOR A PROMOTING ROLE OF SUGAR RING DISTORTION IN A THREE-STEP CATALYTIC CONVERSION OF UDP-GLUCURONIC ACID
T. Eixelsberger[§], S. Sykora[§], S. Egger, M. Brunsteiner, K. L. Kavanagh, U. Oppermann, L. Brecker, B. Nidetzky, *J. Biol. Chem.* 287 (**2012**), 31349-31358
[§] These authors contributed equally to the work.

Scale-Up and Intensification of (*S*)-1-(2-Chlorophenyl)ethanol Bioproduction: Economic Evaluation of Whole Cell-Catalyzed Reduction of *o*-Chloroacetophenone
T. Eixelsberger, J. M. Woodley, B. Nidetzky, R. Kratzer, *Biotechnol. Bioeng.* 110 (**2013**), 2311-2315

Enzymatic Redox Cascade for One-Pot Synthesis of Uridine 5'-Diphosphate Xylose from Uridine 5'-Diphosphate Glucose
T. Eixelsberger, B. Nidetzky, *Adv. Synth. Catal.* 356 (**2014**), 3575-3584

Oral presentations

Characterization and biosynthetic application of human UDP-xylose synthase
T. Eixelsberger, B. Nidetzky, *17th Austrian Carbohydrate Workshop*, **2013**, Graz, Austria

Characterization and biosynthetic application of human UDP-xylose synthase 1
T. Eixelsberger, B. Nidetzky, *27th International Carbohydrate Symposium*, **2014**, Bangalore, India

Multi-enzymatic synthesis of UDP-xylose
T. Eixelsberger, B. Nidetzky, *18th Austrian Carbohydrate Workshop*, **2014**, Vienna, Austria

Poster presentations

Structure and mechanism of human UDP-xylose synthase: evidence for a promoting role of sugar ring distortion in a three-step catalytic conversion of UDP-glucuronic acid
T. Eixelsberger, S. Sykora, S. Egger, M. Brunsteiner, K. L. Kavanagh, U. Oppermann, L. Brecker, B. Nidetzky, *26th International Carbohydrate Symposium*, **2012**, Madrid, Spain

Enzymatic redox cascade for synthesis of nucleotide sugars
T. Eixelsberger, D. Horvat, B. Nidetzky, *Green Chemistry for Pharma*, **2014**, Graz, Austria